COMPREHENSIVE APPROACH TO ENSURE DURABILTY OF EXTERNAL WOODEN STRUCTURES

PETR KUKLÍK, ZDENĚK PROŠEK, ANNA GREGOROVÁ
CZECH TECHNICAL UNIVERSITY IN PRAGUE
CZECH REPUBLIC

ABSTRACT

The article deals with durability of wood, durability of wooden structures and surface modification of wood. We are trying to eliminate the factors causing degradation of wood with the use of photocatalytic materials. Those materials are efficient UV absorbers and they are able to destroy biological aggressors also. The planar particles of titanium oxide TiO_2 were chosen for the purpose of our research and applied on a wooden surface. In our case, we used a water solution of TiO_2. The main goal of our work was to study the interaction between planar particles of TiO_2 and wood matter. The samples of pine wood (*Pinus sylvestris*) were monitored for 255 days and subsequently evaluated using an electron microscope. The use of TiO_2 was compared with reference material and a reference commercial coating.

KEYWORDS: Wood, durability of wood, protection of wood, wooden structures.

INTRODUCTION

Wood is the oldest building material capable of transferring both tension and compression (Thelandersson et al. 2003). Wood also has a very good strength to weight ratio. The problem is biological degradation of wood as a natural material (Blass et al. 1995). Due to that durability considerations are important in ensuring an appropriate life for wooden structures. Durability issues imply that the designer has an expectation of performance of the wooden structures for a given number of years - usually the service life of the structure. Responsible design is focused to appropriate wooden species, sizes that allow the satisfactory performance and appropriate treatment. The protection of wood takes many forms including proper detailing. They are mainly directed towards the prevention of moisture access.

Although wood as raw material has wide utilisation in many industrial sectors, its use is compromised in some applications due to some draw-backs resulting from its variability both between and within wood species as well as its inherent physical-chemical properties

(e.g. anisotropy, hygroscopicity). Wood performs variably in density, strength and durability, while it is susceptible to degradation by UV-light, chemicals, fungi and insects when in humid environments. Moreover, wood lacks dimensional stability because of its property to swell and shrink when being in variable moisture conditions, caused by the large number of hydroxyl groups in the wood structure (Blass et al. 1995). Protective systems ensuring durability of wooden structures take many forms: *a)* design for durability, *b)* chemical treatment where natural durability is not enough, or *c)* maintenance and monitoring (visual, semi-destructive). Nevertheless, it is also necessary to take into account that preservative treatment may affect the strength and stiffness properties of wood (Blass et al. 1995).

One of the semi-destructive methods for evaluation of wooden structures is based on measurement of material resistance against penetration of an indenter. The damage of a wooden structural member is small after the tests. One of the well-known devices is Pilodyn 6J Forest that penetrates the surface layers of wooden element by a short pin with the help of an internal spring. It is possible to determine wood density and even the related mechanical properties based on the input of the depth of the pin penetration (Hasníková et al. 2014).

Wood density is determined by several factors, e.g. cell diameter and cell wall thickness, proportions of earlywood and latewood, cellulose and lignin content etc. Density has a significant influence on mechanical properties of wood (Kasal et al. 2004).

One of the innovative methods particularly suitable for long-term continuous monitoring of stress in wooden structure is the use of a fibre optic sensor. The technology of Fibre Bragg Grating (FBG) sensor is an optical system used for the same purposes as strain gauge sensors. However, unlike strain gauges, deformation measurements and information transmission are realized by means of light. Energy requirements of the system are therefore reduced and the system is significantly more resistant to most potential sources of interference, including electromagnetic interference. The fibre optic sensor is essentially an optical fibre equipped with a special grating (the so-called Bragg grating), which is produced for example by UV laser firing during fibre production. It is a very small, germanium doped portion of the optical fibre which, in the case of joining this fibre with the stretched body, changes its optical properties in a defined manner, and thus it is possible to measure very precisely the elongation of the body. On one fibre there can be several independent FBG sensors, each measuring a different place on the construction and working at a different wavelength. The fibre is equipped with a polymeric sleeve covering which acts as a fibre protection against moisture and mechanical damage. The FBG sensors are based on a principle of reflection of central wavelength of light by the Bragg grating. A part of the emitted light signal passes through the grating and a part of the light spectrum is reflected back. In the measuring unit, it is compared to the reference (unloaded) grating tuned to the same wavelength, the deformation is obtained from the difference of values. In the case of a newly made wooden member, the sensor can be inserted into its body. If an existing wooden member or even historical structure is to be monitored, the sensor can be attached to its surface (Velebil et al. 2016).

Durability of wood

Under ideal conditions wooden structures can be in use for centuries without significant biological deterioration (Thelandersson et al. 2003). However, when conditions are not ideal, many of wood species need a preservative treatment to be protected from the biological agents responsible for wood degradation, mainly fungi and insects. There is also one simple rule for design of wooden structures - "keep wood dry". In this case, the good detailing can be used to reduce biological hazard. Maintenance is also very important during the service life of the structure.

Each type of biological hazard has its own set of conditions that increase the risk of deterioration. Many of them include high levels of moisture. For example, fungal attack on wood is accelerated by the following conditions: moisture content between 20% and 25%, freely available oxygen, temperature range in 5°C to 40°C (ideally 25-40°C), a ready supply of food containing sugars and carbohydrates (i.e. the wood itself, particularly sapwood) (Blass et al. 1995).

Wood and wood-based products shall either have adequate natural durability for the particular application, or be given some preservative treatment. The new EN 335: 2013 gives general definitions of Use classes (previously called Hazard classes) for different service situations to which wood and wood-based products can be exposed.

Surface modification of wood

From a chemical point of view, the wood consists of cellulose, hemicellulose and lignin, while the wood cells also contain at a lesser extent other components like tannins, resins, oils, fats, terpenes, flavonoids, quinines and alkaloids (Hunt et al. 1938). The properties of wood surfaces are influenced by polymer morphology, extractive chemicals and processing parameters and conditions in end-uses. In the case of wood, the cell wall polymers are the main components which must be modified to change the properties of wood.

Generally timber protection materials should prolong lifetime of wooden structures. The main role of the group protective materials based on photocatalysis is to protect wood before color changing, moulds and fungus. The most spread photocatalytic materials for wood protection are TiO_2, ZnO, CeO_2 (Šubrt 2014) and WO_3 (Paola el al. 2012). Photocatalytic materials are applied in nanoform and usually used as a transparent coating. There are two ways to apply, particle of photocatalytic material can be directly mixed with the solution (Allen et al. 2002) or encapsulated into porous, resistant material (Minabe et al. 2000). Furthermore, the article deals with the use of TiO_2 because it is the most available material with photocatalytic properties (Chen et al. 2009).

Material for chemical protection of wood by TiO_2 was chosen planar particles of TiO_2 because it is possible to prepare as photoactive (crystalline) and non-photoactive (amorphous) (Bahtat et al. 1992). We are expecting that the use of the planar particles of TiO_2 (Fig. 1) could be one of the method to ensure durability of wood and wooden structures during their planned service life. This will strengthen the confidence of users (e.g. engineers and architects) and boost the use of wood also in conventional fields of application like building structures etc. The goal of our work is study interaction between planar particles of TiO_2 and wood matter. In our study, we want to observe the direct interaction between wood tissue and particle of

TiO$_2$, so we used an aqueous solution of TiO$_2$. We assume that water evaporates and the particles are bonded by Van der Waals forces directly to wood tissue (Hu et al. 2014).
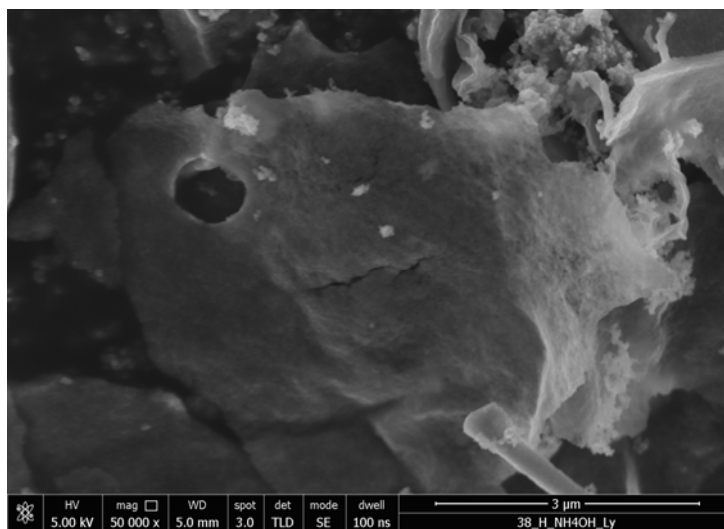

Fig. 1: Planar particle of amorphous TiO$_2$ (Photo: electron microscopy CTU, Prague).

After the application of TiO$_2$, the planar morphology was proved by electron microscopy (Fig. 1). On the picture is possible to see that the surface of the particle is not plain but wavy and also it is not completely continuous. The holes cover 20% of the surface and aggregates cover 10%. Holes and aggregates in this amount have no negative impact on the UV absorption of the material as was proven by UV-VIS spectroscopy.

In the next part of the article is presented the use of chemical protection of wood in the form of TiO$_2$ in comparison with the commonly used commercial protection of wood and unprotected wood.

MATERIAL AND METHODS

Materials

The tested wood was pine (*Pinus sylvestris*) from the forest area in Central Europe. The wood was protected in the form of a coating. Planar TiO$_2$ particles were used as chemical protection of wood. It was a 3% aqueous solution of TiO$_2$, which was evenly applied on the wood surface. The preparation of TiO$_2$ itself was taken from the article by Svora et al. (2020), where elemental composition and structural characterization are also described. Alkyd stain SynolacTM 6005 W from Cray Valley Ltd. was chosen as a representative of commercial chemical protection of wood and was chosen for comparison according to EN 927-3: 2002. Alkyd stain SynolacTM 6005 W with a solids content of 65% uses iron catalysis (bispidon) as drier.

Samples preparation

Three sets of samples were used to describe the effect of wood protection using TiO_2, which were exposed to the outside environment for 255 days. Each set contained six pine samples measuring 20 x 40 x 400 mm, which were placed external environment on the grounds of the University Centre of Energy Efficient Buildings. Tab. 1 shows the identification of individual samples with methods of protection. The samples were continuously visually monitored (Fig. 2) and subsequently, after 255 days, smaller samples were taken from the surface for microscopic sections.

Tab. 1: Methods of UV protection of samples.

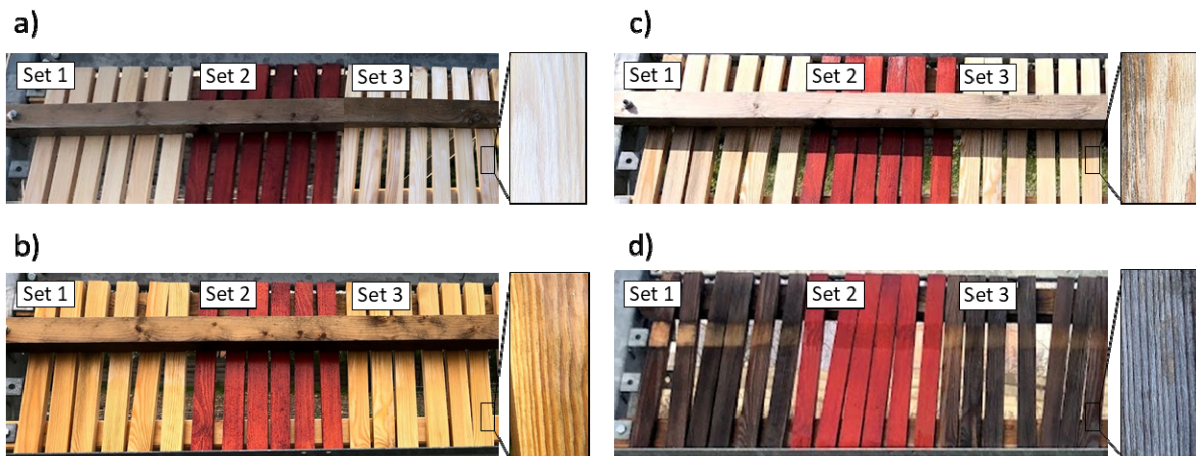| Set	UV protection method
1	without protection
2	alkyd stain
3	3% TiO_2 solution

Fig. 2: Visual monitoring of the samples during exposure to the external environment: a) exposure time 0 days, b) exposure time 44 days, c) exposure time 83 days, d) exposure time 255 days.

Microscopic sections were used for electron microscopy. A small portion of the sample was taken from the wood surface and enclosing in epoxy resin (EpoFix kit from Struers). Subsequently, the sample was ground and polished to achieve the required roughness for electron microscopy and elemental microanalysis. In the first step, silicon carbide foils with a roughness of 500 grains·cm^{-2} were used for 2 min, followed by foils with a roughness of 1200 grains·cm^{-2} and 2000 grains/cm^2 for 4 min and 4000 grains·cm^{-2} for 12 min. The entire preparation was performed on Tegramin 25 from Struers with a pressure on samples of 5 N and performed without the use of water as a wetting agent. The sample thus prepared reached the flatness required for analysis. Finally, the samples were sputtered with 3 nm platinum. Platinum created a conductive layer on the surface of the wood, thus eliminating the charging effect that occurs when using the high current required for elemental microanalysis.

Experimental methods

The experimental methods used describe the surface and microstructure of the tested wood. The article uses a combination of optical and electron microscopy with elemental microanalysis. The experiments methods were performed in the Laboratory of Electron Microscopy and Micro-analysis at the University Centre for Energy Efficient Buildings in Buštěhrad. The Axio Zoom.V16 microscope from ZEISS was used for optical microscopy. This is a stereo zoom microscope and a large field was used to study and describe the surface of the tested samples.

The electron microscopy was performed using the scanning electron microscope (SEM) with a Schottky cathode FEG SEM Merlin from ZEISS. Energy dispersive spectrometer (EDS) from Oxford Instruments was used for qualitative elemental microanalysis of the tested samples. The EDS microanalysis was performed using the element maps of the microstructure and point ID of individual coating. During the SEM analysis, the microscope settings were as follows: resolution 1024×768 pixels with an average time per pixel of 9 μs, a working distance of 8.5 mm, acceleration voltage 20 kV, current 2 nA, and EDS setting were as follows: resolution 2048 pixels, frame live time 79 seconds, frame count 4, process time 3 and the pixel dwell time 25 μs.

RESULTS AND DISCUSSION

Optical microscopy

The surfaces of the tested samples can be seen in Fig. 3. The color of the wood surface can be seen with a protective coating for set of samples 2 and 3. Sample with a commercial protection (Set 2) shows no changes during exposure to the external environment. The surface of the sample without protection against UV degradation (Set 1) shows color changes which are caused degradation of wood by external environment. The color of wood changed from yellow (natural color) to brown for latewood and silver patina acquires on the surface of earlywood.
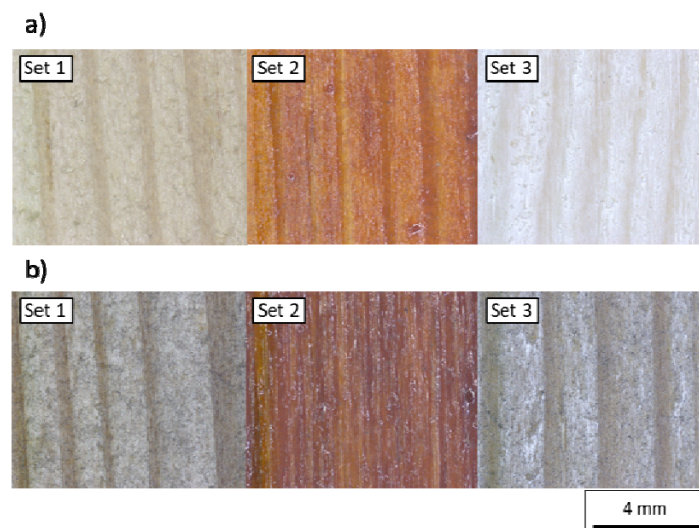
Fig. 3: Optical images of the sample surface: a) exposure time 0 days, b) exposure time 255 days, magnification 10x.

The differences between earlywood and latewood were caused by different bulk densities. The earlywood is more degraded than latewood due to its lower density and thus, a deeper light penetration into wood. A smaller color change effect can also be observed for   a sample with TiO$_2$ protection (Set 3). These results are consistent with other studies dealing with UV degradation of wood (Cogulet et al. 2016). However, it must be noted that these findings were reached for the white spruce (*Picea glauca*) and samples were exposed in a QUV accelerated weathering tester from Q-Lab (USA) for 2000 h.

Electron microscopy

Electron microscopy images of the microstructure (Figs. 4-6) confirmed the results from optical microscopy. The microstructure is composed of 90% by volume of cells, which divide earlywood tracheids or latewood tracheids according to the period in which they grew (Prošek et al. 2015). The remaining microstructure is made up of parenchymal cells and resin channels.

Change in the microstructure of sample without UV protection (Set 1) due to degradation by UV radiation can be seen (Fig. 4). The receding part of earlywood can be seen in the microstructure of the sample, which is more susceptible to UV degradation of wood. In addition, the loss of lignin by means of UV radiation thins the cell walls in the case of an earlywood cell and their impaired connection through the middle lamella, which is rich on lignin. The same effect of UV radiation is described in a study by Rowell (2005).
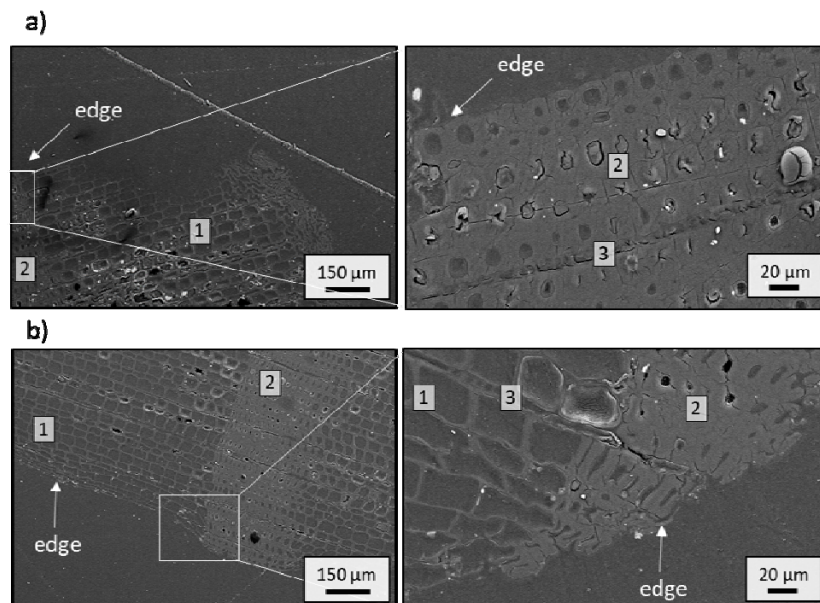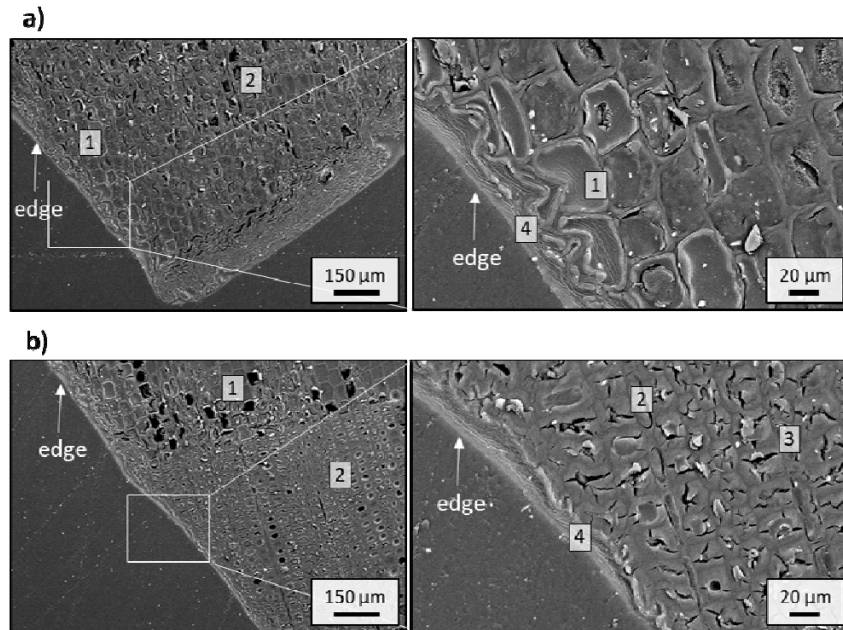

Fig. 4: SEM images of reference sample without a protective layer (Set 1), cross-section, magnification 250 × and for cutout 1k ×: (1) earlywood tracheid, (2) latewood tracheid, (3) parenchymal cell, a) exposure time 0 days, b) exposure time 255 days.

The UV protective coating can be seen in the microstructure (Fig. 5) of samples with commercial protective layer (Set 2). The protective layer is approximately 10 μm thick. The microstructure does not show any significant changes in the cells due to the protective coating and thus UV radiation did not cause degradation of the material. Protective layer,

opaque pigmented coatings, act as very effective UV radiation screen. This is an effect that has been described in several studies (George et al. 2005).

Fig. 5: SEM images of sample with a commercial protective layer (Set 2), cross-section, magnification 250 × and for cutout 1k ×: (1) earlywood tracheid, (2) latewood tracheid, (3) parenchymal cell, (4) protective layer, a) exposure time 0 days, b) exposure time 255 days.

Sample with protection layer of TiO_2 (Set 3) can be seen on Fig. 6. Protection layer of TiO_2 has a thickness of approximately 5 μm. The protective layer of TiO_2 is not visible in the microstructure after exposure to the external environment for 255 days and damaged wood cells of earlywood tracheid can be seen in the microstructure.
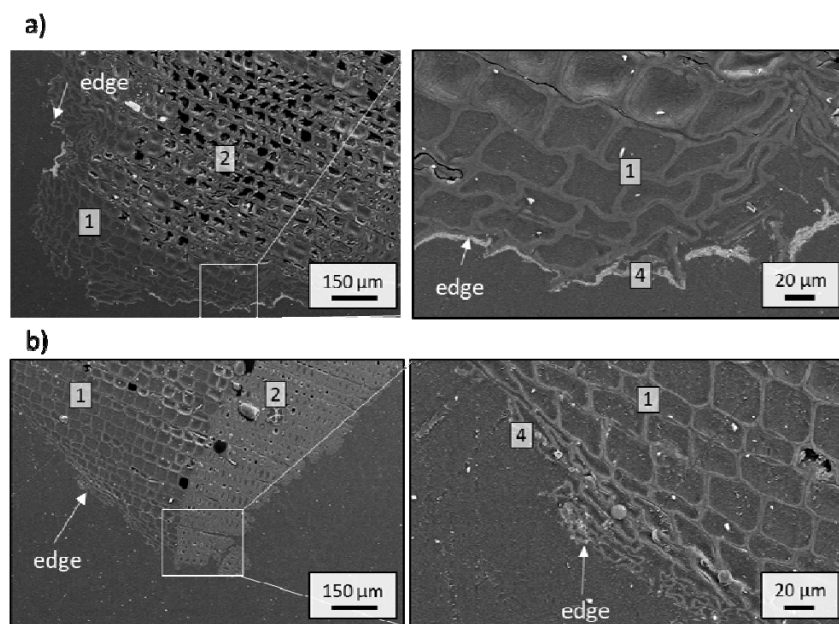
Fig. 6: SEM images of sample with TiO_2 protective layer (Set 3), cross-section, magnification 250 × and for cutout 1k ×: (1) earlywood tracheid, (2) latewood tracheid, (3) parenchymal cell, (4) protective layer, a) exposure time 0 days, b) exposure time 255 days.

Elemental microanalysis

The element map determined by EDS can be seen in the Fig. 7. The commercial protective layer and the 3% aqueous TiO_2 solution layer were rich in iron and titanium, respectively. Therefore, these chemical elements were examined in the microstructure.
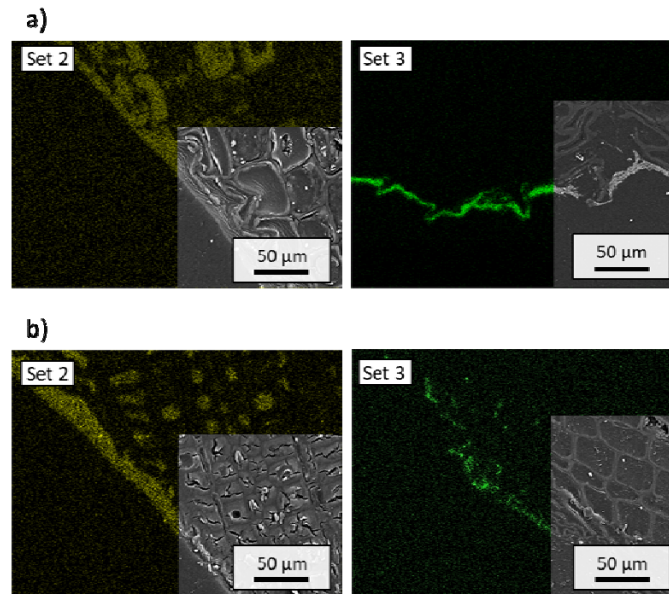

Fig. 7: Elemental microanalysis of samples with a protective layer – BSE detector magnified 1k × with EDS element maps (yellow – iron, green – titanium), a) exposure time 0 days, b) exposure time 255 days.

The high iron (drier) content can be seen in the protective layer with a thickness of 10 μm for the sample with the commercial protective layer (Set 2). In addition, a high content of iron in the cell cavities of the so-called lumen can also be seen, which indicates that the wood is impregnated to a depth of 100 μm and thus reliably protected the wood cells. The depth of impregnation of 100 μm was also confirmed in the work of Rijckaer et al. (2001) who tested Scots pine sapwood in this way.

Samples with a protective TiO_2 layer (Set 3) show a high titanium content in the layer with a width of approximately 5 μm. Furthermore, there is no titanium in the lumen and in the entire microstructure, which means that the wood has not been impregnated. The TiO_2 protective layer is not integral after exposure of the sample to the external environment and this results in a partial degradation of the wood cells. This is the effect of a weak connection between the TiO_2 layer and the wood surface. An aqueous solution of TiO_2 was used because after evaporation of the water, the TiO_2 particles are bonding by Van der Waals forces (Hu et al. 2014). The Van der Waals forces have a low binding effect and, as a result, TiO_2 particles are gradually leached out of the sample surface by rain. This statement is in agreement with the knowledge about the weak connection of particles by Van der Waals forces (Santamarina 2003, Santos et al. 2020).

CONCLUSIONS

Durability of wooden structures is one of the critical limit states which should be considered. Wood protection should be carried out in accordance with the requirements for the specific applications. The protection of wood takes many forms including proper detailing. The effect and interaction between wood mass and amorphous titanium dioxide TiO_2 were investigated in order to improve the quality of surface finish of wooden structures. Coatings with planar particles of titanium dioxide were used for dispersions applied on wooden surface in a transparent layer. The researched wood was pine (*Pinus sylvestris*), which was exposed to the external environment for 255 days and compared with a reference sample and a commercial coating. Based on the results, it can be concluded that: *(1)* the cells of the reference wood were destroyed by the external environment for 255 days, *(2)* commercial protective coating reliably protected wood, *(3)* the protective layer of 3% TiO_2 water solution was not integral and thus the wood cells were damaged, *(4)* the low integrity of the TiO_2 protective coating was caused by the lower bonding of the resulting Van der Waals forces.

Work in progress deal with testing new wood samples, which are protected by TiO_2 coating in a solution of water glass and acrylate. In the case of a water glass solution, the inorganic porous structure is created and particles are surrounded by silicate chains. In the case of acrylic solution, the organic porous structure is created.

ACKNOWLEDGMENT

REFERENCES

1. Allen, N.S., Edge, M., Ortega, A., Liauw, C.M., Stratton, J., McIntyre, R.B., 2002: Behaviour of nanoparticle (ultrafine) titanium dioxide pigments and stabilisers on the photooxidative stability of water based acrylic and isocyanate based acrylic coatings. Polymer degradation and stability 78(3): 467-478.
2. Bahtat, M., Mugnier, J., Lou, L., Serughetti J., 1992: Planar TiO_2 waveguides by the sol-gel process: The relationship of structure to properties. Sol-Gel Optics II 1758: 173-183.
3. Blass, H., Aune, P., Choo, B., Görlacher, R., Griffiths, D., Hilson, B., Racher, P., Steck, G., 1995: Timber Engineering. Centrum Hout. Almere, The Netherlands, 427 pp.
4. Chen, F., Yang, X., Wu, Q., 2009: Antifungal capability of TiO_2 coated film on moist wood. Building and Environment 44(5): 1088-1093.
5. Cogulet, A., Blanchet, P., Landry, V., 2016: Wood degradation under UV irradiation: A lignin characterization. Journal of Photochemistry and Photobiology B: Biology 158: 184-191.

6. EN 335, 1992: Durability of wood and wood-based products - Use classes: definitions, application to solid wood and wood-based products.

7. EN 927-3, 2002: Paints and varnishes. Coating materials and coating systems for exterior wood. Part 3: Natural weathering test.

8. George, B., Suttie, E., Merlin, A., Deglise, X., 2005: Photodegradation and photostabilisation of wood – the state of the art. Polymer Degradation and Stability 88(2): 268-274.

9. Hasníková, H., Kuklík, P., 2014: Various non-destructive methods for investigation of timber members from a historical structure. Wood Research 59(3): 411-420.

10. Hunt, G., Garrett, G., 1938: Wood preservation. McGraw-Hill, Book Company, Inc. New York and London, First Edition, 457 pp.

11. Hu, Z., Zhang, X., Liu, Z., Huo, K., Chu, P.K., Zhai, J., Jiang, L., 2014: Regulating water adhesion on superhydrophobic TiO_2 nanotube arrays. Advanced Functional Materials 24(40): 6381-6388.

12. Kasal, B., Anthony, R., 2004: Advances in situ evaluation of timber structures. Progress in Structural Engineering and Materials 6: 94–103.

13. Maddox, J., Kuklík, P., 2016: Non-destructive testing methods for determining material characteristic values of historic timber structures. In: FORDE CARILLION, MC, ed. Structural Faults & Repair - 2016. 16th International Conference and Exhibition. Edinburgh, 17.05.2016 - 19.05.2016. Edinburgh: Engineering Technics Press Edinburgh.

14. Minabe, T., Tryk, D.A., Sawunyama, P., Kikuchi, Y., Hashimoto, K., Fujishima, A., 2000: TiO_2-mediated photodegradation of liquid and solid organic compounds. Journal of Photochemistry and Photobiology A: Chemistry 137(1): 53-62.

15. Nikolic M., Lawther J.M., Sanadi A.R., 2015: Use of nanofillers in wood coatings: a scientific review. Journal of Coatings Technology and Research 12: 445-61.

16. Paola, A.D., García-López, E., Marcì, G., Palmisano, L., 2012: A survey of photocatalytic materials for environmental remediation. Journal of hazardous materials 211: 3-29.

17. Prošek, Z., Králík, V., Topič, J., Nežerka, V., Indrová, K., Tesárek, P., 2015: A description of the microstructure and the micromechanical properties of spruce wood. Acta Polytechnica 55(1): 39-49.

18. Rijckaert, V., Stevens, M., Van Acker, J., de Meijer, M., Militz, H., 2001: Quantitative assessment of the penetration of water-borne and solvent-borne wood coating in Scots pine sapwood. European Journal of Wood and Wood Products 59(4): 278-287.

19. Rowell, R.M., 2005: Handbook of wood chemistry and wood composites. Taylor & Francis. London, 487 pp.

20. Santamarina, J.C., 2003: Soil behavior at the microscale: Particle Forces. Soil behavior and Soft Ground Construction. Pp 25-56.

21. Santos, T.P. , Cunha, R.L., Tabeling, P., Cejas, C.M., 2020: Colloidal particle deposition on microchannel walls, for attractive and repulsive surface potentials. Physical Chemistry Chemical Physics 30: 17236-17246.

22. Svora, P., Ecorchard, P., Pližingrová, E., Komárková, B., Pawełkowicz, S.S., Murafa, N., Maříková, M., Smržová, D., Wagner, B., Machálková, A., Bezdička, P., 2020: Influence of

inorganic bases on the structure of titanium dioxide-based microsheets. ACS omega 5(37): 23703-23717.

23. Šubrt, J., Pulišová, P., Boháček, J., Bezdička, P., Pližingrová, E., Volfová, L., Kupčík, J., 2014: Highly photoactive 2D titanium dioxide nanostructures prepared from lyophilized aqueous colloids of peroxo-polytitanic acid. Materials Research Bulletin 49: 405-12.

24. Thelandersson, S., Larsen, H., 2003: Timber Engineering. John Wiley & Sons. Chichester, 446 pp.

25. Velebil, L. , Zelený, R., Včelák, J., Dvořák, M., Kuklík, P., Terebesyová, M., Olbrich, M., 2016: Optical fibre sensors as a potential solution for monitoring wooden structures. In: WCTE 2016 CD-ROM Proceedings, Vienna.

PETR KUKLÍK*, ZDENĚK PROŠEK, ANNA GREGOROVÁ
CZECH TECHNICAL UNIVERSITY IN PRAGUE
UNIVERSITY CENTRE FOR ENERGY EFFICIENT BUILDINGS
TŘINECKÁ 1024, 273 43 BUŠTĚHRAD
CZECH REPUBLIC
*Corresponding author: kuklik@fsv.cvut.cz

CHARACTERIZATION OF ANATOMICAL, MORPHOLOGICAL, PHYSICAL AND CHEMICAL PROPERTIES OF KONAR (*ZIZIPHUS SPINA-CHRISTI*) WOOD

MOHAMMAD DAHMARDEH GHALEHNO, BABAK NOSRATI SHESHKAL,
FARHAD KOOL
UNIVERSITY OF ZABOL
IRAN

MIHA HUMAR
UNIVERSITY OF LJUBLJANA
SLOVENIA

MOHSEN BAHMANI
SHAHREKORD UNIVERSITY
IRAN

ABSTRACT

The goal of this research is to investigate some morphological (fibre length, fibre diameter, cell wall thickness, Runkel coefficient, flexibility coefficient, slenderness coefficient, rigidity coefficient, Luce's coefficient, solid coefficient), physical (dry wood density, volumetric shrinkage) and chemical (cellulose, hemicellulose, lignin, ash and acetone soluble extractives contents) composition of Konar (*Ziziphus spina-christi*) wood grown in Hormozgan province, Iran. For this purpose, three normal trees were selected randomly and a disk was cut from each one at breast height. Anatomical inspection revealed that the species was diffuse porous, with distinctive growth rings, simple preformation plate, with polygonal openings, and banded or diffuse-in aggregates parenchyma. The average values of wood dry density, fiber length, fiber diameter, cell wall thickness, Runkel coefficient, flexibility coefficient, felting coefficient, Luce's coefficient, solid coefficient, rigidity coefficient were 0.926, 52.1, 77.85, 0.57, 163 $\times 10^3$ μ^3 and 0.48. Cellulose, hemicellulose, lignin, acetone soluble, extractives, ash contents were 43.34, 19.98, 33.9, 6.42 and 2.78%, resp.

INTRODUCTION

Konar tree (*Ziziphus spina-christi*) is widely distributed in the Middle East and Iran southern provinces due to its compatibility with the unfavorable environmental conditions like dehydration, high environment temperature, pests and diseases. Konar tree is a deciduous hardwood species. Konar zone covers Africa to Middle East including Southern regions of Iran. Konar belongs to Rhamnaceae family which includes 70 genera and 1500 species of shrubs and small to medium-size trees. It is a drought hardy tree that is adapted to grow in water-stressed habitats (Gupta and Saxena 2011). Konar is widely cultivated for its fruit due to its medical features. Other applications of Konar trees are fodder for livestock, stock-proof hedge, living fence and timber. However, new applications of Konar species such as the production of activated carbon (Abshirini et al. 2019), production of cellulose nanocrystals (Hindi 2017), production of silver nanoparticles (Alajmi et al. 2019), and production of surfactants to increase the extraction of oil wells (Shahri et al. 2012) have also been reported. Konar wood is very hard and resistant to termites (Lizardi-Mendozaet al. 2016). For this reason, it is a superior species for producing posts, roofing beams, tool handles, utensils, artistic woodwork, cabinet making, and windows in regions with high possibility of termite attack.

Forests sources in Iran have been recently diminished mainly due to aggressive harvest and unsustainable silvicultural practices (Bahmani et al. 2020, Nazari et al. 2020). For this reason, dry tolerant wood species like Konar have been recently gained much attention. Therefore, understanding the properties of drought-tolerant wood species in arid regions is necessary to optimize their usage as well as encourage forest owners to cultivate them. One of the industries consuming Konar wood in the southern regions of Iran is boat construction which is increasing the number of such boat construction companies at the moment. This led to increasing in the wood demand for this wood species. In addition to *Ziphus spina-christi,* wood species like *Prosopis spicigera*, *Tectona grandis*, and *Acacia nilotica* were also applied in the boat construction industry. Schirarend (1991) measured some anatomical properties of *Ziziphus jujube* and *Ziziphus mauritiana*. He reported that 28 and 10 vessels per square millimeter, 142 and 125 μm, vessel diameter and 352-410 μm, vessel length in *Ziziphus jujube* and *Ziziphus mauritiana*, respectively. The average value of fiber diameter in *Ziziphus jujube* and *Ziziphus mauritiana* were 1002 and 780 μm, respectively. Gupta and Saxena (2011) studied the wood microstructure of the Rhamnaceae family which is native to India. It was stated that the wood species in Rhamnaceae family are diffuse porous with distinct growth rings boundaries. It was reported that the mean value of vessel frequency, vessel diameter and vessel length, were 5-37 mm, 110-145 μm, 352-577 μm, resp. These values for the mean fiber length and fiber diameters were 903-1018 μm and 14-17 μm, resp. To our best knowledge, no studies have been conducted on the wood properties of Konar tree (*Ziziphus spina-christi*) in Iran. Considering the importance of Konar tree in preventing soil erosion and desertification, resistance to pests and drought as well as its wide distribution and application in different industries especially in the boat construction industry in the southern parts of Iran and Middle East, identifying and understanding the wood properties of Konar seems necessary. As *Ziziphus spina-christi* has

considerable potential, the goal of the present study is to investigate wood structural properties, fiber morphology, chemical and physical properties of this wood species.

MATERIAL AND METHODS

Study area and sampling

The study area is located between 54° 4' 34" N and 26° 53' 59" E in the Dahi Kand region of Hormozgan, Iran. The mean annual precipitation and temperature of the study area are 220 mm and 32°C, resp. Three 7-year old *Ziziphus spina-christi* normal trees were selected randomly and a disk 3 cm in thickness, was cut from each one at breast height.

Wood anatomical parameters

Small blocks of about $5 \times 5 \times 20$ mm were cut from each disk. The wood was softened by boiling to remove extra air, followed by immersion in distilled water. 20-30 μm thin transverse, radial and tangential sections were cut with a sliding microtome, bleached, stained and rinsed in an ethanol series (50, 95 and 100%) until all traces of excess stain in an ethanol series (50, 95 and 100%) until all traces of excess stain and water were removed. After bleaching, staining and dehydrating, sections were mounted in Canada balsam for subsequent microscopic examination using optic microscope. The description of the anatomical characters followed the IAWA "List of Microscopic Features for Hardwood Identification" (IAWA 1989).

Biometric properties

Separation of individual wood fibre was performed using Franklin (1964) method through which a wood specimens with the dimension of $15 \times 10 \times 2$ mm were saturated in a mixture (1:1) of acetic acid and oxygenized water in test tubes. Afterwards, the specimens were kept in an oven with 65 ± 3°C for 48 h. After maceration, the specimens were washed (2-3 times) in distilled water and then immersed with distilled water. In the next step, shacked and the biometric parameters, as fiber length (*L*), fiber diameter (*D*), cell wall thickness (*W*), lumen diameter (*d*) were evaluated by light microscopic. From each slice, at least 50 fibers were used for the measurements. From the data, the average morphological properties (fiber indices) were then calculated according to the following equations (Saikia et al. 1997):

Runkel coefficient:　　　2W/d　　　　　　　　　　　　　　　　(1)

Flexibility coefficient:　d/100D　　　　　　　　　　　　　　(2)

Slenderness coefficient:　FL/FD　　　　　　　　　　　　　　(3)

Rigidity coefficient:　　2W/D　　　　　　　　　　　　　　　(4)

Luce's coefficient:　　　D^2-d^2/D^2+d^2　　　　　　　　　　　　(5)

Solid coefficient:　　　　(D^2-d^2) ×L　　　　　　　　　　　(6)

Physical properties

Wood samples were prepared from the disks cut from Konar stem. In detail, samples with dimensions of 30 × 20 × 20 mm were prepared in accordance with ISO 13061-14 (2016) for the investigation of oven-dry density and volumetric shrinkage and volumetric swelling. Sample dimensions were measured in green (saturated) and oven-dry condition with a slide caliper; oven-dry mass was determined with an electric balance to an accuracy of 0.01 g. Volumetric swelling was calculated using the dimensional change from the green to oven-dry condition. The physical properties were calculated according to the following equations:

$$D_0 = P_0 / V_0 \qquad (\text{g}\cdot\text{cm}^{-3}) \tag{7}$$

$$\alpha_v = (V_s - V_0)/ V_0 \qquad (\%) \tag{8}$$

where: D_0 - oven dry density (g·cm^{-3}), α_v - volumetric swelling (%), V_s - volume in the saturate state (cm^3), V_0 - volume in state of oven-dry (cm^3), P_0 - weight in state of oven dry (g).

Chemical properties

The chemical constitutes were performed according to the TAPPI test methods: Cellulose (T 257 cm-85), the lignin (T 222 om-98), ash (T 211 om-93), and solubility alcohol-acetone (T 204 cm-88). The cellulose content of oak wood was determined according to the nitric acid method (Rowell et al. 1997). All measurements were repeated three times, and the mean value was used.

RESULTS AND DISCUSSION

Wood anatomy

Microscopic analysis of the axial planes clearly indicates that wood is diffuse-porous, with distinctive growth rings (Fig. 1). Vessels are located next to radial rows. Mean diameter of the vessel is 124.5 μm. Vessel diameter for the majority of the European wood species is much higher, namely ranging from 100 μm (beech) to 400 μm (oak), what classifies these vessels as extremely large (Wagenfuhr 2007) and about equal to those of *Ziziphus jujube* and *Ziziphus mauritiana* with 142 and 125 μm, respectively (Schirarend 1991). Pores of Konar wood are generally occurred as solitary; thus, we classify them as solitary pores, with 5 to 6 pores per mm (Fig. 1). Vessels are connected through simple preformation plate, with polygonal openings. There are no helical thickenings observed on the cell wall. Tangential vessels are much thinner than axial ones. The diameter of vessel lumina in the tangential direction is 124.5 μm. Besides vessels, there are fibre cells present as well, what classifies Konar wood as wood consisting of fibre with tracheid to minutely bordered pits (Fig. 2). Axial parenchyma is present as well. It is banded or diffuse-in aggregates, include 4-8 cells in the tangential direction (Fig. 3). Distribution of rays is 4 to 5 rays per tangential mm. Average ray high was measured 402 μm. In procumbent ray cells, prismatic crystals were observed.
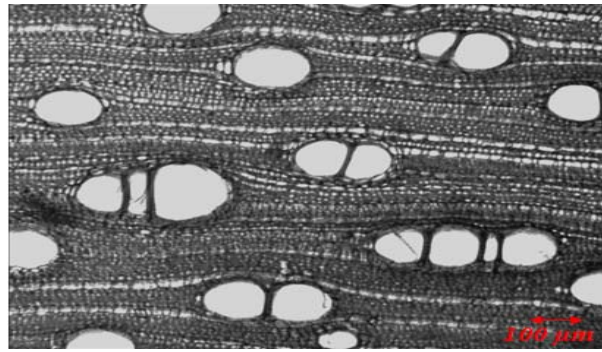
Fig. 1: Cross-section of Konar wood.
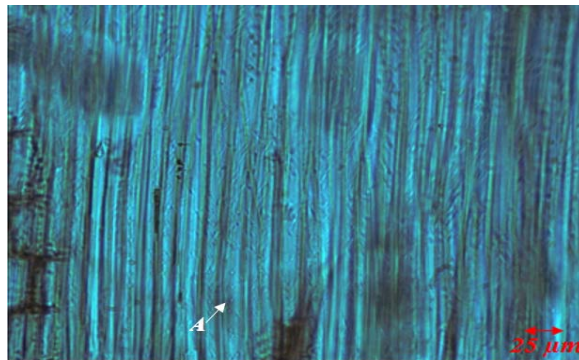
Fig. 2: Radial section of Konar wood: fiber- tracheid.
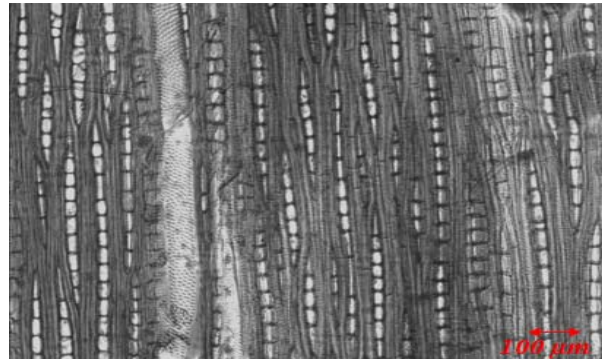
Fig. 3: Tangential section of Konar wood.

Biometric properties

The average fiber length, fiber diameter, lumen diameter and cell wall thickness were measured 1109, 14.24, 7.43, 3.44 µm, resp. Fibers are classified into three groups (IAWA 1989): *(1)* short fibers with a length less 900 µm; *(2)* fibers of medium length between 900-1900 µm including Konar wood with an average fiber length of 1570 µm and fibers longer than 1900 µm.

Morphological properties

In addition to classic wood anatomy measurements, detailed biometric properties were determined according to Franklin method (Franklin 1954, Mehdikhani et al. 2019) to assess Konar wood fibers' suitability the production of lignocellulosic composites.

Runkel ratio is directly affected by cell wall thickness. Runkel ratios higher than one are characteristic thick-walled fibres with stiffer, lesser flexibility and difficult to collapsing properties, creating bulky structures with the lower bonded area and higher porosity (Ezeibekwe et al. 2009). The Runkel ratio lower than one describes fibres with flexibility and wet plasticity and a greater conformability degree. Thus, due to more flexibility, quickly collapsing and forming a structure with the larger bonded area and good strength properties, the fibres Runkel ratios lesser than one is suitable for fibrous networking and bonding (Mehdikhani et al. 2019). The Runkel ratio of Konar wood was 0.926, being very close to value 1. Another factor describing the properties of the fibre is Luce factor. This parameter is derived from fiber diameter and lumen diameter, directly affect fibrous sheet density and pulp digestibility. Fibers with low Luce's shape factor values give better mechanical strength of its pure and composite structures (Kaur and Dutt 2013). Luce factor for Konar wood was 0.57, being in the range of the Eucalyptus species (Ohshima et al. 2005). Solid factor directly affect fibrous sheet density. Similar to Luce's shape factor, species with low solid factor values give better strength of paper. At Konar wood fibres Solid factor of 163×10^3 μ^3 was determined. Rigidity coefficient is also recognized as wall coverage ratio or wall proportion: This parameter is an indicator for bending resistance and is related to fiber flexibility. At Konar wood rigidity factor of 0.48 was determined. Fiber diameter and wall thickness defines the fiber flexibility that can be expressed as flexibility coefficient. At Konar wood this value of 52.1 was measured. Felting ratio is also known as slenderness coefficient. At Konar wood value of 77.85 was determined. This indicator is related positively to pulping yield and negatively to digestibility.

Physical properties

Tab. 1 shows the results for oven-dry density and volumetric swelling for Konar wood. Density of the Konar wood was 0.61 $g^.cm^{-3}$, between density of European beech (0.8 $g^.cm^{-3}$) and Elm (0.56 $g^.cm^{-3}$). Volume and other swelling are rather high (16.1%). For example volume swelling is in the range of the European beech (14-21%) (Wagenfuhr 2007). This is an important limitations of the use of respective wood species in oscillating climate.

Tab. 1: The average physical properties of Konar wood (according to TAPPI test methods).

Wood properties	Dry density (g.cm⁻³)	Longitudinal swelling (%)	Tangential swelling (%)	Radial swelling (%)	Volumetric swelling (%)
Average	0.61	0.47	8.3	6.7	16.1
Standard deviation	0.03	0.06	0.52	0.46	0.83

Chemical properties

Chemical composition of Konar wood can be resolved from Tab. 2. Ash content of 2.78% was measured. Ash content is wood species from temperate zones is much lower, ranging between 0.17% (European beech) and 0.51% (oak) (Voicea et al. 2013). Respective values of Konar wood are closer to ash content in the bark (Tsuchiya et al. 2010). In addition to ash content, Konar wood is characterized by high content of lipophilic extractives (6.42%).

Tab. 2: The average chemical composition of Konar wood (according to TAPPI test methods).

Wood properties	Cellulose (%)	Hemicellulose (%)	Lignin (%)	Acetone soluble extractives (%)	Ash (%)
Average	43.34	19.98	33.90	6.42	2.78
Standard deviation	1.74	-	1.35	0.92	0.26

This value is higher than average. For example, *Eucalyptus pellita* contains only 0.25% of lipophilic extractives (Arisandi et al. 2020), while *Pinus pinea* can contain up to 15% of solvent soluble extractives (De Angelis et al. 2018). Cellulose content in Konar wood was 43.34%. This value is in the range typical for wood from temperate zones, that ranges between 39% (poplar) and 49% spruce. For example, cellulose content is some other wood fibers is much higher, namely 64% (hemp) or 76% (flex) (Madsen and Gamstedt 2013). Lignin content was in the range typical for hardwood species as well (33.9%).

CONCLUSIONS

Konar (*Ziziphus spina-christi*) wood grown in Iran is a diffuse porous hardwood with a semi-heavy density. Its anatomical properties do not differ meaningfully from congeneric. Ash content is lower than that of the wood species from temperate zones but lignin content is in the range of other hardwoods. Konar fibers would be classified as elastic, thin wall fiber resources with felting factor similar to softwoods (70-90). Konar fiber can provide suitable formation and compactness with good bonding ability in 3D cellulosic structures (paper and composites). It is suggested that in further investigations on the natural durability of Konar wood against fungi, insects, and termites.

ACKNOWLEDGEMENT

REFERENCES

1. Abshirini, Y., Foroutan, R., Esmaeili, H., 2019: Cr (VI) removal from aqueous solution using activated carbon prepared from *Ziziphus spina–christi* leaf. Materials Research Express 6(4): 045607.
2. Alajmi, R.A., Al-Megrin, W.A., Metwally, D., Al-Subaie, H., Altamrah, N., Barakat, A.M., Abdel Moneim, A.E., Al-Otaibi, T.T. and El-Khadragy, M., 2019: Anti-toxoplasma activity of silver nanoparticles green synthesized with *Phoenix dactylifera* and *Ziziphus spina-christi* extracts which inhibits inflammation through liver regulation of cytokines in Balb/c mice. Bioscience reports 39(5).
3. Arisandi, R., Ashitani, T., Takahashi, K., Marsoem, S.N., Lukmandaru, G., 2020: Lipophilic extractives of the wood and bark from *Eucalyptus pellita* F. Muell grown in Merauke, Indonesia. Journal of Wood Chemistry and Technology 40(2): 146-154.

4. Bahmani, M., Fathi, L., Koch, G., Kool, F., Aghajani, H., Humar, M., 2020: Heartwood and sapwood features of *Sorbus torminalis* grown in Iranian forests. Wood Research 65: 195-204.

5. De Angelis, M., Romagnoli, M., Vek, V., Poljanšek, I., Oven, P., Thaler, N., Lesar, B., Kržišnik, D. and Humar, M., 2018: Chemical composition and resistance of Italian stone pine (*Pinus pinea* L.) wood against fungal decay and wetting. Industrial crops and products 117: 187-196.

6. Ezeibekwe, I.O., Okeke, S.E., Unamba, C.I.N., Ohaeri, J.C., 2009: An investigation into the potentials of *Dactyladenia bacteri*, *Dialum guineense*, and *Anthonota macrophylia* for paper pulp production. Report and Opinion 1(4): 18-25.

7. Franklin, G.L., 1945: Preparation of thin sections of synthetic resins and wood-resin composites, and a new macerating method for wood. Nature 155(51): 3924.

8. Gupta, S., Saxena, V., 2011: Wood microstructure of ligneous species of Rhamnaceae from India. Journal of Tropical Forest Science 23(3): 239-251.

9. Hindi, S.S., 2017: Nanocrystalline cellulose: synthesis from pruning waste of *Zizyphus spina christi* and characterization. Nanoscience and Nanotechnology 4(3): 106-114.

10. IAWA Committee, 1989: IAWA list of microscopic features for hardwood identification by an IAWA Committee. E.A. Wheeler, P. Baas, P.E. Gasson (eds.) IAWA Bull 10(3): 219-332.

11. ISO 13061-14, 2016: Physical and mechanical properties of wood. Test methods for small clear wood specimens. Part 14: Determination of volumetric shrinkage.

12. Kaur, H., Dutt, D., 2013: Anatomical, morphological and chemical characterization of lignocellulose by-products of lemon and sofia grasses obtained after recuperation of essential oils by steam distillation. Cellulose Chemistry and Technology 47(1-2): 83-94.

13. Lizardi-Mendoza, J., Monal, W.A., Valencia, F.G., 2016: Chitosan in the preservation of agricultural commodities. Academic Press 3: 31.

14. Madsen, B., Gamstedt, E.K., 2013: Wood versus plant fibers: similarities and differences in composite applications. Advances in Materials Science and Engineering 2013: 1-14.

15. Mehdikhani, H., Torshizi, H.J., Ghalehno, M.D., 2019: Deeper insight into the morphological features of sunflower stalk as Biorefining criteria for sustainable production. Nordic Pulp & Paper Research Journal 34(3): 250-263.

16. Nazari, N., Bahmani, M., Kahyani, S., Humar, M., Koch, G., 2020. Geographic variations of the wood density and fiber dimensions of the Persian oak wood. Forests 11(9): 1003.

17. Rowell, R.M., Young, R.A., Rowell, J.K., 1997: Paper and composites from agro-based resource. CRC Lewis publisher, Boca Raton, FL, USA. 446 pp.

18. Saikia, C.N., Goswami, T., Ali, F., 1997: Evaluation of pulp and paper making characteristics of certain fast growing plants. Wood Science and Technology 31(6): 467-475.

19. Schirarend, C., 1991: The systematic wood anatomy of the *Rhamnaceae juss* (Rhamnales). I. Tribe zizipheae. IAWA journal 12(4): 359-388.

20. Shahri, M.P., Shadizadeh, S.R., Jamialahmadi, M., 2012: Applicability test of new surfactant produced from *Zizyphus spina-christi* leaves for enhanced oil recovery in carbonate reservoirs. Journal of the Japan Petroleum Institute 55(1): 27-32.
21. TAPPI Test Method T 204 om-88, 1988: Standard test methods for solvent extractives of wood and pulp.
22. TAPPI Test Method T 211 om 02, 2002: Standard test methods for ash in wood, pulp, paper, and paperboard.
23. TAPPI Test Method T 222 om-98, 1998: Standard test methods for acid-insoluble lignin in wood and pulp.
24. TAPPI Test Method T 257 cm-85, 1988: Standard test methods for sampling and preparing wood for analysis.
25. Tsuchiya, Y., Shimogaki, H., Abe, H., Kagawa, A., 2010: Inorganic elements in typical Japanese trees for woody biomass fuel. Journal of Wood Science 56(1): 53-63.
26. Voicea, I., Danciu, A., Matache, M., Voicu, G., Vladut, V., 2013: Biomass and the thermo-physical-chemical properties of this related to the compaction process. Annals of the Faculty of Engineering Hunedoara 11(1): 59.

MOHAMMAD DAHMARDEH GHALEHNO*, BABAK NOSRATI SHESHKAL,
FARHAD KOOL
UNIVERSITY OF ZABOL
DEPARTMENT OF WOOD AND PAPER SCIENCES AND TECHNOLOGY
ZABOL 98615538
IRAN
*Corresponding author: mmdahmardeh@uoz.ac.ir

MIHA HUMAR
UNIVERSITY OF LJUBLJANA
DEPARTMENT OF WOOD SCIENCE
BIOTECHNICAL FACULTY
1501 LJUBLJANA
SLOVENIA

MOHSEN BAHMANI*
SHAHREKORD UNIVERSITY
DEPARTMENT OF NATURAL RESOURCES AND EARTH SCIENCE
SHAHREKORD 64165478
IRAN
*Corresponding author: mohsen.bahmani@sku.ac.ir

SEGMENT OF WALL PANEL FOR TIMBER STRUCTURES UNDER VERTICAL LOAD

JIŘÍ CELLER, JAKUB DOLEJŠ
CZECH TECHNICAL UNIVERSITY IN PRAGUE
CZECH REPUBLIC

ABSTRACT

The subject of this paper is an experimental and numerical analysis of the stability of the wall panels with one-side board sheathing for timber structures. The reinforcement of the panel is provided using glued timber composite I-shaped element consisting of a web made of a wood-based desk embedded into flanges of solid timber. The mechanism of the behaviour of these panels, mode of the failure and reliable procedure to determine the buckling load-bearing capacity not been fully explored so far. This work describes the behaviour of the wall panel under vertical load and the method of failure using experimental and numerical analysis. The reduction coefficient k_J was determined, which can be used for a simple calculation of the buckling capacity of a wall panel.

KEYWORDS: Timber structures, wall panel, I-stud, one-sided board sheathing, stability, experiments.

INTRODUCTION

A modern and responsible lifestyle focused on sustainable production, higher living comfort, low environmental impact and high quality of production generally brings new and new challenges in the field of civil engineering, to which it is necessary to adequately respond professionally. In the field of fire resistance of timber structures, for example, the question arises of the residual load-bearing capacity of a wall timber panel, the inner load-bearing layer of which has been significantly damaged by fire. The research of ribbed panels with one-sided cladding with a wood-based board took place in recent years at the Faculty of Civil Engineering of the Czech Technical University in Prague.

The light timber frames are one of the most used construction systems for timber structures. Research and experiments of wall panels using studs with a classical rectangular cross-section were performed in history many times. The reinforcing load-bearing capacity of

the walls was determined using advanced methods several times in the past (Brandejs 2006, Girhammar and Källsner 2009, Källsner and Girhammar 2009). Another problem that was solved is e.g. anchoring methods and its stiffness of wall panels (Jára 2018, Tomasi and Sartori 2013) and sheathing-to-framing connections (Sartori and Tomasi 2013, Premrov and Kuhta 2009). Furthermore, experiments of wall panels were performed to show the effect of openings on the overall load-bearing capacity of these elements (Šilih and Premrov 2010, Šilih and Premrov 2011). The load-bearing element in wall panels is often a timber stud with a rectangular cross-section, its behaviour during loading and various failure modes depending on the load is described in (Bäckström and Kliger 2008, Bäckström et al. 2009).

To improve the thermal technical properties of the wall panel, it is possible to replace the classic stud with a rectangular cross-section with a stud with an I-shaped cross-section, or I-stud. Elements with an I-shaped cross-section are now commonly used for beams, i.e. an element in a horizontal position, or I-beams (Racher et al. 2006, Jára et al. 2014, 2015). For I-beams, it is sometimes necessary to make round, square and rectangular openings for installations. The influence of holes on the load-bearing capacity of the beam has been presented in many publications (Zhu et al. 2005, Guan and Zhu 2009, Jára et al. 2015, Afzal et al. 2006). Another possibility of making holes in the web of I-beams represent so-called castellated timber I-joists (Harte and Baylor 2011, Baylor and Harte 2013).

Elements with an I-shaped cross-section are also commonly used in wall panels with double-sided sheathing. I-studs are prone to loss of stability by deviation (buckling) in the plane of the wall. The stability of these panels is ensured by double-sided board sheathing. Stability is not ensured, when one-side sheathing burns out during fire or sheathing is not made from a load-bearing material. The aim of this work is to clarify the behaviour of wall panels with a one-sided board sheathing and with an I-shaped cross-section consisting of a web made of a wood-based desk embedded into flanges of solid timber. The sheathing-to-framing connections were performed using steel staples. The choice of the I-stud was performed with the current requirements for heat-technical properties of exterior perimeter walls. It was especially crucial to achieving the values of the coefficient of heat transfer U ($W^.m^{-2}K^{-1}$) across the walls that correspond to normative values for low-energy and passive houses according to ČSN 73 0540-2 (2012).

MATERIAL AND METHODS

The buckling capacity of the wall panel section was determined by experimental and numerical analyses. Before performing experiments, preliminary analytical calculation and numerical model were created for the purpose of the estimation of the behaviour of the wall panels. The particular steps which have been performed before the experiment including the calculation of the buckling capacity in accordance with (EN 1995-1-1 2004, EN 1999-1-1 2007) were presented in (Celler J. et al. 2016).

Static tests on wall panels with an I-shaped cross-section stiffener made of the wood-glued composite element and one-sided board sheathing were designed and performed within the experimental part of the work. A detailed description of the preparation of the experiment,

execution of the experiment and evaluation of the results were presented in (Celler J. et al. 2019). For completeness of this paper, basic information about the samples for the experiment is also presented. The test set up, the dimensions of each component and the whole sample and method of load are shown in Fig. 1.
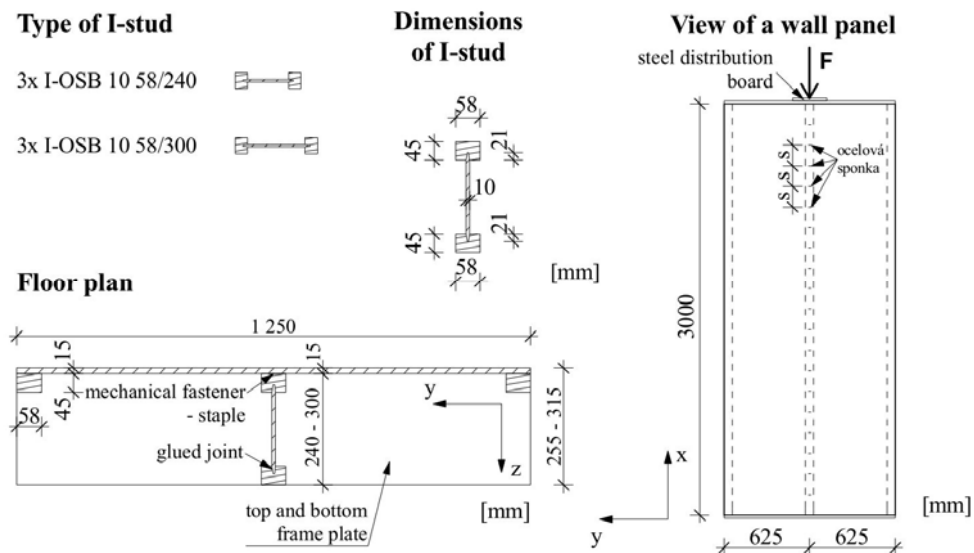

Fig. 1: The test set up for a series of experiments of the wall panel and method of load.

The dimensions of the wall panel were adapted to the real construction. The dimensions of the wall panels are 1250 × 3000 mm. 6 samples of the wall panel section were tested: I-studs with a cross-sectional height of 240 mm (3 samples) and 300 mm (3 samples) were used. The wall panel was placed at the test area gate, fastened with textile straps and loaded (Fig. 2, on the left), the deformed wall panel is shown in Fig. 2 (on the right). The load was applied to the I-stud through the upper frame plate made from the OSB board and the steel distribution board.

Fig. 2: Wall panel placed to the test area: axonometry and front view (on the left), deformed structure: buckling of the free flange of I-stud and deflection of the entire I-stud in the plane of the wall (on the right).

The results of the experiment corresponded to the assumptions from the preliminary analytical calculation and numerical model results.

After performing the experiments, the wall panels were cut and their parts used for material tests and staple joint tests. The material tests were performed for wood and OSB boards. The description of individual experiments and the results of material tests were presented in (Celler J. et al. 2019). The results of material tests were compared with the results obtained in the literature (Dolejš 1997, Pošta 2015).

RESULTS AND DISCUSSION

An important part of the entire wall panel is the connection between the held timber flange and the sheathing from the OSB board. This connection is made using steel staples. In the experimental part, the load-bearing capacity of the staple joint for cutting and pulling out was determined.

Shear capacity of staples: four test specimens were prepared from timber prisms and OSB boards, which were cut from wall panels. The dimensions of the individual components and the whole sample are in Fig. 3.
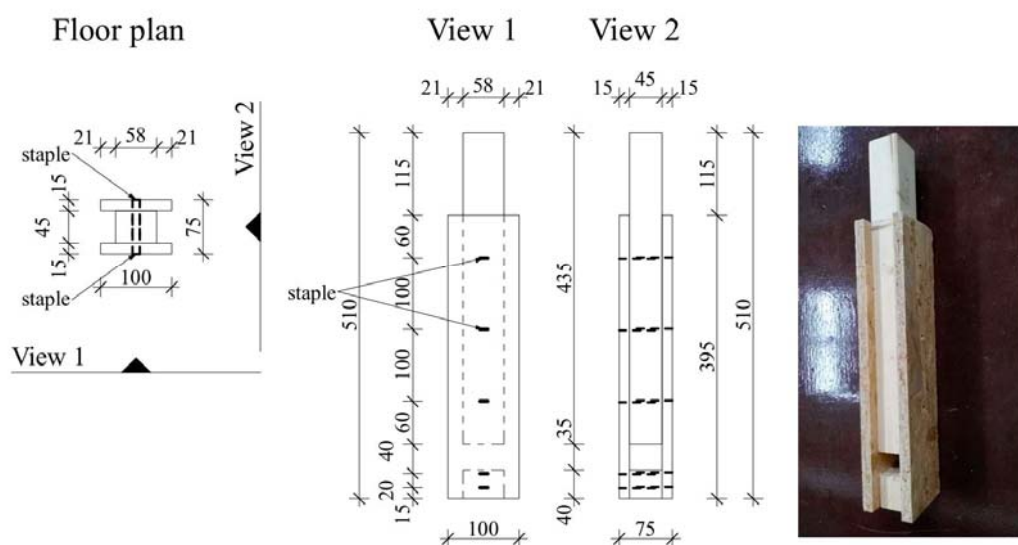

Fig. 3: Dimensions and arrangement of the test specimen for performing staple joints in shear.

The average value of the maximum applied force is 5.71 kN at a displacement of 6.75 mm. For the validation of the numerical model, the stiffness of the staple joint in the shear „$K_{s,exp}$" is determined from the performed experiments as the average value of the stiffness of individual test specimens. The average value of the stiffness of the staple joint in the shear „$K_{s,exp,\varnothing}$" is 1241 N·mm^{-1}.

Axial capacity of staples: six test specimens were prepared from a timber prism and OSB board, which were cut from the wall panels. Connection of prism and OSB board using one steel staple. The dimensions of the individual components and the whole sample are in Fig. 4.
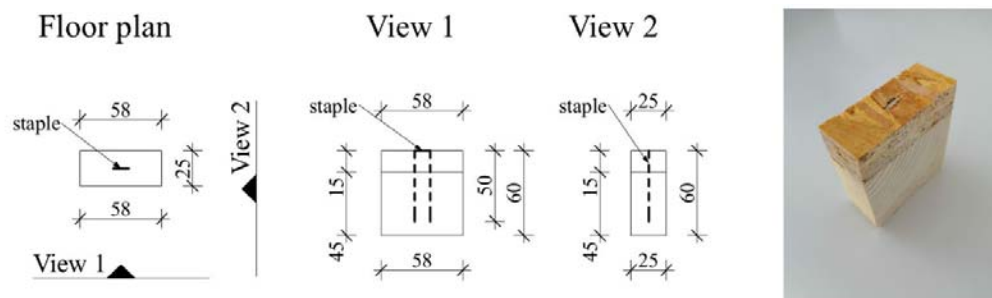
Fig. 4: Dimensions and arrangement of the test specimen for performing the staple joint to pull out the staple.

The average value of the maximum applied force is 361.6 N at a displacement of 0.85 mm. For the validation of the numerical model, the stiffness of the staple joint for extraction „$K_{v,exp}$" is determined from the performed experiments as the average value of the stiffness of individual test specimens. The average value of the stiffness of the staple joint for pulling out „$K_{v,exp,ø}$" is 807 N·mm^{-1}.

Furthermore, a 3D numerical model of a section of a wall panel with a stiffener made of a wood-glued composite element with an I-shaped cross-section and one-sided board sheathing was created within the numerical part of this work. For numerical analysis, knowledge about modelling the timber according to (Hataj 2019, Celler V. 2020, Mikolášek 2012).

Based on preliminary calculations and models, the static calculation program SCIA Engineer working with the finite element method was chosen for the resulting 3D numerical model, which in the current version contains all the necessary tools for numerical analysis, taking into account nonlinearities of all kinds. The model was modified and validated based on performed wall panel experiments, staple joint experiments and material tests. The dimensions, arrangement and material design of the individual elements of the wall panel in the 3D numerical model are the same as in the wall panel assembled for the experiment. The 3D numerical model and dimensions of the individual components are shown in Fig. 5.
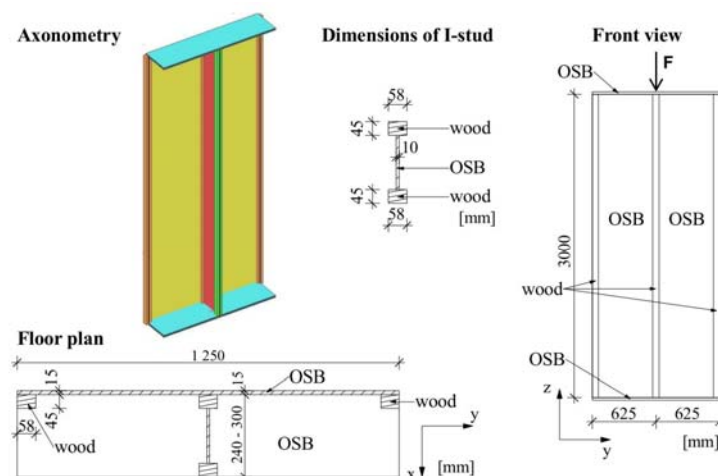

Fig. 5: 2D-elements numerical model: axonometry (on the left), dimensions of the model and individual components (bottom, right).

The 3D model is created using slab-wall elements modelled using the centerline and thickness of the element. Boundary conditions corresponding to the performed experiment were introduced in the model. The semi-rigid connection between the flange of the I-stud and the sheathing is created using an internal joint on the edge of the surface. The individual stiffnesses of the joint are entered as nonlinear using a load-deflection diagram of the dependence of the applied force on the displacement according to the performed experiments. Geometric imperfection - the initial curvature of the free flange of the I-stud and the side timber prisms was introduced into the model using a horizontal line load. A mesh with the size of the elements of a finite element mesh measuring 30 x 30 mm was created on the whole model. The load was considered in several ways. Finally, the line load to the centerline of the flanges and the web of the I-stud was considered for the numerical model. For the analysis of the structure, a nonlinear calculation was performed, taking into account the initial imperfections of the structure using the stability calculation. A modified Newton-Raphson method was chosen for the nonlinear calculation, which is sufficiently accurate and fast for the given type of model.

The deformed structure was drawn for individual nonlinear combinations. For the I-stud with a cross-sectional height of 300 mm (hereinafter I-stud 300), deformed structures were drawn for loads of approximately 30%, 70% and 100% of the maximum applied force (Fig. 6). From the beginning of the loading, the free flange of the I-stud deviates and at the same time, the sheathing is deformed, which corresponds to the experiment. As the load increases, the free flange of the I-stud, including the web, becomes more significantly deformed, which again corresponds to the experiment, where the dominant deformations occurred on the free flange of the I-stud.
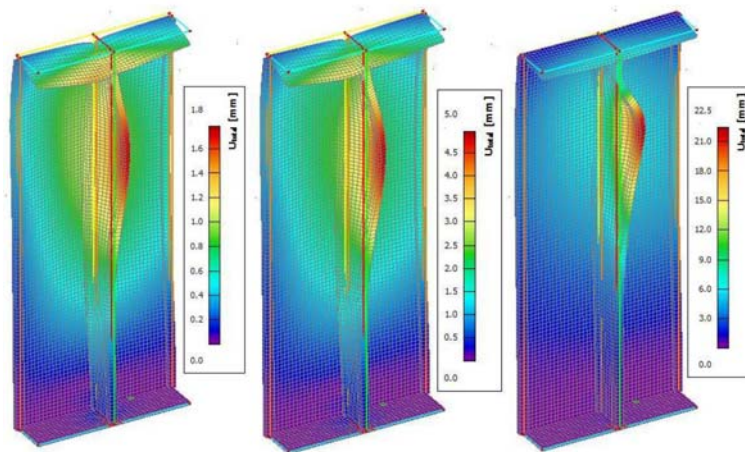
Fig. 6: I-stud 300 - deformed structure for nonlinear calculation, percentage of maximum applied force: 30% (left), 70% (middle), 100% (right).

The results of the numerical model were compared with the experiment. The maximum displacement that occurred on the structure on the free flange of the I-stud was monitored. The dependence of the applied force on the maximum displacement in the numerical model and during the experiment is compared in Fig. 7.
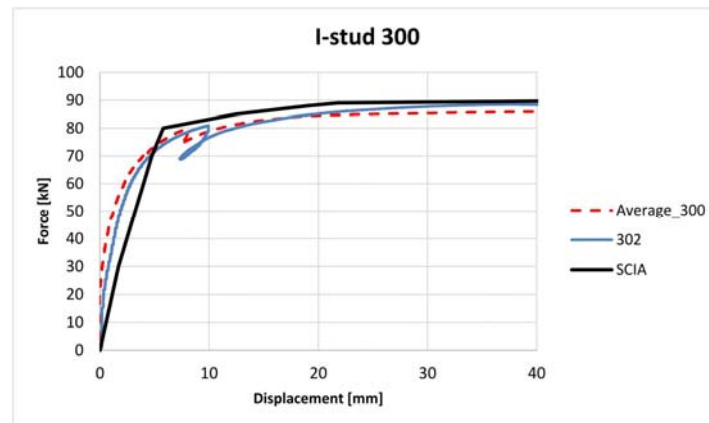
Fig. 7: Comparison of load-deflection diagrams from the experiment and a numerical model for an I-stud with a cross-sectional height of 300 mm.

The maximum force achieved for a test specimen of an I-stud 300 and a distance of steel staples of 100 mm is 88.5 kN. For the numerical model, the maximum force at the top of the load-deflection diagram is 89.0 kN.

To verify the correct setting of all parameters, a numerical experiment was also performed for a section of a wall panel with an I-stud with a cross-sectional height of 240 mm (hereinafter I-stud 240). The course of loading and deformation of the structure was similar to the wall panel with I-stud 300. The dependence of the applied force on the maximum displacement in the numerical model and during the experiment is compared in Fig. 8.
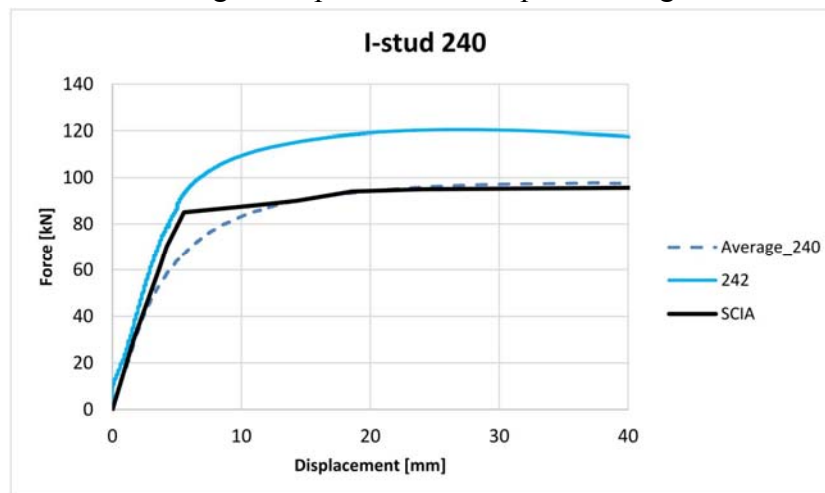
Fig. 8: Comparison of load-deflection diagrams from the experiment and a numerical model for an I-stud with a cross-sectional height of 240 mm.

For test specimens with an I-stud 240, an initial imperfection was measured with much greater variance than for an I-stud 300. In addition, for the I-stud test specimen with the smallest measured imperfection, the smallest distances of steel staples are used. For this reason, the result of the numerical analysis is compared with a test specimen 242, in which the distance of the steel staples is 100 mm, and also with an average load-deflection diagram for all test specimens of the I-stud 240.

The maximum average achieved force for I-stud test specimens with a cross-sectional height of 240 mm is 99.1 kN. In the numerical model, the maximum force at the top of the load-deflection diagram is 94.0 kN, which is 5.1% lower than the average force obtained in the experiment. Compared to sample 242, in which the maximum force reached is 120.4 kN, a larger difference can already be seen compared to the numerical model, which gives a safe reserve for possible larger initial imperfections (geometric and structural) of the I-stud.

When comparing the load-deflection diagrams for an I-stud 240 and an I-stud 300, it can be seen that for I-stud 240, the initial branch of the load-deflection diagram corresponds more to the experiment performed than for I-stud 300. This corresponds to much larger initial imperfections in the I-stud 240 samples than in the I-stud 300.

Based on the results of experiments and a numerical model, a parametric study was prepared. At the beginning of the parametric study, the load-bearing capacity of the wall panel section with dimensional modifications for the tested I-stud cross-sectional heights was determined. Based on the results of the parametric study, the analytical calculation was validated and verified.

From the preliminary analytical calculation considered for several possible ways of deflection of the cross-section of the wall panel performed by I-stud with one-sided board sheathing, the load-bearing capacities were calculated with a large variance of values. None of these values accurately describes the actual state of failure of the wall panel, described in detail in (Celler J. et al. 2016). For this reason, it is necessary to modify the analytical calculation so that the results correspond to the performed experiments and numerical analysis.

First, a numerical analysis was performed for several selected wall panel heights that are used in common construction practice.

Subsequently, the reduction coefficient „k_J" of the total load-bearing capacity of the wall panel section was determined, taking into account the cross-sectional height of the I-stud according to Eq. 1. The reduction factor was determined by back analysis of the analytical calculation and the results of the numerical analysis. The reduction factor was determined for the method of analytical calculation of the flat-plate buckling perpendicular to the "z" axis, i.e. the deviation of the cross-section in the wall plane.

$$k_J = 1.08 - h_2/1\text{m} \quad (\text{-}) \tag{1}$$

where: k_J - reduction factor (-), h_2 - cross-sectional height of the I-stud (m).

The load-bearing capacity of the segment of wall panel from the analytical calculation according to Eq. 2 taking into account the reduction factor „k_J" is plotted in a graph, in which the dependence of load-bearing capacity of the wall panel cross-section and the panel height for I-stud 240 and 300 are plotted (Fig. 9).

$$N_{c,z} = k_J \cdot k_{c,z} \cdot A' \cdot f_{f,c,0,d} \quad (\text{-}) \tag{2}$$

where: k_J - reduction factor (-), $k_{c,z}$ - buckling coefficient for deflection of the wall cross-section perpendicular to the "z" axis, ie in the plane of the wall (-), $A´$ - effective cross-sectional area of the wall panel (mm^2), $f_{f,c,0,d}$ - design value of compressive strength parallel to the fibers of structural timber of strength class C24 (N$\cdot$mm^{-2}).
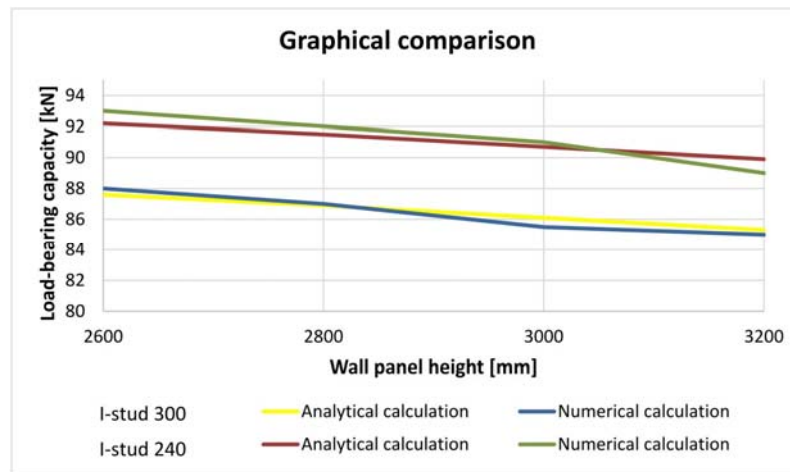

Fig. 9: Comparison of the load-bearing capacity of a wall panel from the analytical calculation and numerical analysis for an I-stud with a cross-sectional height of 240 mm and 300 mm with different wall panel heights.

Within the range of given wall panel heights, which are selected for use in common construction practice, it is clear from the previous results that it is sufficient to consider the linear course of the reduction factor.

The validity of the formula for calculating the load-bearing capacity of a segment of wall panel is for panel heights in the range of 2600 mm to 3200 mm, for the axial distance of I-studs 625 mm and a given type of I-stud with a cross-sectional height of 240 mm and 300 mm. The distance of the steel staples for connecting the OSB board cladding to the flange of the I-stud must not exceed 100 mm.

CONCLUSIONS

Based on experimental and numerical analysis, the mechanism of the behaviour of a section of a wall panel with a reinforcement formed by a stud with an I-shaped cross-section and a one-sided board sheathing under vertical load was clarified and described. Furthermore, a method of failure was described, which occurred either by deflection of the entire I-stud or a free flange of I-stud in the plane of the wall depending on the rigidity of the connection of the sheathing from OSB board to the I-stud flange using steel staples. Based on the analysis of the failure mode of individual test specimens, it is recommended to observe the maximum distance of steel staples given in the standard (DIN 1052: 2004-08 2004). It is 100 mm for the tested specimens.

The results of experiments on the section of wall panels show that the influence of the initial geometric imperfections is crucial for the load-bearing capacity on the buckling. In particular, the deflection of the free I-stud flange is one of the important factors influencing the result. The author recommends limiting the amplitude of this imperfection for similar configurations to 5 mm.

An analytical calculation of the load-bearing capacity of the wall panel was performed for various failure methods (deviation of the cross-section from the wall plane and in the wall plane, spatial buckling). Based on the results of the parametric study and back analysis of the analytical model, the reduction coefficient „k_j" was determined, which can be used for a simple calculation of the buckling capacity of a wall panel consisting of a load-bearing element with an I-shaped cross-section with one-sided board sheathing. In simple terms, the use of this reduction factor can be recommended for wall panels with a height in the range of 2600 to 3200 mm, for the axial distance of I-stud 625 mm and a given type of I-stud with across-sectional height of 240 mm and 300 mm. The distance of the staples in the connection of the OSB sheathing to the flange must not exceed 100 mm.

ACKNOWLEDGMENTS

REFERENCES

1. Afzal, T.M., Lai, S., Chui, Y.H., Pizarda, G., 2006: Experimental evaluation of wood I-joists with web holes. Forest Products Journal 56: 26-30.
2. Bäckström, M., Kliger, I.R., 2008: Timber-framed partition walls and their restraining effect on warp in built-in wall studs - A model for spring. Construction and Building Materials 23: 71-77.
3. Bäckström, M., Al-Emrani, M., Kliger, R., 2009: Timber-framed partition walls and their restrainig effect on warp in built-in wall studs - Model for twist. Construction and Building Materials 23: 3556-3563.
4. Baylor, G., Harte, A.M., 2013: Finite element modelling of castellated timber I-joists. Construction and Building Materials 47: 680-688.
5. Brandejs, R., 2006: Lateral stiffness of timber frame buildings. Prague: Czech Technical University, 112 pp.
6. Celler, J., Dolejš, J., Hlavatá, V., Jára, R., 2016: Hybrid panels with I-shaped stiffeners. In: Central Europe towards Sustainable Building 2016 - Innovations for Sustainable Future. Pp 1030-1035, GRADA Publishing, 1st edition, Prague.
7. Celler, J., Dolejš, J., Posta. J., Jara, R., 2019: Stability of wall panels with one-sided board sheathing for timber structures. In: Central Europe towards Sustainable Building (CESB19). Bristol: IOP Publishing Ltd. IOP Conference Series: Earth and Environmental Science, Prague, 8 pp.

8. Celler, V., 2020: Constitutive modeling of wood using microscopic analysis. Prague: Czech Technical University, 121 pp.

9. ČSN 73 0540-2, Z1, 2012: Thermal protection of buildings. Part 2: Requirements. Technical Standardization Center, CTU in Prague, Faculty of Civil Engineering (in Czech).

10. DIN 1052: 2004-08, 2004: Design of timber structures. General rules and rules for buildings.

11. Dolejš, J., 1997: Non-destructive methods for mechanical properties of timber. Czech Technical University, Prague, 100 pp.

12. EN 1995-1-1, 2004: Eurocode 5: Design of timber structures. Part 1-1: General. Common rules for buildings (CEN).

13. EN 1999-1-1, 2007: Eurocode 9: Design of aluminium structures. Part 1-1: General structural rules (CEN).

14. Girhammar, U.A., Källsner, B., 2009: Elasto-plastic model for analysis of influence of imperfections on stiffness of fully anchored light-frame timber shear walls. Engineering Structures 31(9): 2182-2193.

15. Guan, Z.W., Zhu, E.C., 2009: Finite element modelling of anisotropic elasto-plastic timber composite beams with openings. Engineering Structures 31(2): 394-403.

16. Harte, A.M., Baylor, G., 2011: Structural evaluation of castellated timber I-joists. Engineering Structures 33(12): 3748-3754.

17. Hataj, M., 2019: Numerical and analytical models of traditional carpentry joints. Czech Technical University, Prague, 136 pp.

18. Jára, R., Dolejš, J., Pošta, J., 2014: Glued timber beams I-OSB. Research report 228974. CTU in Prague, Faculty of Civil Engineering, Department of Steel and Timber Structures, Prague, 8 pp.

19. Jára, R., Pošta, J., Dolejš, J., 2015: Experimental analysis of timber beams ISOB. Research report 240953. Buštěhrad, CTU in Prague, UCEEB,19 pp.

20. Jára, R., Pošta, J., Dolejš, J., Pohl, K., 2015: Timber glued beam with I-shaped cross-section. Pp 176-178, Dřevostavby 2015, Volyně.

21. Jára, R., 2018: Anchoring of load-bearing sandwich panels of timber buildings. Czech Technical University, Prague, 90 pp.

22. Källsner, B., Girhammar, U.A., 2009: Plastic models for analysis of fully anchored light-frame timber shear walls. Engineering Structures 31(9): 2171-2181.

23. Mikolášek, D., 2012: Numerical modelling of selected timber joints constructions. Technical University of Ostrava, Ostrava,143 pp.

24. Pošta, J., 2015: Radiometry as a tool for non-destructive in-situ testing of timber elements. Czech Technical University, Prague, 116 pp.

25. Premrov, M., Kuhta, M., 2009: Influence of fasteners disposition on behaviour of timber-framed walls with single fibre–plaster sheathing boards. Construction and Building Materials 23(7): 2688-2693.

26. Racher, P., Bocquet, J.F., Bouchair, A., 2006: Effect of web stiffness on the bending behaviour of timber composite I-beams. Materials & Design 28: 844-849.

27. Sartori, T., Tomasi, R., 2013: Experimental investigation on sheathing-to-framing connections in wood shear walls. Engineering Structures 56: 2197-2205.
28. Šilih, E.K., Premrov, M., 2010: Analysis of timber-framed wall elements with openings. Construction and Building Materials 24: 1656-1663.
29. Šilih, E.K., Premrov, M., 2011: Influence of openings on horizontal load-carrying capacity of timber-frame wall elements with fibre-plaster sheathing boards. Advances in Engineering Software 43: 19-26.
30. Tomasi, R., Sartori, T., 2013: Mechanical behaviour of connections between wood framed shear walls and foundations under monotonic and cyclic load. Construction and Building Materials 44: 682-690.
31. Zhu, E.C., Guan, Z.W., Rodd, P.D., Pope, D.J., 2005: Finite element modelling of OSB webbed timber I-beams with interactions between openings. Advances in Engineering Software 36(11 − 12): 797-805.

JIŘÍ CELLER*, JAKUB DOLEJŠ
CZECH TECHNICAL UNIVERSITY IN PRAGUE
DEPARTMENT OF STEEL AND TIMBER STRUCTURES
THAKUROVA 7, 166 29 PRAHA 6 – DEJVICE
CZECH REPUBLIC
*Corresponding author: jiri.celler@fsv.cvut.cz

INVESTIGATION THE FIRE HAZARD OF PLYWOODS USING A CONE CALORIMETER

ZHIGANG WU, XUE DENG, LIFEN LI, LIPING YU, JIE CHEN
GUIZHOU UNIVERSITY
P.R. CHINA

BENGANG ZHANG, XUEDONG XI
UNIVERSITY OF LORRAINE
FRANCE

QIAOYAN ZHANG
ZHAZUO STATE-OWNED FOREST FARM OF GUIZHOU PROVINCE
P.R. CHINA

ABSTRACT

A high-efficiency fire retardant composition was prepared with dicyandiamide, phosphoric acid, boric acid, borax, urea and magnesium sulfate and it was used to process veneers which were then to prepare the plywood. Meanwhile, heat release and smoke release from combustion of plywood were tested by a cone calorimeter, including heat release rate, mass loss rate, CO yield, CO_2 yield and oxygen consumption. Results showed that the plywood with this fire retardant treatment had the better flame-retardant performance and smoke suppression effect as well as the stronger char-forming capability compared to plywood without fire retardant treatment. The average heat release rate, total heat release, average effective heat of combustion, total smoke release, CO yield and oxygen consumption of the plywood with fire retardant treatment were decreased by 63.72%, 91.94%, 53.70%, 76.81%, 84.99% and 91.86%, respectively. Moreover, the fire growth index of plywood treated by fire retardant was relatively low (3.454 $kW \cdot m^{-2} \cdot s^{-1}$) and it took longer time to reach the peak heat release rate, accompanied with slow fire spreading. The fire performance index was relatively high (0.136 $s \cdot m^2 \cdot kW^{-1}$) and it took longer time to be ignited, thus leaving a long time for escaping at fire accidents. The fire hazard of plywood with fire retardant treatment was low, and its safety level was high.

KEYWORDS: Fire retardant, plywood, combustion performance, fire hazard.

INTRODUCTION

With the intensifying shortage of wood resources around the whole world, developing wood-based panels has become an important way to solve this problem. Plywood is one of the most important products in wood-based panels. The output and demands for plywood which is a major material for indoor decoration are increasing significantly. However, plywood is a type of flammable material (Chung 2010, Nicholas and Siau 1973, Qu 2011). Once plywood is ignited, the fire will spread quickly and release a lot of heats to accelerate formation of indoor flashover. Under this circumstance, it is very difficult for the trapped to escape from the fire accident and for the firefighter to extinguish the fire, thus making it extremely easy to cause considerable economic losses and serious casualties. Therefore, fire retardant treatment of plywood has the important practical significance (Cao 2019, Yu et al. 2020, Cao et al. 2020).

Fire hazards are mainly determined by heat and smoke of combustion. Heat hazard refers to heat damages of life, properties and buildings by spreading heats from combustion to surrounding environment through radiation, convection and conduction. Smoke hazard refers to the damages caused by smoke and toxic gases to life and environment (Altun et al. 2010, Dong and Xu 2019). Fire hazard is essentially a comprehensive manifestation of potential heat risks and smoke risks of materials (Zhang et al. 2014, Xue et al. 2006, Son et al. 2012). Therefore, research and development on fire retardant treatment of plywood are focused on decreasing heat release and smoke release. Studies proved that nitrogen-series fire retardants and phosphorus-series fire retardants are characteristic of low price, small volatility and low toxicity. These two series of fire retardants have good flame retardation, but independent use of these fire retardants fails to achieve satisfying effect. Boron-series compounds are equipped with inflaming retardation, smoke suppression, anti-corrosion and mildew prevention and insect prevention (Chu et al. 2017, Zhang et al. 2016, Zhou et al. 2020, Kartal et al. 2007). Magnesium salt has good flame retardation and strong smoke suppression effect (Pan et al. 2014, Cao 2019). To endow good flame retardation for plywood, a composite fire retardant was prepared with dicyandiamide, phosphoric acid, boric acid, borax, urea and magnesium sulfate. Later, high-quality fire retardant was synthesized by supplementation and synergistic interaction of different components.

The cone calorimeter is recognized worldwide as one of the most acceptable fire testing apparatuses. Its testing results are not influenced by the types and complete combustion state of materials (Kim et al. 2012, Fateh et al. 2014). Moreover, cone calorimeter is highly related with large combustion experiment and it can test multi-aspect indexes related with combustion performances of materials comprehensively, including heat release rate, mass loss rate, oxygen content and CO_2 content. It is a very comprehensive combustion performance testing technique. In this study, cone calorimeter was applied to evaluate combustion performance of plywood processed by the prepared fire retardant and it will lay foundations for the improvement and application of the prepared fire retardant.

MATERIALS AND METHODS

Materials

Masson pine (*Pinus massoniana* Lamb.) with a size of 2200 mm (length) × 130 mm (width) × 2.5 mm (thickness), density 0.48 g·cm^{-3} and moisture content 10-14% was purchased from Rongjiang Guizhou, China. Dicyandiamide (with a purity of 98%), boric acid (with a purity of 99.5%), phosphoric acid (with a purity of 85%), borax (with a purity of 99.5%), urea (with a purity of 99%) and magnesium sulfate (with a purity of 99%) were purchased from Sinopharm Chemical Reagent Co., Ltd. (PR China). All other chemicals mentioned in this work were reagent grade. Powdery urea formaldehyde resin (C360), which was used by mixing with water (mass ratio of resin power to water was 100 : 80) and then adding 0.5% ammonium chloride for the preparation of plywoods, was purchased from Malaysia.

Preparation of fire retardant

Based on a large number of pre-experiments, the compositions of the flame retardant were 4% dicyandiamide, 6% phosphoric acid, 2.25% boric acid, 2.25% borax, 1% urea and 0.5% magnesium sulfate.

Treatments of *Pinus massoniana* veneers with fire retardant

Pinus massoniana veneers were dried in an oven (101-1AB electric blast drying oven) at 60°C ± 5°C until reaching constant weights and then moved out and stored in glass drier to cool down to the room temperature, weighted and then put in vacuum chamber. The fire retardant was poured into the chamber until 5 cm higher than the surface of the piles of wood samples under vacuum conditions (-0.09 MPa, 60 min). Next, the samples were taken out and the surface liquids of each wood sample was removed gently by a piece of filter paper. The wood samples were put in indoor environment for about one week and then dried in an oven at 90°C ± 5°C until the moisture content at 5% - 9%.

Preparation of five-layer plywood

The flame retardant veneers with a double-sided adhesive loading of 220 g·m^{-2} were rested at room temperature for 15-20 min. The assembled veneers were then exposed to single-layer hot press unit (XLB type) at Shanghai Rubber Machinery Plant and pressed with a pressure of 1.5 MPa at 100°C for 15 min to obtain a plywood panel. The moisture content of control plywood was 16.6%, and that of flame retardant treated plywood was 13.5%.

Evaluation of combustion performance and smoke suppression performance

Cone calorimeter tests were performed according to the procedures indicated in the ISO 5660-1-2015 standard using a Fire Testing Technology cone calorimeter FTT2000 (Fire Testing Technology Ltd., UK). The plywood panel was conditioned in the laboratory at 20 ± 2°C and relative humidity of 65% ± 5% for 1 day and then cutting into specimens with dimensions of 100 mm (length) × 100 mm (width) × 10 mm (thickness) prior to testing. The fire

scenario was comprised of four steps: ignition, growth, fully developed, and decay. The tests were conducted with 50 kW·m^{-2} of heat flux which corresponded to the fully developed step.

RESULTS AND DISCUSION

Heat release rate (HRR) analysis

Heat release rate (HRR) refers to the heat release from per unit area of material combustion and it reflects the rate of heat release of materials during combustion, HRR, peak HRR (pk-HRR) and average HRR (av-HRR) are often used to evaluate combustion performances of materials and they all can reflect degree of material combustion and output of volatile combustibles. These three indexes can be used to evaluate spreading trend of flames and rate of fire hazard. The smaller HRR, pk-HRR and av-HRR indicates the lower heat release from material combustion and the lower fire hazards (Li et al. 2019).

The HRR curve during combustion of plywood is shown in Fig. 1. Seen from Fig. 1 that the HRR curve of plywood with fire retardant treatment was relatively stable after 120 s, indicating fire retardant decreased the production rate of combustible volatiles, weakened transmission of heats of plywood from surrounding environment and relieved the risk of plywood pyrolysis in fire accidents. pk-HRR of plywood without fire retardant treatment was 187.13 kW·m^{-2}, which was 40.93% higher than that of plywood with fire retardant treatment (110.53 kW.m^{-2}). The av-HRR of plywood with fire retardant treatment was decreased by 63.73% to 39.48 kW·m^{-2} compared to that of plywood without fire retardant treatment (108.85 kW·m^{-2}). HRR, pk-HRR and av-HRR of plywood with fire retardant treatment were decreased significantly than those of plywood without fire retardant treatment, indicating that the fire hazard caused by plywood after fire retardant treatment was small.
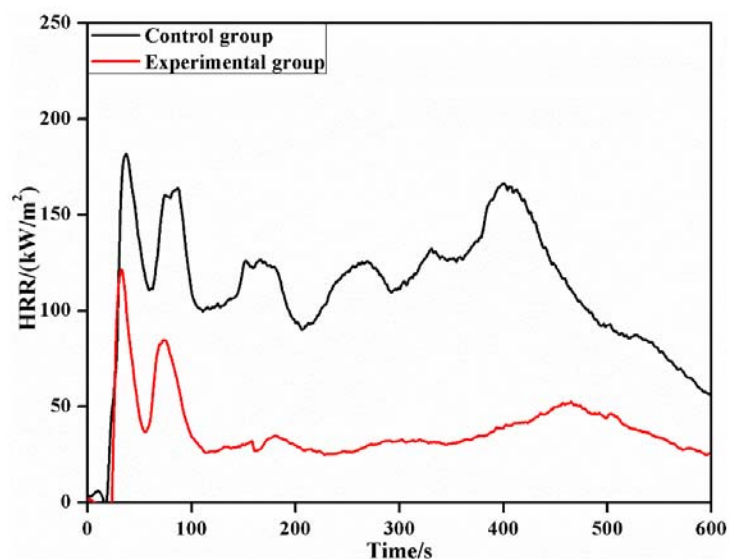

Fig. 1: The HRR curves of plywoods.

Total heat release (THR) analysis

Total heat release (THR) refers to the total heats released by unit area of materials from ignition to extinguishment. The fire hazard is more serious when THR is higher. Combustibility and flame retardation of materials could be evaluated better by combining HRR and THR (Mo et al. 2007). The THR curve during combustion of plywood is shown in Fig. 2. As shown in Fig. 2, heat release begun to be generated by plywoods with and without fire retardant treatment at about 30 s. THR curve of plywood without fire retardant treatment increased quickly as time went on, while THR curve of plywood with fire retardant treatment increased at a stable rate. These also proved the conclusions of HRR. In other words, the introduction of fire retardant decreased the production rate of possible volatiles and releasing of possible volatiles or combustion heats was relatively uniform. THR of plywood without fire retardant treatment was 69.21 MJ$\cdot$m^{-2} and the THR of plywood with fire retardant treatment was 5.58 MJ$\cdot$m^{-2}, showing a difference of 91.94%. This demonstrated that plywood with fire retardant treatment had a small THR during the combustion process, which reflected the very significant flame retardant efficiency. Fire retardant treatment decelerated the growth of surrounding temperature of ignition point in fire accidents significantly, and thereby delayed time and speed of fire spreading effectively.
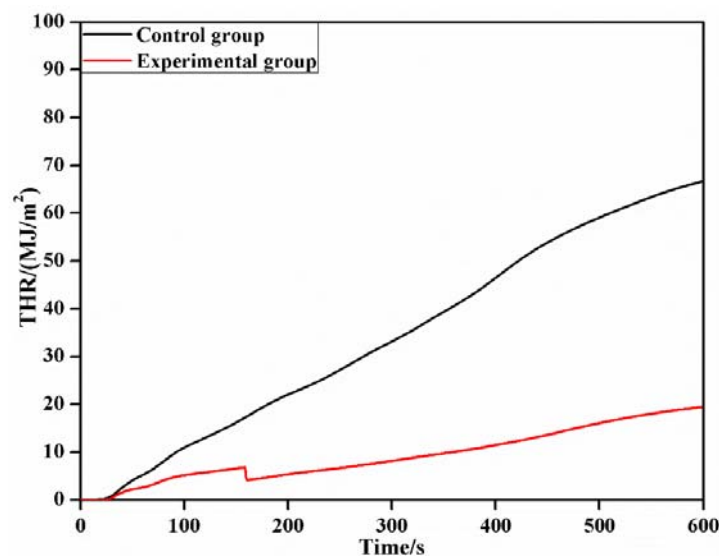
Fig. 2: The THR curves of plywoods.

Effective heat of combustion (EHC) analysis

Effective heat of combustion (EHC) refers to the ratio between heat release and mass loss at a moment, which reflects the burning degree of volatile gases in meteorological flames. The THR curves of plywoods at combustion are shown in Fig. 3.

As shown in Fig. 3 that average EHC of plywood with fire retardant treatment was 5.44 MJ$\cdot$kg^{-1}, which was 53.70% lower than that of plywood without fire retardant treatment (11.75 MJ$\cdot$kg^{-1}). That was because the fire retardant could inhibit pyrolysis of wood effectively and decrease the output of combustible volatiles, thus decreasing EHC significantly.

Fig. 3: The EHC curves of plywoods.
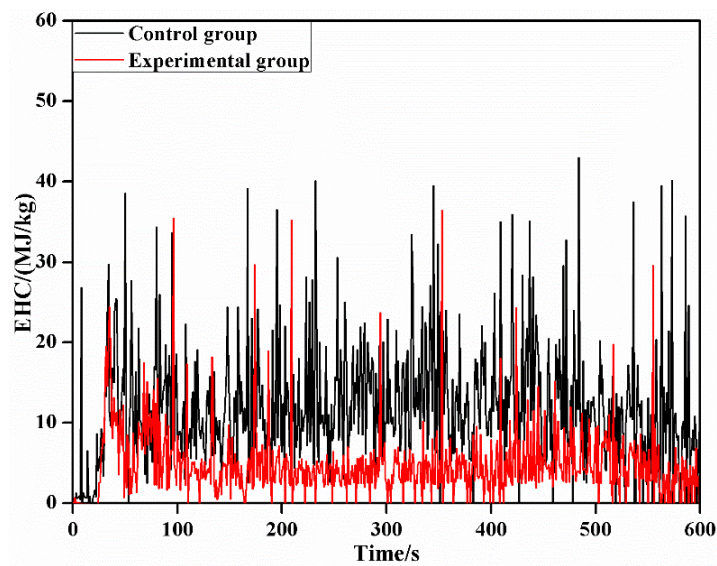
Mass loss (ML) and residual mass (Mass) of plywoods

Mass changes before and after the combustion of plywood are shown in Tab. 1. The ML of plywood without fire retardant treatment was 52.04 g, which decreased to 8.97 g for plywood with fire retardant treatment. This reflected that fire retardant could inhibit plywood combustion effectively and made it difficult for plywood to develop pyrolytic reactions, thus decreasing ML. The Mass of plywood without fire retardant treatment was 18.17%, which amounts to 85.92% for plywood with fire retardant treatment. This indicated that fire retardant inhibited combustion of plywood and accelerated the char-forming rate, thus increasing Mass. As a result, fire retarding plywood also could maintain strength in fire for a long period and it was difficult to collapse.

Tab. 1: The combustion mass change of plywoods.

Plywoods	ML (g)	Mass (%)
Control group	52.04	18.17%
Experimental group	8.97	85.92%

Smoking properties analysis

Total smoke release (TSR), CO yield (COY), CO_2 yield (CO_2Y) and total oxygen consumption (TOC) of plywoods during combustion are shown in Fig. 4 and Tab. 2.

TOC of plywood with fire retardant treatment was 3.6974 g, which was 91.86% lower than that of plywood without fire retardant treatment (45.4428 g). It was because fire retardant accelerated char-forming rate of plywood, decreased the formation of combustible volatiles and inhibited combustion.

TSR, COY and CO_2Y of plywood with fire retardant treatment were 25.99 $m^2 \cdot m^{-2}$, 0.0178 $kg \cdot kg^{-1}$ and 0.6036 $kg \cdot kg^{-1}$, which were decreased by 76.81%, 84.99% and 38.70% compared to those of plywood without fire retardant treatment (112.09 $m^2 \cdot m^{-2}$, 0.1186 $kg \cdot kg^{-1}$ and 0.9847 $kg \cdot kg^{-1}$). TSR, COY and CO_2Y of plywood with fire retardant treatment were

decreased to different extents, which could be explained as follows. Borides and magnesium sulfate in fire retardant had excellent smoke suppression performances and decreased the possibility of smoke asphyxia or toxicity-induced deaths during the occurrence of fire accidents.
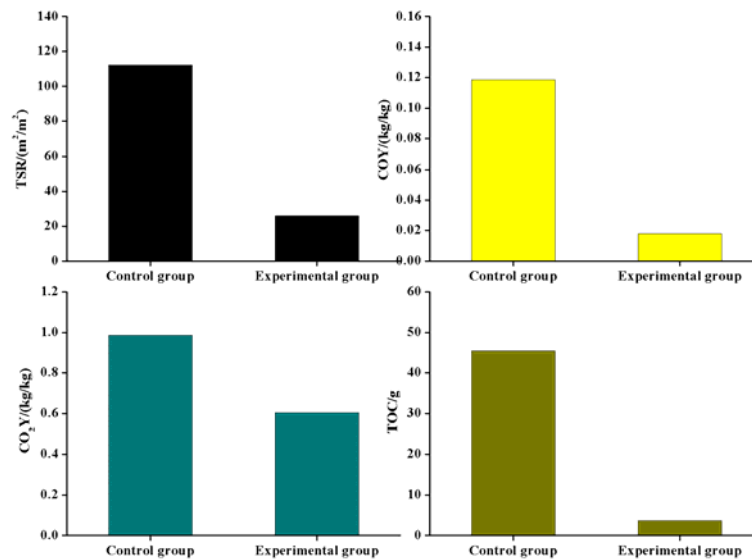

Fig. 4: Smoking effect and oxygen consumption of plywoods.

Tab. 2: The gas emission and total oxygen consumption of plywoods.

Plywoods	TSR ($m^2 \cdot m^{-2}$)	COY ($kg \cdot kg^{-1}$)	CO_2Y ($kg \cdot kg^{-1}$)	TOC (g)
Control group	112.09	0.1186	0.9847	45.4428
Experimental group	25.99	0.0178	0.6036	3.6974

Evaluation of potential fire hazard of plywoods

Fire performance index (FPI) and fire growth index (FGI) were applied to evaluate potential fire hazards comprehensively. FGI reflects the fire spreading capability of plywoods when they are exposed to high-heat environment. The higher value of FGI indicates the greater risks of fire accidents (Fig. 5). FPI reflects the tendency of combustion of plywoods. The smaller value of FPI indicates the smaller fire hazards (Cao 2019, Zhang et al. 2015, Huang et al. 2019).

FGI values of plywoods with and without fire retardant treatment were 3.454 $kW \cdot m^{-2} \cdot s^{-1}$ and 6.148 $kW \cdot m^{-2} \cdot s^{-1}$, indicating that fire retardant could decrease pk-HRR of plywoods, prolong the time to reach the pk-HRR and decelerate fire spreading. FPI values of plywoods with and without fire retardant treatment are 0.136 $s \cdot m^2 \cdot kW^{-1}$ and 0.106 $s \cdot m^2 \cdot kW^{-1}$, resp. This reflects that fire retardant prolonged the ignition time of plywoods and increased the time for escaping from fire accidents. In a word, plywood with fire retardant treatment had relatively high FPI and relatively low FGI, showing a high safety level.
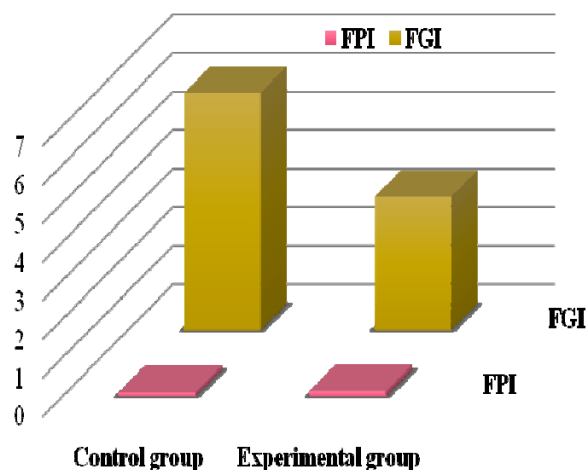
Fig. 5: FPI and FGI of plywoods.

CONCLUSIONS

A high-efficiency fire retardant composition was prepared with dicyandiamide, phosphoric acid, boric acid, borax, urea and magnesium sulfate and it was used to process veneers which were then to prepare the plywood. Meanwhile, heat release and smoke release from combustion of plywood were tested by a cone calorimeter. Results showed that: *(1)* The plywood with fire retardant treatment had the better flame-retardant performance and smoke suppression effect as well as the stronger char-forming capability compared to plywood without fire retardant treatment. *(2)* The average heat release rate, total heat release, average effective heat of combustion, total smoke release, CO yield and oxygen consumption of the plywood with fire retardant treatment were decreased by 63.72%, 91.94%, 53.70%, 76.81%, 84.99% and 91.86%, respectively. *(3)* The fire growth index of plywood treated by fire retardant was relatively low (3.454 $kW \cdot m^{-2} \cdot s^{-1}$) and it took longer time to reach the peak heat release rate, accompanied with slow fire spreading. *(4)* The fire performance index was relatively high (0.136 $s \cdot m^2 \cdot kW^{-1}$) and it took longer time to be ignited, thus leaving a long time for escaping at fire accidents. *(5)* The fire hazard of plywood with fire retardant treatment was low, and its safety level was high.

ACKNOWLEDGMENTS

REFERENCES

1. Altun, S., Ozcifci, A., Senel, A., 2010: Effects of silica gel on leaching resistance and thermal properties of impregnated wood. Wood Research 55(4): 101-112.

2. Cao, J.Z., 2019: A review on wood protectant dispersion systems and their liquid penetration. Journal of Forestry Engineering 4(3): 1-9.

3. Cao, Y., Wang, X., Li, Y., Shen, D., Dai, Y.P., Zhang, S.Z., Zhang, W.G., 2020: Effect of high temperature oil heat treatment on the starch content and mold-resistant property of bamboo. Journal of Forestry Engineering 5(2): 109-115.

4. Chu, D., Mu, J., Zhang, L., 2017: Promotion effect of NP fire retardant pre-treatment on heat-treated poplar wood. Part 2: hygroscopicity, leaching resistance, and thermal stability. Holzforschung 71(3): 217-223.

5. Chung, Y.J., 2010: Comparison of combustion properties of native wood species used for fire pots in Korea. Journal of Industrial and Engineering Chemistry 16(1): 15-19.

6. Dong, W.R., Xu, M., 2019: Effect of nano copper-zinc preservative combined with phenolic resin on properties of rubber wood. Journal of Forestry Engineering 4(1): 39-44.

7. Fateh, T., Rogaume, T., Luche, J., Richard, F., Jabouille, F., 2014: Characterization of the thermal decomposition of two kinds of plywood with a cone calorimeter-FTIR apparatus. Journal of Analytical and Applied Pyrolysis 107: 87-100.

8. Huang, X.D., Huang, J.K., Hse, C.Y., Todd, F.S., Lin, J.G., Li, S.J., 2019: Study on the mold-resistant properties of moso bamboo treated with starch amylase. Journal of Forestry Engineering 4(3): 60-65.

9. Kartal, S.N., Hwang, W.J., Imamura, Y., 2007: Water absorption of boron-treated and heat-modified wood. Journal of Wood Science 53(5): 454-457.

10. Kim, J., Lee, J.H., Kim, S., 2012: Estimating the fire behavior of wood flooring using a cone calorimeter. Journal of Thermal Analysis and Calorimetry 110(2): 677-683.

11. Li, C.Y., Lv, C.Y., Yu, L.L., 2019: Flame retardant treatment of bamboo and its effect on bamboo properties. World Bamboo and Rattan 17(6): 16-20, 24.

12. Mo, T.C., Wang, H.W., Chen, S.Y., 2007: Synthesis and characterization of polyimide-silica nanocomposites using novel fluorine-modified silica nanoparticles. Journal of applied polymer science 104(2): 882-890.

13. Nicholas, D.D., Siau, J.F., 1973: Factors influencing the treatability of wood, in: wood deterioration and its prevention by preservative treatment. New York: Syracuse University Press.

14. Pan, J., Mu, J., Wu, Z., Zhang, X., 2014: Effect of nitrogen-phosphorus fire retardant blended with $Mg(OH)_2/Al(OH)_3$ and nano-SiO_2 on fire-retardant behaviour and hygroscopicity of poplar. Fire and Materials 38(8): 817-826.

15. Qu, H.Q., Wu, W.H., Wu, H.J., Xie, J.X., Xu, J.Z., 2011: Study on the effects of flame retardants on the thermal decomposition of wood by TG-MS. Journal of Thermal Analysis and Calorimetry 103(3): 935-942.

16. Son, D.W., Kang, M.R., Kim, J.I., Park, S.B., 2012: Fire performance of the wood treated with inorganic fire retardants. Journal of the Korean Wood Science and Technology 40(5): 335-342.

17. Xue, S.Q., Li, B., Feng, K.X., 2006: Characteristics and application of water-based fire retardants. Fire Technique and Products Information 8: 25-27.

18. Yu, L.P., Tian, M.F., Li, L.F., Wu, Z.G., Chen, S.C., Chen, J., Xi, X.D., 2020: Study of nano

colloidal silica sol based protectant on the prevention of Masson pine. Wood Research 65(5): 797-808.

19. Zhang, X., Li, D., Xie, H., Wang, D., 2014: Preparation and application of water-based fire retardant of ammonium phosphate. Advanced Materials Research 1015: 287-290.

20. Zhang, X.T., Mu, J., Chu, D.M., Zhao, Y., 2015: Synthesis of fire retardants based on N and P and poly (sodium silicate-aluminum dihydrogen phosphate) (PSADP) and testing the flame-retardant properties of PSADP impregnated poplar wood. Holzforschung 70(4): 341-350.

21. Zhang, X.T., Mu, J., Chu, D.M., Zhao, Y., 2016: A study on the fire performance and hygroscopicity of poplar treated with melamine modified N-P fire retardant. Journal of Central South University of Forestry & Technology 36(2): 119-124.

22. Zhou, Z.X., Du, C.G., Yu, H.L., Yao, X.L., Huang, Q.L., 2020: Promotion effect of nano-SiO_2 on hygroscopicity, leaching resistance and thermal stability of bamboo strips treated by nitrogen-phosphorus-boron fire retardants. Wood Research 65(5): 693-704.

ZHIGANG WU, XUE DENG, LIFEN LI, LIPING YU*, JIE CHEN
GUIZHOU UNIVERSITY
COLLEGE OF FORESTRY
GUIYANG 550025
GUIZHOU
P.R. CHINA
*Corresponding author: wzhigang9@163.com, ylpgzu@163.com

BENGANG ZHANG, XUEDONG XI
UNIVERSITY OF LORRAINE
IUT-LERMAB 88000
EPINAL
FRANCE

QIAOYAN ZHANG
ZHAZUO STATE-OWNED FOREST FARM OF GUIZHOU PROVINCE
GUIYANG 550299
GUIZHOU
P.R. CHINA

COMPARATIVE ANALYSIS OF COMPOSITE TIMBER-CONCRETE CEILING SYSTEMS

KLARA FREUDENBERGER, JAROSLAV SANDANUS
SLOVAK UNIVERSITY OF TECHNOLOGY IN BRATISLAVA
SLOVAKIA

ABSTRACT

This paper compares two concepts of composite timber concrete ceilings and their uncoupled alternatives based on a parametric study by comparing the final deflections of individual variants and at the same time considering according to the ultimate limit state. It includes a comparison of coupled and uncoupled variants while maintaining the same boundary conditions as the load, the thickness of the ceiling structure and the load width. By considering other factors, we can achieve more optimal variant, thanks to more accurate consideration of the required boundary conditions such as the complexity of installation or fire resistance. The purpose of this paper is to simplify the optimal selection of the ceiling structure based on the suitability of the supporting structure.

KEYWORDS: Composite structure, ceiling, cross laminated timber, timber, shear connectors.

INTRODUCTION

At present, the accent is on the usage of materials and structures that leave as little carbon footprint as is possible. As is widely known, wood is the most suitable basic construction material. As part of wood-based material is CLT too. CLT is relatively new material, it was developed just at the end of 20th century (Brandner et al. 2016). It is commonly applied as structure member as ceilings or walls in multi storey buildings or structures with requires longer span like congress halls, galleries, or schools (Ceccotti 2002). High material resistance compared to the weight is main benefit in elements like CLT panels. Each segment consists of three-, five- to seven- layers of lamellas. Each layer is applied perpendicular to layer before (Aicher et al. 2001). It is rule, that outer layers must be in the same way as main load capacity (Bajzecerova et al. 2018). In some cases, CLT panels as ceilings may be insufficient. To use most of the potential of these structures, it is necessary to apply shear connectors. It is well known that by applying a coupling, the ceilings can be more effective by coupling appropriate materials and components, e.g., timber beam with concrete deck (Surovec and

Slivanský 2015). Coupling ensures the interaction of individual materials and increases the load-bearing capacity and rigidity of the structure (Jiang and Crocetti 2019).

By creating a composite cross-section, it can be ensured the interaction of two elements (Fig. 1) (Ahmed and Tsavdaridis 2019). This phenomenon can be verified based on the course of normal stresses along the height of the cross-section (Lukaszewska et al. 2008).
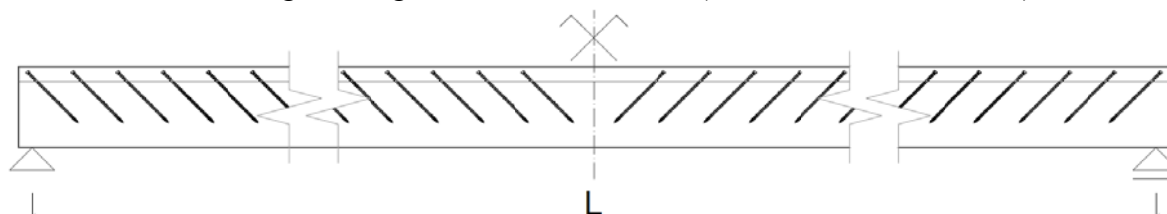

Fig. 1: Longitudinal section of the location of the coupling by self-tapping screws.

In the context of this study, it is specifically the interconnection between timber and concrete elements. To secure the coupling, it is possible to use mechanical coupling by self-tapping screws as well as grooving (Čajka and Burkovič 2013) (Mai et al. 2018), notched conectors (Yuchen and Crocetti 2019) (Loebus et al. 2017) or gluing. The study is aimed on the usage of screws that belong to the category of flexible mechanical shear connectors, especially: Rotho Blaas CTC 9 mm thickness at 240 mm (Rotho Blaas GmbH, 2021: Screws and connectors for timber 2021). The screws are applied at an angle of 45°.

MATERIAL AND METHODS

Composite beam timber-concrete ceiling

At the bottom of the cross-section are used timber beams as construction beams (T) of strength class C24. The cross-sectional dimensions are varied and compared in study. Width (W_T) of beams in this study is used the same, namely 120 mm. A cement-chipboard of constant thickness of 28 mm is used for the formwork. The concrete layer, which is used as part of the composite cross-section, is designed to have a constant thickness (H_{con}) of 50 mm with one row of reinforcement that is used only to avoid excessive confusion of the concrete (EN 1992-1-1, 2004). The same load width of 1m is used in this variant. The effective width is identical to the load width (Fig. 2).
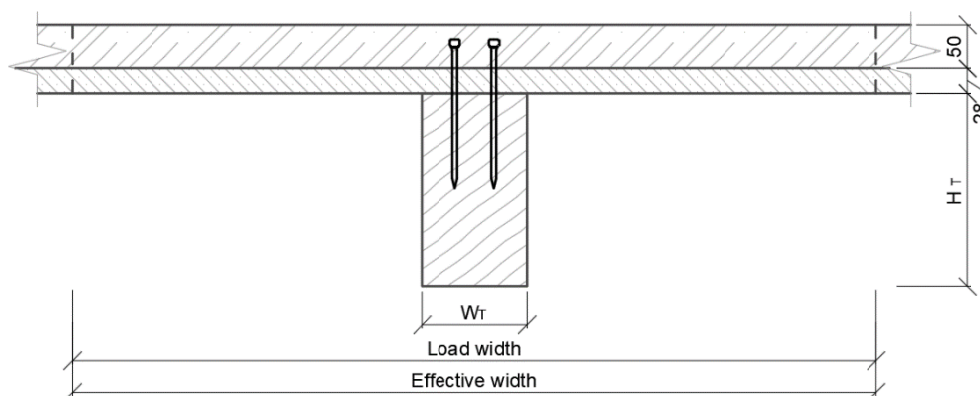

Fig. 2: Cross-section of composite beam timber-concrete ceiling.

Composite slab timber-concrete ceiling

Solid timber panel from cross laminated timber (CLT) is used as part of a coupled cross-section and provides a support function and further replaces the need to use formwork (Fig. 3). The study uses panels intended for application to ceiling structures, which means that the outer layers of the CLT panel are in the longer direction of the slab and at the same time in its direction with higher load-bearing capacity. The thickness and number of layers varies based on the needs of the study. Since it is a slab element, the load width refers to 1m. As it is in previous variant, load width and effective width are equal. Concrete of the same strength class C20/25 of constant thickness with one row of reinforcement is used as another material in the composite ceiling.
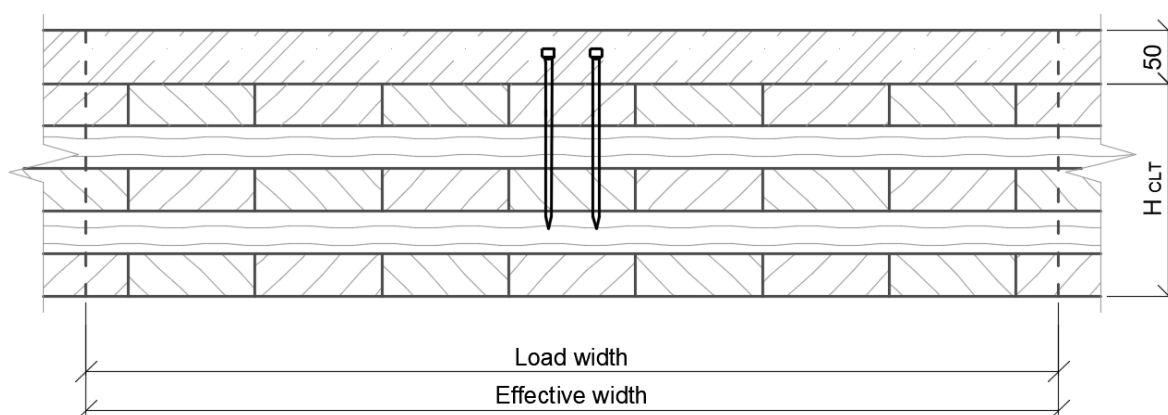

Fig. 3: Cross-section of composite slab timber-concrete ceiling.

Non-composite variants of timber-concrete ceiling

For verification efficiency of coupling were created non-composite variants. To verify the effectiveness of the coupling, uncoupled variants were created. In both cases, the coupling by self-tapping screws were not applied, the following boundary conditions were maintained as in the previous variants.

Test set-up

The analytical study is prepared in the MS Excel program. Algorithm consists of different material parameters and geometric parameters. In the calculation is necessary to account differences between used cross-sections. Used variants have equal values of surface loads consisting of imposed load (2 $kN \cdot m^{-1}$), and predefined loads as load from load-bearing and non-load-bearing walls (2,78 $kN \cdot m^{-1}$), and load of layers of floor (1,2 $kN \cdot m^{-1}$) expect for self-weight load. These values changes based on the change in the thickness and density of used wood-based material (EN 1991-1-1, 2002). In first step, the γ-method is necessary to apply in the variant with CLT panel (EN 1995-1-1, 2004). Based on this method, it is possible to take into the account the efficiency of individual layers and express the corresponding moment of inertia of the effective cross-section of the CLT segment. Subsequently, the method of idealized cross-section is applied, which is based on the creation of an idealized cross-section originally consisting of several materials. This result can be achieved after calculating with the partial coefficient, it is used to obtain effective cross-sectional characteristics specified in

the EN 1995-1-1 Annex B. Method is valid for combination as for CLT and concrete as timber-beam concrete structure.

The sample is assessed as part of the analysis in the first step. The cross-section is assessed for the ultimate limit state (ULS) for various stress methods along the height of the cross-section. The instant deflection is count for serviceability limit state (SLS). In the next step is count is offset further for SLS and ULS at the end of life are evaluated (EN 1991-1-1, 2002).

RESULTS AND DISCUSSION

Comparison of efficiency of support systems

Numbers of factors affect the effectiveness of a design e.g., type of material and geometrical parameters, quantity and type of shear connectors, load width and effective span of the ceiling structure (Dias et al. 2015).

Deflection is one of the factors that determines the ability to use. Exceeding the values does not say that the structure collapses, it expresses comfort and the possibility of use. Excessive curvature of roof can cause some devices to malfunction (Ataei et al. 2019).

Since deflection also corresponds to the time. Due to the effect of time, the joints are loosened, and these results are an increase in the already instant deflection and thus the final deflection created (Hassanieh et al. 2017, Kanócz and Bajzecerová 2012, Khorsandnia et al. 2015). By comparing instant deflection in Figs. 4-7 and final deflection in Figs. 8-11 it can be seen increase in deformation. This has the effect of reducing the scope of the use of span.

Also, it is known that the thickness of the structure affects the final deflection of the structure. The effect of improving parameters of ceiling can be seen gradually in Figs. 4-7. It is shown that the coupled slab ceiling is more effective and can be applied to a range of approximately 9.5 m. On the other hand, a beam-coupled ceiling can only be applied up to a span of approximately 6.5 m with a load width of 1 m. Coupled variants are more efficient as uncoupled variants and is possible to overcome a longer span.

Fig. 4: Comparison of instant deflection depending on thickness of noncoupled beam-concrete and length of span.

Fig. 5: *Comparison of instant deflection depending on thickness of coupled beam-concrete and length of span.*

Fig. 6: *Comparison of instant deflection depending on thickness of noncoupled CPT-concrete and length of span.*
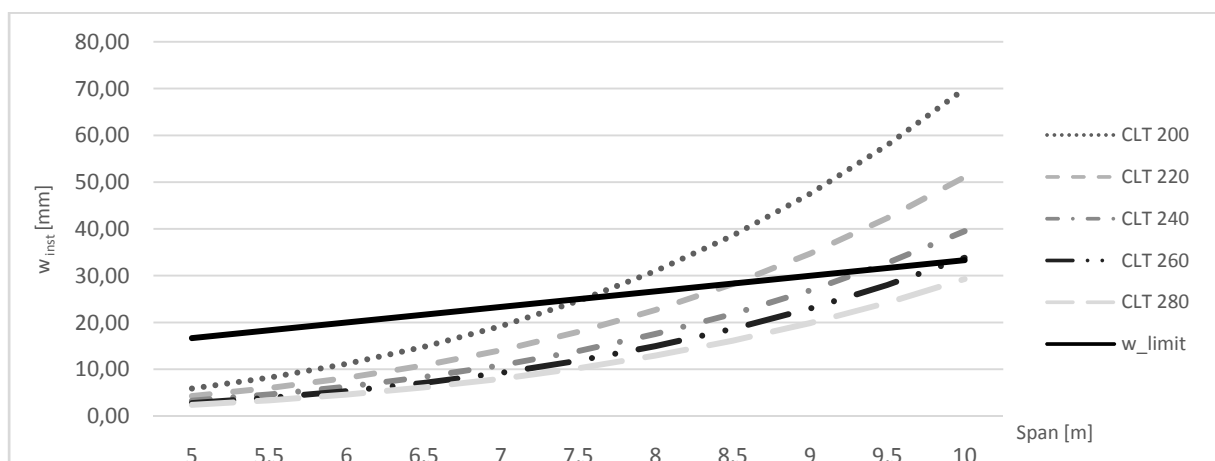
Fig. 7: *Comparison of instant deflection depending on thickness of coupled CLT-concrete and length of span.*
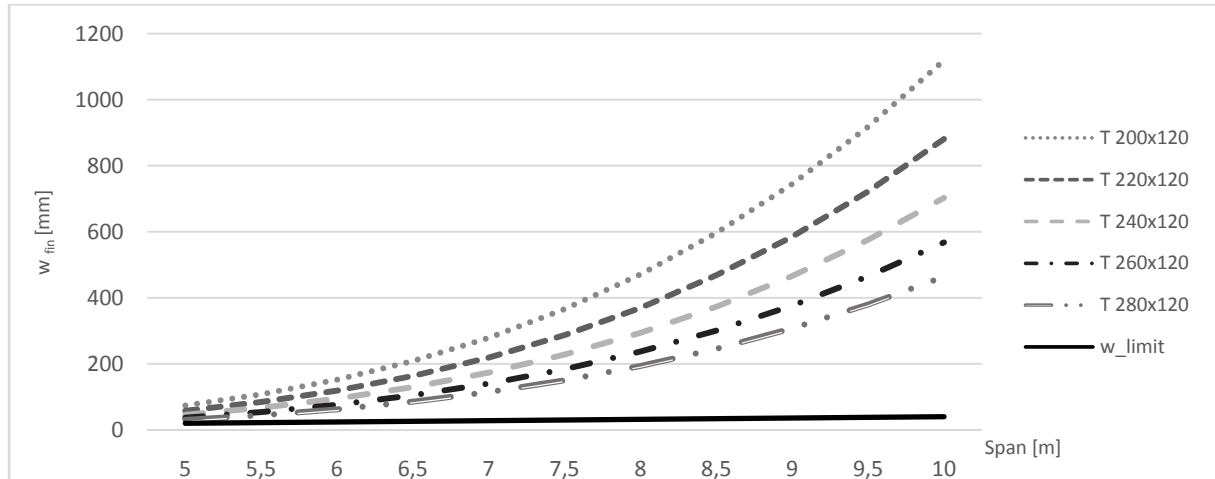
Fig. 8: Comparison of final deflection depending on thickness of noncoupled beam-concrete and length of span.
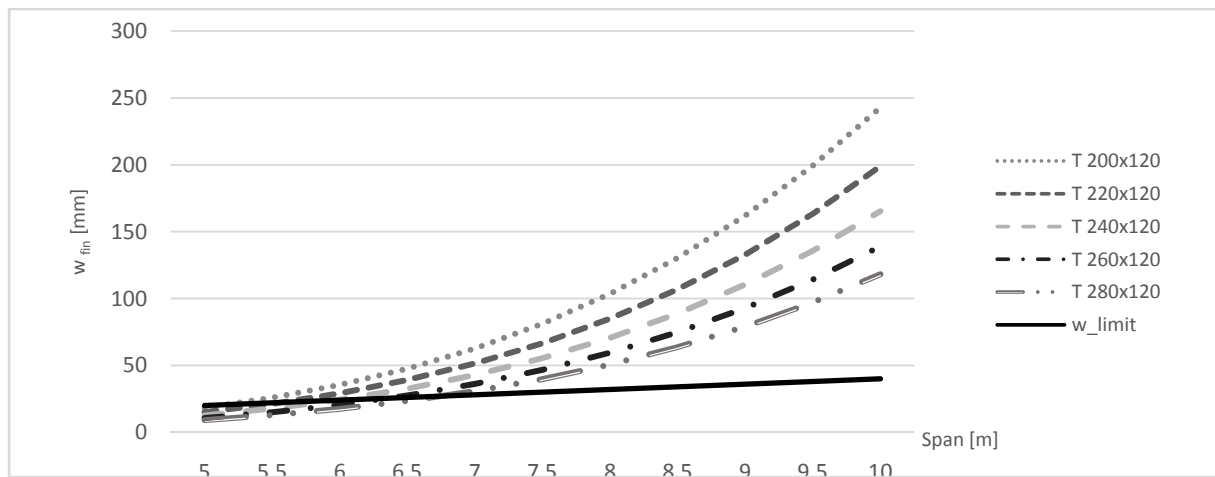
Fig. 9: Comparison of final deflection depending on thickness of coupled bean-concrete and length of span.

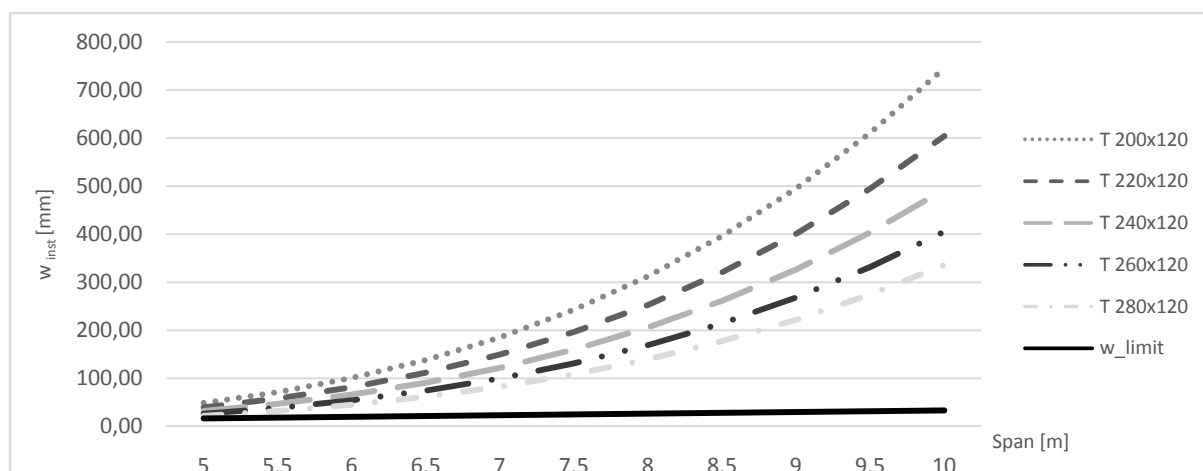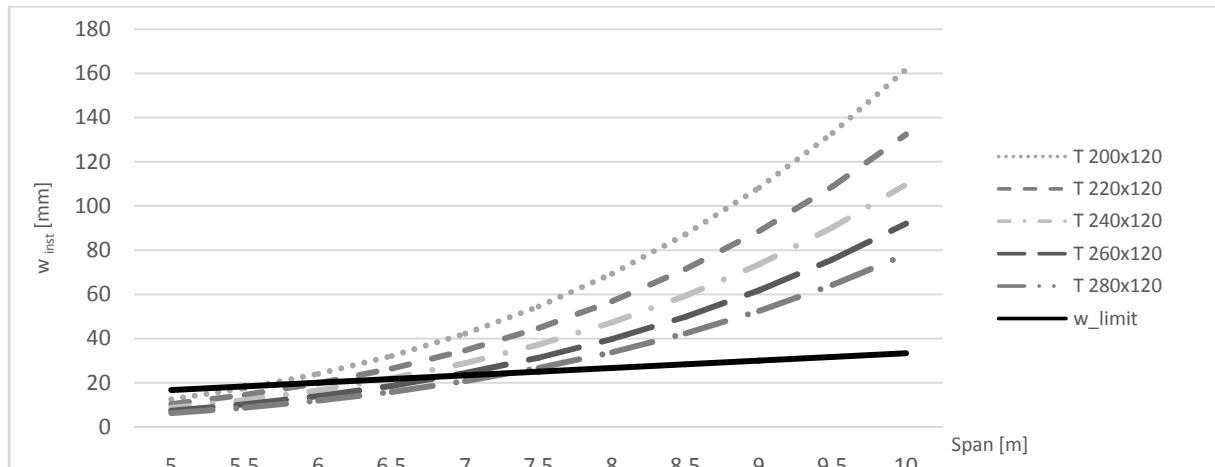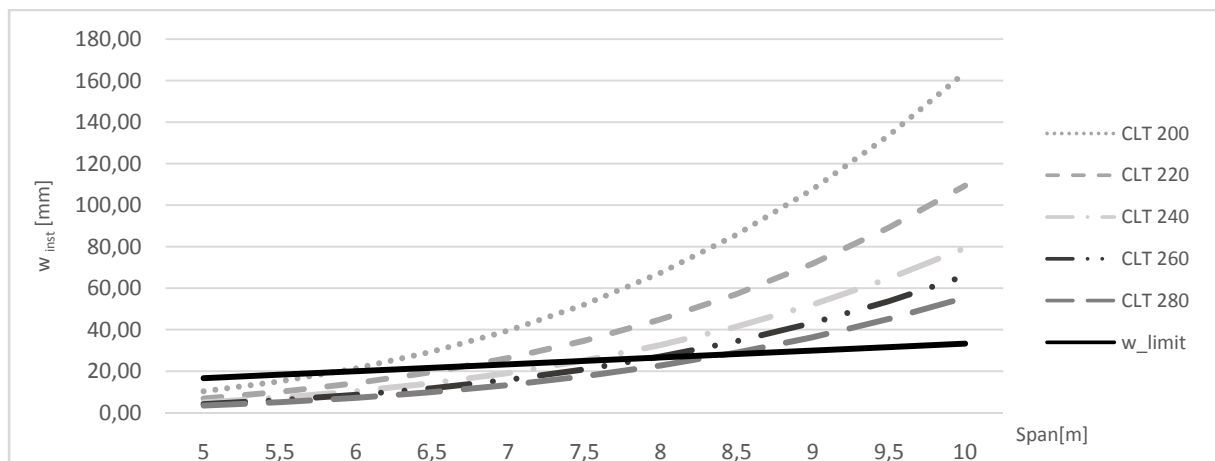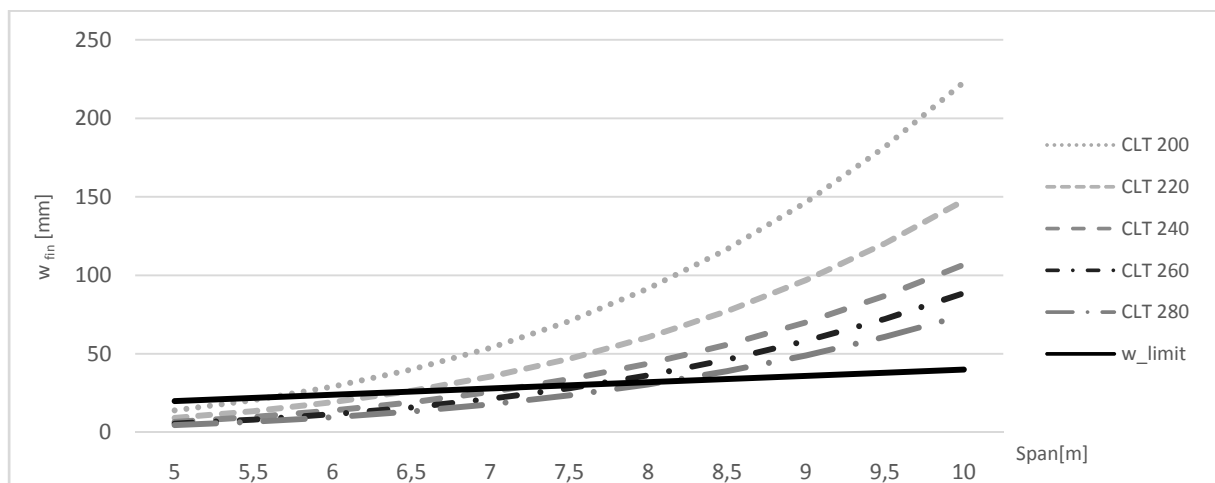*Fig. 10: Comparison of final deflection depending on thickness of noncoupled CLT-concrete and length of span.*
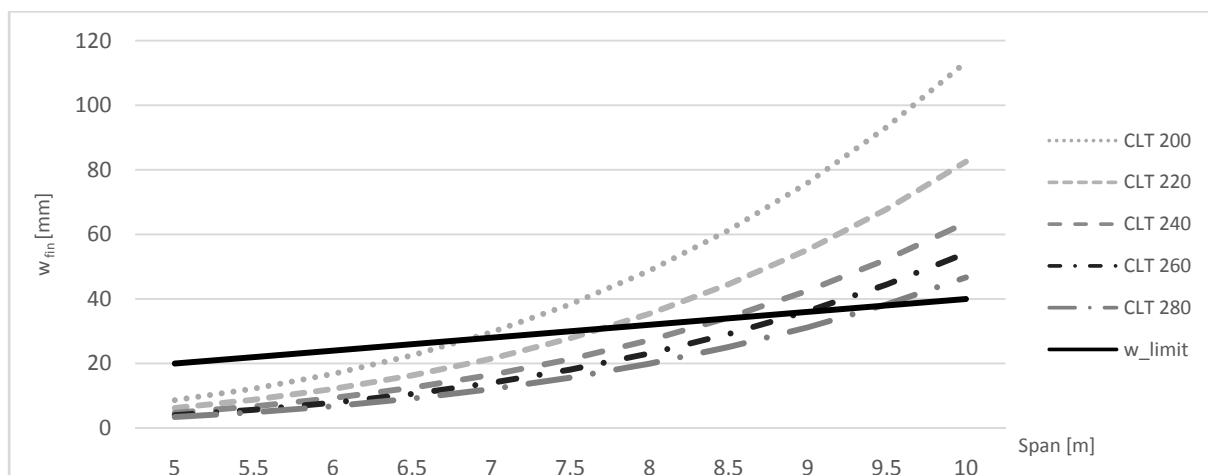
Fig. 11: Comparison of final deflection depending on thickness of coupled CLT-concrete and length of span.

It is necessary to consider assessments at the ultimate limit state as well as usability. As it is obviously presented in Figs. 13 and 14, there may be case where the conditions are fulfilled only for SLS (EN 1991-1-1, 2002). In Fig. 12 are presented distribution of bending stresses cross the height of cross-section.
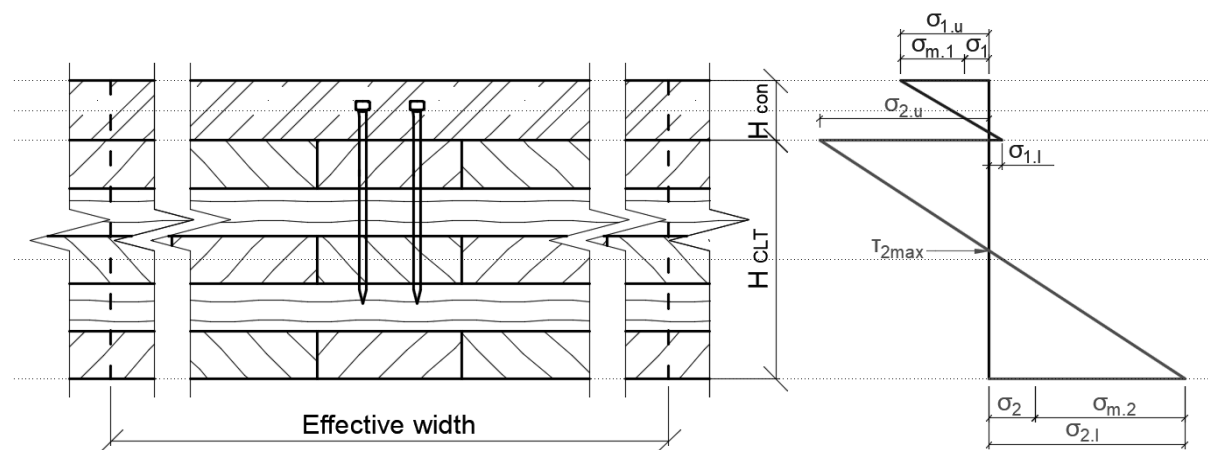
Fig. 12: Cross-section of CLT and distribution of bending stresses.

Similar cross-section of 240 mm thickness was taken for all variants in the comparison. Load width is 1m and span is 5 m, these parameters are similar for this comparison. Segments are shown in their end of live state.

Timber beam variants have higher value stresses along the cross-section comparing to CLT slab variants. Stress at the upper edge of the concrete section can be observed multiply values in the evaluation by 22.1% is the difference between coupled and non-coupled timber-concrete beam, in favour of coupling variant. Selected samples of beam variants show exceeding stress limits. It can be observed that in the case of the coupled beam variant was a decrease of almost 100% compared to the noncoupled variant of value 214.6%. Exceeded values can be seen in evaluation of final deflection. Noncoupled timber beam variant reach values of 230%. Decrease of this value to 63.2% is by using shear connectors in coupled

timber-concrete beam variant. Requirement for limit state of final decline is fulfilled. It is clear, that coupling elements are significantly improving segment according to Tab. 1.

Tab. 1: Evaluation of Assessment at timber-concrete variants with 5 m span.

Coupled timber-concrete ceiling						Non-coupled timber-concrete ceiling					
Cross-section		ULS - end of service life			SLS - end of service life	Cross-section		ULS- end of service life			SLS - end of service life
H_T	W_T	$\sigma_{1.u}/f_{cd}$	σ_{2M}/f_{md+} $\sigma_{2.l}/f_{t.0.d}$	τ_{2max}/f_{vd}	w_{fin}/w_{lim}	H_T	W_T	$\sigma_{1.u}/f_{cd}$	σ_{2M}/f_{md+} $\sigma_{2.l}/f_{t.0.d}$	τ_{2max}/f_{vd}	w_{fin}/w_{lim}
200	120	0.396	1.578	0.500	0.916	200	120	0.843	2.887	0.694	3.705
220	120	0.344	1.368	0.466	0.756	220	120	0.659	2.481	0.656	2.898
240	120	0.302	1.199	0.437	0.632	240	120	0.523	2.146	0.618	2.300
260	120	0.268	1.059	0.411	0.535	260	120	0.420	1.868	0.583	1.850
280	120	0.240	0.943	0.389	0.456	280	120	0.342	1.637	0.550	1.507

Values of stresses at the upper edge of concrete part of section of different CLT variants are slightly similar to each other (Tab. 2). On the other hand, these differences are not so obvious as in timber beam variants. Coupled CLT-concrete slab has 7.12% capacity instead of 13% by noncoupled CLT-concrete slab. Strain at lower part of timber segment is decisive factor. Requirements for ULS and SLS in case of CLT variants are satisfied. Decrease in values is not so observable as in case of beam variants. Coupled variant has decrease of values 5.7%. It is due to higher efficiency of slabs involved their higher stiffness.

Tab. 2: Evaluation of assessment at CLT-concrete variants with 5 m span.

Coupled CLT-concrete ceiling					Non-coupled CLT-concrete ceiling				
Cross-section	ULS - end of service life			SLS - end of service life	Cross-section	ULS - end of service life			SLS - end of service life
H_{CLT}	$\sigma_{1.u}/f_{cd}$	σ_{2M}/f_{md+} $\sigma_{2.l}/f_{t.0.d}$	τ_{2max}/f_{vd}	w_{fin}/w_{lim}	H_{CLT}	$\sigma_{1.u}/f_{cd}$	σ_{2M}/f_{md+} $\sigma_{2.l}/f_{t.0.d}$	τ_{2max}/f_{vd}	w_{fin}/w_{lim}
200	0.213	0.478	0.122	0.432	200	0.153	0.600	0.144	0.702
220	0.162	0.356	0.098	0.310	220	0.101	0.435	0.115	0.464
240	0.130	0.284	0.085	0.236	240	0.072	0.341	0.098	0.335
260	0.114	0.259	0.084	0.200	260	0.060	0.306	0.095	0.278
280	0.101	0.237	0.083	0.171	280	0.050	0.276	0.093	0.234

Tab. 3: Evaluation of assessment at CLT-concrete variants with 8 m span.

Coupled CLT-concrete ceiling					Non-coupled CLT-concrete ceiling				
Cross-section	ULS - end of service life			SLS - end of service life	Cross-section	ULS - end of service life			SLS - end of service life
H_{CLT}	$\sigma_{1.u}/f_{cd}$	σ_{2M}/f_{md+} $\sigma_{2.l}/f_{t.0.d}$	τ_{2max}/f_{vd}	w_{fin}/w_{lim}	H_{CLT}	$\sigma_{1.u}/f_{cd}$	σ_{2M}/f_{md+} $\sigma_{2.l}/f_{t.0.d}$	τ_{2max}/f_{vd}	w_{fin}/w_{lim}
200	0.623	1.196	0.198	1.524	200	0.393	1.531	0.230	2.864
220	0.494	0.885	0.157	1.107	220	0.259	1.110	0.183	1.895
240	0.408	0.703	0.134	0.851	240	0.186	0.872	0.157	1.370
260	0.362	0.644	0.133	0.724	260	0.154	0.782	0.153	1.137
280	0.325	0.593	0.132	0.622	280	0.129	0.707	0.148	0.957

In this comparison were used samples of variants as beam and slab ceilings showed in (Tabs. 1 and 2) with the same span of 5 m. CLT variants are not suitable for shorter spans as it was presented and have potential for considerably higher span and loads. Longer span would be more appropriate for variants consisting of CLT panels. For example (Tab. 3), exceeded capacity can be seen in coupled and noncoupled CLT concrete slab with 8 m span. Overall fulfilled conditions for SLS and ULS are completed in coupled CLT concrete variant. By comparison values of capacity with case of noncoupled variant values are higher by 137% and are no more suitable for SLS. These values are 51.9% higher than in coupled variant. In case of ULS the decisive stresses capacity is in the lower part of CLT panel. Capacity is suitable, but it has higher percentage usage than other assessments.

It is not only resistance or load-bearing capacity that should be taken in consideration during decision-making about the type of ceiling structure (Tab. 4). The design may be suitable for these factors, but it is necessary to consider others, e.g., requirement of structure thickness of each storey, because the thickness of ceiling can also strongly influence total building costs. Advantage of using slab CLT system is not only low thickness and good rigidity, but also simplicity of placement technical equipment of buildings, because of the absence of protruding beams (Bajzecerová and Kanócz 2017).

Tab. 4: Comparison of variants based on suitability for use (darker color indicates higher suitability for use).

Alternatives / Parameters	Non-coupled timber beam concrete ceiling	Coupled timber beam concrete ceiling	Non-coupled CLT-concrete ceiling	Coupled CLT-concrete ceiling
Length of span				
Thickness of ceiling				
Time of realisation				
Fire resistance				
Price				

Level of difficulty in making the ceiling structure is another indicator. It is necessary to use formwork while using the beam system. When classic formwork is used, it must be also removed afterwards. This aspect remains even in the coupled variant where the application of a considerable number of shear connectors are added to the entire assembly process. Necessity to install formwork is eliminated while applying the slab system. In terms of implementation, it is the simplest and least laborious variant. This system can be made more efficient by using shear connectors, but at the expense of laboriousness in laying the self-tapping screws.

In fire situation, compared to steel or concrete is timber as material more effective. Timber not prone to lose strength after reaching a certain temperature, and neither is explosive strub off the surface as it is the habit for the concrete. Charred layer which slows down the overheating of the element at outer side of timber protects surface (Makovická Osvaldová et al. 2016, Chen et al. 2021). It is important to note, that section does not lose its resistance abruptly but continuously (Makovicka Osvaldová 2020).

During the research of a suitable variant, it is also necessary to consider the financial complexity. It is obvious that the cheapest will be the application of the simplest solution - the

beam ceiling noncoupled, but it is inefficient way. The usage of CLT panels can make construction considerably more expensive, but nevertheless it is possible to realize ceiling structures with larger spans. It is also required to consider the necessity of using the shear connectors. Price of self-tapping screws is not negligible due to their quantity and quantity of additional work. Also, must be account necessity of usage temporary supports while applying coupled variants.

CONCLUSIONS

Coupling appears to be an effective way to achieve higher strength of the ceiling structure. While comparing the beam variants, it was found that the proposed coupling was able to eliminate the stresses to approximately half the values compared to the uncoupled variant. The slab variants have been found to be unnecessarily oversized at 5 m spans. Further research will need to focus on the use of slimmer boards (Van Thai et al. 2020). It would be beneficial to focus on the effectiveness of the coupling, in which case, a higher degree of coupling could also be verified. Alternatively, verify other methods of coupling (Kanócz et al. 2013). Coupling with the aid of screws appears to be a highly laborious alternative and it would be appropriate to compare the coupling efficiency also with the variant where the shear connectors would be used as a perforated steel strip shear connectors or grooves.

REFERENCES

1. Ahmed, I.M., Tsavdaridis, K.D., 2019: The evolution of composite flooring systems: applications, testing, modelling and eurocode design approaches. Journal of Constructional Steel Research 155: 286–300.
2. Aicher, S., Dill-Langer, G., Höfflin, L., 2001: Effect of polar anisotropy of wood loaded perpendicular to grain. Journal of Materials in Civil Engineering 13(1): 2–9.
3. Ataei, A., Chiniforush, A.A., Bradford, M., Valipour, H., 2019: Cyclic behaviour of bolt and screw shear connectors in steel-timber composite (STC) beams. Journal of Constructional Steel Research 161: 328–340.
4. Bajzecerova, V., Kovac, M., Kanocz, J., 2018: Structural analysis of cross-laminated timber slabs subjected to bending – state of the art. Selected Scientific Papers - Journal of Civil Engineering 13(1): 133–140.
5. Bajzecerová, V., Kanócz, J., 2017: Parameters of various timber-concrete composite connection systems. Advances and Trends in Engineering Sciences and Technologies II - Proceedings of the 2nd International Conference on Engineering Sciences and Technologies, ESaT 2016, Pp 21–26.
6. Brandner, R., Flatscher, G., Ringhofer, A., Schickhofer, G., Thiel, A., 2016: Cross laminated timber (CLT): overview and development. European Journal of Wood and Wood Products 74(3): 331–351.
7. Ceccotti, A., 2002: Composite concrete-timber structures. Progress in Structural Engineering and Materials 4(3): 264–275.

8. Čajka, R., Burkovič, K., 2013: Technologie spřažení dřevo betonových stropních konstrukcí pomocí lepených smykových lišt (Coupling technology of wood concrete ceiling structures using glued shear strips).

9. Chen, Z., Lu, W., Bao, Y., Zhang, J., Wang, L., Yue, K., 2021: Numerical investigation of connection performance of timber-concrete composite slabs with inclined self-tapping screws under high temperature. Journal of Renewable Materials 9(12): 89–104.

10. Dias, A.M.P.G., Martins, A.R.D., Simões, L.M.C., Providência, P.M., Andrade, A.A.M., 2015: Statistical analysis of timber-concrete connections - Mechanical properties. Computers and Structures 155: 67–84.

11. EN 1992-1-1, 2004: Eurocode 2: Design of concrete structures. Part 1.1: General rules and rules for buildings.

12. EN 1991-1-1, 2002: Eurocode 1: Actions on structures. Part 1.1: General actions. Densities, self-weight, imposed loads for buildings.

13. EN 1995-1-1+A1, 2004: Eurocode 5: Design of timber structures. Part 1-1: General rules and rules for buildings, Annex B (Informative): Mechanically jointed beams.

14. Hassanieh, A., Valipour, H.R., Bradford, M.A., 2017: Experimental and numerical investigation of short-term behaviour of CLT-steel composite beams. Engineering Structures 144: 43–57.

15. Jiang, Y., Crocetti, R., 2019: CLT-concrete composite floors with notched shear connectors. Construction and Building Materials 195: 127–139.

16. Jiang, Y., Crocetti, R., 2019: CLT-concrete composite floors with notched shear connectors. Construction and Building Materials 195: 127–139.

17. Kanócz, J., Bajzecerová, V., 2012: Influence of rheological behaviour on load-carrying capacity of timber-concrete composite beams under long term loading. Procedia Engineering 40: 20–25.

18. Kanócz, J., Bajzecerová, V., Šteller, Š., 2013: Timber–concrete composite elements with various composite connections. Part 1: Screwed connection. Wood Research 58(4): 555-570.

19. Khorsandnia, N., Schänzlin, J., Valipour, H., Crews, K., 2015: Coupled finite element-finite difference formulation for long-term analysis of timber-concrete composite structures. Engineering Structures 96: 139–52.

20. Lukaszewska, E., Johnsson, H., Fragiacomo, M., 2008: Performance of connections for prefabricated timber-concrete composite floors. Materials and Structures/Materiaux et Constructions 41(9): 1533–1550.

21. Loebus, S., Structures, T., Winter, S., 2017: Two-way spanning timber-concrete-composite-slabs. Development of construction and design methods for two-way spanning Timber-Concrete-Composite constructions Objective and initial situation of the research project Realization of the research project Shea, 6 pp.

22. Mai, K.Q., Park, A., Nguyen, K.T., Lee, K., 2018: Full-scale static and dynamic experiments of hybrid CLT–concrete composite floor. Construction and Building Materials 170: 55–65.

23. Makovická Osvaldová, L., Gašpercová, S., Mitrenga,P., Osvald, A., 2016: The influence of density of test specimens on the quality assessment of retarding effects of fire retardants. Wood Research 61(1): 35–42.

24. Makovicka Osvaldová, 2020: Wooden façades and fire safety effects of joint type on ignition behaviour. Springer Nature, 88 pp.

25. Surovec, L., Slivanský, M., 2015: Teoretická analýza spriahnutého drevo-betónového stropu RD v Stupave (Theoretical analysis of a composite wood-concrete ceiling of a family house in Stupava).

26. Van Thai, M., Ménard, S., Elachachi, S.M., Galimard, P., 2020: Performance of notched connectors for CLT-concrete composite floors. Buildings 10(122): 21 pp.

KLARA FREUDENBERGER, JAROSLAV SANDANUS*
SLOVAK UNIVERSITY OF TECHNOLOGY IN BRATISLAVA
FACULTY OF CIVIL ENGINEERING
DEPARTMENT OF STEEL AND TIMBER STRUCTURES
RADLINSKÉHO 2766/11
810 05 BRATISLAVA
*Corresponding author: jaroslav.sandanus@stuba.sk

RESEARCH ON SHEAR PERFORMANCE OF COMPONENTS CONNECTED BY BEECH AND SELF-TAPPING SCREW COMPOSITE DOWELS

XUDONG ZHU[1,2,3]
[1]NANJING FORESTRY UNIVERSITY
[2]YANGZHOU POLYTECHNIC INSTITUTE
[3]YANGZHOU UNIVERSITY
CHINA

YINGYING XUE, XUEWEN ZHANG, PENGFEI QI, JIE SHEN
YANGZHOU POLYTECHNIC INSTITUTE
CHINA

CHANGTONG MEI
NANJING FORESTRY UNIVERSITY
CHINA

ABSTRACT

This study examined the properties of components connected by beech and self-tapping screw composite dowels (group C). As a contrast, the components connected by beech dowels and self-tapping screws individually were tested. The test results indicated that the properties of the components connected by beech dowels (group B) were better than those connected by self-tapping screws (group S), except the ductility coefficient, final displacement, and energy consumption. On the other hand, the main failure modes of groups B and S were the broken beech dowel and the bent self-tapping screw, respectively. For group C, two peak values could be found which were larger than the maximum load of groups B and S, respectively. The properties of group C were better than those of groups B and S, except that the final displacement and energy consumption were located between those of groups B and S. Meanwhile, the linear equation in two unknowns have be found between groups B, S and C.

KEYWORDS: Beech dowel, self-tapping screw, composite dowel, shear performance.

INTRODUCTION

With the development of wood based engineering materials, especially laminated timber and cross-laminated timber (CLT), self-tapping screw (STS) connection was studied (Chen et al. 2019). Meanwhile, traditional wood dowels were also used to connect the CLT as a green and low carbon alternative (Hao et al. 2020, Bui et al. 2020, Li et al. 2020). Furthermore, a new wood dowel friction welding technology was another attempt (Bocquet et al. 2007, Bocquet et al. 2017, Girardon et al. 2014, Satoshi et al. 2017).

For the properties of components connected by STS, the lateral resistance performance of hex-head STS joint was better than that of wire nail joint except deforming ability (Sun et al. 2019). Considering the thread, the maximum load of screws with both double-threaded sections and fully threaded shanks were higher than those of single-threaded screws (Yeh et al. 2014). In the field of connecting the glulam, STS was often used with steel plate. Komatsu et al. (2019) studied the relationship between predicted nonlinear behaviors and observed ones. On the other hand, the influence of the angle of inclined screws was a research highlight. It was found that Tomasi model could be used to analyze the slip modulus of steel-wood joints when the angle between 45° to 90° (Lu et al. 2020). However, in the other study, an insertion angle of 30° had a larger stiffness and strength than a 45° angle (Mirdad et al. 2019, 2020a,b). Furthermore, if the length of STS was longer, the joint could increase the screwed in depth, then a higher shear properties obtained. Meanwhile, in this paper, Wang et al. (2020) proposed to use tapper washers to steady the inclined screws.

Based on the application of STS in the CLT. With the increased diameter and length, the shear strength could be improved (Sullivan et al. 2018, Dong et al. 2018). The stiffness and strength of specimens increased with the increase of angle too (Brown et al. 2020, Chang et al. 2019). Compared to the mortise-tenon connections in CLT, the STS connections failed before the damage of CLT, while the mortise-tenon connections did not failed (Lin et al. 2019). According to the Eurocode 5 and the study of Hossain et al. (2019), the group effect was 0.9n for all joints under static loading. In case of cyclic loading, a more pronounced group effect was observed that can be expressed as $n^{0.9}$ (n was the number of connected joints). Besides, self-tapping screws were used to connect the wooden parallel chord trusses. Fatal pull-out of self-tapping screws occurred by accompanying with bottom chord bending failure (Komatsu et al. 2018).

With the extending of using time, the cracks of the glulam and mortise-tenon joints occurred. Several researches have been studied the reinforcement by STS. The STS reinforcement could improve the capacity of glulam beam with cracks. This reinforcement method could prevent the development of cracks in the glulam beam during the bearing process (Petrycki et al. 2020, Zhang et al. 2019a,b). Johan et al. (2005) have found that the capacity of the reinforcement beams could improve 50% compared to the unreinforced beams. The compressive behavior increased obviously for the glulam specimens with self-tapping screws reinforcement. The length, number and the arrangement of the self-tapping screws had great influences on the failure modes and the load-carrying capacity (Tang et al. 2021). While in the reinforcement of mortise-tenon joints, the 5th percentile value of the capacity of beams with half-lap joint and round dovetail joint reinforced by self-tapping screws could reach

75.8-76.7% and 75.9-77.5% of that of the intact beams, respectively (Li et al. 2019). Song et al. (2018) studied the lateral performance of traditional heavy timber frames with mortise-tenon joints retrofitted using STS. The retrofitted frames exhibited smaller stiffness, larger deformability, higher damping ratio, and similar strength degradation from primary cycles to trailing cycles. In the research of Sun et al. (2018), it concluded that steel plates and STS are suitable for the strengthening of mortise-tenon joints, the strength or rigidity of which is obviously inadequate.

In this study, a new beech and self-tapping screw composite dowel was proposed. This composite dowel could have both of the features of STS and wood dowel. In the study of Zhu et al. 2017, 2018, 2019), the wood dowel could be broken by twisting. On the other hand, Liu et al. (2019) found that the twisting would be avoided when compressed wood was used, and the pullout resistance of compressed wooden dowel rotary friction welding could be increased. While in this paper, the twisting should also be avoided by using beech dowel instead of birch dowel, and the new composite dowel structural form. The shear performance of the component connected by the composite dowels was studied in this paper.

MATERIAL AND METHODS

Materials

Wood dowels, 12 mm in diameter and 70 mm in length, were fabricated from beech wood (*Zelkova schneideriana*, Crownhomes, Jiangsu, China). The dried density at 2% MC of the beech dowel was 703 kg·m^{-3}. Self-tapping screws (Moregood, Shanghai, China), 5.2 mm in diameter and 70 mm in length, was covered by hot galvanizing. Spruce-pine-fir (SPF; Crownhomes, Jiangsu, China) slats with the dimensions of 89 mm (width, W) × 38 mm (thickness, T) × 300 mm (length, L) were used as substrates. The air dried density at 9.7% MC of the larch was 495 kg·m^{-3}.

Specimen preparation

Group B (two beech dowels group): the wood substrates with the dimensions of 89 × 38 × 300 mm were pre-drilled with holes 10 mm in diameter and 70 mm in depth. Next, the wood dowels were welded into the pre-drilled holes in the substrates to create bonded joints at a high-speed rotation of 1500 rpm (Fig. 1b). Three specimens were prepared for each group.

Group S (two self-tapping screws group): the wood substrates with the dimensions of 89 × 38 × 300 mm were pre-drilled with holes 3 mm in diameter and 70 mm in depth. Next, the self-tapping screws were screwed into the pre-drilled holes in the substrates by electric hand drill. Three specimens were prepared for each group.

Group C (two composite dowels group): the wood dowels were pre-drilled with holes 3 mm in diameter and 70 mm in depth using a drilling machine. Then the self-tapping screws were screwed into the pre-drilled holes. Meanwhile, the wood substrates with the dimensions of 89 mm × 38 mm × 300 mm were pre-drilled with holes 10 mm in diameter and 70 mm in depth using a drilling machine. Next, the wood dowels were welded into the pre-drilled holes in the substrates to create bonded joints at a high-speed rotation of 1500 rpm (Fig. 1b). Three specimens were prepared for each group.
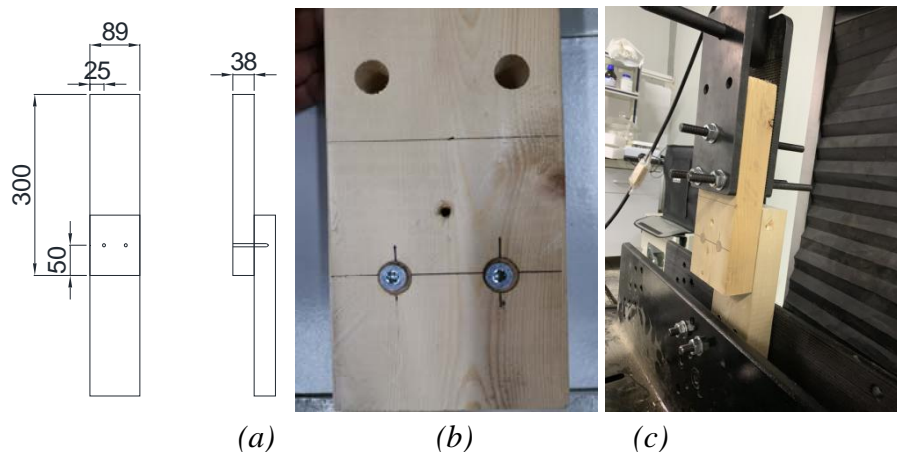
(a) *(b)* *(c)*

Fig. 1: The size of shear performance samples (a), samples of group C (b), and WDW-300E universal testing equipment.

Methods

Pullout resistance test

All the specimens were conditioned at 20°C and 60% relative humidity for 7 days before the tests were conducted. The pullout resistance of the specimens was tested using a universal testing machine (Fig. 1c, WDW-300E; Jinan Popwil, Jinan, China) at a speed of 5 mm·min^{-1}.

Analysis method of characteristic value

All the force-displacement curves were obtained from the shear performance tests. Then each force-displacement curve was analyzed by analysis method of characteristic value (Fig. 2). According to this analysis, seven parameters which were maximum load (Pmax), ultimate load (Pu), yield load (Py), initial stiffness (Ki), ductility coefficient (µ), energy consumption (S) and final displacement (Du) could be calculated in Tabs. 1-3. From Fig. 2, six lines could be calculated and derived from the force-displacement curve. They were listed below:

I - the line connected by the points 0.1·Pmax and 0.4·Pmax;

II - the line connected by the points 0.4·Pmax and 0.9·Pmax;

III - move the line II to the tangent point of the force-displacement curve;

IV - draw a horizon line at the intersection of line I and III, extend the horizon line to the force-displacement curve, then the ordinate value was Py, the abscissa value was Dy;

V - the line connected by the point (0, 0) and (Dy, Py), the slope of the line was initial stiffness Ki;

VI - draw a line created the shadow area of figure which was equal to the area created by the force-displacement curve, X-ray, and the line X=Du, the ratio of Du and Dv was ductility coefficient µ.
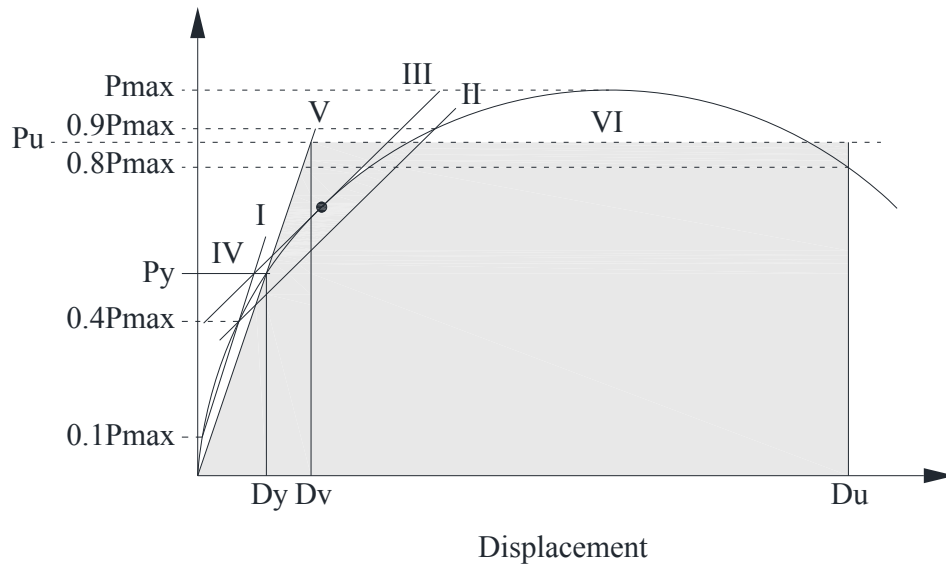
Fig. 2: Analysis method of characteristic value.

RESULTS AND DISCUSSION

The analysis of the curves and failure modes

All the curves of specimens were showed in Fig. 3. From Fig. 3a, all the maximum loads of group S were located at the displacement range of 20-25 mm. From Fig. 3b, three differences could be observed. First of all, the maximum loads of all the groups B were located at the displacement range 5-11 mm which were much smaller than those of the groups S. Second, when the loads were reached to the maximum value, they were decreased sharply to the zero. In the study of Hao et al. (2020) and Li et al. (2020), broken wood dowels were the main form of failure during the shear test. The similar phenomena were found in Fig. 5a, the broken beech dowels were the main failure modes of groups B. While from Fig. 4, the bending of self-tapping screws were the primary failure modes of group S. On the other hand, from Fig. 4d, the broken self-tapping screws after bending were the alternative failure modes of groups S. The failure modes of self-tapping screws were in accordance with Dong et al. (2018) and Lin et al. (2019). Third, the data diversity of groups B was much larger than that of groups S. The properties of self-tapping screws were similar to each other because the self-tapping screws were made from metal which was isotropic material. But beech wood was anisotropic material.

From Fig. 3c, one obvious difference could be found. Two peak values were observed. The first peak value was located at the range of 5-10 mm. And the second peak value was located at the range of 20-25 mm. The failure modes of groups C were showed in Fig. 5b. All the specimen showed the same failure mode. During all the test process, the bent of self-tapping screws and broken of beech dowels occurred simultaneously. On the other hand, combined with the two peak values, the beech dowels were broken when the curves reached to the first peak value. The self-tapping screws were bent to the limit state when the curves reached to the second peak value.
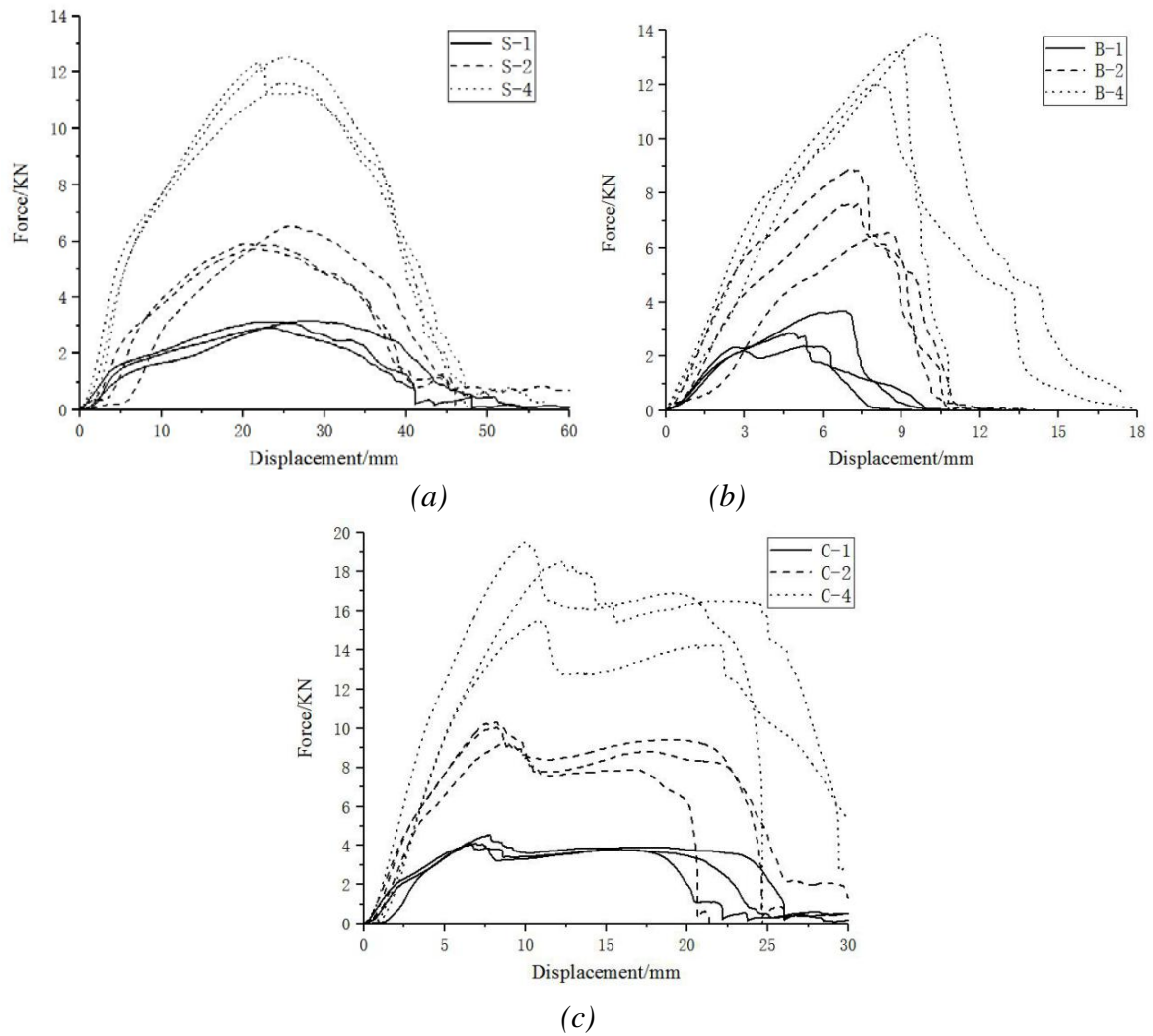
(a) *(b)*

(c)

Fig. 3: Force displacement curves of group S (a), B (b), and C (c).

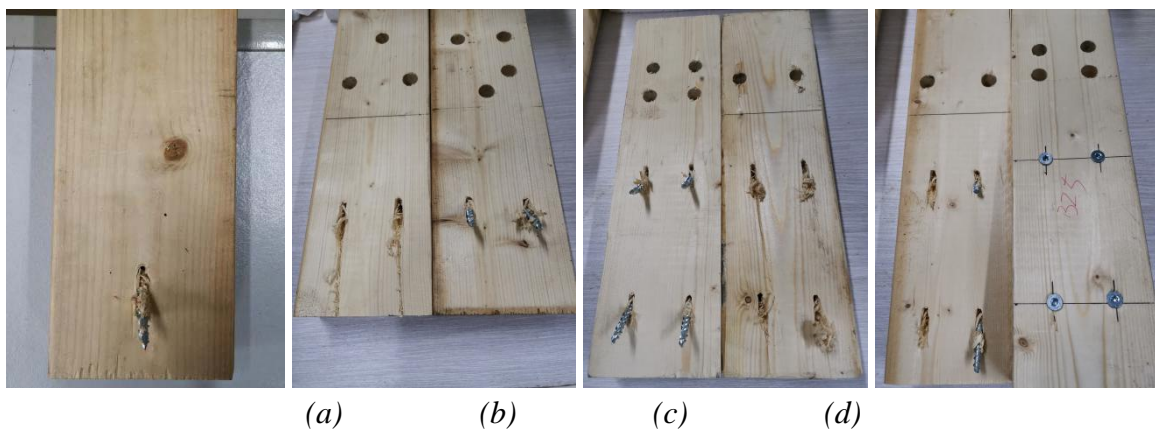*(a)* *(b)* *(c)* *(d)*

Fig. 4: Failure mode of group S-1 (a), S-2 (b), S-4-1 (c), and S-4-3 (d).

(a)   *(b)*
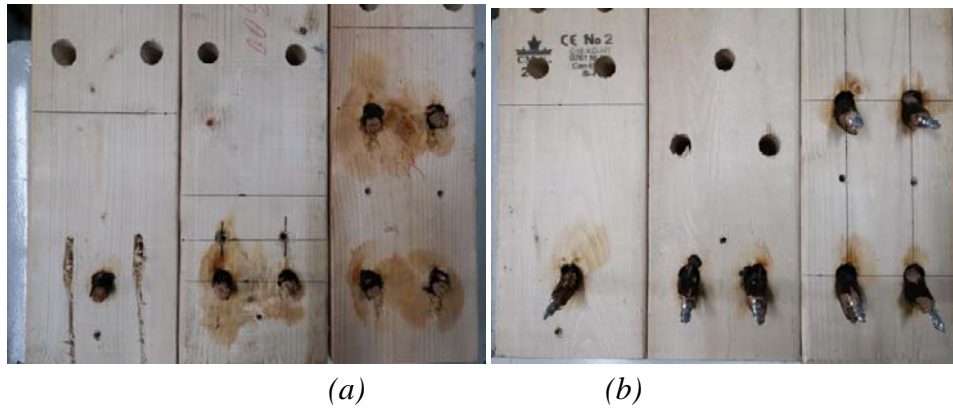
Fig. 5: Failure mode of group B (a), and C (b).

Tab. 1: Shear performance of group S.

Parameters	S-1			S-2			S-4		
	S-1-1	S-1-2	S-1-3	S-2-1	S-2-2	S-2-3	S-4-1	S-4-2	S-4-3
Maximum load (kN)	2.910	3.150	3.130	5.910	5.740	6.540	11.300	12.350	12.520
	3.063(0.133)[1]			6.063(0.421)			12.057(0.661)		
Yield load (kN)	1.340	1.316	1.430	3.010	2.555	3.023	5.330	5.065	5.660
	1.362(0.060)			2.863(0.267)			5.532(0.298)		
Ultimate load (kN)	2.420	2.627	2.640	5.216	5.000	5.550	9.865	10.360	10.895
	2.562(0.123)			5.255(0.277)			10.373(0.515)		
Initial stiffness (kN·mm^{-1})	0.294	0.219	0.366	0.404	0.457	0.288	0.903	1.099	0.897
	0.293(0.074)			0.383(0.086)			0.966(0.115)		
Ductility coefficient	3.761	3.134	4.283	2.467	2.920	1.788	3.189	3.446	2.798
	3.726(0.575)			2.392(0.570)			3.144(0.326)		
Final displacement (mm)	30.948	37.529	30.908	31.838	31.912	34.503	34.854	32.490	33.973
	33.128(3.811)			32.751(1.518)			33.772(1.195)		
Energy consumption (kN·mm)	64.938	82.850	72.053	132.41	132.26	137.96	289.97	287.75	304.04
	73.280(9.019)			134.21(3.248)			293.92(8.834)		

[1]Values in parentheses are the standard deviation.

Tab. 2: Shear performance of group B.

Parameters	B-1			B-2			B-4		
	B-1-1	B-1-2	B-1-3	B-2-1	B-2-2	B-2-3	B-4-1	B-4-2	B-4-3
Maximum load (kN)	3.690	2.380	2.860	6.560	7.610	8.900	13.200	12.050	13.900
	2.977(0.663)			7.690(1.172)			13.050(0.934)		
Yield load (kN)	1.945	2.052	1.647	4.440	3.690	4.910	7.676	7.322	5.612
	1.881(0.210)			4.347(0.615)			6.870(1.104)		
Ultimate load (kN)	3.068	2.128	2.478	5.580	6.343	7.630	11.620	10.253	12.533
	2.558(0.475)			6.518(1.036)			11.469(1.148)		
Initial stiffness (kN·mm^{-1})	0.982	0.804	0.873	0.946	1.477	1.946	1.953	2.185	1.634
	0.886(0.090)			1.456(0.500)			1.924(0.277)		
Ductility coefficient	2.300	2.378	1.892	1.543	1.865	1.975	1.562	1.895	1.420
	2.190(0.261)			1.794(0.225)			1.626(0.244)		
Final displacement (mm)	7.185	6.292	5.370	9.103	8.008	7.745	9.295	8.895	10.886
	6.282(0.908)			8.285(0.720)			9.692(1.053)		
Energy consumption (kN·mm)	17.240	10.570	9.792	33.366	37.175	44.128	73.415	67.139	88.370
	12.534(4.094)			38.223(5.457)			76.308(10.904)		

Tab. 3: Shear performance of group C.

Parameters	C-1			C-2			C-4		
	C-1-1	C-1-2	C-1-3	C-2-1	C-2-2	C-2-3	C-4-1	C-4-2	C-4-3
Maximum load (kN)	4.030	4.540	4.120	10.040	9.280	10.300	19.520	18.510	15.500
	4.230(0.272)			9.873(0.530)			17.843(2.091)		
Yield load (kN)	1.862	1.890	2.400	4.634	4.766	4.776	9.640	9.404	8.832
	2.051(0.303)			4.725(0.079)			9.292(0.415)		
Ultimate load (kN)	3.576	3.747	3.601	8.457	7.832	8.967	16.613	16.232	13.326
	3.641(0.092)			8.419(0.568)			15.390(1.798)		
Initial stiffness (kN.mm-1)	1.055	0.881	0.695	1.805	1.502	1.775	2.625	1.917	1.882
	0.877(0.180)			1.694(0.167)			2.141(0.419)		
Ductility coefficient	6.214	4.198	4.614	4.796	3.455	4.446	3.373	2.957	3.252
	5.009(1.064)			4.232(0.696)			3.194(0.214)		
Final displacement (mm)	21.061	17.847	23.911	22.477	18.019	22.464	21.345	25.039	23.028
	20.940(3.034)			20.987(2.570)			23.137(1.849)		
Energy consumption (kN·mm)	69.254	58.908	76.766	170.281	120.702	178.779	302.040	337.707	259.691
	68.309(8.966)			156.587(31.367)			299.813(39.056)		

The difference of parameters among group B, S, and C

From Tabs. 1-3 and Fig. 6a, the maximum load increased with the number for all the groups which was illustrated above (Liu et al. 2015, Hossain et al. 2019). The maximum loads of groups C were higher than those of groups B and S individually, but lower than the sum of groups B and S. On the other hand, the second peak values were existed in groups C beside the maximum loads. The sum of the two peak values was much higher than the sum of the group B and S.

From Fig. 6b, the initial stiffness of groups S was the lowest. While the initial stiffness of groups B was a little lower than that of groups C. From the curves of Fig. 3, in the displacement range of 0-5 mm, the curve shape of groups C was similar to that of groups B which increased sharply. The curve shape of groups S increased slowly. Based on these phenomena, the initial stiffness of groups S was much lower than that of the other two groups (Dong et al. 2015, Xiong et al. 2011). With the increased connector number, the initial stiffness showed the increasing trend.

From Fig. 6c, the final displacement of groups S was the largest. On the contrast, the final displacement of groups B showed the lowest value. While the final displacement of groups C was situated between the groups B and S. For the same groups, the final displacement of different connector number did not show obvious difference. From Fig. 6d, the ductility coefficient of groups B was the lowest because the final displacement of groups B was the lowest. For the groups C, the ductility coefficient was the highest, because the final displacement of them was higher than that of groups B, the initial stiffness of groups C was higher than that of groups S. On the other hand, the initial stiffness increased with the connector number (Liu et al. 2015), while the final displacement did not showed the obvious change with the connector number. Based on this, the ductility coefficient showed the downward trend with the connector number. From Fig. 6e, the changing trend of energy consumption was similar to that of maximum load in Fig. 6a.
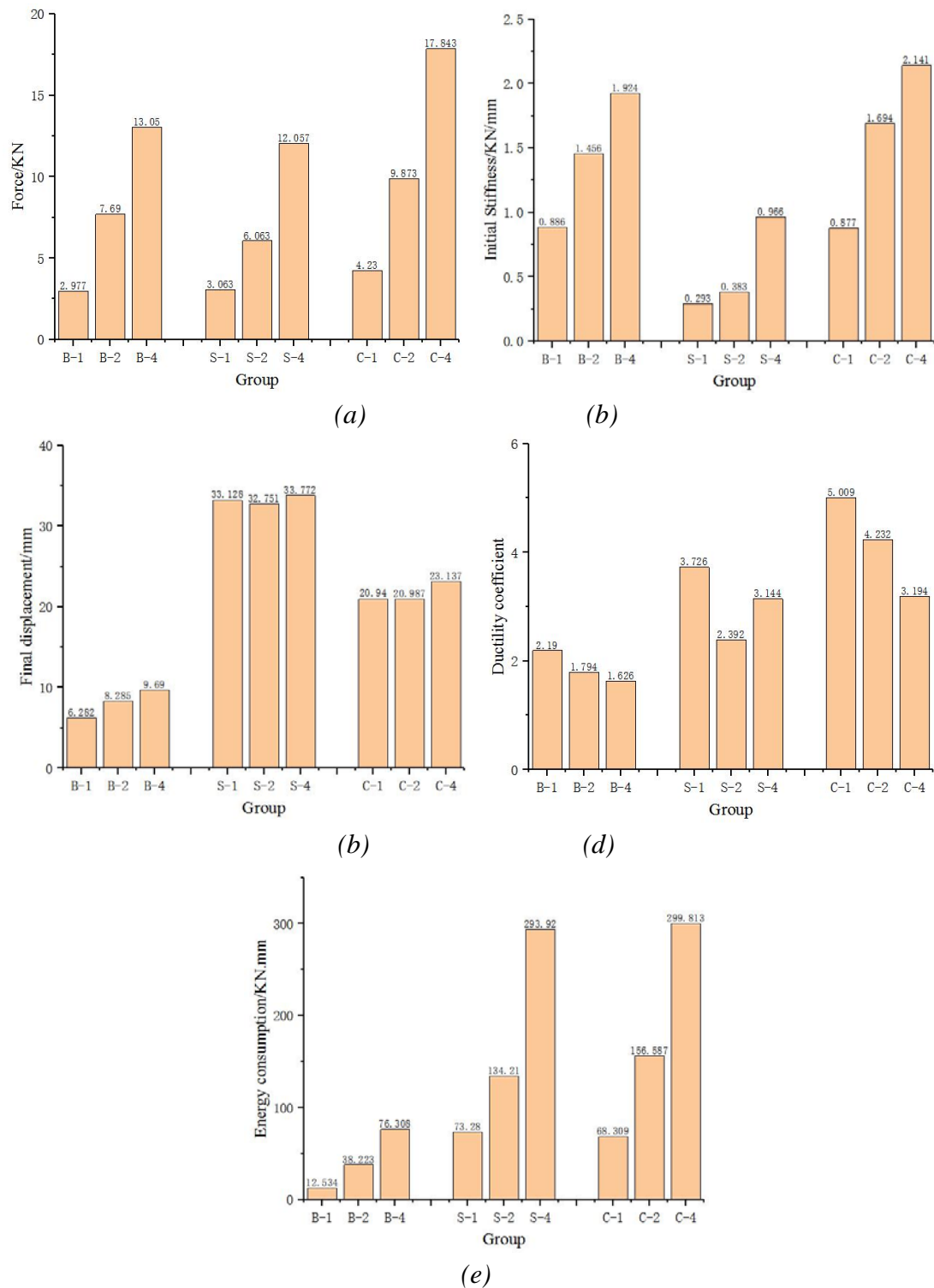
Fig. 6: The difference of maximum load (a), initial stiffness (b), final displacement (c), ductility coefficient (d), and energy consumption (e) between group B, S, and C.

The relationship between group B, S, and C

The relationship between groups B, S, and C was studied below (Xue et al. 2020). The value of group B-1, and B-2 was set as *x*, the value of group S-1, and S-2 was set as *y*, and the value of group C-1 and C-2 was set as *z*. Then the linear equation in two unknowns could be

observed. And then using the formulas, the calculated values of groups C-3 could be found in Tab. 4. On the other hand, the errors between calculated values and testing values could also be found in Tab. 4. The errors of the parameters of yield load, initial stiffness, and ductility coefficient were higher than 10%. So this evaluation method could not be used in these three parameters reasonably. However, in the other five parameters, this analysis method could be a good choice, especially the maximum load, the second peak value, and ultimate load. According to this study, the maximum load, the second peak value, and ultimate load of groups C could be calculated accurately. In the future study, more evidence of the relation between groups B, S, and C could be explored:

Maximum load: $z = 0.57x + 0.835y$ (1)

The second maximum load: $z = 0.707x + 0.575y$ (2)

Yield load: $z = 0.052x + 1.053y$ (3)

Ultimate load: $z = 0.674x + 0.748y$ (4)

Initial stiffness: $z = -2.566x + 1.839y$ (5)

Ductility coefficient: $z = -0.195x + 2.619y$ (6)

Final displacement: $z = 0.606x + 0.138y$ (7)

Energy consumption: $z = 0.579x + 2.062y$ (8)

Tab. 4: The difference between calculated value and test value.

Parameters	Maximum load	The second maximum load	Yield load	Ultimate load
Calculated value	17.762	16.026	7.520	15.574
Test value	17.843	15.877	9.292	15.390
Error (%)	0.45	0.94	19.07	1.19
Parameters	Initial stiffness	Ductility coefficient	Final displacement	Energy consumption
Calculated value	1.058	3.645	21.799	327.666
Test value	2.141	3.194	23.137	299.813
Error (%)	50.57	14.13	5.78	9.29

CONCLUSIONS

(1) The maximum load, yield load, ultimate load, and initial stiffness of groups B were better than those of groups S. The ductility coefficient, final displacement, and energy consumption of groups B were lower than those of groups S. The main failure mode of groups B was the broken beech dowel. While for groups S, the bent self-tapping screw was the main failure mode. *(2)* The maximum load, yield load, ultimate load, initial stiffness, and ductility coefficient of groups C were better than those of groups B, and S. Two peak values could be found in groups C. The first and second peak values were larger than those of groups B and S, respectively. The final displacement and energy consumption of groups C were located between those of groups B and S. *(3)* The linear equation in two unknowns have be found between groups B, S and C. It could be used to calculate the maximum load, the second peak value, and ultimate load of groups C, when the parameters of groups B and S were obtained.

ACKNOWLEDGMENTS

REFERENCES

1. Bocquet, J.F., Pizzi, A., and Despres, A., Mansouri, H.R., Resch, L., Michel, D., Letort, F., 2017: Wood joints and laminated wood beams assembled by mechanically-welded wood dowels. Journal of Adhesion Science and Technology 21(3/4): 301- 317.
2. Bocquet, J.F., Pizzi, A., Resch, L., 2007: Full-scale industrial wood floor assembly and structures by welded-through dowels. European Journal of Wood and Wood Products 65(2): 149-155.
3. Brown, J.R., Li, M.H., Tannert, T., Moroder, D., 2020: Experimental study on orthogonal joints in cross-laminated timber with self-tapping screws installed with mixed angles. Engineering Structures 228(1): 1-14.
4. Bui, T.A., Oudjene, M., Lardeur, P., Khelifa, M., Rogaume, Y., 2020: Towards experimental and numerical assessment of the vibrational serviceability. Engineering Structures 216: 1-10.
5. Chang, C., Fang, Y.F., Liu, Y.F., Que, Z.L., 2019: Study on pull-out performance of tilted self-tapping screw in cross-laminated timber. Architecture Technology 50(4): 416-418.
6. Chen, H., Liu, Z.B., Li, S.Z., He, X.P., 2019: A summary of research on the connection performance of new self-tapping screws in wood structures. Shanxi Architecture 45(1): 34-35.
7. Dong, W.B., Gao, Y., Yu, Z.M., Yuan, T.G., 2015: Experimental research on MIDPLY shear wall nail joints of light wood structures. Building Structure 45(6): 54-57.
8. Dong, W.Q., Yao, Y., Song, H., Qi, Y.Y., Ren, H.Q., Wang, Z.Q., 2018: Shear strength of cross-laminated timber connected with self-tapping screws. China Wood Industry 32(5): 1-5.
9. Girardon, S., Barthram, C., Resch, L., Bocquet, J.F., Triboulot, P., 2014: Determination of shearing stiffness parameters to design multi-layer spruce beams using welding-through wood dowels. European Journal of Wood and Wood Products 72(6): 721-733.
10. Hao, J.X., Xu, L., Wu, X.F., Li, X.J., 2020: Analysis and modeling of the dowel connection in wood T type joint for optimal performance. Composite Structures 253:1-11.
11. Hossain, A., Popovski, M., Tannert, T., 2019: Group effects for shear connections with self-tapping screws in CLT. Journal of Structural Engineering 145(8): 1-9.

12. Johan, J., 2005: Load carrying capacity of curved glulam beams reinforced with self-tapping screws. Holz. als Roh- und Werkstoff 63: 342-346.

13. Komatsu, K., Teng, Q.C., Li, Z.R., Zhang, X.L., Que, Z.L., 2018: Experimental and numerical analyses on nonlinear behaviour of wooden parallel chord trusses composed of self-tapping screws. Journal of Wood Science 64(2): 776-793.

14. Komatsu, K., Teng Q.C., Li, Z.R., Zhang, X.L., Que, Z.L., 2019: Experimental and analytical investigation on the nonlinear behaviors of glulam moment-resisting joints composed of inclined self-tapping screws with steel side plates. Advances in Structural Engineering 22(15): 3190-3206.

15. Li, H.M., Lam, F., Qiu, H.X., 2019: Comparison of glulam beam-to-beam connections with round dovetail and half-lap joints reinforced with self-tapping screws. Construction and Building Materials 227: 1-11.

16. Li, Q., Song, H., Wang, Z.Q., 2020: Bending performance of timber composite beam fastened with bamboo/wood dowels. Journal of Northwest Forestry University 35(2): 218-222.

17. Lin, Q. Y., Wen, C. S., Diao, Y., Yan, L. R., Gao, Y., 2019: Mechanical properties of CLT shear connections between self-tapping screws and mortise tenons. Journal of Beijing Forestry University 41(11): 146-154.

18. Liu, K., 2019: Study on pullout resistance of compressed wooden dowel rotary friction welding. Master's thesis. Pp 34-48, Dalian University of Technology, China.

19. Liu, H.F., He, M.J., 2015: Effects of self-tapping screw on performance of glulam beam-to-column connections. Journal of Building Structures 7: 148-156.

20. Lu, X.R., Teng, Q.C., Li, Z.R., Zhang, X.L., Wang, X.M., Komatsu, K., Que, Z.L., 2020: Study on shear property of spruce glulam and steel plate connected with inclined screw. Journal of Forestry Engineering 5(3): 48-53.

21. Mirdad, M.A.H., Chui, Y.H., 2019: Load-slip performance of mass timber panel-concrete (MTPC) composite connection with Self-tapping screws and insulation layer. Construction and Building Materials 213: 696-708.

22. Mirdad, M.A.H., Chui, Y.H., 2020: Stiffness prediction of mass timber panel-concrete (MTPC) composite connection with inclined screws and a gap. Engineering Structures 207: 1-11.

23. Mirdad, M.A.H., Chui, Y.H., 2020: Strength prediction of mass-timber panel concrete-composite connection with inclined screws and a gap. Journal of Structural Engineering 146(8): 1-13.

24. Petrycki, A., Salem, S., 2020: Structural integrity of bolted glulam frame connections reinforced with self-tapping screws in a column removal scenario. Journal of Structural Engineering 146(10): 1-13.

25. Satoshi, F., Keita, O., Masaki, N., Yamasaki, M., Sasaki, Y., 2017: Shear properties of metal-free wooden load-bearing walls using plywood jointed with a combination of adhesive tape and wood dowels. European Journal of Wood and Wood Products 75(3): 429-437.

26. Song, X.B., Li, K., Crayssac, E., Wu, Y.J., 2018: Lateral performance of traditional heavy timber frames with mortise-tenon joints retrofitted using self-tapping screws. Journal of Structural Engineering 144(10): 1-10.

27. Sullivan, K., Miller, T.H., Gupta, R., 2018: Behavior of cross-laminated timber diaphragm connections with self-tapping screws. Composite Structures 168: 505-524.

28. Sun, Y.H., Jiang Z.H., Zhang X.B., Sun, Z.J., Liu, H.R., 2019: Behavior of glued laminated bamboo and bamboo-oriented strand board sheathing-to-framing connections. European Journal of Wood and Wood Products 77: 1189-1199.

29. Sun, Z.Y., Cheng, X.W., Lu, W.D., 2018: Experimental study on seismic performance of damaged straight mortise-tenon joints of ancient timber buildings strengthened with steel plates and self-tapping screws. Structural Engineers 34(5): 106-112.

30. Tang, L.Q., Xu, W., Yang, H.F., Tan, G.H., Chen, Y., 2021: Compressive strength tests perpendicular to the grain of glulam reinforced with self-tapping screws. Journal of Nanjing Technology University (Natural Science Edition) 43(1): 94-100.

31. Wang, C.L., Lyu, J.F., Zhao, J., Yang, H.F., 2020: Experimental investigation of the shear characteristics of steel-to-timber composite joints with inclined self-tapping screws. Engineering Structures 215(15): 1-17.

32. Xiong, H.B., Pan, Z.F., Kang, J.H., Hua, M.X., 2011: Test study on behavior of stud-to-sheathing nail joints under monotonic load in light wood frame constructions. Structural Engineers 6: 106-112.

33. Xue, Y.Y., Zhu, X.D., 2020: Study on the relationship between the MOE of lumbers and nail-laminated timbers. China Forest Products Industry 5:16-20.

34. Yeh, M.C., Lin, Y.L., Huang, G.P., 2014: Investigation of the structural performance of glulam beam connections using self-tapping screws. Journal of Wood Science 60: 39-48.

35. Zhang, C., Guo, H.B., Jung, K., Harris, R., Chang, W.S., 2019: Screw reinforcement on dowel-type moment-resisting connections with cracks. Construction and Building Materials 215: 59-72.

36. Zhang, C., Guo, H. B., Jung, K., Harris, R., Chang, W. S., 2019: Using self-tapping screw to reinforce dowel-type connection in a timber portal frame. Engineering Structures 178: 656-664.

37. Zhu, X.D., Gao, Y., Yi, S., Ni, C., Zhang, J., Luo, X., 2017: Mechanics and pyrolysis analyses of rotation welding with pretreated wood dowels. Journal of Wood Science 63(3): 216-224.

38. Zhu, X.D., Xue, Y.Y., Zhang, S.J., Zhang, J., Shen, J., Yi, S.L., Gao, Y., 2018: Mechanics and crystallinity/thermogravimetric investigation into the influence of the welding time and $CuCl_2$ on wood dowel welding. BioResources 13(1): 1329-1347.

39. Zhu, X.D., Xue, Y.Y., Shen, J., Zhang, S.J., 2019: Withdrawal strength of welded dowel joints made of birch and larch wood. Wood Research 64(5): 921-934.

XUDONG ZHU[1,2]
[1]NANJING FORESTRY UNIVERSITY
JIANGSU, 210037
[2]YANGZHOU POLYTECHNIC INSTITUTE
[3]YANGZHOU UNIVERSITY
JIANGSU, 225100
CHINA

YINGYING XUE, XUEWEN ZHANG, PENGFEI QI, JIE SHEN
YANGZHOU POLYTECHNIC INSTITUTE
JIANGSU, 225100
CHINA

CHANGTONG MEI[*]
NANJING FORESTRY UNIVERSITY
JAINGSU, 210037
CHINA
*Corresponding author: mei@njfu.edu.cn

THE INFLUENCE OF ENCLOSURE ON BURNING CHARACTERISTICS OF OSB FURNISHINGS

VLADIMÍR MÓZER, PETR HEJTMÁNEK, DANIELA PITELKOVÁ
CZECH TECHNICAL UNIVERSITY IN PRAGUE
CZECH REPUBLIC

HASALOVÁ LUCIE
TECHNICAL INSTITUTE OF FIRE PROTECTION IN PRAGUE
CZECH REPUBLIC

ABSTRACT

This paper presents a series of full-scale tests conducted with office furniture made from OSB boards. Ignition source (30 kW gas burner) position and enclosure effects, free burn vs. ISO 9705 room, were evaluated from the perspective of instantaneous (HRR) and total heat (THR) released by the fuel packages. It was found that both of the evaluated factors have impact primarily on HRR – the peak ranging from 874 kW to 1 154 kW was delayed by approx. 50 to 60 s in the free-burn experiments; the THR remained relatively consistent at approx. 875 ± 30 MJ, meaning that in the observed period very similar amounts of fuel were burned. The thermal feedback within the enclosure seemed to be partially counteracted by the lack of oxygen, resulting in slightly higher HRR in free-burn test following the first peak. The findings of the research are applicable to fire hazard prediction by fire modelling.

KEYWORDS: OSB, thermal feedback, oxygen concentration, heat release rate, room corner test.

INTRODUCTION

Agglomerated wood, or sheet wood materials are extensively used in construction, furniture manufacture and many other industries. As per the Global forest products facts and figures report 2018 (2019) reconstituted panels (OSB, particle boards and fibreboards) dominate other product categories in Northern America and Europe. In addition, OSB and particle board had the fastest growth in production, increasing by 25% and 13% respectively

over the period from 2014 to 2018. Most of this growth for both products occurred in Eastern Europe including the Russian Federation.

OSB (oriented strand board) boards are made from compressed-oriented wood strands in layers (usually 3) combined by adhesives. In Europe, the boards are mostly produced from pine and spruce, but for production is possible to use wood with density between 350-700 kg·m^{-2}. Individual strips of coniferous wood are about 0,4-0,8 mm × 6-25 mm × 75-130 mm. Longer strips are used for surface layers, smaller ones are in the middle of the board (Böhm et al. 2012). Their strength depends on used glue and thickness. Although the production companies in North America are still use PF adhesives in bigger share, PMDI, a mixture of monomeric diphenylmethane di-isocyanate and methylene-bridged oligo-aromatic isocyanates (Lay and Cranley 2003), is the primary adhesive system used in OSB production in Europe (Grunwald and Stroobants 2014, Grunwald 2014). Other types of glue used in production of OSB are urea formaldehyde (UF), melamine urea formaldehyde (MUF) of phenol-formaldehyde (PF). There are two standard formats of OSB boards sold in our region. The basic dimensions of the board with groove are 2 500 mm × 625 (675) mm. The dimensions of the plain-edge board are 2500 mm × 1250 mm. The thickness of OSB boards varies from 12 mm to 25 mm. They are divided into 4 types by their strength and moisture resistance (OSB-1 to OSB-4) according to EN 300 (2006).

Fire properties and hazards

The boards are usually classified according to EN 13501-1 to reaction-to-fire class D-s1,d0 (ČSN 73 0810 2016). This base classification is established in through the Classification without further testing (CWFT) principle. In case of OSB boards fulfilling EN 300 requirements, with a minimum density of 600 kg·m^{-3} and a minimum thickness of 15 mm, they may be classified as D-s2, d0 for applications excluding flooring and D_{FL}-s1 for flooring applications (Commision decision of 17 January 2003 establishing the classes of reaction-to-fire performance for certain construction products. Notified under document number C(2002) 4807 as amended). Further information on CWFT for wood-based products may be found in (Mikkola and Östman 2004, Östman and Mikkola 2006).

Since some applications require better fire performance, the market offers OSB boards with better reaction-to-fire classes, e.g. board called Kronospan OSB Firestop with reaction-to-fire class B-s1, d0.

To achieve better fire classification and improve fire performance of agglomerate wood products, various fire-retarding components are added to the binder and/or the outermost covering layers or protective films. Among recent research, Martinka et al. (2021) studied the effects of aluminium hydroxide; a comprehensive overview may be found in Aseeva et al. (2014).

Apart from construction material, OSB boards are also used to make furnishing. It is therefore necessary to understand fire hazards associated with such use. Important characteristics, from the fire-spread perspective, include the combination of critical heat flux and time to ignition. (Martinka et al. 2020) examined various OSB configurations and found the time to ignition to be as low as 19 s for the radiant heat flux of 19 kW·m^{-2} and the lowest critical heat flux to be below 10 kW·m^{-2}. Unlike massive wood elements (Dúbravská et al.

2020), sheet wood products, including OSB may be prone to twisting and bending particularly at lower thicknesses, leading to early disintegration of protective char layer.

When considering fire hazards in enclosures, it is important to be able to predict fire severity based on the limited experimental data available. Kadlic (2018) investigated various possibilities of prescribing burning fuel items and discussed differences in modelling results when free-burn and enclosure data were used. Wade (2019) proposed a mathematical approach to account for the enclosure effects on fuel packages and combustible constructions. This model accounts for thermal effects, vent mixing flow and oxygen concentration. Still, the appropriate experimental setup and data representation for fire modelling and engineering remain a significant question, as Babrauskas notes in (Hurley et al. 2016).

MATERIALS AND METHODS

The conducted full-scale fire tests are part of a complex research "Pyroboard" focusing on the computational modelling of pyrolysis and should serve for data validation. The main objective of the project is to describe the pyrolysis and burning of agglomerated wooden materials through a range of parameters collected by micro-, mid- and full-scale experimental research. This will allow proper mathematical modelling of wood burning.

The test specimens are made from Oriented strand board (OSB) satisfying requirements of EN 300. Since the objective was to establish the properties for plain furniture, no further materials are included in fire tests. Test setup represents an office desk with drawers under the desk next to its right leg and a shelf cabinet on the right side of the desk: Office desk consists of desk 1 600 × 800 mm with two board legs 800 × 800 mm and board trestle 1600 × 400 mm. Chest of drawers 400 mm wide, 600 mm deep and 700 mm high with 4 openable drawers 150 mm high. Shelf cabinet 400 mm wide, 400 mm deep and 1 600 mm high with 4 uniform shelf spaces. For slight fire load decrease the OSB boards of thickness 12.5 mm were used. Selected properties of the OSB boards are summarized in Tab. 1.

Tab. 1: Selected properties of OSB boards used as fuel load.

Property	Value
Density	610.7 kg·m^{-3}
Thermal conductivity at 20°C	0.19 ± 0.02 W·m^{-1}·K^{-1}
Specific heat (dry) at 20°C	1.18 kJ·kg^{-1}·K^{-1}

The boards were joined together mechanically with screws. Fire source that simulates fire of a trash bin is a gas burner put under the table. The heat output of the burner is constant 30 kW and the duration of the ignition period is 480 s (8 min). The whole process was done in the Fire laboratory of University centre of energy efficient building of Czech Technical University in Prague, where the Room corner test apparatus is installed. Room corner test (ISO 9705-1: 2016) consists of a small room (3.6 × 2.4 m and 2.4 m high) with one door opening and the exhaust hood 3.0 m × 3.0 m in front of the room. Exhaust fumes proceed to the analysers to obtain data of the heat release rate, so this apparatus can serve as a furniture calorimeter. Ventilation unit has maximal volume flow 3.5 m^3·s^{-1} (approx. 13.000 m^3 per hour).

There were four constellations executed differing firstly in the test setup location itself where the smoke and temperature accumulation is crucial and secondly in location of the burner: *(1)* If the furniture is located inside the room, it represents single-person office where the effect of single burning item should be more noticeable while installation under the exhaust hood where the fumes go straight to the ventilation is similar to well-ventilated open spaces with larger area to heat up (Fig. 1). It is assumed the fire inside the single-person office is more intensive and faster. *(2)* The burner was put either to the left next to the left table leg or to the right side of the working space next to the drawer chest (Fig. 2). Various location was chosen just to see whether any difference of the heat release occurs.
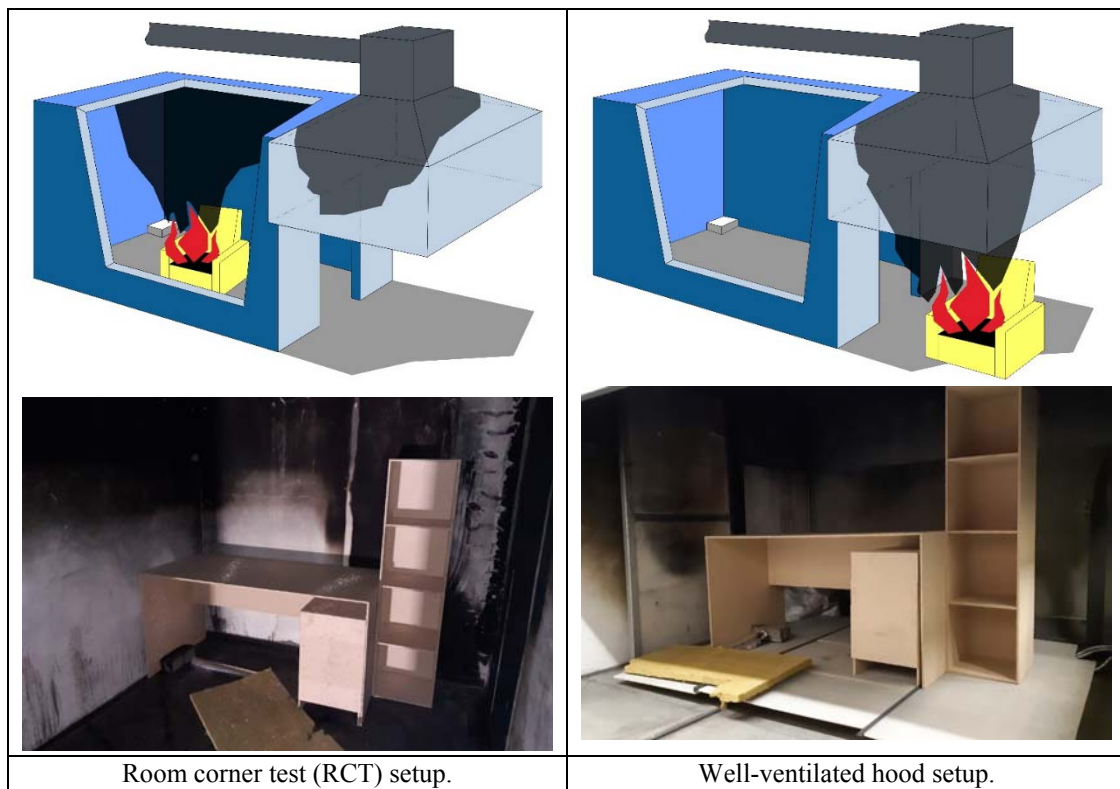

| Room corner test (RCT) setup. | Well-ventilated hood setup. |

Fig. 1: Indicative display of test configurations.

As mentioned before, the ventilation of the space, or exhausting the heated fumes respectively, seems to be crucial and can affect the test result in several ways. It is needed to say that due to calculation processes any change of the volume flow during the test results in the change of HRR (measurement error about 5% or more when the test is over ventilated). Constant flow is therefore favoured. The question was nevertheless which flow. On the one hand, higher volume flow, especially in the ignition phases of the well-ventilated test, entrained the flame causing a significant delay of the flame spread. On the other hand, in HRR peak times the hood was not capable to exhaust all the smoke products. Finally, there needed to be separate types of ventilation scenarios for the room and well-ventilated test: the room test setup had constant volume flow 60% (around 2.0 $m^3 \cdot s^{-1}$), the well-ventilated test setup started at 30% (1.0 $m^3 \cdot s^{-1}$) and after 500 s, when the furniture was definitely ignited, the volume flow

increased to 80% (2.8 m^3·s^{-1}). And there were situations when even such volume flow was not enough to exhaust all the fumes and had to be increased to 100%.

Fire experiment has no pre-set duration. Test started in T= 0 s with ventilation on according to the test setup and data collection, time step was set to t = 3 s. After 120 s, the gas burner was ignited (T = 120 s) and burned for 480 s (T = 600 s). Test procedure for both constellations can be found in Tab. 2.

Tab. 2: Timeline of the experiment.

Time (s)	Room corner test	Well-ventilated
0	test start, data collection extraction capacity @ 60%	test start, data collection extraction capacity @ 30%
120	burner 30 kW	burner 30 kW
500	—	extraction capacity @ 80%
600	burner off	burner off
Until burnout	Free burn	

Except the quantities characteristic for furniture calorimeter, such as heat release rate, smoke production rate or optical density, surface temperature at 10 points of the model furniture were collected (Fig. 2 and Tab. 3). Cable thermocouples type K, 2×0,5 mm^2 with mineral insulation were used. Tip of the thermocouples were shielded by 3 mm thick mineral fibre board. In this article, only thermocouples T02 a T03 will be discussed.
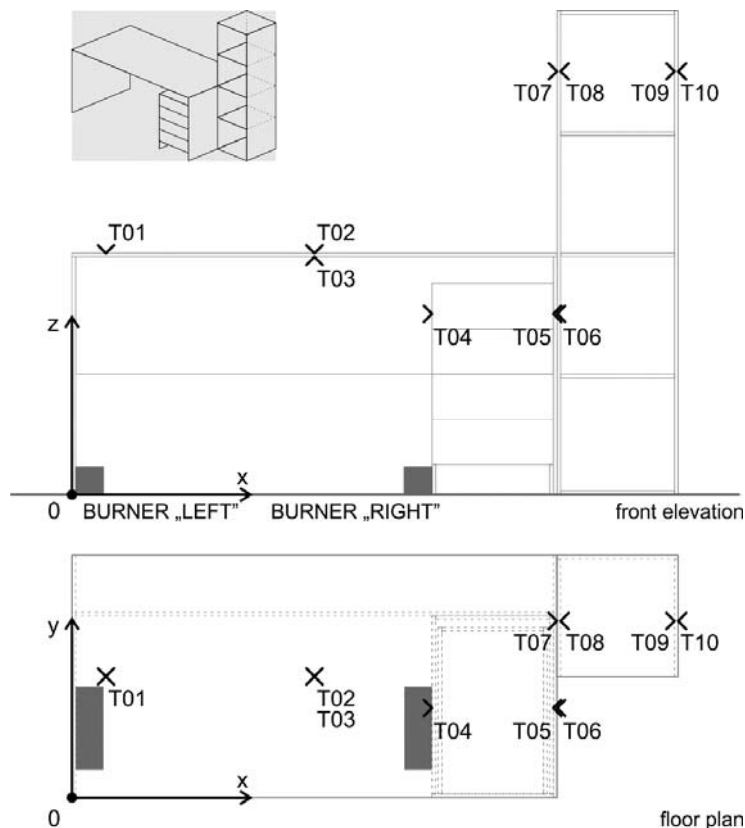

Fig. 2: Test setup with thermocouples location.

Tab. 3: Thermocouples T02 a T03 locations.

Txx	Location	x (mm)	y (mm)	z (mm)
02	On the upper side of the table desk	800	400	800
03	On the bottom side of the table desk	800	400	788

RESULTS AND DISCUSSION

The results from the first series of test burns conducted inside the ISO 9705 room are shown in Fig. 3. The results were shifted back by 120 s to discount the pre-burn period when the gas burner (ignition source) was off. After an initial delay of approximately 100 s there is a growth period until the first peak. The maximum HRR values reached for this scenario were 1132 kW (at 524 s) for ignition on the left side and 874 kW (at 510 s) for ignition on the right side.
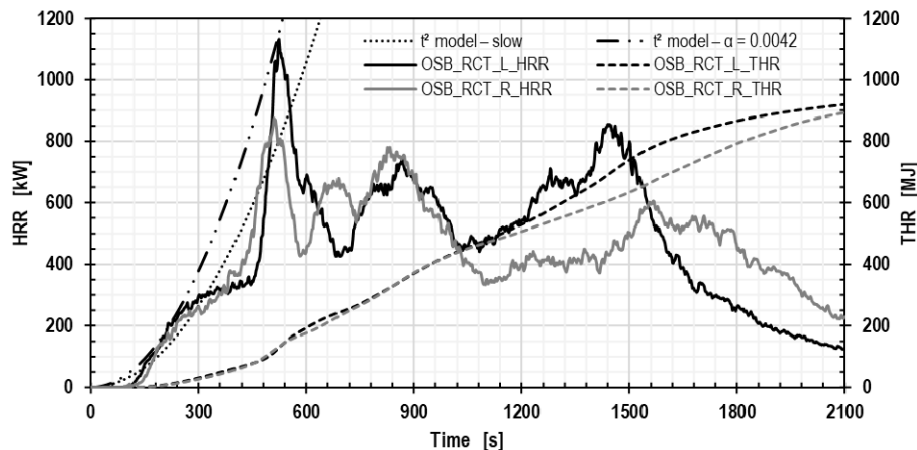

Fig. 3: Room corner test results for office furniture made from OSB; dotted line represents a t^2-model fit with α = 0.00293 kW·s^{-2} (slow) and α = 0.0042 kW·s^{-2} (custom).

The results from the second series of test burns conducted as free-burn tests under the hood are shown in Fig. 4. The results were again shifted back by 120 s to discount the period when the gas burner (ignition source) was off. After an initial delay of approximately 100 s there is a growth period until the first peak. Until approx. 600 s, the growth is relatively slow, followed by a steeper growth period for the next 50 - 100 s until the first peak is reached. This peak is associated with the fire spread under the desktop and rapid release of flammable pyrolysis gases from its surface as it is heated underneath. The subsequent development of fire and HRR is driven by progressive collapse of the furniture. The second prominent peak in the RCT_L scenario is caused by fire development on the shelves side. When fire was initiated on the right side (RCT_R) the peak is not as prominent.

Similar trends in HRR and the overall development of fire was observed in tests conducted in well-ventilated conditions under the hood, see Fig. 4. Due to the lack of thermal feedback, the effect of the enclosure, the development phase is prolonged, nonetheless after reaching approx. 375 - 400 kW there is a steep increase in HRR until the first peak is reached. There is

also a difference in the peak HRR between the burner locations, left and right, however a less significant one.

The first peak HRR occurs approx. 30 s after the burner is turned off in the tests conducted inside the RCT and approx. 90 s in the free-burn tests. The contribution of the burner is subtracted from the analysed HRRs, i.e. the values presented in Figs. 3 and 4 represent net heat release of the OSB furnishings. The burner flames contribute to the initial flame spread on the OSB surfaces, however, it was not possible to quantify this effect. It is expected that shorter duration of ignition period would delay the onset of exponential growth period described below.

An overview of the main fire severity parameters is provided in Tab. 4. It may also be seen, that the total released amount of heat does not differ significantly. Over the considered period of 2 100 s (35 min), the difference between the maximum and minimum THR is 61 MJ, which is approximately 3.6 kg of fuel, assuming $h_{c,eff} = 17$ MJ·kg^{-1}. This is less than 10% if the minimum THR is considered a baseline.

The first difference that is apparent when comparing HRR shown in Figs. 3 and 4 is the prolonged fire growth stage up until approx. 400 kW. The fire growth until 400 kW takes about 100 - 150 s longer in tests under the hood. It is likely due to the lack of thermal feedback, since the heat in the fire and smoke plume is extracted rapidly, hence, the smoke layer cannot form fully and there is no construction to re-radiate heat back to the fuel. Since the heat is contained better in the RCT tests, the surfaces of the furniture heat up more rapidly, aiding the flame spread.
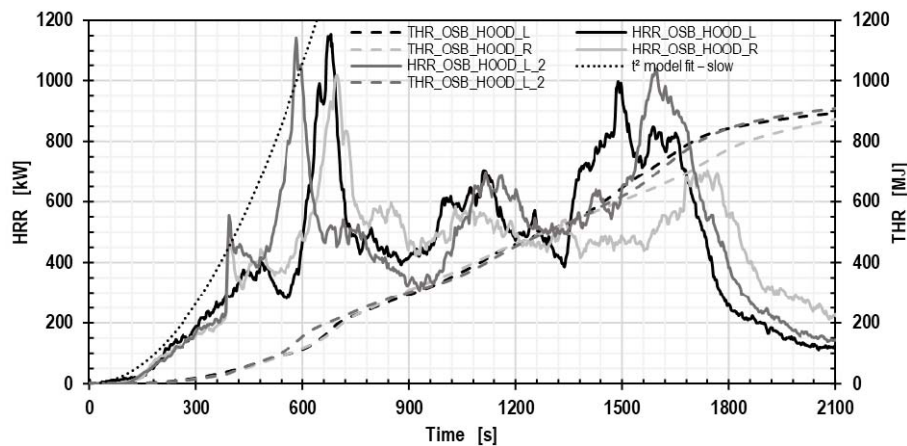
Fig. 4: Free-burn test results for office furniture made from OSB; dotted line represents a t^2-model fit with $\alpha = 0.00293$ kW·s^{-2} (slow).

Tab. 4: Overview of the main parameters of the burn tests.

Value	RCT_L	RCT_R	HOOD_R	HOOD_L	HOOD_L_2
Peak HRR (kW)	1 132	874	1 017	1 154	1 143
Time to peak (s)	524	510	580	560	583
Time to 1MW (s)	510	—	577	547	579
THR (MJ) (0–2100 s)	902	861	841	878	889

The above assumption is also supported by the temperature development on the top and bottom surfaces of the desktop (Fig. 5). It may be seen that there are significant temperature differences in the temperatures on the bottom side of the desktop. These are likely caused by the significant airflow for scenarios where the burning furniture is placed directly under the extraction hood – well-ventilated free burn experiments (HOOD). This airflow affects the heat transfer patterns under the desk and since approx. 70 - 75% of the produced heat is transferred through convection in the fire and smoke plume (Heskestad and Delichatsios 1989, Karlsson and Quintiere 2002).

Hence the combined effect of reduced thermal feedback and increased heat removal in the free burn experiments, appears to cause slower fire growth and delays the first peak. Due to very transient nature of the flow patterns (even between the experiments in the same configuration) it is, however, difficult to quantify these effects precisely. The steep increase in HRR seems to corelate with the charring temperature of wood ≈ 300°C – for RCT scenario at approx. 480 s and for HOOD scenarios 560 s and 620 s, respectively. It must be noted, however, that there are multiple other factors affecting the growth phase, e.g. structural deterioration, which are difficult to quantify. The greater peak (1 132 kW) for the configuration with the burner on the left side may be attributed to the position of the desk – the left side is in the corner of the room, i.e. the flames are enclosed on two sides, so more heat is directed at the desk.
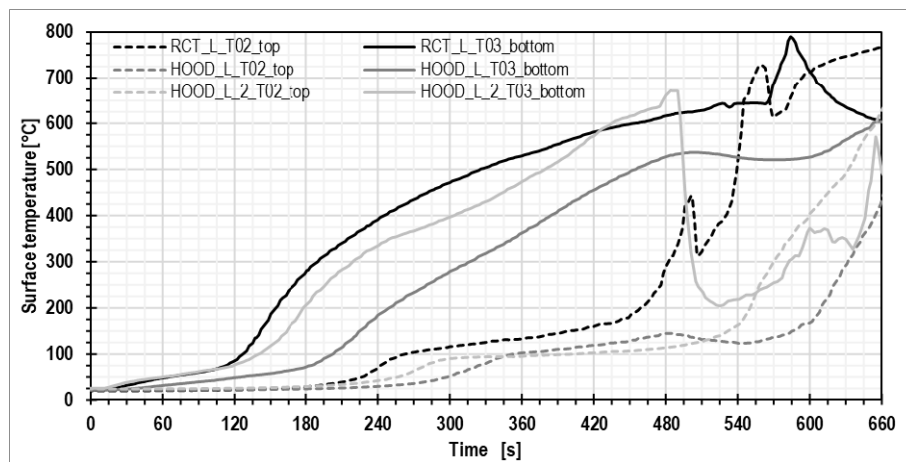
Fig. 5: Temperatures at top and bottom surfaces in the centre the desktop.

Fire growth phase is an important characteristic from the fire safety engineering perspective. It may be approximated as an exponential function, t^2 model, which follows (Heskestad and Delichatsios 1979):

$$\dot{Q} = \alpha \cdot t^2 \tag{1}$$

where: $\dot{Q}$ – heat release rate (HRR) (kW), α – fire growth rate coefficient (kW·s^{-2}), t – time (s).

There are four standardised fire growth rate coefficients (NFPA 72 2017): slow 0.00293 kW·s^{-2}, medium 0.01172 kW·s^{-2}, fast 0.0469 kW·s^{-2}, and ultrafast 0.1876 kW·s^{-2}.

These fire growth rate coefficient are characteristics of various products and occupancies (PD 7974-1 2003, Mayfield and Hopkin 2011, BS 9999 2017).

The t^2 fire growth model was fitted to the experimental data. From the standardised fire growth rate coefficients, $\alpha = 0.00293$ kW·s^{-2} (slow) follows the development stage the closest, dotted lines in Figs. 3 and 4. In the case of the RCT tests, the value of α was increased to 0.0042 kW·s^{-2}, since the time to reach the peak HRR was underestimated. As indicated in Fig. 3, the custom fire growth curve is still relatively close to the slow fire growth curve (about ¼ of the slow→medium band). Overall, the experiments indicate that there is a relatively slow fire growth stage for this type of furniture and initiation source.

Mayfield and Hopkin (2011) fitted the t^2 fire growth model to a well-ventilated free-burn experiment with an office furniture setup, and they found the fire growth phase also to be rather slow. In fact, for the investigated period $500 < t \le 1200$ s, they derived $\alpha = 0.0003$ kW·s^{-2}, which is an order of magnitude lower than for the slow fire growth rate. For an unsprinklered reception area they derived $\alpha = 0.003$ kW·s^{-2} for the investigated period $180 < t \le 1400$ s, which may be considered almost equal to the slow fire growth rate ($\alpha = 0.00293$ kW·s^{-2}). Although, there were other fuel items present, in the above experiments, primary fuel load consisted of an office desk with a chest of draws and shelving units.

Similar results for office furniture were recorded by (Walton and Budnick 1988). Again, significant variations were present, particularly between free burn and enclosure experiments. In free burn experiments the fire growth was found to be within the slow–medium zone.
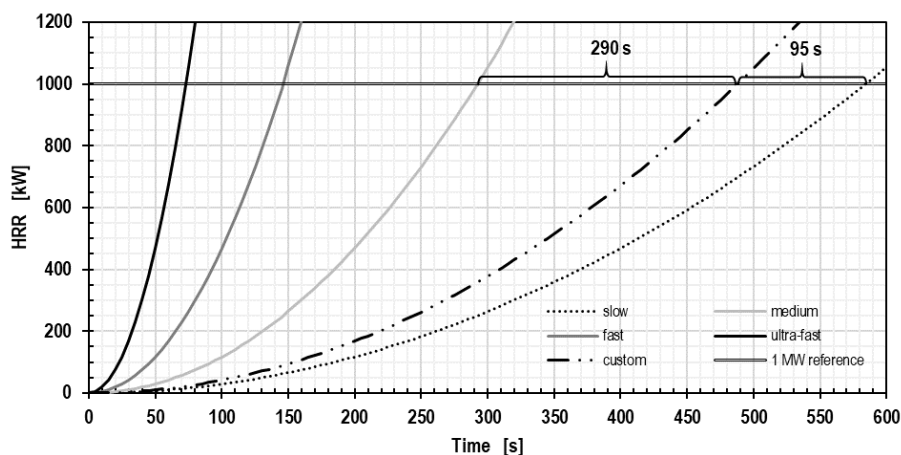
Fig. 6: Comparison of fire growth rates; custom – $\alpha = 0.0042$ kW·s^{-2}.

As regards the overall fire severity, there is no clear trend. HRR and THR curves in Figs. 3 and 4 indicate somewhat less severe course of fire for scenarios in which the burner was on the right side, both in the enclosure as well as freeburn. The decay phase, however, compensates for this (longer and/or higher HRR) to a certain extent. There are competing effects of heat balance (thermal feedback and gas extraction) and oxygen availability. For enclosure tests thermal feedback is expected to be more prominent and less heat is directly extracted due to the airflow affecting directly on the fire zone. The reduced airflow also means reduced oxygen concentration, which in turn reduces the burning and heat release rate. On the

contrary there is sufficient oxygen available in the free burn experiments, however, more heat is lost due to the increased airflow and absence of established hot layer and deflected flames.

There are also limitations as to what is the extent of HRR enhancement by thermal feedback within the enclosure. Babrauskas (Hurley et al. 2016) discusses various aspects affecting thermal feedback and states, that there is approx. 20% enhancement possible for fires in the 100 - 1000 kW range. The effect is also dependent on the proportion of fuel surface able to "see" radiating surfaces, gases, and flames. Since, the tested fuel packages had large surfaces facing "inside", e.g. shelve compartments, desk underside, drawers, etc., thermal feedback enhancement of heat release rate is expected to be limited. As Pokorny and Malerova (2017) and Pokorny and Gondek (2016) note, the fire location (corner, wall and free standing) and ventilation conditions have a significant impact too, which is in line with the findings summarised in (Wade 2019).

CONCLUSIONS

As part of a greater research project, this paper discusses the differences in fire behaviour of office furniture made from OSB boards when located inside an enclosure and directly under an extraction hood (free-burn). The test enclosure and extraction system are as per the room corner test (RCT), specified by ISO 9705.

After piloted ignition (30 kW burner) the development of fire was observed with the objective to identify them main factors causing the differences. The purpose for this comparison was the accuracy and mutual replaceability of enclosure and free-burn test results. Very often such results are applied as design fire in fire engineering, which may lead to under or overestimation of fire hazards. The investigated furniture set-up comprising a desk, chest of drawers and a shelving unit is typical for an office occupancy or home workstation. Differences were found both due to the location of the burner (ignition source) as well as burning environment − enclosed vs. free-burn. Although the total heat released remained relatively consistent, THR ≈ 875 ± 30 MJ.

The instantaneous heat release rate, however, shows significant variability for both ignition and enclosure conditions. The first HRR peak is delayed by about 50 - 60 s for free-burn conditions. On the other hand, despite faster peak onset, the following HRR appears to be less severe for RCT (enclosed) tests. In case right side ignition (chest of drawers), the peak HRR does not even reach 1 MW. It appears, that the thermal feedback effect enhancing the burning rate is limited due to the geometry of the fuel (significant internal surfaces) and the oxygen-deprived atmosphere inside the enclosure hampers fire development and burning rate. As regards applicability to fire modelling for fire hazard predictions, the data obtained provide a useful insight on the variability associated with more complex geometries of solid fuel packages. Although there are options to model burning rate enhancement in various fire models (B-Risk, FDS) one should be careful not to over- or underpredict fire severity. In particular, zone models offer only a limited capability for fuel geometry representation (2D and 3D simple rectangular shapes) and the burning rate enhancement models are sensitive particularly to the amount and orientation of surface exposed to radiating heat.

ACKNOWLEDGEMENT

REFERENCES

1. Aseeva, R., Serkov, B., Sivenkov, A., 2014: Fire behavior and fire protection in timber buildings. Springer Series in Wood Science. Dordrecht: Springer Netherlands, 290 pp.
2. Böhm, M., Reisner, J., Bomba, J., 2012: Materiály na bázi dřeva. 1. (Wood-based materials). Česká zemědělská univerzita v Praze, Fakulta lesnická a dřevařská, Katedra zpracování dřeva. 183 pp.
3. BS 9999, 2017: Fire safety in the design, management and use of buildings. Code of Practice.
4. ČSN 73 0810, 2016: Požární bezpečnost staveb. Společná Ustanovení. (Fire protection of buildings. General requirements). (In Czech).
5. EN 300, 2006: Oriented strand boards (OSB). Definitions, classification and specifications.
6. Dúbravská, K., Tereňová, Ľ., Štefková, J., 2020: CLT construction performance under thermal loading. Wood Research 65(4): 605–14.
7. Grunwald, D., Stroobants, J., 2014: Wood based panels with enhanced properties. What is possible with MDI today? In: Adhesives for Wood-Based Boards. Pp 104-116, Karadeniz Technical University, Trabzon, Turkey.
8. Heskestad, G., Delichatsios, M., 1979: The initial convective flow in fire. Symposium (International) on Combustion 17(1): 1113–23
9. Heskestad, G., Delichatsios M., 1989: Update: The initial convective flow in fire. Fire Safety Journal 15(6): 471–75.
10. Hurley, M.J., Gottuk, D., Hall Jr., J.R., Harada, K., Kuligowski, E., Puchovsky, M., Torero, J., Watts Jr., J.M., Wieczorek, Ch., 2016: SFPE Handbook of fire protection engineering. 5th ed. Springer, New York, 3493 pp.
11. ISO 9705-1, 2016: Reaction to fire tests. Room corner test for wall and ceiling lining products. Part 1: Test method for a small room configuration.
12. Kadlic, M., 2018. Impact of variability and uncertainty of input parameters on the quality of fire model outputs. PhD. Thesis. University of Zilina, 114 pp.
13. Karlsson, B., Quintiere, J., 2002: Enclosure fire dynamics. Boca Raton, Taylor & Francis. 338 pp.
14. Lay, D., Cranley, P., 2003: Polyurethane adhesives. In: Handbook of Adhesive Technology. Pp 695–718.
15. Martinka, J., Mantanis, G., Lykidis, C., Antov, P., Rantuch, P., 2021: The effect of partial substitution of polyphosphates by aluminium hydroxide and borates on the technological and fire properties of medium density fibreboard. In: Wood Material Science & Engineering. Pp 1–7.

16. Martinka, J., Štefko, T., Wachter, I., Rantuch, P., 2020: Impact of electrical cables embedded into oriented strand board on critical heat flux. Wood Research 65(2): 257–70.

17. Mayfield, C., Hopkin, D., 2011: Design fires for use in fire safety engineering. Bracknell, IHS BRE Press, 74 pp.

18. Mikkola, E., Östman, B., 2004. European classes for the reaction to fire performance of wood products (except floorings). Stockholm. Tratek, 36 pp.

19. NFPA 72, 2017: National fire alarm and signaling Code.

20. Östman, B., Mikkola, E., 2006: European classes for the reaction to fire performance of wood Products. Holz Als Roh- Und Werkstoff 64(4): 327–37.

21. PD 7974-1, 2003: Part 1. Initiation and development of fire within the enclosure of origin.

22. Pokorny, J., Gondek, H., 2016: Comparison of theoretical method of the gas flow in corridors with experimental measurement in real scale. Acta Montanistica Slovaca 21(2): 146–53.

23. Pokorny, J., Malerova, M., 2017: Fire plume characteristics and their application in assessment of a local fire. In: International Scientific Conference on Fire Protection, Safety and Security. TU Zvolen. Pp 1–4.

24. Wade, C., 2019: A theoretical model of fully developed fire in mass timber enclosures. PhD. Thesis. University of Canterbury, 293 pp.

25. Walton, W.D., Budnick, E., 1988: Quick response sprinklers in office configurations. Fire test results. NBSIR 88-3695. Gaithersburg, MD, NIST, 84 pp.

VLADIMÍR MÓZER[*]
CZECH TECHNICAL UNIVERSITY IN PRAGUE
FACULTY OF CIVIL ENGINEERING
CZECH REPUBLIC
*Corresponding author: Vladimir.Mozer@cvut.cz

PETR HEJTMÁNEK[1,2]
[1]CZECH TECHNICAL UNIVERSITY IN PRAGUE
[2]UNIVERSITY CENTRE OF ENERGY EFFICIENT BUILDINGS
CZECH REPUBLIC

DANIELA PITELKOVÁ[1,2]
CZECH TECHNICAL UNIVERSITY IN PRAGUE
[1]FACULTY OF CIVIL ENGINEERING
[2]UNIVERSITY CENTRE OF ENERGY EFFICIENT BUILDINGS
CZECH REPUBLIC

HASALOVÁ LUCIE
TECHNICAL INSTITUTE OF FIRE PROTECTION IN PRAGUE
PÍSKOVÁ 42, 143 00 PRAHA 12
CZECH REPUBLIC

EFFECT OF EDGE DISTANCES ON STIFFNESS OF SHEAR-TENSION MODE IN GLULAM CONNECTIONS WITH INCLINED SCREWS

YIFAN LIU[1], ZIYIN YAO[1], FEIBIN WANG[1], HUI HUANG[2], ZELI QUE[1]
[1]NANJING FORESTRY UNIVERSITY
P.R. CHINA
[2]JIANGXI ACADEMY OF FORESTY
P.R. CHINA

ABSTRACT

The effects of edge distances on stiffness in glulam connections with inclined self-tapping screws were studied in this paper. Under four anchorage angles (A-45°, A-60°, A-75°, A-90°) and three edge distances (EG-2D, EG-4D, EG-6D) conditions, the shear-tension tests were carried out on the timber structure connections with inclined self-tapping screws, and the stiffness and other properties of the connections were tested. Based on the results, the effects of edge distances on stiffness in joints were quantified using the equivalent energy elastic-plastic (EEEP) model. The results showed that the edge distances had a certain impact on the yield mode and load-carrying performance of the joints. Within a certain range of variation, as the edge distance increased, the stiffness of the connections increased gradually, showing a positive correlation. The stiffness of specimen EG-2D is 4.41 kN·mm^{-1}. The stiffness of specimen EG-4D is 10.04 kN·mm^{-1}, which increases by 128% compared with the specimen EG-2D. The stiffness of specimen EG-6D is 12.08 kN·mm^{-1}, which increases by 174% compared with the specimen EG-2D. However, the ductility coefficient, yielding load, and energy dissipating have no significant change. Within a reasonable edge distance, only ductile damage occurred.

KEYWORDS: Inclined self-tapping screw, edge distances, edge distances, stiffness, glulam.

INTRODUCTION

Modern dowel-type fasteners, self-tapping screws (STS) have higher strength and stiffness compared with a traditional screw, which is widely used in mass timber structure (Blass and Bejtka 2001, Ringhofer et al. 2015) as shown in Fig. 1. This type of screw mostly features a continuous thread over the whole length (fully-thread) which leads to a more

uniform load transfer between the screw and the wood material (Dietsch et al. 2015, Jockwer et al. 2014). In recent years, many experimental (Yang et al. 2020, Zhang et al. 2019) and numerical studies (Brandner et al. 2018) concern about how the increase of screw inclination provides an increase of load-carrying capacity of the joints and concludes that is a significant change (Tomasi et al. 2010, Bejtka and Blass 2002, Wang et al. 2019, Komatsu et al. 2019, Yang et al. 2018, Que et al. 2020, Lu et al. 2020, Teng et al. 2020, Chen et al. 2020, Chang et al. 2019). Blass and Bejtka first clarified and proposed theoretical equations for the load-carrying capacity of inclined STS joint based on Johansen's theory (Johansen 1949). However, the inclined STS have more complex behavior in laterally loading condition which governed by the embedment behavior of the timber, withdrawal action on the screw and rope effect for large deformations. The assessment of the stiffness of the inclined STS has been studied by a few researchers (Girhammar et al. 2017, Symons et al. 2010, Tomasi et al. 2010).

Fig. 1: The engineering application of self-tapping screw.

According to Eurocode 5 (EN 1995-1-1, 2009), the slip modulus of the connector is depends on the timber properties and diameter of STS. It can be expressed as:

$$k_{ser} = \rho_m^{1.5} \cdot d / 23 \tag{1}$$
$$k_{ser} = \rho_m^{1.5} \cdot d^{0.8} / 30 \tag{2}$$

where: k_{ser} is the slip modulus of a connector for design at serviceability limit state (N·mm^{-1}); ρ_m is the density of the timber (kg·m^{-3}). The values of d mean the effective diameter of STS where the effective diameter is 1.1 times the thread root diameter (mm).

The Eq. 1 applies to nails without pre-drilling and Eq. 2 applies to screw. This equation can predict the stiffness of shear-compression stress in some cases. However, for the screws subjected to shear-tension stress, the equation is not able to accurately evaluate the stiffness. Therefore, Tomasi et al. (2010) further proposed the mechanic-based model to estimate the properties of STS connection. It can be expressed as:

$$k_{ser} = k_{\perp} \cdot cos\alpha \cdot (cos\alpha - \mu \cdot sin\alpha) + k_{\parallel} \cdot sin\alpha \cdot (sin\alpha + \mu \cdot cos\alpha) \tag{3}$$

where: $k_\perp$ is the connector stiffness for lateral loading; $k_\parallel$ is the connector stiffness for withdrawal loading; α is the angle of inclination of the STS; μ is the friction coefficient of the wood element.

According the Eq. 3 the stiffness of this connection can be seen by the two parts that lateral stiffness and the withdrawal stiffness of the screw. The lateral and withdrawal stiffness were affected of two parameters which is the interface friction of wood element and the inclined angle of the screw. As the angle changes, these two stiffnesses contribute differently to the overall stiffness of the connection. For example, the angle of inclination is 0°, the overall stiffness of the node is the vertical component of the screw, which is completely borne by the compressive bearing stiffness of the screw. This trend can also be reflected in the Fig. 2. The figure showed the stiffness for the screw subjected to shear-tension stress versus the inclination angle for the case where the friction coefficient has different value. The "willow leaf" enclosed area represents the node stiffness of the self-tapping screw subjected to shear-tension stress could appear possible area.
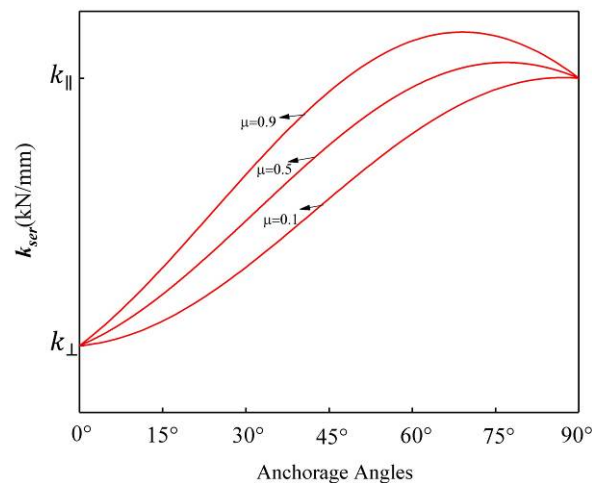
Fig. 2: The influence of the inclination (α) on the stiffness value.

Tomasi's model (Tomasi et al. 2010) is only a theoretical derivation model, but in actual engineering, the stiffness of self-tapping screws will change differently under the influence of different margins, end distances, and group effects.

The above research did not even address the edge distance effect of the stiffness for the STS. For the real project, the calculation formula given in the standard Eurocode 5 (EN 1995-1-1, 2009) has restrictions, the edge distances, end distances, and spacing lead to more complex mechanisms of the STS. This paper aims to introduce and experimentally verify the effect of edge distance on the stiffness of the timber structure joint connected with STS used the glulam material.

MATERIAL AND METHODS

Materials

The specimens were fabricated in factory that glulam made of Douglas fir (*Pseudotsuga menziesii*), of strength class SZ1 according to GB 50005-2017 (2017), and PUR adhesive (Polyurethane Reactive). The lamina of the glulam thickness was 35 mm. The average moisture content was 10.5%, and the average air-dry density was 0.538 g·cm^{-3}. The manufacture of glulam processing with adhesive spread 250 g·m^{-2}, compacting pressure 1.0 MPa, pressure time 4 h, processing temperature 25°C.

The self-tapping screws are FTLD (product number) cylindrical head with full thread structure. The diameter × length of self-tapping screws is 6 mm × 140 mm, as showing in Fig. 3 and Tab. 1. Withdrawal and bending tests carried out on the self-tapping screws in compliance with LY/T 2377-2014 (2014), LY/T 2059-2012 (2012), and ASTM F 1575-17 (2017), the average result of withdrawal strength is 25.79 N·mm^{-2}, and the average bending yield strength is 1064 MPa.
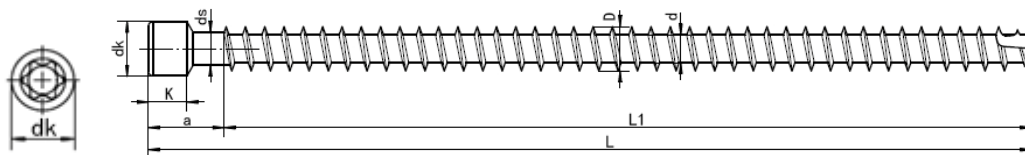
Fig. 3: FTLD self-tapping screw.

Tab. 1: The dimensions of FTLD self-tapping screw (units: mm).

Type	L	L1	D	d	dk	K
FTLD	140.0	130.0	6.0	4.0	8.4	5.5

The plan of the experiment

The specimen was designed by reference to the Chinese national standard GB 50005 2017 (2017) and the European standard Eurocode 5. The samples usually study in push-out tests, for example, it consists of two lateral wood (70 × 90 × 300 mm) elements and a central one (140 × 90 × 300 mm), held together by self-tapping screws: *(a)* The different anchored angle of single inclined self-tapping screws working only under shear-tension load (A-45°, A-60°, A-75°, A-90°); *(b)* The different edge distance of single inclined self-tapping screws working only under shear-tension load (EG-2*D*, EG-4*D*, EG-6*D*).

In the study, the influence of the screw angle, two self-tapping screws are screwed in from both sides of the lateral wood elements, the edge distance is 36 mm, the end distance is 108 mm, and the inclined angle is 45°, 60°, 75°, and 90° resp. To analyze the influence of the screw edge distance, were set to 2 *D* (12 mm), 4 *D* (24 mm), 6 *D* (36 mm), a total of three sets of specimens. The test was repeated six times for each group, and the test design was shown in Fig. 4.
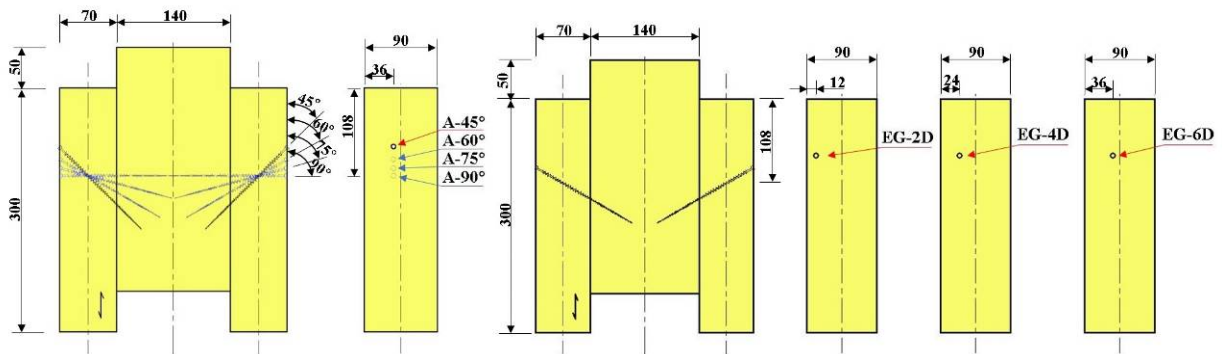
Fig. 4: The schematic plans of specimens with different angles and edge distances. Units (mm).

Test protocol and instruments

The protocol of the push-out test was referenced in American standard ASTM D1761-12 (2012) the deformation speed of the mechanical test machine was set 0.9 mm·min^{-1} ($\pm$ 50%) by monotone displacement control of this test. Under this loading condition, the push-out test gets the maximum load within 5 - 20 min. During the experiment, when the load of the specimen has fallen to less than 80% of the maximum load, the loading is to stop, while using date collection system TDS-530, four linear variable differential transformer transducers (LVDT) and mechanical load sensor, acquisition of force and displacement data. The protocol of the loading is shown in Fig. 5.
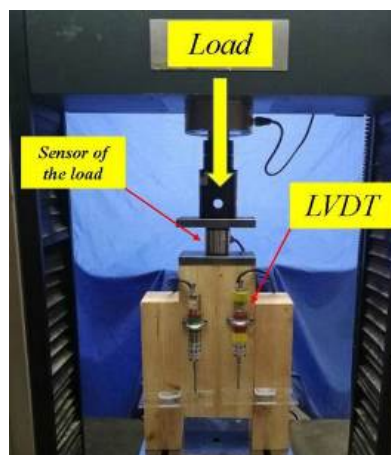
Fig. 5: Apparatus of the testing.

RESULTS AND DISCUSSION

Equivalent energy elastic-plastic method

The test results are shown in Fig. 6 and Fig. 7. It is significant to know the yield point when the plastic deformations occurred in seismic. In seismic design, plastic deformations are allowed for ductile structures. Therefore, it is important to know the yield point, when the plastic deformation begins, and ductility, how much plastic deformation the structure can undergo without significant loss of strength (Williams et al. 2008).
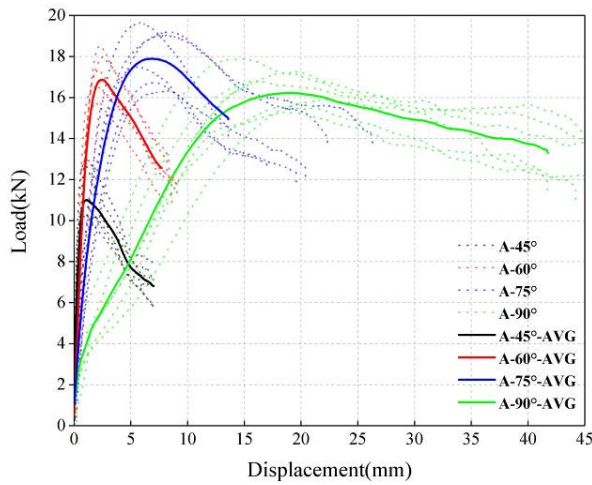
Fig. 6: The load-slip curves of specimens with different anchorage angles.
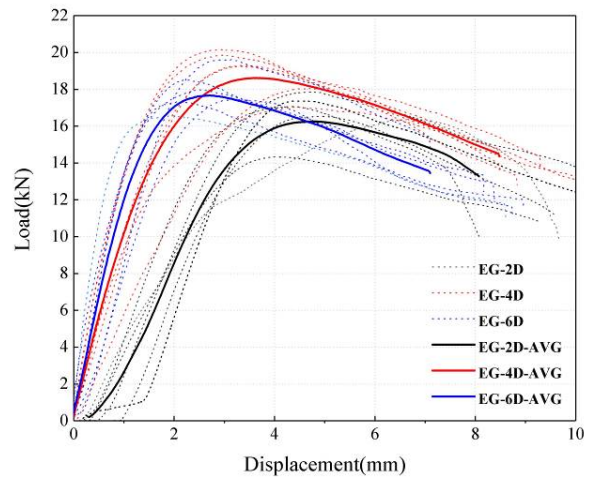
Fig.7: The load-slip curves of specimens with different edge distances.

There are several methods around the world to quantify these properties for timber structures. In this paper adopted the equivalent energy elastic-plastic (EEEP) curve method that usually analysis the shear walls in ASTM E2126-19 (2019). The bilinear curve represents the accurate elastic-plastic behavior of the connection. The area below the test curve is equal to the area under the bilinear curve. The initial stiffness defined by 0% and 40% of the maximum load. Deformation at failure is defined as the deformation at 80% of the maximum load. The yield load can be calculated using this following equation:

$$p_y = \left[\Delta_{failure} - \sqrt{\Delta_{failure}^2 - 2w_{failure}/K} \right] \times K \tag{6}$$

where: p_y is yield load; $\Delta_{failure}$ is deformation at failure; and $w_{failure}$ means energy dissipated until failure.

Then we can equivalent the test curve to the bilinear curve directly. The first line of the bilinear curve corresponds to the initial stiffness and yield load. Once the yield load is defined, the yield deformation can be determined. The ductility of the connection can be calculated.

Equivalent energy elastic-plastic analysis for different anchorage angles

As is shown in the Fig. 8, the load-slip curves and bi-linear models of specimens with different anchorage angles. The stiffness of the joint is the largest at 45°, and as the anchorage angle increases, the stiffness of the joint gradually decreases. That is consistent with the slope part of the bi-linear model.
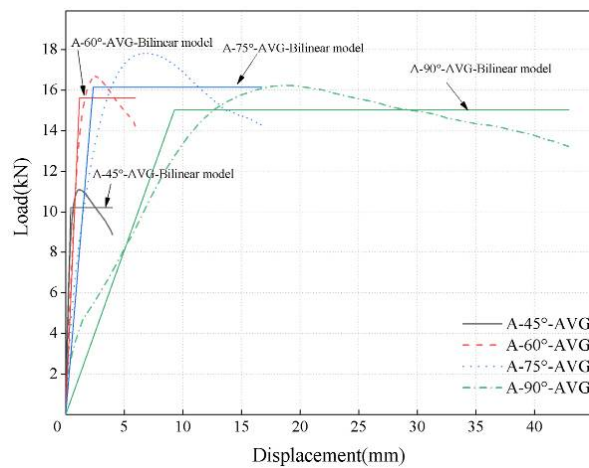
Fig. 8: The bi-linear models of specimens with different anchorage angles.

The area enclosed by the load-slip curve is the energy dissipation of this joint during the test. In terms of energy dissipation, as the anchorage angle of the self-tapping screw increases, the energy dissipation of the joint increases. In order to show this difference, the initial stiffness, yield load, ductility coefficient and energy dissipation of the joints were calculated quantitatively by pick point software (Karube et al. 2001).
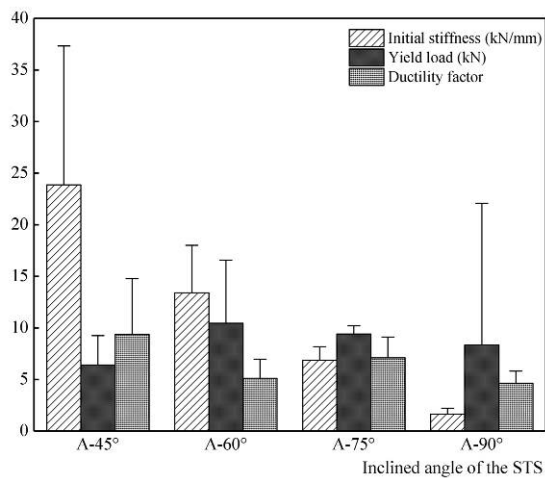
Fig. 9: The properties of specimens with different anchorage angles.
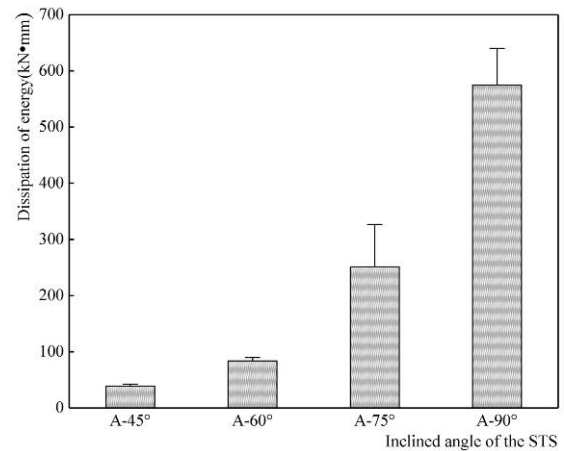
Fig. 10: The dissipation of energy of specimens with different anchorage angles.

Tab. 2: The characteristic parameter of specimens with different anchorage angles.

Anchorage angles test ID	Maximum load (kN)	Initial stiffness (kN·mm^{-1})	Yield load (kN)	Ductility factor	Dissipation of energy (kN·mm)
A-45°-AVG	11.09 (±1.16)	23.87 (±13.44)	6.40 (±2.84)	9.37 (±5.41)	38.65 (±3.71)
A-60°-AVG	16.70 (±1.00)	13.38 (±4.62)	10.45 (±6.11)	5.10 (±1.85)	84.00 (±5.81)
A-75°-AVG	17.83 (±1.28)	6.84 (±1.32)	9.40 (±0.80)	7.09 (±2.03)	250.96 (±75.50)
A-90°-AVG	16.23 (±0.94)	1.62 (±0.58)	8.31 (±13.76)	4.62 (±1.19)	574.76 (±65.29)

Note: The standard deviation of the six specimens in the brackets.

The load-displacement diagram was fitted by the bilinear model using EEEP method, then extract all kinds of properties of this connection draw the bar chart as Fig. 9 and Fig. 10. As Fig. 9 demonstrated that with the increase of self-tapping screw angle, initial stiffness is on the decline. In Tab. 2, the average of the initial stiffness of the specimen A-45° is 23.87 kN·mm^{-1}. The average of the initial stiffness of the specimen A-60° is 13.38 kN·mm^{-1} compared with the A-45° which was reduced 43.9%. The average of the initial stiffness of the specimen A-75° is 6.84 kN·mm^{-1}. Compared with the A-45° that was reduced 45%. The average of the initial stiffness of the specimen A-90° is 1.62 kN·mm^{-1}, which is only 6.8% of the average initial stiffness at A-45°. That means the initial stiffness is inversely proportional to the anchorage angle. But for yielding load, the specimen of A-60° has the maximum value. In the same condition, the inclined angle 45° is always easy to yield. Compared with energy dissipation, Fig. 10 shows the trend of exponential growth, the energy dissipation is a positive correlation with anchorage angle.

When single the angle is considered changing, the effective length of self-tapping screws deep into the main material also changes. That is why the bearing capacity values of A-45° are low. On the other hand, the effective length of the embedded main wood element did no effect on the stiffness of this single shear-tension connection.

For the specimen of A-45°, with the increase in load, the self-tapping screw first bears the bending resistance of the glulam under the action of the force. When this action increases with the increase in force, the reaction force of the screw cap also increases gradually, and finally presents the failure mode of pulling out the screw. With the change of the anchorage angle, the failure mode of the specimens also changed. The specimens of A-45°and A-60° were appeared screw pulling failure, and the specimens of A-75°and A-90° showed obvious bending failure.

This phenomenon illustrates the effect of the effective length of the connector on the failure mode of the connection.

Experimental phenomena and failure modes of different anchorage angles

During the loading process, with the increase in load and displacement, this joint transitions from the elastic stage to the plastic stage. At the beginning of the yield displacement point of the specimen, the cracking occurred along with the sound. The sound is more intense near the maximum load, and the head of the screw with the angles of 75° and 90° are pulled into the lateral wood elements about 7 mm and 15 mm, respectively.

As the cross-section of the specimens in Fig. 11, the failure mode can be observed. For A-45° specimens there are no significant changes about the way of screws, but the self-tapping screw was pulled out from the main wood element. The reason is the anchorage length of the screw into the main wood element is short, which caused the effective length of the embedded main wood element was not enough. In this case, the withdraw capacity was much bigger than the yield capacity of the screw. The self-tapping screw of the A-60° specimen was bent at the shear plane, and a plastic hinge appeared. The self-tapping screws of the A-75° and A-90° specimens were bent on both sides of the connection, and two plastic hinges appeared. The bending degree of the 90° specimen was greater, and the bending

symmetrical distribution occurred at both sides of the shear plans, which resulted in the failure mode of "two-hinge yield".

Fig. 11: Inside phenomena of different anchorage angles.

Equivalent energy elastic-plastic analysis for different edge distance

Similarly, the load-displacement diagram was fitted with a bilinear model to extract the properties of specimens with different edge distance (Fig. 12). As can be seen from Fig. 13 and Fig. 14, the initial stiffness showed an upward trend with the increase of the edge distance.
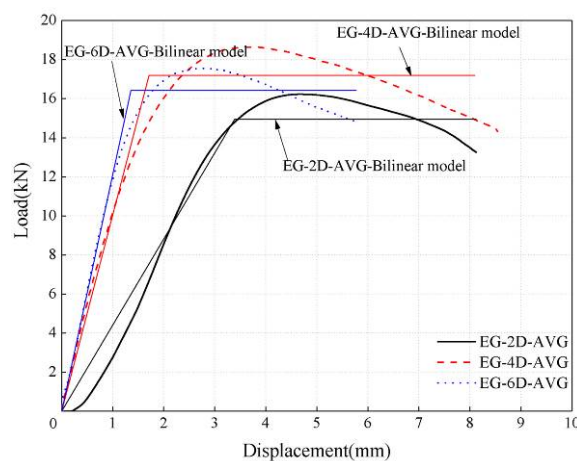
Fig. 12: The bi-linear models of specimens with different edge distances.

In Tab. 3, the average of the initial stiffness of the specimen EG-2D is 4.41 kN·mm^{-1}. The average of the initial stiffness of the specimen EG-4D is 10.04 kN·mm^{-1}. The average of the initial stiffness of the specimen EG-6D is 12.08 kN·mm^{-1}. The trend of average yield load and average ductility factor is relatively uniform, while the average energy dissipation of the specimen EG-4D is the largest (124.57 kN·mm), and the average energy dissipation of

EG-6D is the smallest (83.63 kN·mm), which decreases by 32.9% compared with the specimen EG-4D.
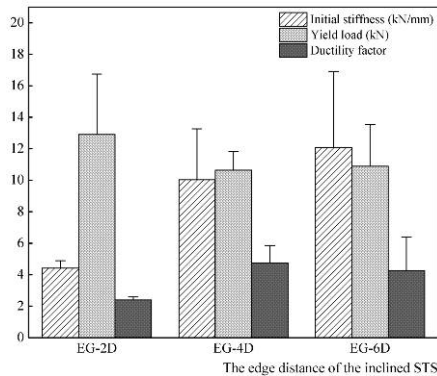
Fig. 13: The properties of specimens with different edge distances.
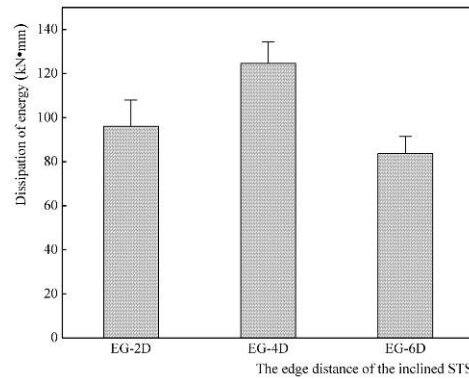
Fig. 14: The dissipation of energy of specimens with different edge distances.

Tab. 3: The characteristic parameter of specimens with different edge distances.

Edge distances test ID	Maximum load (kN)	Initial stiffness (kN·mm⁻¹)	Yield load (kN)	Ductility factor	Dissipation of energy (kN·mm)
EG-2D-AVG	16.23 (±1.12)	4.410 (±0.48)	12.91 (±3.83)	2.40 (±0.19)	96.10 (±11.91)
EG-4D-AVG	18.65 (±1.07)	10.04 (±3.22)	10.64 (±1.17)	4.73 (±1.12)	124.57 (±9.78)
EG-6D-AVG	17.55 (±0.97)	12.08 (±4.83)	10.89 (±2.64)	4.24 (±2.15)	83.63 (±7.85)

Note: The standard deviation of the six specimens in the brackets.

Experimental phenomena and failure modes of different edge distance

During the loading process, the specimen surface has no obvious phenomenon. After unloading, the shear plane has about 2 mm gap, separated the specimen, and examined the failure modes of different edge distances. Results show that the screw was a bend in the shear plane of different edge distances and "one hinge yield" failure occurred. Moreover, these results more remarkable in the specimen EG-4D. The way of the screw and screw failure mode in the members after a load of each group of specimens was shown in Fig. 15 and   Fig. 16.

Fig. 15: Inside phenomena of specimens with different edge distances.

Fig. 16: The failure mode of the self-tapping screw.

CONCLUSIONS

The push-out test was conducted with self-tapping screws at four anchorage angles (A-45°, A-60°, A-75°, and A-90°), three edge distances (EG-2D, EG-4D, and EG-6D). Using the energy elastic-plastic curve method (EEEP) method to study the effect of edge distances on stiffness and other properties of the joint.

The results showed that the anchorage angles of STS had a significant impact on the initial stiffness of this joint, with the increase of self-tapping screw angle, initial stiffness is on the decline. In terms of initial stiffness, the specimen of A-45° is 23.87 kN·mm^{-1}, but it is the easiest to buckle, and has lower energy dissipation and ductility. The maximum yield load at the specimen of A-60° is 10.45kN. For the specimen of A-45°, the stiffness of the connection is the smallest, and the energy dissipation value is the largest 574.76 kN·mm.

With the increase of the edge distances, the initial stiffness increased, and the yield load, ductility coefficient, and energy dissipation were uniform. The stiffness of specimen EG-2D is 4.41 kN·mm-1. The stiffness of specimen EG-4D is 10.04 kN·mm-1, which increases by 128% compared with the specimen EG-2D. The stiffness of specimen EG-6D is 12.08 kN·mm-1, which increases by 174% compared with the specimen EG-2D. However, the ductility coefficient, yielding load, and energy dissipating have no significant change.

Experimental results presented in this research the effect of the edge distances has a significant impact on the stiffness of the connection. The effective range of the STS has to be considered in the future test.

ACKNOWLEDGEMENTS

REFERENCES

1. ASTM F1575-17, 2017: Standard test method for determining bending yield moment of nails.
2. ASTM D1761-12, 2012: Standard test methods for mechanical fasteners in wood.
3. ASTM E2126-19, 2019: Standard test methods for cyclic (reversed) load test for shear resistance of vertical elements of the lateral force resisting systems for buildings.
4. Blass, H.J., Bejtka, I., 2001: Screws with continuous threads in timber connections. Pp 193-201, Proceedings PRO 22. International RILEM symposium on joints in timber structures. Stuttgart, Germany.
5. Bejtka, I., Blass, H.J, 2002: Joints with inclined screws. Pp 141-154, In: Meeting, international council for research and innovation in building and construction working commission W18-timber structures. Kyoto, Japan. (Paper No. CIB-W18/35-7-4).
6. Brandner, R., Ringhofer, A., Grabner, M., 2018: Probabilistic models for the withdrawal behavior of single self-tapping screws in the narrow face of cross laminated timber. European Journal of Wood Products 76: 13–30.
7. Chang, C., Fang, Y.F., Liu, Y.F., Que Z.L., 2019: Study on pull-out performance of tilted self-tapping screw in cross-laminated timber. Architecture Technology 50(04): 416-418. (In Chinese)
8. Chen, Z.Y., Wang, X.M., Dang, W.J., Dong, L., Chen, J., Que, Z.L., 2020: Study on performance of steel-to-timber joints with inclined self-tapping screws for cross-laminated timber structures. Architecture Technology 51(03): 288-291. (In Chinese).
9. Dietsch, P., Brandner, R., 2015: Self-tapping screw and threaded rods as reinforcement for structural timber elements. A state-of-the-art report. Construction and Building Materials 97: 78-89.
10. EN 1995-1-1, 2009: Eurocode 5: Design of timber structures part 1-1: general-common rules and rules for buildings.
11. Girhammar, U.A., Nicolas J., Bo, K., 2017: Stiffness model for inclined screws in shear-tension mode in timber-to-timber joints. Engineering Structures 136: 580-595.
12. GB 50005-2017, 2017: The standard for the design of timber structures. (In Chinese)
13. Johansen, K., 1949: Theory of timber connection. Bridge Structural Engineering 9: 249-262.
14. Jockwer R., Steiger R., Frangi A., 2014: Design model for inclined screws under varying load to grain angles. Pp 141-153, Meeting 47 of the International Network for Timber Engineering Research INTER. Bath, United Kingdom. (Paper No. INTER/47-7-5).
15. Komatsu, K., Teng, Q.C., Li, Z.R., Zhang, X.L., Que Z.L., 2019: Experimental and analytical investigation on the nonlinear behaviors of glulam moment-resisting joints composed of inclined self-tapping screws with steel side plates. Advances in Structural Engineering 22(15): 3190-3206.
16. Karube, M., Harada, M., Hayashi, T., 2001: A proposal of bi-linear modeling tool for assess its method and problem in common tool for load-deformation curves of wooden

structures. Digests of Annual Meeting of Architectural Institute of Japan C-1(3): 215-216. (In Japanese).

17. LY/T 2377, 2014: Test methods for the joint performance with dowel type fasteners used in wooden structural material (In Chinese).

18. LY/T 2056, 2012: Steel nails for timber structures (In Chinese).

19. Lu, X.R., Teng, Q.C., Li, Z.R., Zhang, X.L., Wang, X.M., Komatsu, K., Que, Z.L., 2020: Study on shear property of spruce glulam and steel plate connected with inclined screw. Journal of Forestry Engineering 5(3): 48-53. (In Chinese).

20. Que, Z.L., Han, C., Teng, Q.C., Hu, C.S., Luo, W.S., 2020: Study on anti-side performance of glulam beam-column joints with inclined screw. China Forest Products Industry 57(05): 34-40. (In Chinese).

21. Ringhofer, A., Brandner, R., Schickhofer, G., 2015: Withdrawal resistance of self-tapping screws in unidirectional and orthogonal layered timber products. Materials and Structures 48: 1435–1447.

22. Symons, D., Persaud, R., Stanislaus, H., 2010: Slip modulus of inclined screws in timber-concrete floors. Structures and Buildings 163(4): 245–55.

23. Teng, Q.C., Wang, F.B., Que Z.L., Zeng, N., 2020: Effects of angles on the screw and nail withdrawal strength in dimension lumber. Scientia Silvae Sinicae 56(01): 154-161.

24. Tomasi, R., Crosatti, A., Piazza, M., 2010: Theoretical and experimental analysis of timber-to-timber joints connected with inclined screws. Construction and Building Materials 24(9): 1560-1571.

25. Williams, M., Mohammad, M., Alexander, S., Pierre, Q., 2008: Determination of yield point and ductility of timber assemblies: In search for a harmonized approach. Pp 1064-1071, 10th World Conference on Timber Engineering, Miyazaki, Japan.

26. Wang, F.B., Wang, X.M., Cai, W.Z., C., Chang, C., Que Z.L., 2019: Effect of inclined self-tapping screw connecting laminated veneer lumber on the shear resistance. Bioresources 14(2): 4006-4021.

27. Yang, X.J., Ma, L., Que Z.L., Yu, Y.H., 2018: Enduring performance of self-tapping screw connection in wood members and WPC members. Wood Research 63(5): 833-842.

28. Yang, R.Y., Zhang X.F., Yuan Q., Sun Y.F., Wu Y.H., 2020: Research of pin slot embedding yield strength parallel to grain of *Larix gmelinii*. Journal of Forestry Engineering 5(05): 131-138.

29. Zhang Y., Liu X.Y., Hu Q.B., Gao Y., 2019: Influence of old panel on the mechanical properties of nailed joints in light wood frame structure. Journal of Forestry Engineering 4(01): 51-58.

YIFAN LIU, ZIYIN YAO, ZELI QUE[*]
NANJING FORESTRY UNIVERSITY
COLLEGE OF MATERIALS SCIENCE AND ENGINEERING
NANJING 210037
P.R. CHINA
*Corresponding author: zelique@njfu.edu.cn

FEIBIN WANG
NANJING FORESTRY UNIVERSITY
COLLEGE OF LANDSCAPE ARCHITECTURE
NANJING 210037
P.R. CHINA

HUI HUANG
JIANGXI ACADEMY OF FORESTY
INSTITUTE OF FOREST PRODUCTS INDUSTRY
NANCHANG 330032
P.R. CHINA

ANATOMICAL PROPERTIES OF STRAW OF VARIOUS ANNUAL PLANTS USED FOR THE PRODUCTION OF WOOD PANELS

RADOSŁAW MIRSKI, ALEKSANDRA BANASZAK, EWA FABISIAK, JOANNA SIUDA
POZNAŃ UNIVERSITY OF LIFE SCIENCES
POLAND

ABSTRACT

The aim of this study was to determine basic anatomical features of annual plant fibers used as wood substitutes for the production of wood-based panels. For this purpose rye, wheat, triticale, rape and corn straw were used. The determination of the morphological features of the fibers was conducted on the macerated material. Fiber lengths, fiber diameters and lumens were measured, and then the fiber wall thicknesses and slenderness ratios were calculated. The result clearly showed significant differences among all fiber characteristics of the tested plants. The strength and direction of the relationship between the anatomical properties determined in the study and the physicomechanical properties of the boards produced with straw from the tested annual plants were identified.

INTRODUCTION

The shortage of wood and its increasing prices lead to continuous work on re-placing the traditionally used particles in the production of particleboards (Mirski et al. 2020). Mainly trying to replace pine, spruce or birch chips with particles obtained from other lignocellulosic materials. One of the possibility is used straw of annual plants e.g. dried stalks of cereal crops, maize or rape. Term "straw" is commonly used in the case of cereals, legumes, flax and rape plants. In the EU countries, a significant amount of straw is observed as a residue from agriculture (Meyer et al. 2018). The straw of cereals, corn and rape is a by-product of agricultural production. In the case of rape, the demand to use straw results from the fact that rape is still the basic biocomponent in the production of biofuels (Markiewicz and Muślewski 2020). One of them is the use of straw as a lignocellulosic raw material in the broadly understood wood industry (for the production of large-size boards).

In Poland, in the years 1999–2018, the average annual surplus of straw harvested over agricultural consumption equaled 12.5 million tons (4.2 Mtoe) (Gradziuk et al. 2020). Cereal straw and other annual plants are different from wood, e.g. chemical composition. Depending on the species cereal straw contains 45-55% cellulose, 26-32% hemicellulose (pentosans) and 16-21% lignin (Paukszta 2006). Despite some technological difficulties, the incentives to use straw for the production of particleboards are its lower price, wide availability, its lower hygroscopicity, better thermal insulation and lower weight density (Dziurka and Mirski 2013). The concept of using these raw materials in the broadly understood wood industry is not new. The first at-tempts in this area were made in the 1960s. However, such boards have not been produced on an industrial scale. These limitations are partly due to incomplete knowledge about the properties of these raw materials, and thus the properties of the boards that can be produced under various technological conditions. The selection of wood substitutes should ensure compliance with the requirements, in terms of mechanical properties and water resistance, for boards used in the construction industry (Moriarty 2002).

The properties of oriented strand boards (OSB), in which the wood was partially or completely replaced with straw of cereals or rape, were investigated by e.g. Cheng et al. (2013), Mirski et al. (2016). Bekhta et al. (2013), Boquillon et al. (2004), Hafezi and Hosseini (2014) determined the properties of particle boards in which wheat straw was used as a substitute for wood. Dziurka and Mirski (2013), Huang et al. (2016) used rapeseed straw for the production of boards. Research also shows that white mustard can be used as a substitute for wood (Azizi et al. 2011, Bekhta et al. 2013, Boquillon et al. 2004, Dukarska et al. 2015, Grigoriou 2000, Mo et al. 2003). Moreover, Kurokochi and Sato (2015), Li et al. (2011) showed that rice straw can be use. Wu et al. (2015) conducted a study of the properties of boards produced with the use of corn straw, while Papadopoulos and Hague (2003) used flax and hemp. Papadopoulos et al. (2004), Xu et al. (2004) also applied bamboo and kenaf as a substitute for wood. Dukarska et al. (2012) for manufacture particleboards used evening primrose straw. An interesting option is also the replacement of wood particles with tomato and grape stalks, kiwi, coffee or tea waste (Bekalo and Reinhardt 2010, Guuntekin et al. 2009, Nemli et al. 2003). Medium-density fibreboards (MDF) enriched with corn or cotton stalk fibers were studied by Kargarfard and Latibari (2011). The cited studies carried out in various research centers show that not all lignocellulosic materials provide the boards produced with the physical and mechanical properties required in construction. This is the result of e.g. diversified anatomical structure, chemical composition and particle size of alternative raw materials.

Moreover, various technological conditions for the production of boards, as well as the types of adhesives used, make it difficult to compare the properties of the produced boards and to select the most appropriate substitutes for wood. In the case of gluing straw particles of annual plants, the presence of waxy substances on their surface hinders the gluing of the particles, which make worse the strength and water resistance of the boards. This problem can be solved by using iso-cyanate-based pMDI resins (Grigoriou 2000, Mo et al. 2003). For replace currently using materials, knowledge a specification of straw and their influence on particleboards properties is necessary.

Until now, research related to alternative materials instead of wood, especially straw from annual plants used in the production of particle boards or fiberboards, has focused mainly on determining the physical and mechanical proper-ties of boards made of these materials. One of the factors determining the possibilities of using straw from annual plants for the production of panels is the varied anatomical structure of these materials. The comparison of the properties of boards in which straw is the substitute for wood from different annual plants is possible if they were produced under the same technological conditions. Therefore, the aim of these studies was to determine the morphological features of straw fibers of annual plants and to determine the strength and direction of the relationship between the microstructure features and the physicomechanical properties of the boards, determined in previous studies on the same experimental material and produced according to the same methodology (Mirski et al. 2018).

MATERIAL AND METHODS

Material

In this research rape straw (*Brassica napus* L. var. Napus) (Ra), triticale straw (*Triticosecale* Witt.) (Tr), rye straw (*Secale* L.) (Ry), corn straw (*Zea mays* L.) (Co), wheat straw (*Triticum* L.) (Wh) were used. This material was obtained from the harvest in the same year, in Wielkopolska province (Poland), in the form of bales. It has been crushed and stripped of mineral impurities.

Methods

The morphological features of the straw anatomical elements were marked on the macerated material. Maceration was carried out with a mixture of acetic acid and hydrogen peroxide (30%) in the proportion 1:1, at the temperature of 60°C for 20 h. From the obtained macerates, microscopic preparations were made. Length and diameter of the fibers as well as the diameter of the lumens were measured. From each tested raw material, 30 fibers were measured, and their diameters were determined at the widest points of the tested cells. Based on the performed measurements, the thickness of the fiber walls and the slenderness ratio, which is the ratio of the length to the diameter of the fibers, were calculated. Measurements were performed using a Primo Star light microscope (Carl Zeiss Microscopy, Germany) coupled with a computer image analyzer (Motic Images Plus 4.0, Motic In-corporation Ltd, Hong Kong, China). The macrostructure of the longitudinal surfaces of the tested lignocellulosic materials was observed using a stereoscopic microscope made by Olympus (Olympus Poland) coupled with a computer image analyzer using the Motic Images Plus 2.0 program (Motic Incorporation, Ltd., Hong Kong, China).

Statistical analysis was performed using Statistica 13.0 software (Dell, Round Rock, TX, USA). The descriptive statistics and one-way analysis of variance (ANOVA) were applied. All tests were performed at the significance level of $p < 0.05$.
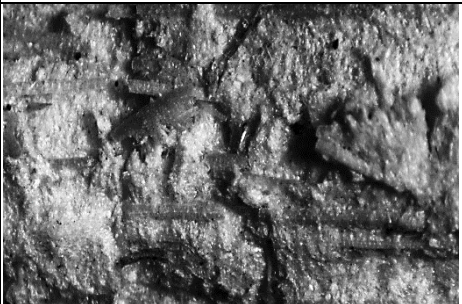
In order to numerically determine the relationship between the anatomical properties determined in the study and the physicomechanical properties of the boards (made with the use

of straw from the studied annual plants) taken from authors previous research, a correlation matrix was used.

RESULTS AND DISCUSSION

The straws of the examined annual plants differ in their macro- and microscopic structure. Rye, wheat, triticale and corn belong to the grasses, and rape is a variety of cabbage. The most important part of the straw is the tube-shaped stalk, separated by elbows into segments called internodes (Liu et al. 2018). Straw from annual plants is characterized by high morphological heterogeneity. They consist of fibers and other structural elements such as vessels and parenchymal cells. The straw walls consist of three layers. The outer layer is made of a covering tissue whose cells are characterized by serrated edges. The middle layer is made of slender, pointed bast fibers with thick walls. Apart from them, in this layer there are slightly shorter and less slender sclerenchymatic strengthening cells, concentrated mainly in the nodes forming the so-called elbows. The inner layer consists mainly of parenchymal cells, vessels and bast fibers. During the growth of these plants, their parenchyma quickly disappears and the stalk, except for the nodes, be-comes empty inside. The exception is maize, in which the nodes and internodes are filled with parenchyma (spongy core). Rapeseed, on the other hand, is a plant of the type of cabbage, hence its straw has a structure different from that of other plants and is not suitable for fodder or bedding. The parenchyma is undesirable from the point of view of adhesion and mechanical properties. From the point of view of suitability for the wood-based panels industry, the bast fibers are the most valuable cells in the straw composition. In the structure of the stem, the fiber is its most durable structural element. In addition, they have a favorable strength to density ratio and have good thermal and acoustic insulation properties.

The macrostructure images of the longitudinal sections are presented in Fig. 1. The tested lignocellulosic raw materials differ in the structure of external and internal longitudinal surfaces. The outer surfaces of the straw are smoother. On the other hand, the inner surfaces are rough due to the presence of parenchymal cells. The surface roughness is desirable as it contributes to better adhesion with the binder matrix (glue) for greater strength. It should also be noted that the particles of different straws show the presence of contaminants from the storage environment. Similar results were observed by Bouasker et al. (2014).

Material	Inner layer (magnification 60 x)	Inner layer (magnification 180 x)
Corn straw		
Triticale	Outer layer (magnification 130 x)	Inner layer (magnification 130 x)

Straw		
	Outer layer (magnification 130 x)	Inner layer (magnification 130 x)
Rape straw		
	Outer layer (magnification 130 x)	Inner layer (magnification 130 x)
Rye straw		
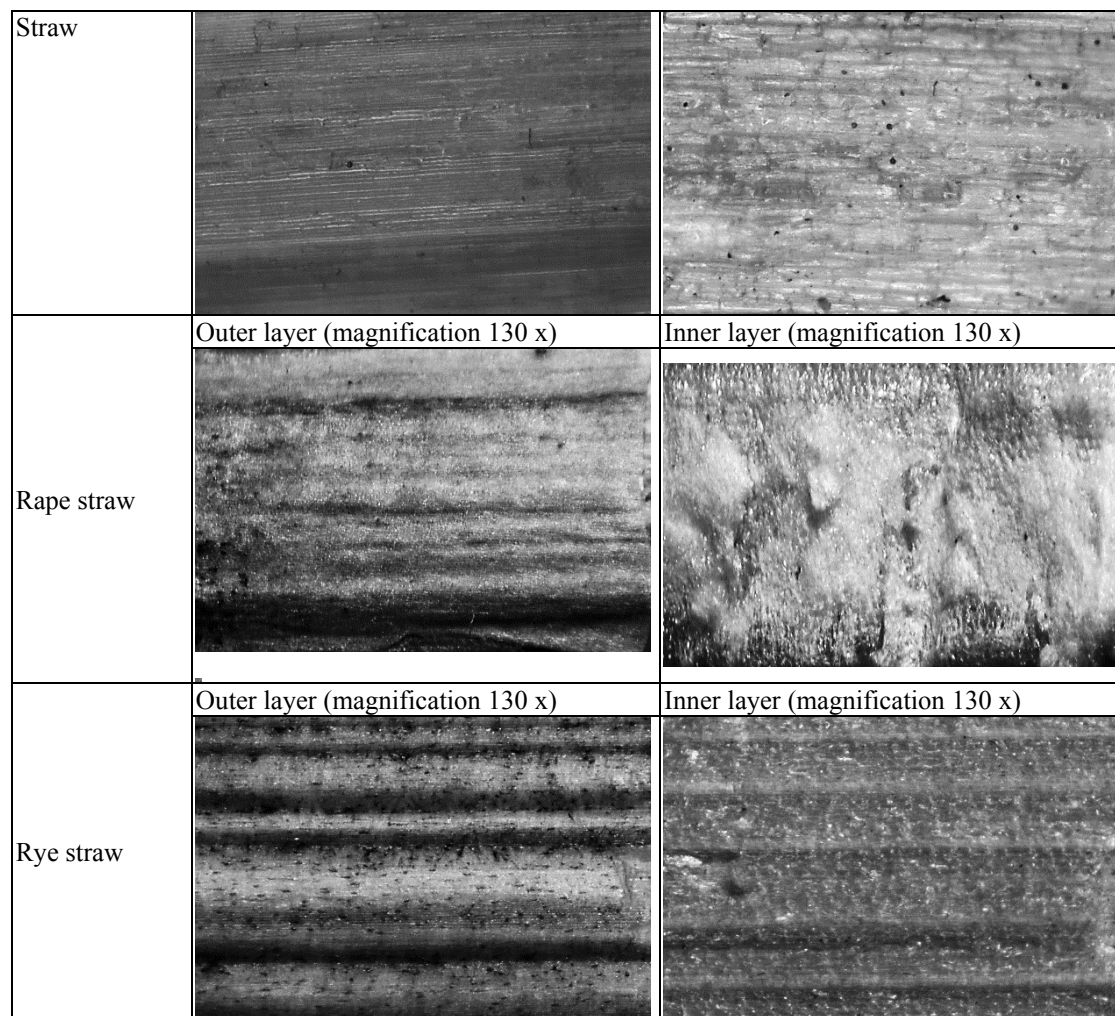
Fig. 1: Macrostructure of longitudinal sections of external and internal layers of the investigated straws of annual plants.

The results of the determination of the anatomical properties of the fibers of the tested lignocellulosic raw materials are presented in Fig. 2. The first stage of the straw morphological analysis was started with the comparison of the fiber length. Wheat has the longest fibers, the average length of these cells is 1820 µm. Literature data indicate that wheat straw fiber length was smaller (970 µm) in comparison with results of presented research (Ferdous et al. 2020). In turn, the shortest fibers were recorded for rape, as their average length was 800 µm. In the case of corn, the fibers from the inner zones of the cross-section were about 40% shorter (their average length was approximately 985 µm) compared to the outer zones. Rape had the largest diameter fibers (21.9 µm). According to these dimensions, these fibers showed the smallest slenderness, which did not exceed the value of 40. The diameters of the fibers of the tested plants were more even than their length.

The thickness of the fiber walls is also an important dimension influencing the physical and mechanical properties of the boards. Triticale and wheat fibers (about 5.6 µm) were characterized by very similar and at the same time the thickest walls. According to Ferdous et al. (2020) fiber wall thickness of wheat straw was 1.99 µm. The wall thicknesses of rye and

rape fibers were about 20% smaller, and that of maize about 36%, compared to the average thickness of triticale and wheat. In the case of maize, the thickness of the fiber walls (outer and inner part) was practically the same (3.7 µm). Comparing the coefficients of variation of the measured values, it can be concluded that the highest values occurred for the fiber length and they ranged from 19% for wheat to 42% for rape. For the fiber diameter and wall thickness, the coefficients of variation were smaller and amounted to, respectively, from 21% to 30% and from 23% to 32%.
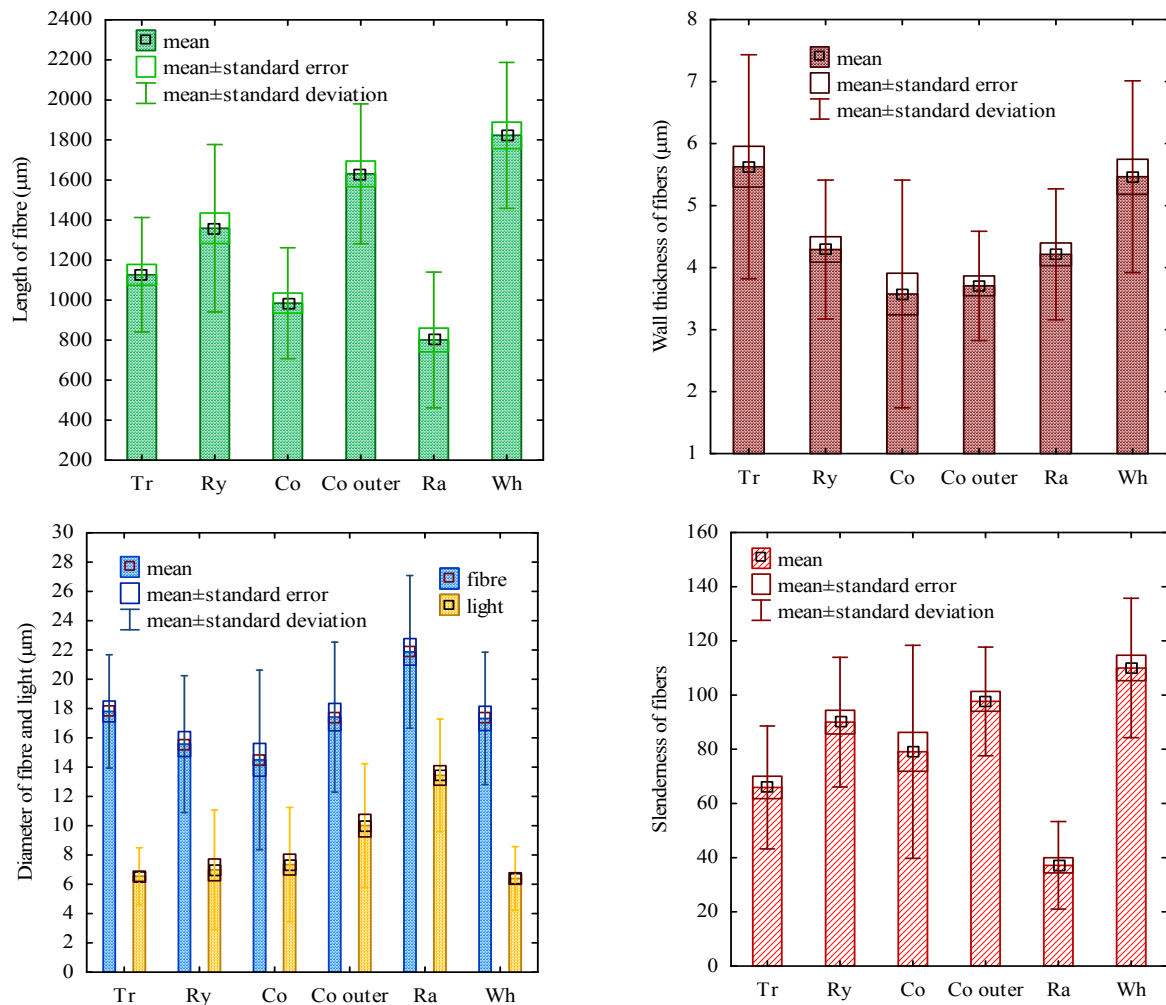
Fig. 2: Length, diameter of fibers and lumens, thickness and slenderness of fibers of tested lignocellulosic materials (Tr – triticale; Ry - rye; Co - corn; Ra - rape; Wh – wheat).

The Anova analysis of variance showed that at the significance level of 0.05, the differences in all measured fiber dimensions and the slenderness ratio of the tested plants are statistically significant. The values of the calculated Fisher F test statistics are greater than the table statistics (Tab. 1).

Tab. 1: Analysis of variance (ANOVA) of selected properties anatomical of the examined fibrous materials.

Source of variation	$F_{estimated}$ $F_{(5;177;0.05)}$	$F_{tabular}$ $F(5;177;0.05)$	p
Fiber lengths (μm)	40.339		0.000
Fiber diameters (μm)	8.215		0.000
Thickness of wall of fibres (μm)	11.381	2.265	0.000
Slenders ratio	32.455		0.000

Note: df- degrees of freedom, F- value of test Fisher, p- level of significance.

In previous studies, Mirski et al. 2018 determined the physicomechanical proper-ties of three-layer boards, in which the middle layer was made of industrial pine chips and the outer layers were straw particles of the annual plants studied in this study. Physical and mechanical properties of the boards were different for the individual plants. In order to demonstrate which anatomical features of the fibers of the studied plants have an impact on the physicomechanical properties and to determine the strength of this correlation, a correlation matrix was prepared based on their mean values (Tab. 2).

Tab. 2: Density correlation matrix (ρ), modulus of rigidity (MOR), modulus of elasticity (MOE), thickness swelling (TS24) and water absorption (WA24h), fiber lengths (L), fiber diameters (Dw), lumen diameters (Dl), slenderness fibers (S) and wall thickness fibers (T) of the annual plants tested.

Correlation coefficients (p < 0.05)									
	ρ	MOR	MOE	TS24h	WA24h	L	D_w	D_l	S	T
ρ	1.000	**0.7015**	**0.7588**	-0.4335	-0.6512	0.5065	-0.0402	-0.5425	0.1686	**0.9554**
MOR		1.0000	**0.9476**	**-0.8109**	**-0.9374**	**0.9571**	-0.4248	-0.6910	0.6680	0.5224
MOE			1.0000	**-0.9043**	**-0.9884**	**0.9271**	-0.5962	**-0.8744**	**0.7559**	0.5430
TS24h				1.0000	**0.9545**	**-0.9165**	**0.8725**	**0.9426**	**-0.9613**	-0.1504
WA24h					1.0000	**-0.9600**	0.6903	**0.8970**	**-0.8436**	-0.4091
L						1.0000	-0.6349	**-0.7677**	**0.8437**	0.2721
D_w							1.0000	**0.8603**	**-0.9453**	0.2513
D_l								1.0000	**-0.8682**	-0.2771
S									1.0000	-0.1279
T										1.0000

The obtained high values of correlation coefficients indicated that the increase in fiber length resulted in an increase in modulus of rigidity (MOR) and modulus of elasticity (MOE) and a decrease in both thickness swelling (TS) and water absorption (WA) after 24 h of soaking the tested boards in water. These correlations were statistically significant at the level of 0.05 with respect to the stiffness and water absorption modulus of the boards. The increase in fiber lumen diameter facilitates access and increases the possibility of water penetration into their interior, which influenced water absorption and swelling after 24 hours of soaking the boards in water and reduced the modulus of elasticity. It should be noted, however, that these correlations are strong, as these coefficients range from 0.8744 to 0.9426, but are statistically insignificant. On the other hand, the increase in the slenderness of the fibers significantly reduces the

swelling of the boards after 24 hours of soaking in water. A strong and positive, although statistically insignificant, relationship was found between slenderness and modulus of elasticity, and a strong and negative correlation was found between slenderness and water ab-sorption after 24 h of soaking. On the other hand, the correlation coefficient between the thickness of the fiber walls and the density of the boards indicates that this relationship is strong and statistically significant, as it reaches the value of 0.9554.

CONCLUSIONS

(1) The tested straws of annual plants show statistically significant differences at the level of 0.05 for all analyzed anatomical features of the fibers. *(2)* The longest fibers were recorded for wheat and these values were over two times higher than those of rape, where these cells were the shortest. Due to small differences in fiber diameters in the analyzed plants, the slenderness ratio was determined by the fiber length. The differentiation of the mean values of this coefficient was almost threefold. *(3)* The thickness of the fiber walls was similar for wheat and triticale (approx. 5.5 μm) as well as rye and rape (approx. 4.5 μm) and they were respectively approx. 35% and approx. 15% higher than corn fibers. *(4)* A strong positive correlation was demonstrated between fiber length and modulus of rigidity (MOR) and modulus of elasticity (MOE) and a strong but negative correlation between fiber length and swelling and water absorption after 24 h of soaking the panels. *(5)* A strong, positive correlation was also obtained for the relationship between the diameter of the lumen of the fibers and the thickness swelling and water absorption after 24 h of soaking the panels. On the other hand, high, but negative correlation coefficients were established between the slenderness of the fibers and the analyzed physical properties of the boards. Slightly smaller, positive values of the correlation coefficients were obtained between the slenderness of the fibers and the modulus of rigidity (MOR) and modulus of elasticity (MOE).

REFERENCES

1. Azizi, K., Tabarsa, T., Ashori, A., 2011: Performance characterizations of particleboards made with wheat straw and waste veneer splinters. Composites Part B: Engineering 42(7): 2085–2089.
2. Bekalo, S.A., Reinhardt, H.-W., 2010: Fibers of coffee husk and hulls for the production of particleboard. Materials and structures 43: 1049–1060.
3. Bekhta, P., Korkut, S., Hiziroglu, S., 2013: Effect of pretreatment of raw material on properties of particleboard panels made from wheat straw. BioResources 8(3): 4766–4774.
4. Boquillon, N., Elbez, G., SchÖnfeld, U., 2004: Properties of wheat straw particleboards bonded with different types of resin. Journal of Wood Sciences 50: 230–235.
5. Bouasker, M., Belayachi, N., Hoxha, D., Al-Mukhtar, M., 2014: Physical characterization of natural straw fibers as aggregates for construction materials applications. Materials 7(4): 3034–3048.

6. Cheng, W., Han, G., Fang, D., 2013: Oriented structural boards from split wheat straw: effects of straw length, panel density, and resin content. BioResources 8(3): 4497–4504.

7. Dukarska, D., Bartkowiak, M., Stachowiak- Wencek, A., 2015: White mustard straw as an alternative raw materials in the manufacture of particleboards resonated with different amounts of urea-formaldehyde resin. Drewno 58(194): 49–63.

8. Dukarska, D., Łęcka, J., Czarnecki, R., 2015: The effect of wood chip substitution with evening primrose waste on properties of particleboards depending on the type of binding agent. Electronic Journal of Polish Agricultural Universities: 15(2): 5.

9. Dziurka, D., Mirski, R., 2013: Lightweight boards from wood and rape straw particles. Drewno 56(190): 19-31.

10. Ferdous, T., Quaiyyum, M.A., Bashar, S., Jahan, M.S., 2020: Anatomical, morphological and chemical characteristics of kaun straw (*Seetaria italika*). Nordic Pulp & Paper Research Journal 35(2): 288–298.

11. Gradziuk, P., Gradziuk, B., Trocewicz, A., Jendrzejewski, B., 2020: Potential of straw for energy purposes in Poland. Forecasts based on trend and causal models. Energies 13: 5054.

12. Grigoriou, A.H., 2000: Straw-wood composites bonded with various adhesive systems. Wood Science and Technology 34: 355–365.

13. Guuntekin, E., Uner, B., Karakus, B., 2009: Chemical composition of tomato (*Solanum lycopersicum*) stalk and suitability in the particleboard production. Journal of environmental biology 30(5): 731-734.

14. Hafezi, S.M., Hosseini, K.D., 2014: Surface characteristics and physical properties of wheat straw particleboard with UF resin. Journal of the Indian Academy of Wood 11: 168–173.

15. Huang, L., Xia, P., Liu, Y., Fu, Y., Jiang, Y., Liu, S., Wang, X., 2016: Production of biodegradable board using rape straw and analysis of mechanical properties. BioResources 11(1): 772–785.

16. Kargarfard, A., Latibari, A.J., 2011: The performance of corn and cotton stalks for medium density fiberboard production. BioResources 6(2): 1147–1157.

17. Kurokochi, Y., Sato, M., 2015: Effect of surface structure, wax and silica on the properties of binderless board made from rice straw. Industrial Crops and Products 77: 949–953.

18. Li, X., Cai, Z., Winandy, J.E., Basta, A.H., 2011: Effect of oxalic acid and steam pretreatment on the primary properties of UF-bonded rice straw particleboards. Industrial Crops and Products 33(3): 665–669.

19. Liu, Z., Wang, H., Hui, L., 2018: Pulping and papermaking of non-wood fibers. Pulp and Paper Processing 1: 4–31.

20. Madej, A., 2016: Bilans słomy w Polsce w latach 2010-2014 oraz prognoza do 2030 roku (Straw balance in Poland in the years 2010-2014 and forecast to the year 2030). Roczniki Naukowe Stowarzyszenia Ekonomistów Rolnictwa i Agrobiznesu 18: 163–168.

21. Markiewicz, M., Muślewski, Ł., 2020: Survey performance and emission parameters of diesel engine powered by diesel oil and fatty acid methyl esters using fuzzy logic techniques. Fuel 277: 118179.

22. Meyer, A.K.P, Ehimen, E.A., Holm-Nielsen J.B., 2018: Future European biogas: Animal manure, straw and grass potentials for a sustainable European biogas production. Biomass and Bioenergy 111: 154-164.

23. Mirski, R., Dziurka, D., Banaszak, A., 2018: Properties of particleboards produced from various lignocellulosic particles. BioResources 13(4): 7758–7765.

24. Mirski, R., Dziurka, D., Czarnecki, R. 2016: The possibility of replacing strands in the core layer of oriented strand board by particles from the stems of rape (*Brassica napus* L. Var. Napus). BioResources 11(4): 9273–9279.

25. Mirski, R., Kawalerczyk, J., Dziurka, D., Wieruszewski, M., Trociński, A., 2020: Effects of using bark particles with various dimensions as a filler for urea-formaldehyde resin in plywood. BioResources 15(1): 1692–1701.

26. Mo, X., Cheng, E., Wang, D., Sun, X.S., 2003: Physical properties of medium-density wheat straw particleboard using different adhesives. Industrial Crops and Products 18: 47–53.

27. Moriarty, C.J., 2002: The effect of lab-made flakes on physical and mechanical property variability of laboratory flakeboard. Forest Products Journal 52: 69–73.

28. Nemli, G., Kırcı, H., Serdar, B., Ay, N., 2003: Suitability of kiwi (*Actinidia sinensis* Planch.) prunings for particleboard manufacturing. Industrial Crops and Products 17: 39–46.

29. Paukszta, D., 2006: Skład Chemiczny Zdrewniałej Części Łodygi Słomy Rzepakowej (Chemical composition of wooden parts of rape stem). Rośliny Oleiste – Oilseed Crops XXVII: 143–150.

30. Papadopoulos, A.N., Hague, J.R., 2003: The potential for using flax (*Linum usitatissimum* L.) shiv as a lignocellulosic raw material for particleboard. Industrial Crops and Products 17: 143–147.

31. Papadopoulos, A.N., Hill, C.A.S., Gkaraveli, A., Ntalos, G.A., Karastergiou, S.P., 2004: Bamboo chips (*Bambusa vulgaris*) as an alternative lignocellulosic raw material for particleboard manufacture. Holz als Roh-und Werkstoff 62(1): 36–39.

32. van Duren, I., Voinov, A., Arodudu, O., Firrisa, M.T., 2015: Where to produce rapeseed biodiesel and why? Mapping European Rapeseed Energy Efficiency. Renewable Energy 74: 49–59.

33. Wu, T., Wang, X., Kito, K., 2015: Effects of pressures on the mechanical properties of corn straw bio-board. Engineering in Agriculture, Environment and Food 8(3): 123–129.

34. Xu, J., Sugawara, R., Widyorini, R., Han, G., Kawai, S., 2004: Manufacture and properties of low-density binderless particleboard from kenaf core. Journal of Wood Science 50: 62–67.

RADOSŁAW MIRSKI*, ALEKSANDRA BANASZAK, EWA FABISIAK,
JOANNA SIUDA
POZNAŃ UNIVERSITY OF LIFE SCIENCES
DEPARTMENT OF WOOD BASED MATERIAL
28 WOJSKA POLSKIEGO STR., 60-637
POZNAŃ, POLAND
*Corresponding author: radoslaw.mirski@up.poznan.pl

INVESTIGATION OF EFFECT OF USING NANO COATING ON WOODEN SHEDS ON DYNAMIC PARAMETERS

SERTAÇ TUHTA, FURKAN GÜNDAY

ONDOKUZ MAYIS UNIVERSITY

TURKEY

ABSTRACT

In this article, the dynamic parameters (frequencies, mode shapes, damping ratios) of the uncoated wooden shed and the coated by silicon dioxide are compared using the operational modal analysis method. Ambient excitation was provided from micro tremor ambient vibration data on ground level. Enhanced frequency domain decomposition (EFDD) was used for output. Very best correlation was found between mode shapes. Nano-SiO_2 gel applied to the entire outer surface of the red oak shed has an average of 14.54% difference in frequency values and 13.53% in damping ratios, proving that nanomaterials can be used to increase internal rigidity in wooden slabs. High adherence of silicon dioxide to wooden surfaces was observed as another important result of this study.

KEYWORDS: Operational modal analysis, nanomaterial, wooden, EFDD, SiO_2.

INTRODUCTION

Nanotechnology can produce products with many unique properties that can improve existing building materials: lighter and stronger structural composites, less maintenance coatings, more useful cement-based materials, products with better thermal insulation properties, etc. (Akbaş 2020). In addition, nanomaterials applied to the surfaces of structural elements of buildings can contribute to environmental cleaning and energy generation through photocatalytic reactions (Akbaş 2020). As many become interested in pursuing good health, environmental and protection in the use of wood products becomes increasingly critical (Jing et al. 2019). Thanks to nanotechnology, wood can be stronger, more durable and easier to place, steel can be made tougher, glass self-cleaning, and paints can be made more insulating and water-repellent (Tang et. al. 2018).

The reason for using silicon dioxide in the study is that its mechanical properties are as good as conventional materials (AFRP, BFRP, CFRP, GFRP, etc.) used in reinforcement (Arriaga et al. 2011, Motlagh et al. 2012, Prachasaree and Limkatanyu 2013, Glišović et

al. 2016, Kisitotalla et al. 2017, Dave et al. 2018, Doubek et al. 2018). Nano-SiO$_2$ gel has large specific surface area and strong adsorption properties, which may help to prevent water-based fire retardant from running off (Zhongxi et al. 2020).

Operational modal analysis method is an up-to-date experimental method that is frequently used in determining the dynamic parameters of structures. The basic principle of the method is based on obtaining dynamic parameters such as frequency, mode shapes and damping ratios by processing the output data received from the structure. In addition, operational modal analysis is used to determine the damage levels of the existing structures, to check the validity of the assumptions made while constructing the finite element model, to update the initial numerical model of the existing structures according to the experimental data, to determine the dynamic characteristics of the structures by the experimental modal analysis method when the numerical model of the existing structures cannot be formed and to follow the structural health is widely used in the process (Alvin and Park 1994, Tseng et al. 1994, Aliev and Larin 1998, Ljung 1999, Lus et al. 2003, Roeck 2003).

It is necessary to estimate sensitivity of reaction of examined system to change of random or fuzzy parameters of a structure. Investigated measurement noise perturbation influences to the identified system modal and physical parameters. Estimated measurement noise border, for which identified system parameters are acceptable for validation of finite element model of examine system. System identification is realized by observer Kalman filter (Kalman 1960, Trifunac 1972, Ibrahim 1977, Juang 1994). In special case observer gain may be coincide with the Kalman gain. Stochastic state-space model of the structure is simulated by Monte-Carlo method. As a result of these theoretical and experimental studies, the importance of temperature change and humidity has emerged once again from the environmental factors affecting the odal parameters. The effects of temperature and humidity on modal parameters have been the subject of thorough examination in the last 15 years (Kasımzade and Tuhta 2017, Tuhta 2018, 2019).

It was observed that three types of definitions were used in the engineering structures: modal parameter identification; structural-modal parameter identification; control-model identification methods are used. In the frequency domain the identification is based on the singular value decomposition of the spectral density matrix and it is denoted frequency domain decomposition (FDD) and its further development enhanced frequency domain decomposition (EFDD). In the time domain there are three different implementations of the Stochastic Subspace Identification (SSI) technique: Unweighted principal component (UPC); Principal component (PC); Canonical variety analysis (CVA) is used for the modal updating of the structure (Sestieri and Ibrahim 1994, Balmes 1997, Bendat 1998, Marwala 2010).

In this study, the EFFD method was used in the signal processing. The Enhanced Frequency Domain Decomposition technique is an extension to Frequency Domain Decomposition (FDD) technique. This technique is a simple technique that is extremely basic to use. In this technique, modes are easily picked locating the peaks in Singular Value Decomposition (SVD) plots calculated from the spectral density spectra of the responses. FDD technique is based on using a single frequency line from the Fast Fourier Transform

_____

analysis (FFT), the accuracy of the estimated natural frequency based on the FFT resolution and no modal damping is calculated. On the other hand, EFDD technique gives an advanced estimation of both the natural frequencies, the mode shapes and includes the damping ratios (Jacobsen et al. 2006). In EFDD technique, the single degree of freedom (SDOF) Power Spectral Density (PSD) function, identified about a peak of resonance, is taken back to the time domain using the Inverse Discrete Fourier Transform (IDFT). The natural frequency is acquired by defining the number of zero crossing as a function of time, and the damping by the logarithmic decrement of the correspondent single degree of freedom (SDOF) normalized auto correlation function Peeters (2000).

The aim of this study is to determine the effects of silicon dioxide usage on the dynamic parameters of the wooden sheds. For this purpose, the dynamic parameters (frequencies, mode shapes, damping ratios) of the wooden shed (red oak) and the dynamic parameters (frequencies, mode shapes, damping ratios) of the entire outer surface of the 80-micron thick silicon dioxide are compared using the operational modal analysis method.

MATERIAL AND METHODS

Description of wooden shed model

The wooden shed was produced from red oak slabs with a thickness of 20 mm with density 630 $kg \cdot m^{-3}$ in the Ondokuz Mayıs University Civil Engineering Laboratory. Modulus of elasticity E = 11300 MPa was determined according to used materials property, Poisson ratio $\mu = 0.35$ was determined according to used materials property. The wooden shed model and dimensions is shown in Fig. 1.
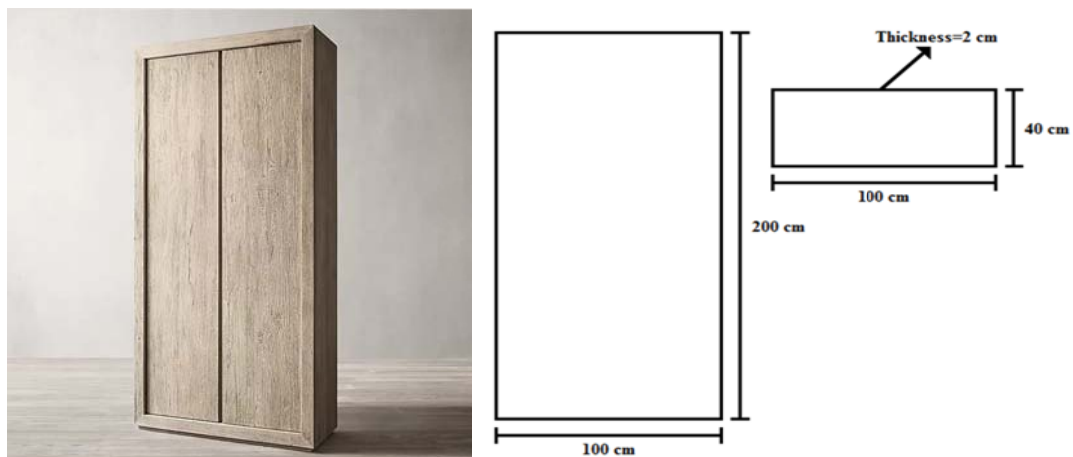
Fig. 1: Wooden shed model and dimensions.

In the case of coated wooden shed, the following studies are made on it to check and examine the efficiency of using SiO_2 coating: entire outer surface of the 80 μm thick of wooden shed are coated with multi-layer SiO_2 coating. SiO_2 coating and its components YKS is product of YKS Corporation. The properties of the slab coated with SiO_2 are: E = 7.5E10 $N \cdot m^{-2}$, Poisson ratio $\mu = 0.17$, mass per unit volume $\rho = 22000$ $N \cdot m^{-3}$, thickness = 0.00008 m. The entire outer surface of the wooden shed is covered of silicon dioxide. Approximately amount of

180 g of paint is used in 1 m^2. The surface is expected to dry during each application approximately 1 hour of curing in order to prepare a surface for application of silicon dioxide. After these setups, ambient vibration tests are followed by curing to obtain experimental dynamic characteristics similar to previously used properties in order to obtain comparative measurements.

Operational modal analysis of wooden shed

In this study, the operational modal analysis method was used to obtain the modal parameters. Three accelerometers are used to measure ambient vibrations. One of them is always assigned as the reference sensor located at the bottom of shear wall. The acceleration record was measured in two data sets. For the two data sets, 2 and 3 accelerometers were used, respectively. Accelerometers were calibrated and used, thus preventing possible measurement errors. 100 min were recorded for each data set. Selected measurement points and directions are shown in the figure. Ambient stimulation was achieved using microtremor data recorded at ground level. Matlab software and Artemis modal pro software were used to obtain modal parameters. First setup and second setup are given in Fig. 2.

Fig. 2: First setup and second setup for OMA.

RESULTS AND DISCUSSION

Ambient excitation data from the recorded micro tremor data on ground level is given in Fig. 3. Singular values of spectral density matrices of wooden shed are given in Fig. 4.
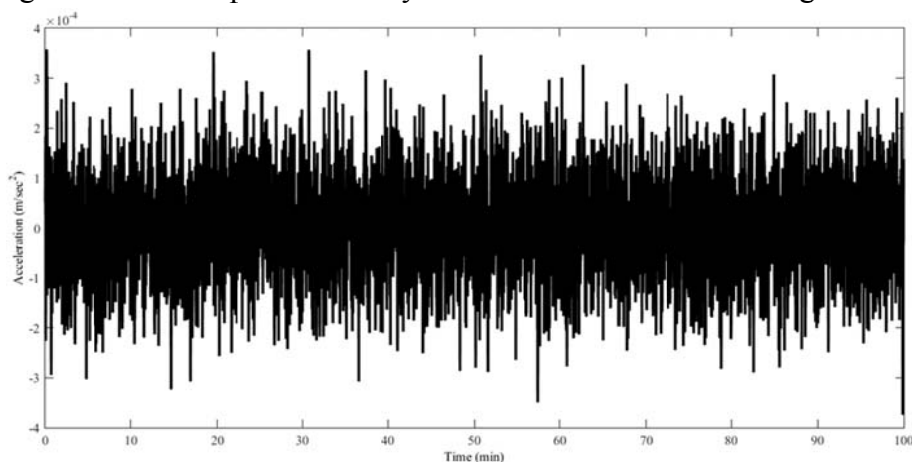
Fig. 3: Ambient excitation data from the recorded micro tremor data on ground level.
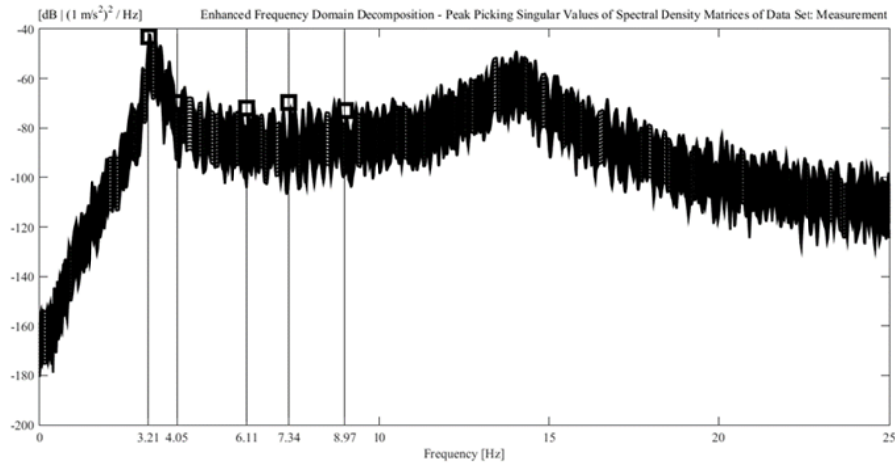
Fig. 4: Singular values of spectral density matrices of wooden shed model.

The first five mode shapes extracted from experimental modal analyses are given in Fig. 5. Natural frequencies and modal damping ratio acquired from all measurement setups with operational modal analyses are given in Tab. 1. When all measurements are examined, it can be seen that a best accordance is found between experimental mode shapes. In addition, when both setup sets are experimentally identified modal parameters are checked with each other, it can be seen that there is a best agreement between the mode shapes in the operational modal analyses.

Fig. 5: The first five mode shapes respectively.

Tab. 1: Operational modal analysis result at the wooden shed model.

Mode number	1	2	3	4	5
Frequency (Hz)	3.21	4.05	6.11	7.34	8.97
Modal damping ratio (ξ)	1.34	1.18	0.91	1.02	0.84

Operational modal analysis of coated wooden shed model

Care is taken to ensure that the measurements are the same as those made in the wooden shed model. SVSDM are shown in Fig. 6. The first five mode shapes extracted from experimental modal analyses are given in Fig. 7.
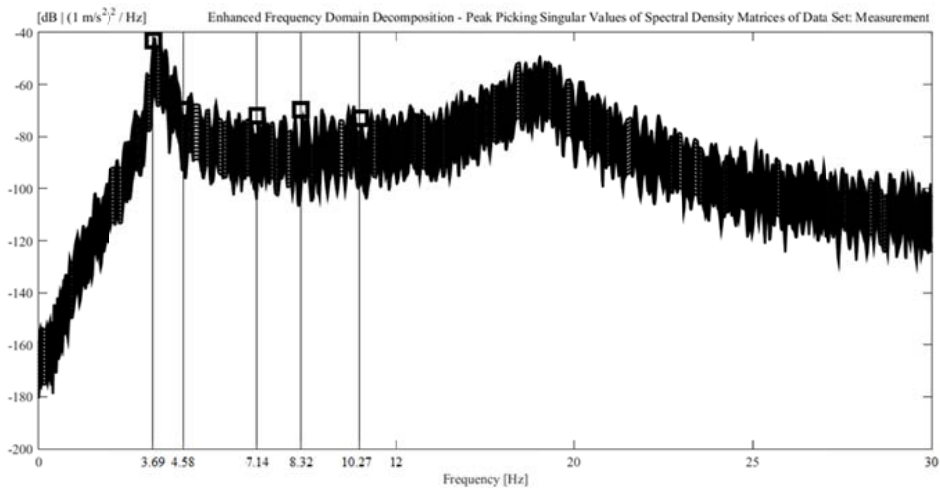
Fig. 6: Singular values of spectral density matrices of coated wooden shed model.

Fig. 7: The first five mode shapes respectively.

It is clear that using silicon dioxide seems to be very effective for strengthening wooden members along with increasing stiffness; this research aims to determine how SiO_2 implementation affects structural response of wooden shed by changing of dynamic characteristics. Natural frequencies and modal damping ratio acquired from all measurement setups with operational modal analyses are given in Tab. 2.

Tab. 2: Operational modal analysis result at the coated wooden shed model.

Mode number	1	2	3	4	5
Frequency (Hz)	3.69	4.58	7.14	8.32	10.27
Modal damping ratio (ξ)	1.07	0.98	0.82	0.93	0.74

Comparison of existing and coated wooden shed models frequency results are given in Tab. 3. Where E is the existing wooden shed model and C is coated shed model. Comparison of Existing and Coated Shed Damping Ratio Results are given Tab. 4. Where E is the existing wooden shed model and C is coated shed model.

Tab. 3: Comparison of existing and coated wooden shed model frequency results.

Mode number	1	2	3	4	5
Frequency (Hz)-E	3.21	4.05	6.11	7.34	8.97
Frequency (Hz)-C	3.69	4.58	7.14	8.32	10.27
Difference (%)	14.95	13.08	16.85	13.35	14.49

Tab. 4: Comparison of existing and coated shed damping ratio results.

Mode number	1	2	3	4	5
Modal damping ratio (ξ) - E	1.34	1.18	0.91	1.02	0.84
Modal damping ratio (ξ) - C	1.07	0.98	0.82	0.93	0.74
Difference (%)	20.14	16.94	9.89	8.82	11.90

CONCLUSIONS

In this research, the conducted were both operational modal analysis of existing wooden shed and silicon dioxide coated wooden shed. Comparing the result of study, the followings are noticed: *(1)* From the ambient vibration test, the first five natural frequencies are attained experimentally, which range between 3 and 11 Hz. *(2)* When comparing the existing and coated wooden shed results, it is clearly seen that there is very best agreement between mode shapes. *(3)* It has been determined that there is an average of 14.54% difference between the frequency values of the existing wooden shed and the silicon dioxide coated wooden shed. *(4)* It has been determined that there is an average of 13.53% difference between the damping ratios of the existing wooden shed and the silicon dioxide coated wooden shed. *(5)* Silicon dioxide applied to the entire outer surface (80 micron thick) of the wooden shed has an average of 14.54% difference in frequency values (Tab. 3) and 13.53% in damping ratios (Tab. 4), proving that nanomaterials can be used to increase rigidity in wooden sheds, in other words, for reinforcement. *(6)* The fact that no negative chemical reaction was observed between wood and silicon dioxide during the examination revealed that such nano-coatings can be used in wooden structures. *(7)* Another important result determined in the study is that it has been observed that the adherence of silicon dioxide and similar nanomaterials mentioned in the introduction to wooden shed surfaces is at the highest level.

REFERENCES

1. Akbaş, Ş.D., 2020: Modal analysis of viscoelastic nanorods under an axially harmonic load. Advances in Nano Research 8(4): 277-282.
2. Aliev, F.A., Larin, V.B., 1998: Optimization of linear control systems. Analytical Methods and Computational Algorithms. Florida, CRC Press, 279 pp.
3. Alvin, K.F., Park, K.C., 1994: Second-order structural identification procedure via state-space-based system identification. AIAA Journal 32(2): 397-406.
4. ANSI S2.47-1990, 1990: Vibration of buildings. Guidelines for the measurement of vibrations and evaluation of their effects on buildings.
5. Arriaga, F., Íñiguez-Gonzáles, G., Esteban, M., 2011: Bonding shear strength in timber and GFRP glued with epoxy adhesives. Wood Research 56(3): 297-310.
6. Balmes, E., 1997: New results on the identification of normal modes from experimental complex modes. Mechanical Systems and Signal Processing 11(2): 229-243.
7. Bendat, J.S., 1998: Nonlinear systems techniques and applications. USA, Wiley, 488 pp.

8. Brincker, R., Zhang, L., Andersen, P., 2000: Modal identification from ambient responses using frequency domain decomposition. Proceedings of the 18th International Modal Analysis Conference (IMAC), Pp 625-630, San Antonio, Texas, USA.

9. Dave, M., Pandya, T., Stoddard, D., Street, J., Blake, C., Ly, P., 2018: Dynamic and damping properties of novel bio-composites using the hammer excitation vibration technique. Wood Research 63(2): 215-226.

10. Doubek, S., Borůvka, V., Zeidler, A., Reinprecht, L., 2018: Effect of the passive chemical modification of wood with silicon dioxide (silica) on its properties and inhibition of moulds. Wood Research 63(4): 599-616.

11. Glišović, I., Stevanović, B., Todorović, M., Stevanović, T., 2016: Glulam beams externally reinforced with CFRP plates. Wood Research 61(1): 141-154.

12. Günday, F., 2018: GFRP retrofitting effect on the dynamic characteristics of model steel structure using SSI. International Journal of Advance Engineering and Research Development 5(4): 1160-1173.

13. Günday, F., 2018: OMA of RC industrial building retrofitted with CFRP using SSI. International Journal of Advance Engineering and Research Development 5(5): 759-771.

14. Ibrahim, S.R., 1977: Random decrement technique for modal identification of structures. Journal of Spacecraft and Rockets 14(11): 696-700.

15. Jacobsen, N.J., Andersen, P., Brincker., R., 2006: Using enhanced frequency domain decomposition as a robust technique to harmonic excitation in operational modal analysis. International Conference on Noise and Vibration Engineering (ISMA), Leuven, Belgium.

16. Jing, Q., Jinpeng, L., Zhenyu, W., Lijie, Q., Yu, D., Songlin, Y., Zhengbin, H., 2019: Effects of wax and dimethyl silicone oil mixed impregnation on dimensional stability of two hardwoods. Wood Research 64(1): 165-176.

17. Juang, J.N., 1994: Applied system identification. New Jersey, Prentice Hall, 394 pp.

18. Kalman, R.E., 1960: A new approach to linear filtering and prediction problems, Journal of Basic Engineering 82(1): 35-45.

19. Kasimzade, A.A., Tuhta, S, 2017: Application of OMA on the bench-scale earthquake simulator using micro tremor data. Structural Engineering and Mechanics 61(2): 267-274.

20. Kasimzade, A.A., Tuhta, S, 2017: OMA of model steel structure retrofitted with CFRP using earthquake simulator. Earthquakes and Structures 12(6): 689-697.

21. Kisitotalla, P., Atchounga, P.K., Mtopi, B., 2017: Kalman filtering of gauges noise on the creep behavior of *Entandrophragma cylindricum* (Sapelli) under a constant stress. Wood Research 62(3): 341-352.

22. Ljung, L., 1999: System identification: Theory for the user. New Jersey, Prentice Hall, 640 pp.

23. Lus, H., De Angelis, M., Betti, R., Longman, R.W., 2003: Constructing second-order models of mechanical systems from identified state space realizations. Part I: Theoretical discussions. Journal of Engineering Mechanics 129(5): 477-488.

24. Marwala, T., 2010: Finite element model updating using computational intelligence techniques: Applications to Structural Dynamics. USA, Springer Science-Business Media, 250 pp.

25. Motlagh, B., Gholipour Y., Ebrahimi G., 2012: Experimental investigation on mechanical properties of old wood members reinforced with FRP composite. Wood Research 57(2): 285-296.
26. Peeters, B., 2000: System identification and damage detection in civil engineering. PhD. dissertation, Katholieke Universiteit Leuven, Leuven, Belgium, 238 pp.
27. Prachasaree, W., Limkatanyu., S., 2013: Performance evaluation of FR Preinforced para wood glued laminated beams. Wood Research 58(2): 251-264
28. Roeck, G.D., 2003: The state of the art of damage detection by vibration monitoring: the SIMCES experience. Journal of Structural Control 10(2): 127-134.
29. Sestieri, A., Ibrahim, S.R., 1994: Analysis of errors and approximations in the use of modal coordinates. Journal of Sound and Vibration 177(2): 145-157.
30. Tang, Z., Yu, L., Zhang, Y., Zhu, L., Ma, X., 2018: Effects of nano-SiO_2/polyethylene glycol on the dimensional stability modified ACQ treated southern pine. Wood Research 63(5): 763-770.
31. Trifunac, M.D., 1972: Comparisons between ambient and forced vibration experiments. Earthquake Engineering and Structural Dynamics 1(2): 133-150.
32. Tseng, D.H., Longman, R.W., Juang, J.N., 1994: Identification of the structure of the damping matrix in second order mechanical systems. Spaceflight Mechanics 167-190.
33. Tuhta, S., 2018: GFRP retrofitting effect on the dynamic characteristics of model steel structure. Steel and Composite Structures 28(2): 223-231.
34. Tuhta, S., 2019: OMA of model chimney using bench-scale earthquake simulator. Earthquakes and Structures 16(3): 321-327.
35. Zhongxi, Z., Chungui, D., Huilong, Y., Xiaoling, Y., Qiuli, H., 2020: Promotion effect of nano-SiO_2 on hygroscopicity, leaching resistance and thermal stability of bamboo strips treated by nitrogen-phosphorus-boron fire retardants. Wood Research 65(5): 693-704.

SERTAÇ TUHTA, FURKAN GÜNDAY[*]
ONDOKUZ MAYIS UNIVERSITY
FACULTY OF ENGINEERING
DEPARTMENT OF CIVIL ENGINEERING
55139, ATAKUM
SAMSUN
TURKEY
*Corresponding author: furkan.gunday@omu.edu.tr

THE SOY FLOUR AS AN EXTENDER FOR UF AND MUF ADHESIVES IN BIRCH PLYWOOD PRODUCTION

JAKUB KAWALERCZYK, JOANNA SIUDA, DOROTA DZIURKA,
RADOSŁAW MIRSKI, MAGDALENA WOŹNIAK, KINGA STUPER-SZABLEWSKA
POZNAŃ UNIVERSITY OF LIFE SCIENCES
POLAND

ABSTRACT

Formaldehyde emission still remains a major disadvantage of widely applied formaldehyde-containing amino resins such as UF (urea-formaldehyde) resin and MUF (melamine-urea-formaldehyde) resin. The compositions of adhesives for plywood manufacturing have to contain a proper extenders in order to adjust their viscosity. Thus, the aim of the study was to investigate the effect of protein-rich soy flour (SF) as the extender for adhesives. The composition of flours and their ability to absorb the formaldehyde were determined. Properties of liquid resins such as gel time, viscosity, pH and solid content were investigated. The possible chemical interaction between the extenders and resins were assessed with the use of FTIR spectroscopy. Plywood panels manufactured using UF and MUF adhesives with the soy flour introduced as the extender in various concentrations were tested in terms of shear strength and formaldehyde release. Studies have shown that soy flour has a favorable composition and formaldehyde-scavenging ability. The addition of SF affected resins properties such as viscosity and gel time but showed no influence on their pH and solid content. FTIR analysis has not explained the chemical interaction between resin and extender. The application of soy flour in the concentration of 15% for UF resin and 10% for MUF resin allowed to produce plywood characterized by improved bonding quality and decreased formaldehyde emission.

KEYWORDS: Amino resins, soy flour, extender, plywood.

INTRODUCTION

The start of innovative wood composites production had a major effect on wood utilization by its fragmentation to a particles and bonding them together. In addition to the suitable use of scarce raw material, the developed boards were characterized by a properties that were not available from solid wood. Since then, wood-based panels such as plywood, medium- and high

density fiberboards became more popular and as their global production increases, the consumption of wood adhesives also increases (Bekhta et al. 2020, Kawalerczyk et al. 2019a). Because of that, there are many ongoing studies concerning the invention of new adhesives or the refinement of the already existing ones (Frihart 2015).

Nowadays the amino resins such as urea-formaldehyde (UF) and melamine-urea-formaldehyde (MUF) are the main adhesives used in the industry for the preparation of wood-based materials (Lei and Frazier 2015). UF resins have gained a wide applications mostly due to their good adhesion to wood, fast curing and low cost (Costa et al. 2013). On the other hand, MUF resins are characterized by a higher moisture resistance which allows to extend the possible applications and include the panels intended for kitchen, floor and structural use (Mirski et al. 2020a). However, the common disadvantage of these resins is the release of formaldehyde (HCHO) from the finished boards, especially those for indoor applications (Antov et al. 2020a, Mirski et al. 2020b).

The effective way to reduce the harmful emissions from plywood is to select a suitable extender for the adhesive (Kawalerczyk et al. 2020b). The compositions of the adhesive mixture in plywood manufacturing have to contain the additives called the fillers or the extenders in order to adjust their viscosity (Chen and Yan 2018, Dukarska and Czarnecki 2016). Many studies have been carried out in order to find a new proteinaceous filling substances for plywood manufacturing. Hogger et al. (2020b) investigated the possibility to introduce wheat flour, wheat starch and wheat protein in various concentrations to PF (phenol-formaldehyde) and UF resin. Studies have shown that the amount of the extender added was determined by the increase in viscosity. The extenders had no major effect on pH values, curing behavior and the course of FTIR (Fourier transform infrared spectroscopy) spectra. Moreover, the properties of plywood containing the various wheat extenders were investigated. It was concluded that the wheat flour and wheat starch can be applied as a suitable filling substances for UF and PF adhesives. However, the amount of wheat protein added was limited by the viscosity of the mixtures to 30% for both resins. The type of extender had no significant effect on the formaldehyde emission (Hogger et al. 2020a). Waage et al. (1991) added up to 40% pecan shell flour and 33% wheat flour to PF resin and determined the influence on its curing properties by thermal analysis (dynamic mechanical thermal analysis and differential scanning calorimetry). The obtained results indicated no significant changes of the extender on the curing process. Ding et al. (2013) added the wheat flour, wheat starch mixed with gluten and maize powder to the UF resin. The strength properties of bond layer between the veneers was not affected by the type of additive. Moreover, it was found that the gluten addition resulted in the highest increase of the viscosity values. Ong et al. (2018) tested the possibility to apply the palm kernel meal (PKM) and palm shell (PS) to the composition of MUF adhesive. Authors optimized the extenders concentration in the range from 13 to 18% where the decrease in formaldehyde emission was at a minimum at 18% and the shear strength increase was at a maximum at 13%. Babcock and Smith (1947) investigated the possibility of using corn gluten and soybean meal as the vegetable proteinaceous extenders for phenolic adhesive in plywood production. Formulas including resin and protein materials in the ratio of 6:4 was characterized by the rapid curing time and the strength properties which meet the

requirements for the exterior plywood. Hojilla-Evangelista (2013) studied the application of wet-milled corn germ protein as the extender for phenolic resin. Investigations have shown that the best properties of plywood panels were achieved with the corn germ protein extract included in the adhesive compositions. Taghiyari et al. (2020) conducted the research on the use of soy flour and a micron-sized wollastonite as the fillers for UF resin. On the basis of the results it was found that 10% of soy flour and 5% of wollastonite in the adhesive formulation provided plywood with the lowest formaldehyde emission and the most optimal mechanical and physical properties.

This study is a continuation of the research concerning the incorporation of various flour types into the adhesives applied in the plywood manufacturing process. The following five types of flours were investigated as the potential UF resin extenders: hemp, rye, coconut, pumpkin and rice. The outcomes showed that the influence on viscosity and gel time varied depending on the introduced flour type. Moreover, the plywood panels were tested in terms of shear strength, modulus of elasticity and modulus of rupture. The best results were noted in variants containing the rye and pumpkin flour. The values of formaldehyde emission indicated that the hemp flour can be also used as a formaldehyde scavenger (Kawalerczyk et al. 2019b). However, the hemp flour addition resulted in the decrease of UF glue line strength and the plywood mechanical properties. Thus, Authors conducted the studies aimed to adjust the amount of introduced extender in order to achieve a proper viscosity level and to confirm the effect on lowering the harmful emissions from MUF adhesives. The addition of hemp flour to MUF resin in the concentrations of 20% and 25% led to obtain the equally good properties of the manufactured panels with the formaldehyde emission lowered by up to 26% when compared to reference plywood (Kawalerczyk et al. 2020c). Since the advantageous effect was probably related to the high protein content Authors decided to investigate how the addition of soy flour affects the plywood properties.

The soy flour has been used in wood glues for decades (Zhang et al. 2017). According to Vnučec et al. (2017) the application of soy in wood bonding is a reasonable choice due to its high production volume and the small use of soy meal-based products for human food consumption. Moreover, the low cost, high protein content and easy processing are listed among its the most important advantages. There are many ongoing studies on using soy products in the formulation of formaldehyde-free wood adhesives containing also e.g. glyoxal (Amaral-Labat et al. 2008), polyepoxide resins (Huang et al. 2012), polyamidoamine (Gui et al. 2013) also for plywood manufacturing (Huang and Li 2008, Li et al. 2014). However, a low water-resistance can be still a limiting factor for some applications.

In summary, the production of amino resins is expected to increase further especially in the developing regions (Gonçalves et al. 2018). However, since the formaldehyde is classified as the carcinogenic and mutagenic substance it is very important to continue the research on the reduction of the adverse emissions. Moreover, both the global production of plywood and the availability of soy products are also constantly growing. Thus, the aim of this study was to determine the possibility to apply soy flour as the extender for UF and MUF adhesives in the production of plywood characterized by good mechanical properties and significantly lowered formaldehyde emission.

MATERIAL AND METHODS

Materials

A commercially available UF and MUF resins with a properties presented in Tab. 1 were purchased from the market. Ammonium nitrate (20 wt%) was applied as a hardener for the adhesives. Both the soy flour and the rye flour (used for comparison purpose) were obtained from the market. Plywood was prepared with the use of birch (Betula L.) veneer sheets with the average density of 570 kg·m^{-3}, average thickness of 1.4 mm, moisture content $4 \pm 1\%$ and the dimensions of 320×320 mm.

Tab. 1: Properties of adhesives.

Property	UF	MUF
Viscosity (mPa × s)	1211	981
Solid content (%)	69	67
pH	8.1	9.6
Gel time at 100°C (s)	65	68

Determining the compositions of flours

The purchased flours were subjected to a basic composition analysis. The investigations involved the water content based on EN ISO 712 (2012) and the share of following compounds: crude protein content according to Kjeldahl method EN ISO 5983-1 (2006), the content of mineral compounds in the form of ash according to EN ISO 2171 (2010), total fat content according to EN ISO 6492 (2005) and carbohydrates content according to EN ISO 6865 (2002).

Determining the ability of flours to absorb the formaldehyde

In order to determine the ability of flours to absorb the formaldehyde an 0.1 M aqueous solution of formaldehyde was prepared. In order to prepare 0.1 M formaldehyde solution 5 drops of concentrated sulphuric acid were mixed with 100 ml of 15% formaldehyde solution and then refluxed for 15 min to depolymerize the paraformaldehyde. The solution after cooling was neutralized with NaOH to pH 7 and diluted with distilled water. Then, an appropriate amount of flour was added to this solution. After that, the prepared water-formaldehyde solutions of flours were kept in laboratory oven for 3 hours at 65°C. The obtained solution was filtered and the content of formaldehyde was investigated with the use of sodium sulfite titrimetric method. 25 ml of 0.1 M Na_2SO_3 and 2 ml of 0.1 M NaOH were added to a 10 ml aliquot of the formaldehyde-containing filtrate. The titration was performed with 0.05 M HCl solution (phenolphthalein as an indicator). A control test was carried out with the same procedure excluding the formaldehyde. Moreover, the analysis of formaldehyde solution incubated for 3 hours at 65°C without flours was also performed. The analysis involved three repetitions for each solution (Bekhta et al. 2019, 2021).

Adhesive preparation

The amounts of introduced additives such as flours and hardener were adjusted depending on the variant (Tab. 2). The amount of introduced extender has been adjusted based on

the viscosity of purchased resins. Both experimental and reference variants were mixed manually until the proper homogenization was achieved.

Tab. 2: Compositions of adhesive mixtures.

Variant label	Resin type	Quantity (pbw* per 100 g of solid resin)			
		Soy flour	Rye flour	Water	Hardener
UF-R	UF	0	20	10	2
UF-15	UF	15	0	10	2
UF-20	UF	20	0	10	2
UF-25	UF	25	0	10	2
MUF-R	MUF	0	15	10	2
MUF-10	MUF	10	0	10	2
MUF-15	MUF	15	0	10	2
MUF-25	MUF	20	0	10	2

*- pbw means parts by weight.

FTIR analysis

The FTIR analysis was performed in order to assess a chemical interactions between the extenders and resins. The flour-filled adhesive mixtures were cured in the laboratory oven at 120°C and 140°C in case of UF and MUF resins, respectively. After that it was grinded with the use of laboratory mill and sieved in order to obtain a dimensional fraction of 0.125×0.125 mm^2. The cured adhesive in the form of powder was mixed with KBr at a 1/200 mg ratio. Spectra was registered with the use of Nicolet iS5 spectrophotometer with Fourier transform within a range of 500 to 4000 cm^{-1} at a resolution of 4 cm^{-1}, registering 16 scans. The same preparations were completed for pure adhesives without any extender.

Determining the properties of adhesive mixtures

A viscosity is an essential parameter in plywood manufacturing process (Kawalerczyk et al. 2021). Thus, the effect of the adhesive composition on the viscosity of prepared mixtures was investigated right after the resin preparation with the use of Brookfield DV-II + pro viscometer. Moreover, the following properties listed by Gonçalves et al. (2019) among the commonly used industrial indicators for adhesives such as pH, solid content and gel time at 100°C were determined according to relevant standards: EN 1242 (2011), EN 827 (2005) and PN-C-8952-3 (1996), respectively.

Plywood manufacturing and testing

In order to manufacture a three-layered plywood the UF and MUF adhesives were applied on the surface of the external veneer sheets in the amount of 170 g·m^{-2}. The veneers glued with UF resin were pressed at 120°C and unit and 1.4 MPa for 4 min. In case of variants containing MUF resin pressing process was conducted at 140°C for 4 min with the unit pressure of 1.3 MPa. The manufactured panels were tested in terms of formaldehyde emission using a flask methods according to EN 717-3 (1996) initially and after 8 weeks of samples conditioning at an ambient room temperature. In order to determine a bonding quality of plywood the shear strength test was carried out according to EN 314-1 (2004). Plywood glued with UF adhesive

was tested in dry state and after soaking in water (20 ± 3°C) for 24 hours. Panels bonded with MUF adhesive were tested after 24 hours of soaking in water and after pretreatment consisting of boiling in water for 6 h and cooling in water for 1 hour at 20 ± 3°C which was briefly called boiling when describing the results. The determination of formaldehyde emission involved 5 samples from each variant and shear strength involved 12 samples from each variant. The obtained results were subjected to a multivariate statistical analysis ANOVA. Moreover, in order to distinguish homogeneous groups the Tukey test on a significance level of α = 0.05 was performed using Statistica 13.0 software.

RESULTS AND DISCUSSION

The results of flour compositions determinations are summarized in Tab. 3. On the basis of presented outcomes it can be concluded that the soy flour was characterized by significantly higher proteins content than rye flour.

Tab. 3: The composition of flours.

Type of flour	Percentage content of the components (%)				
	Water	Proteins	Ash	Fat	Carbohydrates
Rye flour	14.39 ± 0.36	12.53 ± 0.32	1.51 ± 0.09	1.54 ± 0.10	70.36 ± 0.47
Soy flour	6.49 ± 0.86	50.71 ± 0.31	7.33 ± 0.10	1.25 ± 0.04	34.22 ± 0.48

The high protein content is a favorable feature for the extender and it indicates that the soy flour can be possibly applied as a bio-based scavenger. The proteins in soy flour contains many potentially reactive side-chain amino acid groups (Fan et al. 2011). The numerous groups occurring in amino acids, proteins and peptides demonstrate the ability to undergo the addition and condensation reactions with HCHO (French and Edsall 1945). The formaldehyde reacts with amino and thiol groups and methylol derivatives are formed. Subsequently the part of methylol adducts are dehydrated and the Schiff-bases are formed which consequently allows the further type of cross-linking reactions with other amino acid residues (Hoffman et al. 2015, Metz et al. 2004). Fig. 1 shows the results of investigations regarding the ability of flours to absorb the formaldehyde.

Studies have shown that probably due to the higher protein content the soy flour absorbed the formaldehyde more efficiently when compared to the rye flour. The higher flours content in the solution was, the more noticeable the tendency was. It probably resulted from the increased amount of protein introduced with the soy flour. Similar effects were observed in the investigations concerning the addition of a bark particles and sludge to the formaldehyde solutions. Moreover, the application of these substances as fillers in the adhesive compositions resulted in a decreased HCHO emissions from plywood bonded with UF resin (Bekhta et al. 2019, 2021).
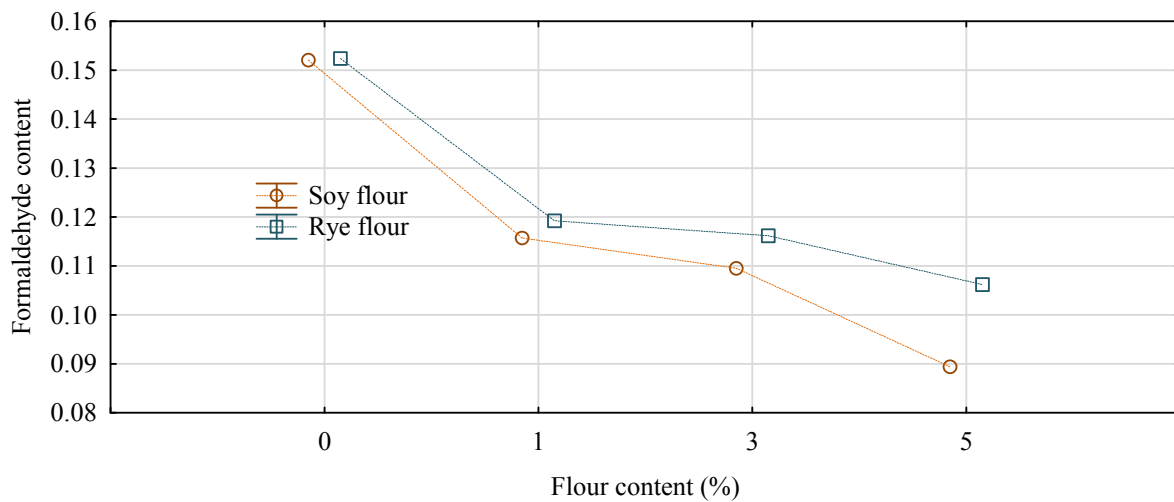
Fig. 1: Formaldehyde content in the aqueous solution of formaldehyde with soy and rye flour.

The FTIR spectra of UF resin, UF resin with the rye flour and the soy flour as extenders are presented in Fig. 2. Since the course of the spectra of adhesives containing the soy flour in various concentrations were the same only one variant was presented. The broadband observed in the 3390 cm^{-1} range was corresponded to the O-H and N-H groups (Ghahri et al. 2018). Two peaks in the 2970 cm^{-1} and 2890 cm^{-1} were attributed to C-H symmetric and asymmetric stretching of CH$_2$ and CH$_3$ groups, respectively (Ghahri et al. 2018, Wang et al. 2008). The bands at 1650 cm^{-1}, 1540 cm^{-1} were assigned to C=O stretching and N-H bending bands in amide I and II (Su et al. 2010, Zhang et al. 2017). Moreover, a peak at 1240 cm^{-1} was also observed and it was corresponded to C-N stretching and N-H bending vibrations of amide III (Ghahri et al. 2018). The above-mentioned bands were considered constant across the all adhesive formulations. Additionally, in case of introducing soy and rye flour as the extenders, an overlapping of the bands from the resin components and the components of filling materials, mainly proteins and carbohydrates, were observed.
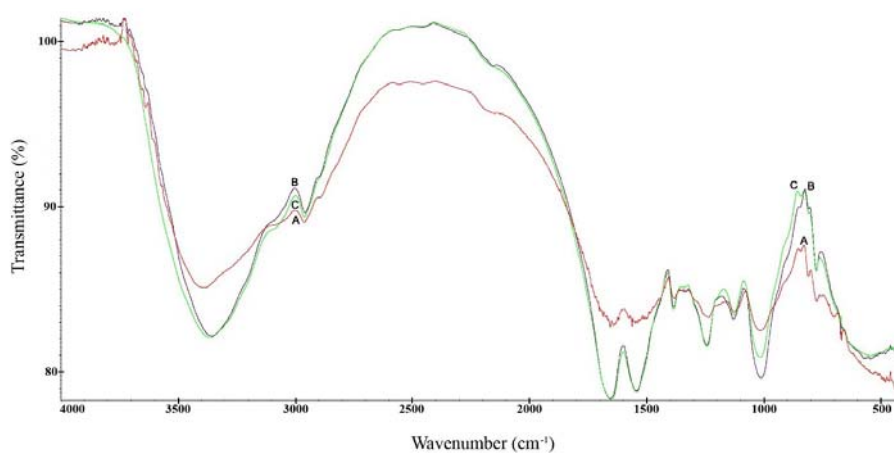

Fig. 2: FTIR spectra of: A – UF resin without any extender, B – variant labeled as UF-20, C – variant labeled as UF-R.

The spectra of both the pure and flour-filled MUF adhesives are presented in Fig. 3. The weak peak at 1657 cm^{-1} was corresponding to the NH$_2$ band and it occurred for MUF resin (Yuan et al. 2016). Band at 1554 cm^{-1} was detected and according to Luo et al. (2015) this band was caused by secondary amides (-CONH-). The bands from a triazine ring of melamine was occurred at 812 cm^{-1} (Luo et al. 2015, Reimschuessel and McDevitt 1960). Moreover, in the spectra of flour-filled MUF resin, there were bands observed at 1011, 1165 and 1370 cm^{-1}, which could be connected with presence of polysaccharides in soy and rye flours. Many polysaccharides were presented by a specific band in the 1200-1000 cm^{-1} region and dominated by the ring vibrations overlapped with the vibrations of C-OH group and C-O-C glycosidic bond (Kačuráková et al. 2000). In turn, the band at 1370 cm^{-1} can be attributed to bending vibration of C-H and C-O groups of the aromatic rings in polysaccharides (De Rosa et al. 2011). The spectrum marked with A symbol was characterized by higher intensity of these bands, than spectrum labeled as B, which is connected with higher content of polysaccharides in rye flour than in soy flour. The investigations of chemical interaction between the resins and the extenders showed only the presence of flours but based on that, it cannot be unambiguously stated that the chemical reactions occurred. Similar effect was observed in studies concerning the addition of e.g. wheat derivatives and nanocellulose as the filling substances for UF resin (Hogger et al. 2020a, Kawalerczyk et al. 2020b).
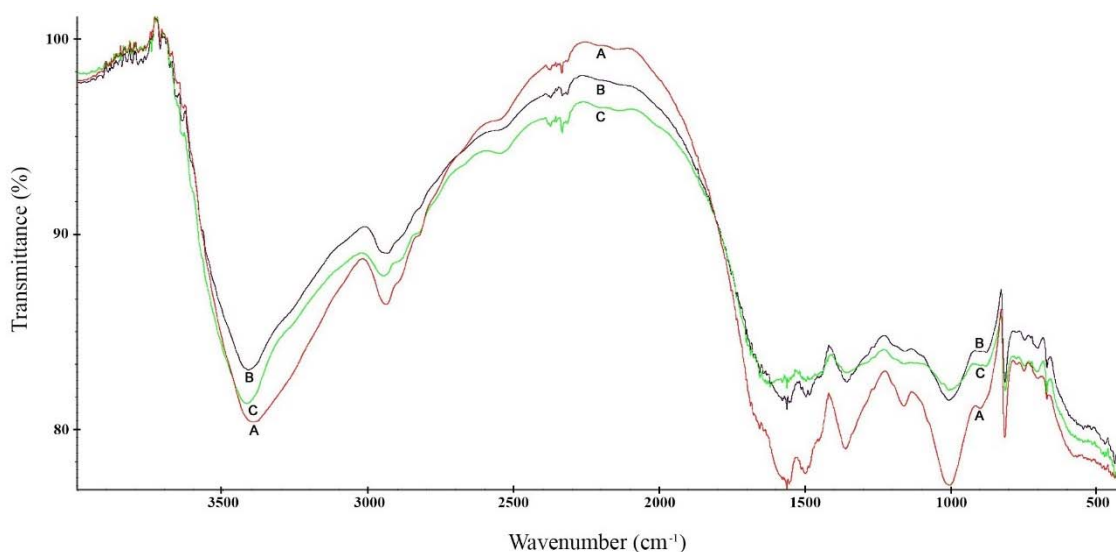
Fig. 3: FTIR spectra of: A – variant labeled as MUF-R, B – variant labeled as MUF-15, C – MUF resin without any extender.

Tab. 4 shows the results of adhesives properties investigations. The outcomes indicate that the type of extender influenced especially such properties as the viscosity and the gel time. Viscosity is an essential parameter in adhesive application during the plywood manufacturing. Too low viscosity results in deterioration of bonding strength because of the excessive resin penetration into the porous veneer surfaces. Consequently, the amount of remaining bonding agent is insufficient to ensure good strength of the glue lines (Kawalerczyk et al. 2020a).

Tab. 4: Properties of adhesive mixtures.

Variant label	Viscosity (mPa×s)	Solid content (%)	pH	Gel time (s)
UF-R	4798 ± 12	71.41 ± 0.09	7.0 ± 0.1	89 ± 2
UF-15	3465 ± 21	69.33 ± 0.11	7.1 ± 0.2	73 ± 1
UF-20	3681 ± 18	71.32 ± 0.04	7.0 ± 0.1	71 ± 2
UF-25	3996 ± 14	72.41 ± 0.07	7.1 ± 0.2	69 ± 2
MUF-R	4661 ± 23	68.19 ± 0.03	7.8 ± 0.1	94 ± 2
MUF-10	3007 ± 18	68.03 ± 0.09	7.7 ± 0.3	85 ± 2
MUF-15	3113 ± 11	68.11 ± 0.02	7.7 ± 0.3	82 ± 1
MUF-25	3519 ± 13	68.49 ± 0.08	7.7 ± 0.1	75 ± 2

The reference variants containing rye flour were characterized by a higher viscosity than the soy flour-filled mixtures. The adhesives mixed with soy flour reached values in the range between the 2000 – 4000 mPa×s assigned to machine application by a glue applicator (Dunky and Niemz 2013). The increased viscosity may be caused by the higher content of carbohydrates. Studies performed by Bekhta et al. (2014) showed that the viscosity of PF adhesive heightened with the increasing amount of starch. The starch is able to absorb the water and swell which leads to intensive rise of viscosity. Studies performed by Hogger et al. (2020b) described a slightly different tendency in case of wheat extenders, however, the rye starch is characterized by a significantly lower gelatinization temperature than the wheat starch (Verwimp et al. 2004). It seems like the type of extenders has not affected the solid content which increased along with the increasing share of filling particles contained in the composition. The pH values reached the similar values regardless of the type of flour. The gel time of MUF adhesive was longer in comparison with UF resin which corresponds with the Zhang et al. (2013) observations on an adverse effect of melamine addition on resin curing behavior. Moreover, the gel time varied depending on the introduced flour. The application of soy flour was beneficial since the curing time was shortened. It can possibly lead to the shortening of pressing time or to the reduction of plywood pressing parameters (Mirski et al. 2011). The gelation process was faster probably due to the higher amount of proteins. The proteins contained in the flour composition shows high reactivity with the methylol groups of amino adhesives which leads to obtain a highly cross-linked polymer structure in the shorter period of time (Fan et al. 2011). Similar effect was observed in case of applying hemp flour characterized by the high proteins content (Kawalerczyk et al. 2020c).

Fig. 4 presents the results of the formaldehyde emission from manufactured plywood panels measured initially and after 8 weeks of storage in an ambient room temperature. The hazardous formaldehyde emission is still a major disadvantage of amino resins especially in the indoor environments since the HCHO was classified as the known human carcinogen (Antov et al. 2020c,b, Réh et al. 2019). As expected, plywood bonded with UF resin was characterized by the higher formaldehyde emission in comparison with panels glued with MUF resin because of the melamine scavenging ability (Dutkiewicz 1984, Paiva et al. 2012). The addition of soy flour had a positive effect and led to a decrease in the amount of formaldehyde emitted from the plywood. The more soy flour was included in the adhesive composition, the less amount of HCHO was emitting from the panels.
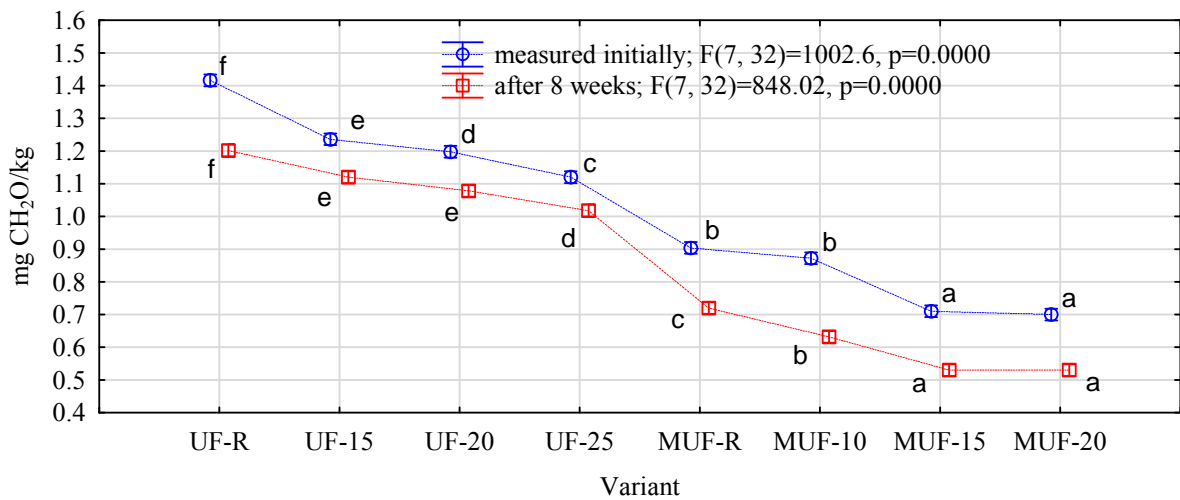
Fig. 4: Formaldehyde emission from plywood (F(x,y)=z,p where F– Roland Fisher's test method, x– number of degrees of freedom, y – number of tests, z– value of F test, p– probability level).

The emissions measured initially decreased by up to 20% in case of plywood glued with UF resin and up to 22% in case of plywood with MUF resin in variants assuming the highest concentrations of soy flour. The measurements conducted after 8 weeks of storage showed a decrease by up to 15% and 25% for plywood bonded with UF and MUF adhesives, respectively. The application of soy flour led to a significant reduction in formaldehyde emissions because of the proteins molecules which contain many functional groups such as amines and amides. These groups can easily react with HCHO (Xing et al. 2013). Similar effect was observed in studies concerning the addition of protein-rich hemp flour to the UF and MUF adhesives in plywood production (Kawalerczyk et al. 2019b, 2020c).

(A)
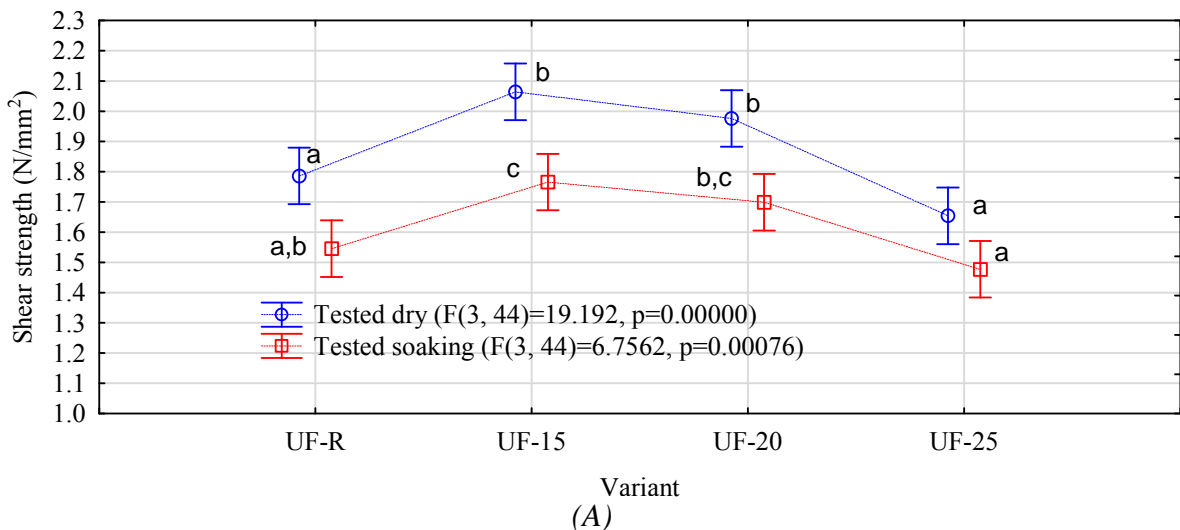
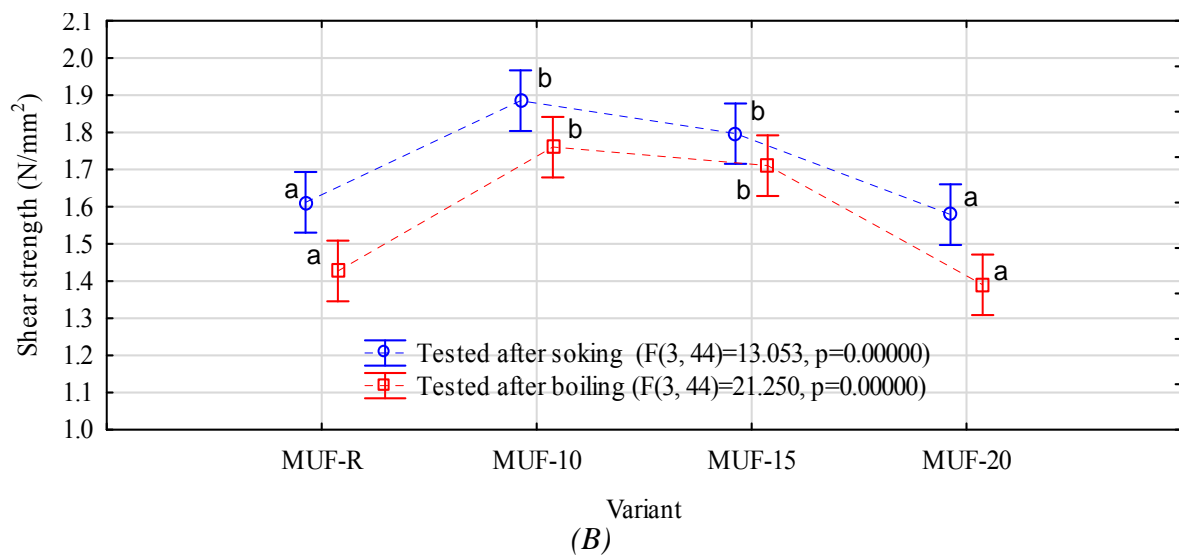*Fig. 5: Shear strength of: (A) plywood bonded with UF resin; (B) plywood bonded with MUF resin (F(x,y)=z,p where F – Roland Fisher's test method, x – number of degrees of freedom, y – number of tests, z – value of F test, p – probability level).*

In order to assess the effect of the rye flour replacement with the soy flour on plywood bonding quality, the shear strength test was carried out. The results are presented in Fig. 5. The best results for UF resin were obtained for variant assuming the soy flour application in the concentration of 15%. It resulted in the increase in shear strength by up to 13% for plywood tested in dry conditions and after soaking in water. Further addition of soy flour in the amount of 20% also resulted in the statistically significant improvement. Similar tendency was noted in variants glued with MUF adhesive. The most advantageous effect was obtained for plywood bonded with the mixture containing a 10% of soy flour. The increase of bonding strength was up to 14% and 19% in the tests conducted after soaking and after boiling, respectively.

As expected, plywood glued with the MUF adhesive reached higher values after soaking in comparison with the UF resin due to the increased water resistance resulting from the melamine addition (Zanetti and Pizzi 2003). The improvement in bonding quality was probably caused because of the high content of proteins included in the soy flour composition. According to Wang and Pizzi (1997) a secondary amido groups contained in the protein chain skeleton show a high reactivity with formaldehyde and the methylol groups of resin. The ongoing chemical bonding leads to the intensification of the cross-linking reactions. However, regardless of the adhesive type, the addition of soy flour in maximum concentration led to a slight decrease in plywood bonding quality. The results were comparable with the reference panels and there were no statistically significant changes noted. Too excessive water absorption by the extenders may lead to a lack of water which participates in forming a three-dimensional crosslinking structure of the resin (Réh et al. 2019). Moreover, the introduction of the extenders in that high concentrations can cause a formation of agglomerates. It leads to the weakening of bonding strength due to the stress accumulation in the certain points of glue line.

CONCLUSIONS

The results of investigations concerning the composition of flours and the ability of flours to absorb the formaldehyde indicate that soy flour can be applied to the amino resins as a scavenger reducing the formaldehyde emissions. The course of FTIR spectra revealed mainly functional groups of adhesives and the presence of proteinaceous extenders but the analysis has not explained the chemical interaction between the flour and the polymer. The replacement of rye flour with the soy flour affected the viscosity values and led to the acceleration of gel time. The type of extender has not influenced the solid content and the pH values. The introduction of soy flour to the UF and MUF adhesive compositions resulted in manufacturing plywood characterized by improved bonding quality and reduced formaldehyde emission.

ACKNOWLEDGMENTS

REFERENCES

1. Amaral-Labat, G.A., Pizzi, A., Goncalves, A.R., Celzard, A., Rigolet, S., Rocha, G.J.M., 2008: Environment-friendly soy flour-based resins without formaldehyde. Journal of Applied Polymer Science 108(1): 624-632.
2. Antov, P., Jivkov, V., Savov, V., Simeonova, R., Yavorov, N., 2020a: Structural application of eco-friendly composites from recycled wood fibres bonded with magnesium lignosulfonate. Applied Sciences 10(21): 7526.
3. Antov, P., Mantanis, G.I., Savov, V., 2020b: Development of wood composites from recycled fibres bonded with magnesium lignosulfonate. Forests 11(6): 613.
4. Antov, P., Savov, V., Neykov, N., 2020c: Sustainable bio-based adhesives for eco-friendly wood composites. A Review. Wood Research 65(1): 51-62.
5. Babcock, G.E., Smith, A.K., 1947: Extending phenolic resin plywood glues with proteinaceous materials. Industrial & Engineering Chemistry 39(1): 85–88.
6. Bekhta, P., Ortynska, G., Sedliacik, J., 2014: Properties of modified phenol-formaldehyde adhesive for plywood panels manufactured from high moisture content veneer. Drvna industrija 65(4): 293–301.
7. Bekhta, P., Sedliačik, J., and Bekhta, N. 2020: Effect of Veneer-Drying Temperature on Selected Properties and Formaldehyde Emission of Birch Plywood. Polymers 12(3): 593.
8. Bekhta, P., Sedliačik, J., Kačík, F., Noshchenko, G., Kleinová, A. 2019: Lignocellulosic waste fibers and their application as a component of urea-formaldehyde adhesive composition in the manufacture of plywood. European Journal of Wood and Wood Products 77(4): 495–508.
9. Bekhta, P., Sedliačik, J., Noshchenko, G., Kačík, F., Bekhta, N. 2021: Characteristics of beech bark and its effect on properties of UF adhesive and on bonding strength and

formaldehyde emission of plywood panels. European Journal of Wood and Wood Products 79: 423-433.

10. Chen, H., Yan, N., 2018: Application of Western red cedar (*Thuja plicata*) tree bark as a functional filler in pMDI wood adhesives. Industrial Crops and Products 113: 1–9.

11. Costa, N.A., Martins, D., Pereira, J., Martins, J., Ferra, J., Cruz, P., Mendes, A., Magalhães, F.D., Carvalho, L.H., 2013: 13C NMR study of presence of uron structures in amino adhesives and relation with wood-based panels performance. Journal of Applied Polymer Science 130(6): 4500–4507.

12. De Rosa, I.M., Kenny, J.M., Maniruzzaman, M., Moniruzzaman, Md., Monti, M., Puglia, D., Santulli, C., Sarasini, F., 2011: Effect of chemical treatments on the mechanical and thermal behaviour of okra (*Abelmoschus esculentus*) fibres. Composites Science and Technology 71(2): 246–254.

13. Ding, R., Su, C., Yang, Y., Li, C., Liu, J., 2013: Effect of wheat flour on the viscosity of urea-formaldehyde adhesive. International Journal of Adhesion and Adhesives 41: 1-5.

14. Dukarska, D., Czarnecki, R., 2016: Fumed silica as a filler for MUPF resin in the process of manufacturing water-resistant plywood. European Journal of Wood and Wood Products 74(1): 5–14.

15. Dunky, M., Niemz, P., 2013: Holzwerkstoffe und Leime: Technologie und Einflussfaktoren. Pp 437-438, Springer-Verlag.

16. Dutkiewicz, J., 1984: Preparation of cured urea–formaldehyde resins of low formaldehyde emission. Journal of Applied Polymer Science 29(1): 45–55.

17. EN 1245, 2011: Adhesives. Determination of pH.

18. EN 314-1, 2004: Plywood . Bonding quality. Test methods.

19. EN 713-7, 1996: Wood-based panels. Determination of formaldehyde release. Part 3: formaldehyde release by the flask method.

20. EN 827, 2005: Adhesives. Determination of conventional solid content and constant mass solids content.

21. EN ISO 2171, 2010: Cereals, pulses and by-products. Determination of ash yield by incineration.

22. EN ISO 5983-1, 2005: Animal feeding stuffs. Determination of nitrogen content and calculation of crude protein content . Part 1: Kjeldahl method.

23. EN ISO 6492, 1999: Animal feeding stuffs . Determination of fat content.

24. EN ISO 6865, 2000: Animal feeding stuffs. Determination of crude fibre content. Method with intermediate filtration.

25. EN ISO 712, 2012: Cereal and cereal products. Determination of moisture content. Reference method.

26. Fan, D.B., Qin, T.F., Chu, F.X., 2011: A soy flour-based adhesive reinforced by low addition of MUF resin. Journal of Adhesion Science and Technology 25(1–3): 323–333.

27. French, D., Edsall, J.T., 1945: The reactions of formaldehyde with amino acids and proteins. In: Advances in Protein Chemistry. Pp 277-335, Elsevier.

28. Frihart, C.R., 2015: Introduction to special issue: wood adhesives: past, present, and future. Forest Products Journal 65(1–2): 4–8.

29. Ghahri, S., Mohebby, B., Pizzi, A., Mirshokraie, A., Mansouri, H.R., 2018: Improving water resistance of soy-based adhesive by vegetable tannin. Journal of Polymers and the Environment 26(5): 1881–1890.

30. Gonçalves, C., Paiva, N.T., Ferra, J.M., Martins, J., Magalhães, F., Barros-Timmons, A., Carvalho, L., 2018: Utilization and characterization of amino resins for the production of wood-based panels with emphasis on particleboards (PB) and medium density fibreboards (MDF). A review. Holzforschung 72(8): 653–671.

31. Gonçalves, M., Paiva, N.T., Ferra, J.M., Martins, J., Magalhães, F.D., Carvalho, L., 2019: Chemical composition of melamine-urea-formaldehyde (MUF) resins assessed by near-infrared (NIR) spectroscopy. International Journal of Adhesion and Adhesives 93: 102327.

32. Gui, C., Liu, X., Wu, D., Zhou, T., Wang, G., Zhu, J. 2013: Preparation of a new type of polyamidoamine and its application for soy flour-based adhesives. Journal of the American Oil Chemists' Society 90(2): 265–272.

33. Hoffman, E.A., Frey, B.L., Smith, L.M., Auble, D.T., 2015: Formaldehyde crosslinking: A tool for the study of chromatin complexes. Journal of Biological Chemistry 290(44): 26404–26411.

34. Hogger, E.M., Herwijnen, H.W.G.V., Moser, J., Kantner, W., Konnerth, J., 2020a: Systematic assessment of wheat extenders in formaldehyde-condensation plywood resins: Part II: Mechanical properties of plywood panels. The Journal of Adhesion DOI: 10.1080/00218464.2020.1756788 (online).

35. Hogger, E.M., Herwijnen, H.W.G. van, Moser, J., Kantner, W., Konnerth, J., 2020b: Systematic assessment of wheat extenders in condensation resins for plywood production: Part I: Physico-chemical adhesive properties. The Journal of Adhesion DOI: 10.1080/00218464.2020.1776123 (online).

36. Hojilla-Evangelista, M.P., 2013: Evaluation of corn germ protein as an extender in plywood adhesive. Journal of Adhesion Science and Technology 27(18–19): 2075–2082.

37. Huang, J., Li, C., Li, K., 2012: A new soy flour-polyepoxide adhesive system for making interior plywood. Holzforschung 66(4): 427–431.

38. Huang, J., Li, K., 2008: A new soy flour-based adhesive for making interior type II plywood. Journal of the American Oil Chemists' Society 85(1): 63–70.

39. Kačuráková, M., Capek, P., Sasinková, V., Wellner, N., Ebringerová, A., 2000: FT-IR study of plant cell wall model compounds: pectic polysaccharides and hemicelluloses. Carbohydrate Polymers 43(2): 195–203.

40. Kawalerczyk, J., Dziurka, D., Mirski, R., Grześkowiak, W., 2019a: The effect of veneer impregnation with a mixture of potassium carbonate and urea on the properties of manufactured plywood. Drewno 203: 107–116.

41. Kawalerczyk, J., Dziurka, D., Mirski, R., Siuda, J., 2021: The reduction of adhesive application in plywood manufacturing by using nanocellulose-reinforced urea-formaldehyde resin. Journal of Applied Polymer Science 138(7): 49834.

42. Kawalerczyk, J., Dziurka, D., Mirski, R., Siuda, J., Szentner, K., 2020a: The effect of nanocellulose addition to phenol-formaldehyde adhesive in water-resistant plywood manufacturing. BioResources 15(3): 5388–5401.

43. Kawalerczyk, J., Dziurka, D., Mirski, R., Szentner, K., 2020b: Properties of plywood produced with urea-formaldehyde adhesive modified with nanocellulose and microcellulose. Drvna Industrija 71(1): 61–67.

44. Kawalerczyk, J., Dziurka, D., Mirski, R., Trociński, A., 2019b: Flour fillers with urea-formaldehyde resin in plywood. BioResources 14(3): 6727–6735.

45. Kawalerczyk, J., Siuda, J., Mirski, R., Dziurka, D., 2020c: Hemp flour as a formaldehyde scavenger for melamine-urea-formaldehyde adhesive in plywood production. BioResources 15(2): 4052–4064.

46. Lei, H., Frazier, C.E., 2015: Curing behavior of melamine-urea-formaldehyde (MUF) resin adhesive. International Journal of Adhesion and Adhesives 62: 40–44.

47. Li, H., Li, C., Chen, H., Zhang, D., Zhang, S., Li, J., 2014: Effects of hot-pressing parameters on shear strength of plywood bonded with modified soy protein adhesives BioResources 9(4): 5858–5870.

48. Luo, J., Zhang, J., Luo, J., Li, J., Gao, Q., 2015: Effect of melamine allocation proportion on chemical structures and properties of melamine-urea-formaldehyde resins. BioResources 10(2): 3265–3276.

49. Metz, B., Kersten, G.F.A., Hoogerhout, P., Brugghe, H.F., Timmermans, H.A.M., Jong, A., Meiring, H., Hove, J. ten, Hennink, W.E., Crommelin, D.J.A., Jiskoot, W., 2004: Identification of formaldehyde-induced modifications in proteins reactions with model peptides. Journal of Biological Chemistry 279(8): 6235–6243.

50. Mirski, R., Dziurka, D., Łęcka, J., 2011: Potential of shortening pressing time or reducing pressing temperature for plywood resinated with PF resin modified using alcohols and esters. European Journal of Wood and Wood Products 69(2): 317–323.

51. Mirski, R., Kawalerczyk, J., Dziurka, D., Siuda, J., Wieruszewski, M., 2020a: The application of oak bark powder as a filler for melamine-urea-formaldehyde adhesive in plywood manufacturing. Forests 11(12): 1249.

52. Mirski, R., Kawalerczyk, J., Dziurka, D., Wieruszewski, M., Trociński, A., 2020b: Effects of using bark particles with various dimensions as a filler for urea-formaldehyde resin in plywood. BioResources 15(1): 1692–1701.

53. Ong, H.R., Khan, M.M.R., Prasad, D.R., Yousuf, A., Chowdhury, M.N.K., 2018: Palm kernel meal as a melamine urea formaldehyde adhesive filler for plywood applications. International Journal of Adhesion and Adhesives 85: 8–14.

54. Paiva, N.T., Henriques, A., Cruz, P., Ferra, J.M., Carvalho, L.H., Magalhães, F.D., 2012: Production of melamine fortified urea-formaldehyde resins with low formaldehyde emission. Journal of Applied Polymer Science 124(3): 2311–2317.

55. PN-C-89352-3, 1996: Wood adhesives test methods. Determination of gelation time.

56. Réh, R., Igaz, R., Krišťák, Ľ., Ružiak, I., Gajtanska, M., Božíková, M., Kučerka, M., 2019: Functionality of beech bark in adhesive mixtures used in plywood and its effect on the stability associated with material systems. Materials 12(8): 1298.

57. Reimschuessel, H.K., McDevitt, N.T., 1960: Infrared spectra of some 1,3,5-triazine derivatives. Journal of the American Chemical Society 82(14): 3756–3762.

58. Su, J.-F., Huang, Z., Yuan, X.-Y., Wang, X.-Y., Li, M., 2010: Structure and properties of carboxymethyl cellulose/soy protein isolate blend edible films crosslinked by Maillard reactions. Carbohydrate Polymers 79(1): 145–153.

59. Taghiyari, H.R., Hosseini, S.B., Ghahri, S., Ghofrani, M., Papadopoulos, A.N., 2020: Formaldehyde emission in micron-sized wollastonite-treated plywood bonded with soy flour and urea-formaldehyde resin. Applied Sciences 10(19): 6709.

60. Verwimp, T., Vandeputte, G.E., Marrant, K., Delcour, J.A., 2004: Isolation and characterisation of rye starch. Journal of Cereal Science 39(1): 85–90.

61. Vnučec, D., Kutnar, A., Goršek, A., 2017: Soy-based adhesives for wood-bonding – a review. Journal of Adhesion Science and Technology 31(8): 910–931.

62. Waage, S.K., Gardner, D.J., Elder, T.J. 1991: The effects of fillers and extenders on the cure properties of phenol–formaldehyde resin as determined by the application of thermal techniques. Journal of Applied Polymer Science 42(1): 273–278.

63. Wang, S., Pizzi, A. 1997: Improving UF plywood adhesives water resistance by coreaction with proteins. Holz als Roh- und Werkstoff 55(2–4): 158–158.

64. Wang, W.H., Li, X.P., Zhang, X.Q., 2008: A soy-based adhesive from basic modification. Pigment & Resin Technology 37(2): 93-97.

65. Xing, S., Riedl, B., Deng, J., Nadji, H., Koubaa, A., 2013: Potential of pulp and paper secondary sludge as co-adhesive and formaldehyde scavenger for particleboard manufacturing. European Journal of Wood and Wood Products 71(6): 705–716.

66. Yuan, X., Luo, K., Zhang, K., He, J., Zhao, Y., Yu, D. 2016: Combinatorial vibration-mode assignment for the FTIR spectrum of crystalline melamine: A strategic approach toward theoretical IR vibrational calculations of triazine-based compounds. The Journal of Physical Chemistry A 120(38): 7427–7433.

67. Zanetti, M., Pizzi, A., 2003: Low addition of melamine salts for improved melamine-urea-formaldehyde adhesive water resistance. Journal of Applied Polymer Science 88(2): 287–292.

68. Zhang, J., Wang, X., Zhang, S., Gao, Q., Li, J., 2013: Effects of melamine addition stage on the performance and curing behavior of melamine-urea-formaldehyde (MUF) resin. BioResources 8(4): 5500–5514.

69. Zhang, X., Zhu, Y., Yu, Y., Song, J., 2017: Improve performance of soy flour-based adhesive with a lignin-based resin. Polymers 9(7): 261.

JAKUB KAWALERCZYK*, JOANNA SIUDA, DOROTA DZIURKA,
RADOSŁAW MIRSKI
POZNAŃ UNIVERSITY OF LIFE SCIENCES
FACULTY OF FORESTRY AND WOOD TECHNOLOGY
DEPARTMENT OF WOOD-BASED MATERIALS
WOJSKA POLSKIEGO 28, 60-637 POZNAŃ
POLAND
*Corresponding author: jakub.kawalerczyk@up.poznan.pl

MAGDALENA WOŹNIAK, KINGA STUPER-SZABLEWSKA
POZNAŃ UNIVERSITY OF LIFE SCIENCES
FACULTY OF FORESTRY AND WOOD TECHNOLOGY
DEPARTMENT OF CHEMISTRY
WOJSKA POLSKIEGO 75, 60-637 POZNAŃ
POLAND

SURFACE IRREGULARITIES OF OAK WOOD AFTER TRANSVERSAL CUTTING WITH A CIRCULAR SAW

MONIKA SARVAŠOVÁ KVIETKOVÁ, MIROSLAV GAŠPARÍK
CZECH UNIVERSITY OF LIFE SCIENCES
CZECH REPUBLIC

ABSTRACT

This paper deals with the effect of saw blade type (24, 40 and 60 teeth) and sawn distance on the primary profile (P_z) of tranvesre surface of European oak (*Quercus robur* L.) after transversal cutting. Transversal cutting was provided at constant cutting speed $v_c = 62$ m⋅s^{-1} and with manual feeding using circular saw blade. An additional parameter was to determine the maximum sawn distance for each type of saw blade up to the point where the saw blade overheated, as well as the beginning of the blackening of the wood surface. The highest values of the primary profile (P_z) were achieved with a saw blade with 24 teeth, lower values were measured on wood cut with a 40 tooth blade and the lowest values after cutting with a 60 tooth blade. As the saw distance increased, there was no rapid and steep increase in the primary profile values, but these values gradually increased slightly, probably due to the gradual blunting of the tool.

KEYWORDS: Circular saw, surface quality, primary profile (P_z), saw blade, tranversal cutting.

INTRODUCTION

Global wood consumption is on the rise and wood is considered a strategic raw material. The wood mass of our forests is a reproducible raw material while respecting all propositions. At the moment, the maximum effort for a comprehensive and ecological solution to the problem of the use of wood raw material with an orientation towards finalization from the aspect of quality and economy of its processing is in place. As energy and raw material costs rise, it is increasingly important to reduce the cost of machining (Orlowski and Walichnowski 2013) as well as improve the quality of the surface after machining (Krenke et al. 2017a,b).

In the woodworking and furniture industries, wood cutting using a saw blade plays a very important role (Williams and Patel 2016), which is undoubtedly the most commonly used type of tool for cutting wood and wood-based materials (Mikleš et al. 2010, Walker 2006, Nasir et al. 2018). The process of cutting wood materials using a saw blade, whether

solid or treated, laminated or agglomerated wood, is a very complex process (Nasir and Cool 2020), which is influenced by a large number of simultaneous factors as well as variables (Fig. 1) (Kvietková 2015).
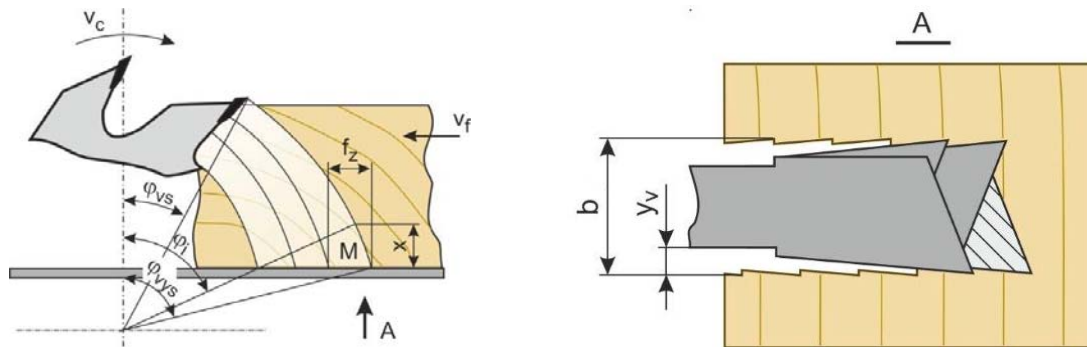
(Note: v_c - cutting speed, v_f - feed speed, f_z - feed per tooth, φ_{vs} - feed angle of the cutting edge entry into the wood, φ_{vys} - feed angle of the cutting edge exit from the wood, φ_i - feed local angle corresponding to the monitored point M, b - cut gap width, and y_v - saw teeth setting) (Kminiak and Gaff 2015).

Fig. 1: Cutting parameters of the saw blade and the principle of surface formation in transversal cutting of wood: (left) arc shaped traces, and (right) forming of cut kerf.

For practice, it is necessary to know the phenomena of mutual interaction of the tool with the workpiece, from the point of view of optimization and intensification of the machining process. The cutting process itself is conditioned by various factors (Gündüz et al. 2008) that strongly affect the output indicators of the process, such as unevenness of the machined surface, noise associated with the energy of the sawing process, as well as indicators related to the tool in terms of wear - cutting edge durability, service life, instability (Tesařová et al. 2010). Knowing the interrelationships between the mentioned indicators and the kinematics of the sawing process itself is an attempt to get closer to the most optimal outputs while keeping the costs of the process itself in terms of efficiency, effectiveness and economy of sawing while respecting the principles of safety and health at work (Wasielewski et al. 2012). It is very important that the whole process of cutting wood takes place with the least possible energy requirements and with the best possible quality of the final surface.

Each technological operation leaves characteristic inequalities on the surface, which can affect the function of these surfaces (Budakçı et al. 2011, 2013). A characteristic feature of the surface of wood sawn with circular saws are the arc traces on the transverse surface.

When the workpiece interacts with the saw blade, the chip thickness changes as a result of the cut indication, with which the pressures on the tooth face change and with them the deformations of the wood mass near the tooth edge. As stated by Lisičan (1996), the formation of grooves is directly proportional to the feed of the workpiece and the size of the tooth distribution of the saw blade. On the other hand, the grooves are inversely proportional to the height of the tooth, the number of revolutions and the number of teeth on the saw blade. Such a workpiece surface is not smooth, but scratches caused by the passage of the saw blade, especially its toothing, can be seen on it. During transversal cutting, the workpiece comes into contact with the saw blade in a plane perpendicular to the saw

blade. This results in the cutting of the structural elements of the wood by the toothing of the saw blade. There are clear surface irregularities on the surface after cutting. Before measuring the surface roughness, it is necessary to determine l_n (evaluated length). The evaluated length includes six basic lengths and is considered as a normal length. The evaluated length l_n, at which the values of the surface quality parameters are evaluated, may comprise one or more basic lengths (Fig. 2).
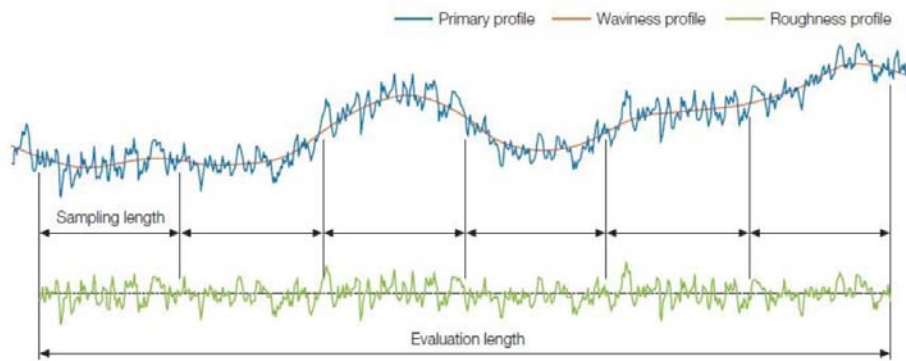

Fig. 2: Basic characteristics of wood surface quality (Khandoker 2020).

Surface unevenness (waviness + roughness) is evaluated in a system in which the spatial character of inequalities, created in the implementation process, is reduced to a plane. In this plane, a profile is obtained, which is evaluated with respect to the center line of the profile, called the primary profile (Pernikář et al. 2001).

Assuming absolute rigidity of saw tools and "vibration-free" movement of cutting tools, the cut surface will be grooved with traces of saw teeth, the depth (height or profile respectively) of which depends on the feed per tooth, mutual distance of teeth (spacing) and the degree of teeth setting. Whenever two surfaces come into contact with each other, the quality of the joined parts plays an important role in the use and wear of these parts (Gurau et al. 2005, 2012).

The height, shape, finishing and direction of surface irregularities on the workpiece depend on many factors such as technological parameters, e.g. feed rate, cutting speed, depth of cut, cutting tool geometry (cutting wedge angle, face angle and back angle), combination of workpiece and tool material as well as their mechanical properties, at last but not least from the quality and type of machine and tool used. It also depends on the attachment used and the vibration between the workpiece, the machine and the tool (Chuchala et al. 2012).

Surprisingly, despite research efforts, there are still several major problems and inconsistencies. This is especially visible in the field of woodworking, where the immediate characterization of the residual surface is needed for further development. The overall assessment of surface evenness has two main reasons, namely the assumption of the possibility of surface formation and monitoring of the production process.

European oak (*Quercus robur* L.) wood was chosen for this research. Oak wood was cut in the transverse direction using a circular saw with three different blades with 24, 40 and 60 teeth. The sawn distance was set at 750 m, but in addition, the maximum possible sawn distance was evaluated separately for each saw blade. The transverse surface after cutting was

evaluated using an Olympus Lext OLS 4100 laser microscope and the primary profile (P_z) was determined.

MATERIAL AND METHODS

Material

European oak (*Quercus robur* L.) wood were used for the experiment. The flat-sawn samples had dimensions of 20 × 100 × 500 mm (Fig. 3). Clear samples were conditioned in a conditioning chamber (relative humidity (ϕ) = 65 ± 5% and temperature (t) = 20 ± 2°C) to achieve their equilibrium moisture content (EMC) of 12%. The average oven-dry density of oak wood was 795 kg·m^{-3}. Whole experiment contained 216 samples.
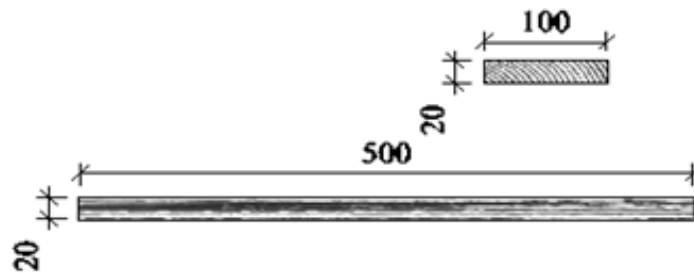
Fig. 3. Oak sample.

Methods
Circular saw

The GCM 10S Professional circular saw (Robert Bosch GmbH, Germany) was chosen for tranversal cutting of oak wood.

Saw blades

Three commonly used circular saw blades Premium (EXTOL, Czech Republic) with sintered carbide tips having 24, 40, and 60 teeth, respectively, were selected for the transverse cutting (Fig. 4). All saw blades had identical diameters (D = 250 mm), thicknesses (b = 3.2 mm), as well as angle geometries (clearance angle α = 15°, wedge angle β = 60°, rake angle γ = 15°). All saw blades had a alternating set teeth.

Fig. 4: Circular saw blades with a) 24 teeth, b) 40 teeth, and c) 60 teeth.

Transversal cutting

During the transversal cutting of the wood, which was provided with a Bosch circular saw, the feeding was carried out manually. As part of the cutting, the 10 mm thick pieces (slices) were cut from the longitudinally placed samples. The whole experiment was carried

out at a constant cutting speed v_c = 62 m⋅s^{-1} and 4700 RPM. The movement of the saw blade was carried out through an arc trajectory using the same principle as in the previous work Kminiak et al. (2015).

Measurements

The primary profile (P_z) values of the transverse surface were determined using the Olympus Lext OLS 4100 Laser microscope (Fig. 5.) which was placed on the special Olymext anti-vibration table. This laser microscope operates on a contactless surface scanning principle.
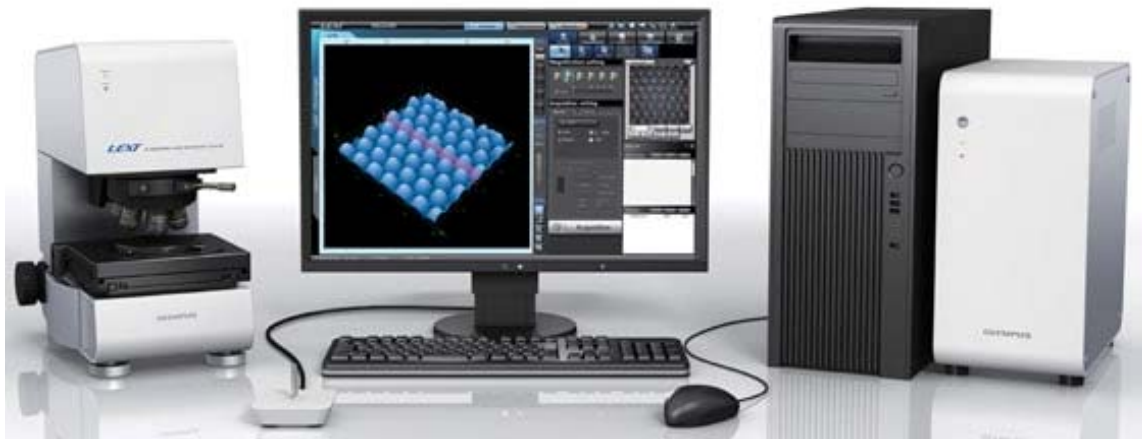
Fig. 5: *Laser microscope Olympus Lext OLS 4100 with additional equipment.*

The surface quality was evaluated based on the arithmetic mean of the primary profile, P_z. Primary profile (P_z) measurements were carried out in three horizontal paths equidistant from one another along the sample width (2.5, 10, and 22.5 mm from the sample margin) (Fig. 6). The measuring path length was 60 mm. The primary profile was measured at a predetermined final sawn distance of 750 m.
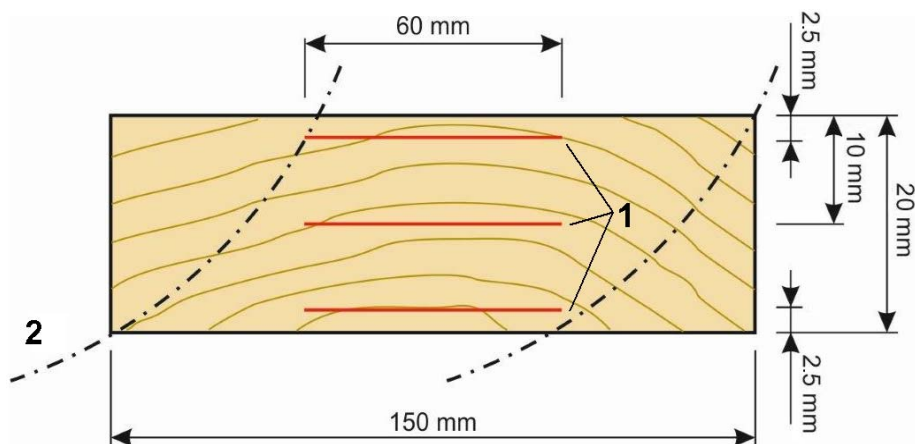
Fig. 6: *The schematic representation of measuring locations on the transversal surface: (1) measuring paths; and (2) track teeth of the saw blade.*

In addition, for each type of saw blade, the maximum sawn distance was determined, which is the longest possible sawn distance where the sawn blade has not yet overheated due

to its friction with wood and dulling of teeth, which is also reflected in blackening of the wood transverse surface.

The acquired data were recorded and exported to MS Excel within the special Olympus software. The primary profile (P_z) values were then evaluated by using STATISTICA 13 software (TIBCO Inc., USA). Two-factor analysis of variance was carried out to a certain the effect of saw blade type and sawn distance on the primary profile (P_z) of transverse area based on the p-value with 95% confidence level. Correlation analysis was performed for a maximum sawn distance of individual saw blade.

Calculations and evaluation

Density was calculated according to ISO 13061-2 (2014) and Eq. 1:

$$\rho = \frac{m}{hbl} = \frac{m}{V},$$

(1)

where: ρ - density of the sample (kg·m^{-3}), m - mass (weight) of the sample (kg), h, b, l - the height, width, and length of the sample (m), V - the volume of the sample (m^3).

The moisture content was calculated according to ISO 13061-1 (2014) and Eq. 2:

$$w = \frac{m_w - m_0}{m_0} * 100,$$

(2)

where: w - moisture content of the samples (%), m_w - mass (weight) of the sample at certain moisture w (kg), m_0 - mass (weight) of the oven-dry test samples (kg).

An oven-dry state was carried out according to the ISO 13061-1 (2014).

RESULTS AND DISCUSSION

Based on the significance level "P" values given in Tab. 1, the effects of the number of teeth and sawn distance could be deemed statistically significant. For the purposes of the statistical evaluation of the results, the sawn distance interval was reduced to 750 m.

Tab. 1: Statistical evaluation of the impact of factors on the primary profile P_z.

Monitored factor	Sum of squares	Degree of freedom	Variance	Fisher's F - test	Significance level P
Intercept	22.66398	1	22.66398	13456.62	0.00
Number of teeth	0.62682	2	0.31341	186.08	0.00
Sawn distance	0.52245	30	0.01741	10.34	0.00
Number of teeth × Sawn distance	1.24936	60	0.02082	12.36	0.00
Error	0.31327	186	0.00168		

The dependence of the height of the primary profile (P_z) on the used saw blade is considerable (Fig. 7). The highest values of the primary profile were recorded using a saw blade with 24 teeth (24T) and, conversely, the lowest values with a saw blade with 60 teeth (60T). Although all saw blades had the same parameters, the unevenness of the machined surface depended on the number of teeth of each saw blade. Although all three saw blades cut at the same RPM, the smallest chip was removed at the 24T saw blade, which affected the unevenness of the machined surface. On the contrary, the saw blade 60T had the smallest value of feed per tooth, which was reflected even after the transversal cutting of oak wood in the form of a lower value of unevenness. This course could also be influenced by the structure of the wood.
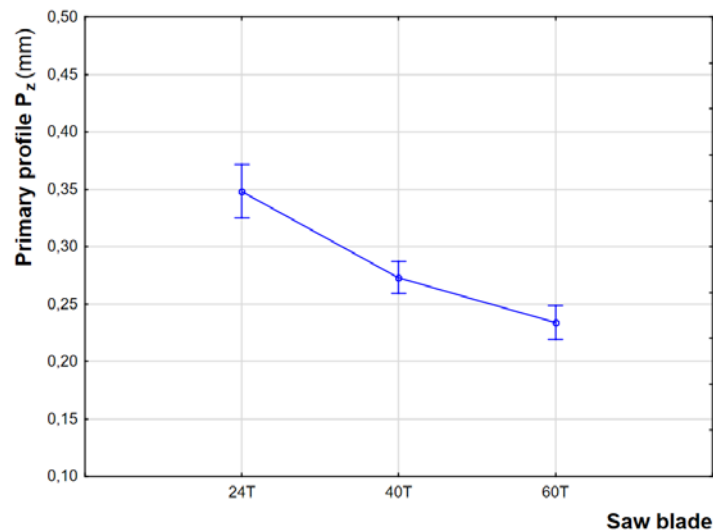

Fig. 7: 95% confidence interval showing the influence of the saw blade type on the primary profile P_z.

An expression of the dependence of primary profile on the sawn distance is presented in Fig. 8, where the ascension can be seen.
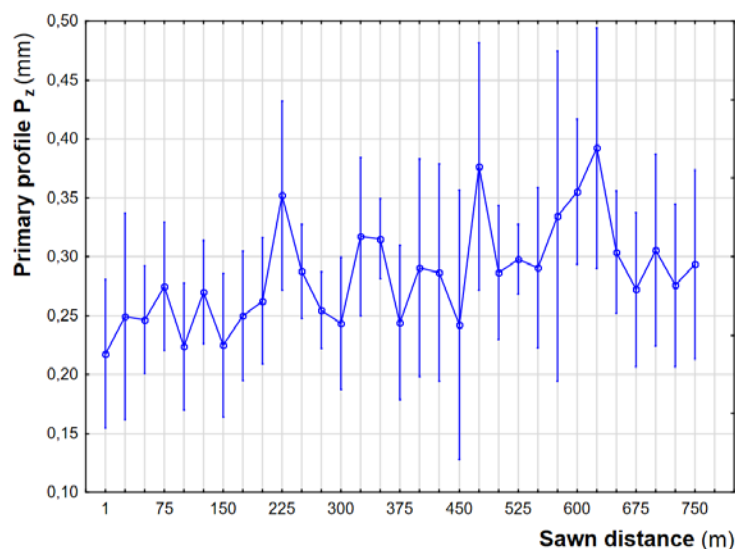
Fig. 8: 95% confidence interval showing the influence of the sawn distance on the primary profile P_z.

Towards the end, the curve of the values of the primary profile has a decreasing tendency, which may be caused by the beginning overheating of the saw blade and the consequent resulting partialy burning of the wood surface.

As can be seen in Fig. 9, the largest differences in the measured values of the primary profile were observed with the saw blade 24T, followed by the saw blade 40T, and the lowest values were shown in the saw blade 60T. Also, the largest variance of the measured values of the primary profile was highest at the 24T saw blade and the lowest values were found at the 60T saw blade. The sawn distance did not have a significant effect on the values of the primary profile when using the saw blades 40T and 60T, but when using the saw blade 24T, the values of the primary profile also increased with the increase of the sawn distance.
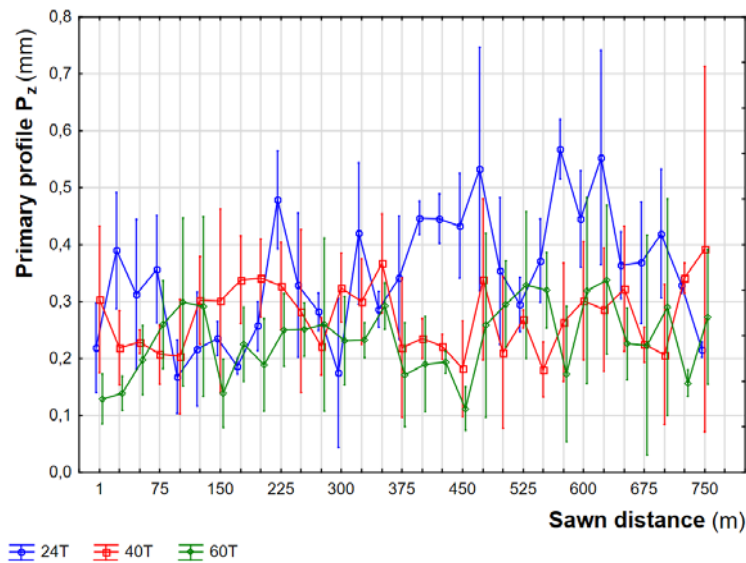
Fig. 9: 95% confidence interval showing the mutual influence of the saw blade type and sawn distance on the primary profile P_z.

The correlation pattern for the 24T saw blade (Fig. 10) shows the variance of the smallest and largest values of the primary profile. When using this saw blade, the variance of values is the largest of all saw blades.

Fig. 10: Correlation of primary profile P_z and maximum sawn distance for saw blade 24T.

Correlation equation of maximum primary profile (P_z) and maximum sawn distance for saw blade 24T: $P_z = 0.2705 + 0.0003*x$.

Figs. 10 – 12 describe the course of correlation of the height of the unevenness profile from the cut distances by individual types of saw blades. Use a 60T saw blade caused the lowest variance of the minimum and maximum values of the primary profile of all three saw blades. This fact was influenced by the largest number of teeth of the saw blade, and thus also the smallest feed per tooth.

Fig. 11: Correlation of primary profile P_z and maximum sawn distance for saw blade 40T.

Correlation equation of maximum primary profile (P_z) and maximum sawn distance for saw blade 40T: $P_z = 0.2564 + 5.9685E\text{-}5*x$.

Fig. 12: Correlation of primary profile P_z and maximum sawn distance for saw blade 60T.

Correlation equation of maximum primary profile (P_z) and maximum sawn distance for saw blade 60T: $P_z = 0.2071 + 7.043E - 5_*x$.

Tab. 2: Average Primary profile P_z for individual saw blades.

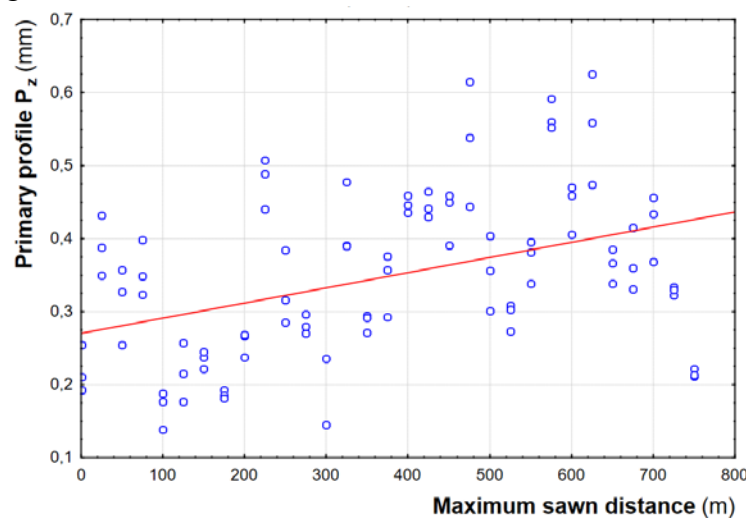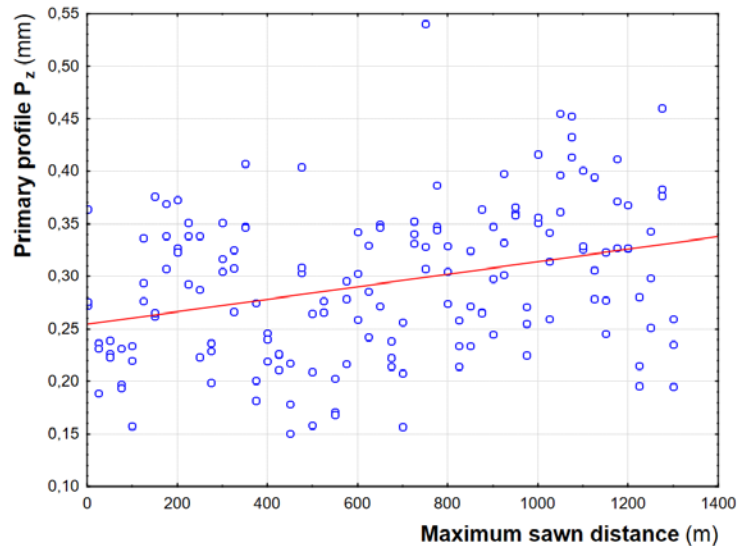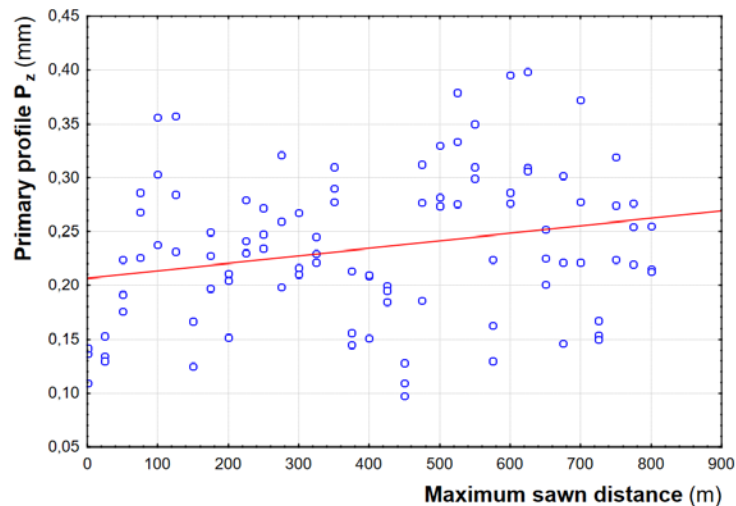| Saw blade	Sawn distance (m)	Average primary profile P_z (mm)			Sawn distance (m)	Average primary profile P_z (mm)			Average per group
		Mean	-95.0%	+95.0%		Mean	-95.0%	+95.0%	
24 teeth	1	0.219	0.140	0.298	400	0.447	0.417	0.476	0.348 (0.112)
	25	0.390	0.288	0.492	425	0.445	0.402	0.489	
	50	0.313	0.182	0.444	450	0.433	0.341	0.525	
	75	0.357	0.262	0.451	475	0.533	0.319	0.746	
	100	0.168	0.104	0.232	500	0.354	0.225	0.482	
	125	0.217	0.117	0.316	525	0.295	0.247	0.342	
	150	0.235	0.205	0.265	550	0.372	0.298	0.445	
	175	0.186	0.172	0.200	575	0.568	0.515	0.621	
	200	0.257	0.214	0.300	600	0.445	0.360	0.530	
	225	0.479	0.392	0.565	625	0.553	0.365	0.741	
	250	0.328	0.202	0.455	650	0.363	0.305	0.422	
	275	0.282	0.249	0.316	675	0.369	0.262	0.475	
	300	0.175	0.044	0.306	700	0.419	0.306	0.533	
	325	0.419	0.295	0.544	725	0.329	0.315	0.342	
	350	0.286	0.255	0.317	750	0.215	0.202	0.228	
	375	0.342	0.234	0.450					
40 teeth	1	0.304	0.175	0.433	400	0.235	0.200	0.270	0.273 (0.068)
	25	0.219	0.153	0.284	425	0.221	0.199	0.243	
	50	0.229	0.208	0.250	450	0.182	0.098	0.266	
	75	0.207	0.155	0.259	475	0.339	0.198	0.480	
	100	0.204	0.103	0.304	500	0.211	0.078	0.343	
	125	0.302	0.225	0.379	525	0.269	0.253	0.285	
	150	0.301	0.139	0.463	550	0.181	0.132	0.229	
	175	0.338	0.261	0.415	575	0.264	0.160	0.367	
	200	0.341	0.272	0.410	600	0.301	0.197	0.406	
	225	0.327	0.250	0.404	625	0.286	0.177	0.394	
	250	0.283	0.140	0.426	650	0.322	0.212	0.432	
	275	0.221	0.171	0.271	675	0.225	0.194	0.256	
	300	0.324	0.264	0.385	700	0.207	0.084	0.330	
	325	0.300	0.225	0.375	725	0.342	0.315	0.368	
	350	0.367	0.280	0.454	750	0.392	0.072	0.713	
	375	0.219	0.097	0.341					
60 teeth	1	0.129	0.086	0.173	400	0.190	0.106	0.274	0.234 (0.071)
	25	0.139	0.109	0.169	425	0.193	0.174	0.213	
	50	0.197	0.137	0.258	450	0.111	0.073	0.150	
	75	0.260	0.183	0.337	475	0.259	0.097	0.420	
	100	0.299	0.151	0.447	500	0.295	0.220	0.371	
	125	0.291	0.134	0.448	525	0.329	0.200	0.458	
	150	0.139	0.079	0.199	550	0.320	0.254	0.386	
	175	0.225	0.160	0.290	575	0.172	0.054	0.291	
	200	0.189	0.108	0.270	600	0.319	0.156	0.483	
	225	0.250	0.186	0.314	625	0.338	0.207	0.468	
	250	0.251	0.204	0.298	650	0.226	0.163	0.289	
	275	0.260	0.107	0.412	675	0.223	0.030	0.416	
	300	0.231	0.154	0.309	700	0.290	0.101	0.480	
	325	0.232	0.202	0.262	725	0.157	0.134	0.179	
	350	0.292	0.252	0.333	750	0.273	0.155	0.391	
	375	0.171	0.080	0.262					

*Note: ± 95% confidence interval of variance; values in parentheses represent ±SD.

As the sawn distance increased, the wear of the cutting edge also increased, which also caused higher values of the primary profile. Tool wear is not only an important parameter for assessing tool life, but also directly affects the surface quality of machining. This fact was also confirmed in their research by Wei et al. (2018).

Tab. 2 shows the average values of the primary profile measured for each type of blade. When comparing the results, it can be concluded that the observed trends of the influence of individual parameters in the transverse cutting of oak wood are confirmed. Homogeneity and density of sawn wood influences the created surface quality (Kúdela and Lagaňa 2010). As reported by Caceres et al. (2018) the reason for the different courses of surface irregularities could be the heterogeneity of the wood material (wood density, deflection of wood fibers), as well as the kinematics of the sawing process (the angle at which the wood fibers are cut, cutting model, imperfect parallelism of fibers with the cutting path) or the occurrence of random effects sawing (crooked cut due to movement caused by deformation of the saw blade shape or vibrations). These factors also affect measurement deviations (Sandak and Martino 2006). This statement fully corresponds with Krilek et al. (2014), Droba and Svoreň (2012) as well as Nasir and Cool (2019), who found that the design of the saw blade directly affects the force relationships in the cutting process, which is subsequently reflected in the quality of the created surface.

At small feeds per tooth, when the chip thickness approaches the existing cutting radius of the edge, there is a hyperbolic increase in the specific cutting resistance (k_c), also known as the so-called size effect (Curti et al. 2017, Atkins 2009), which in turn affects the primary profile such as can also be seen from our results. The specific cutting resistance decreases with increasing chip thickness. This phenomenon is known mainly from the field of metalworking, but it has also been recorded in wood cutting, especially in the case of saw blade cutting (Siklienka et al. 2013). Koleda et al. (2019) state that higher feed rates can be used when cutting with a saw blade, and the durability of the cutting edge can be extended with increasing overhang, but other factors, such as e.g. the diameter of the saw blade (impact on the price, but also on the width of the cutting gap), increasing the cutting power and reducing the quality of the cut must be considered. Ensuring these conditions, of course, leads to further operations, which are undesirable and there is an effort to prevent them both in terms of time and money.

CONCLUSIONS

(1) The value of the primary profile depends on the value of the feed per tooth. These measurements confirmed the theory that the greater the feed per tooth (feed rate), the higher the values of the largest height of the primary profile. The feed rate (feed per tooth) has a significant effect not only on the cutting power, but also on the final quality of the machined surface. *(2)* The shear force acts on the workpiece by means of cutting wedges (teeth). With increasing number of teeth, an almost proportional decrease in the primary profile, i.e. essentially also the surface roughness, was found. *(3)* A similar surface quality as in the case of face milling can also be achieved by transversal sawing. This fact depends on the actual cutting model, the type of wood, the type of saw blade and the feed force.

Depending on the indicated chip length, the quality of the machined surface deteriorates, which is also caused by wear of the cutting tool.

ACKNOWLEDGMENTS

REFERENCES

1. Atkins, T., 2009: The science and Engineering of cutting. The mechanics and process of separating, scratching and puncturing biomaterials, metals and non-metals. 1st ed., Oxford: Butterworth-Heinemann, 432 pp.
2. Budakçı, M., İlçe, A.C., Gürleyen, T., Utar, M., 2013: Determination of the surface roughness of heat-treated wood materials planed by the cutters of a horizontal milling machine. BioResources 8(4): 3189-3199.
3. Budakçı, M., İlçe, A.C., Korkut, D.S., Gürleyen, T., 2011: Evaluating the surface roughness of heat-treated wood cut with different circular saws. BioResources 6(4): 4247-4258.
4. Cáceres, C.B., Uliana, L., Hernández, R.E., 2018: Orthogonal cutting study of wood and knots of white spruce. Wood and Fiber Science 50(1): 55–65.
5. Curti, R., Marcon, B., Collet, R., Lorong, P., Denaud, L., Pot, G., 2017: Cutting forces and chip formation analysis during green wood machining. In: Proceedings of the 23rd International Wood Machining Seminar, Pp 152–161.
6. Chuchala, D., Orlowski, K., Krzosek S., 2012: The effect of the late wood share upon density of the Polish pine wood as a function of its origin. Annals of WULS-SGGW, Forestry and Wood Technology 77: 118-224.
7. Droba, A., Svoreň, J., 2012: Vplyv konštrukčného vyhotovenia pílových kotúčov pre zníženie hluku a výslednú kvalitu obrobeného povrchu (Influence of the design of saw blades for noise reduction and the resulting quality of the machined surface). Zvolen, (in Slovak). *Acta Facultatis Technicae* XVII(1): 15-23.
8. Gurau, L., Mansfield-Williams, H., Irle, M., 2005: Processing roughness of sanded wood surfaces. Holz als Roh - und Werkstoff 63(1): 43-52.
9. Gurau, L., Mansfield-Williams, H., Irle, M., 2012: A quantitative method to measure the surface roughness of sanded wood products. In: Wood and Wood Products, J.P. Davim (ed.), NOVA Science Publishers, Inc., Hauppauge, New York, USA, Pp 1-23.
10. Gündüz, G., Korkut, S., Korkut, D.S., 2008: The effects of heat treatment on physical and technological properties and surface roughness of Camiyani black pine (*Pinus nigra* Arn. subsp. pallasiana var. pallasiana) wood. Bioresource Technology 99(7): 2275-2280.

11. ISO 13061-1, 2014: Physical and mechanical properties of wood. Test methods for small clear wood specimens. Part 1: Determination of moisture content for physical and mechanical tests.

12. ISO 13061-2, 2014: Physical and mechanical properties of wood. Test methods for small clear wood specimens. Part 2: Determination of density for physical and mechanical tests.

13. Khandoker, A.R., 2020: Applicability of liquid-like nano polydimethylsiloxane from 1,3-dichlorotetramethyldisiloxane to the wetting of rough surfaces. Master Thesis, University of British Colombia, Vancouver, Canada, 137 pp.

14. Koleda, P., Barcík, Š., Svoreň, J., Naščák, Ľ., Dobrík, A., 2019: Influence of cutting wedge treatment on cutting power, machined surface quality, and cutting-edge wear when plane milling oak wood. BioResources 14(4): 9271-9286.

15. Kúdela, J., Lagaňa, R., 2010: Wood Structure and Properties. Arbora Publishers, 233 s.

16. Kminiak, R., Gaff, M., 2015: Roughness of surface created by transversal sawing of spruce, beech, and oak wood. BioResources 10(2): 2873 - 2887.

17. Kminiak, R., Gašparík, M., Kvietková, M., 2015: The dependence of surface quality on tool wear of circular saw blades during transversal sawing of beech wood. BioResources 10(4): 7123 - 7135.

18. Kvietková, M., 2015: Obrábění dřeva (Wood processing). Praha: CARTER, 295 pp. (In Czech).

19. Krenke, T., Frybort S., Müller, U., 2017a: Determining cutting force parameters by applying a system function. Machining Science and Technology 21(3): 436–451.

20. Krenke, K., Frybort, S., Müller, U., 2017b: Cutting force analysis of a linear cutting process of spruce. Wood Material Science & Engineering 13(5): 279–285.

21. Krilek, J., Kováč. J., Kučera, M., 2014: Wood crosscutting process analysis for circular saws. BioResources 9(1): 1417-1429.

22. Lisičan, J., 1996: Teória a technika spracovania dreva (Theory and technique of wood processing). Zvolen: Matcentrum, (in Slovak), 625 pp.

23. Mikleš, M., Kováč, J., Krilek, J., 2010: Výskum rezných podmienok priečneho pílenia dreva (Research of cutting process of cross-cutting wood). Research study. Zvolen, Technická univerzita vo Zvolene, (in Slovak), 69 pp.

24. Nasir V., Mohammadpanah A., Cool J., 2018: The effect of rotation speed on the power consumption and cutting accuracy of guided circular saw: Experimental measurement and analysis of saw critical and flutter speeds. Wood Material Science & Engineering 15: 140–146.

25. Nasir, V., Cool, J., 2019: Optimal power consumption and surface quality in the circular sawing process of Douglas-fir wood. European Journal of Wood and Wood products 77(4): 609-617.

26. Nasir, V., Cool, J., 2020: A review on wood machining: Characterization, optimization, and monitoring of the sawing process. Wood Material Science & Engineering 15: 1–16.

27. Oberg, E., Jones, F.D., Horton, H.L., Ryffel, H.H., 2004: Surface metrologic guide. Machinery`s handbook 27th Edition. Pp 724-729, Industrial Press. Inc., New York.

28. Orlowski, K.A., Walichnowski, A., 2013: Economic analysis of upper layer production of engineered floorings. Drewno 56(189): 115–126.

29. Pernikář, J., Tykal, M., Vačkář, J., 2001: Jakost a metrologie. Část metrologie.1.vyd. Brno: Akademické nakladatelství CERM, s.r.o., 151 pp. (In Czech).

30. Sandak, J., Martino, N., 2006: Wood surface roughness – what is it? In: Proceedings of the 17th International wood machining Seminar. Pp 242-250, Rosenheim, Vol. 1, Germany.

31. Siklienka, M., Kminiak, R., Argay, F., 2013: Vplyv uhlovej geometrie pílového kotúča na rezný výkon pri priečnom pílení bukového dreva (Saw blade angle geometry effect on cutting output power by cross-cutting of beech wood). Acta Facultatis Xylologiae Zvolen 55(1): 91-99.

32. Tesařová, D., Chladil, J., Čech, P., 2010: Ekologické povrchové úpravy (Ecological finished surfaces). Mendel University in Brno, 126 pp. (In Czech).

33. Walker, J., 2006: Primary wood processing: principles and practice. 2nd ed., Springer, 596 pp.

34. Wasielewski, R., Orlowski, K.A., Szyszkowski, S., 2012: Economical wood sawing with circular saw blades of a new design. Drvna Industria 63(1): 27–32.

35. Wei, H., Guo, X., Zhu, Z., Cao, P., Wang, B., Ekevad, M., 2018: Analysis of cutting performance in high density fiberboard milling by ceramic cutting tools. Wood Research 63(3): 455-466.

36. Williams, J.G., Patel, Y., 2016: Fundamentals of cutting. Interface Focus 6(3): 20150108.

MONIKA SARVAŠOVÁ KVIETKOVÁ, MIROSLAV GAŠPARÍK*
CZECH UNIVERSITY OF LIFE SCIENCES
FACULTY OF FORESTRY AND WOOD SCIENCES
DEPARTMENT OF WOOD PROCESSING AND BIOMATERIALS
KAMÝCKÁ 1176
CZ-165 00 PRAGUE 6 - SUCHDOL
CZECH REPUBLIC
*Corresponding author: gathiss@gmail.com

THE IMPORTANCE OF USING MULTIPLE ANALYSES TECHNIQUES TO DETERMINE THE PHYSICAL CONDITION OF THE WATERLOGGED WOOD NEAR THE CORRODED PARTS

ASLI GÖKÇE KILIÇ, NAMIK KILIÇ
ISTANBUL UNIVERSITY

CEM AKGÜN
YILDIZ TECHNICAL UNIVERSITY

ABSTRACT

In this study, three samples taken from the planks of the Yenikapı 29 shipwreck were analysed. Firstly, the maximum water content (MWC) and basic density values of the samples were calculated. MWC of the IK13-1 was 164% and the MWC of the SK6-1 was 87%. Because of these low MWC values, samples could be classified as non-degraded. When the SEM images of these two samples were examined, it was understood that the IK13-1 sample was non-degraded but the SK6-1 sample was penetrated with corrosion product and could not be classified as non-degraded. With these analyses, the XRF method was used to measure the iron amounts of the samples. The iron amount of the SK6-1 was 32.3% and the corrosion accumulation in this sample was also proved with XRF. In order to avoid incorrect results, multiple analysis techniques should be used for determining the physical condition of the waterlogged wood near the corroded parts.

KEYWORDS: Basic density, maximum water content, SEM, waterlogged wood, Yenikapı shipwrecks.

INTRODUCTION

During burial under water and/or wet land for many years, the wood transforms into a waterlogged form. Due to this transformation, the physical and chemical properties of the wood change. At first sight, the excavated waterlogged woods seem to be in a good condition because the pores of the wood are saturated with water. This sight can commonly be misleading and the wood in waterlogged form might as well be degraded. The age of the wood, species of the wood, intended purpose of the wood, the ambient conditions under which it is buried and the time it spends under these conditions affect the degree of the degradation of the waterlogged wood. In addition, the chemical and biological degradations of the wood cause the changes in the physical condition of the wood. Therefore, the determination of physical and chemical condition of the waterlogged wood is crucial for

understanding the degradation process of the waterlogged wood. In addition, the waterlogged wood is classified according to its degradation degree. A classification system, which relates maximum water content (MWC), is commonly used (Broda et al. 2015a,b, Koman and Feher 2015, Christensen 1970, De Jong 1977, Fix 2015, Grattan 1987, Hamilton 1996, Hedges 1990, Florian 1990, Kaye and Cole-Hamilton 1998, McConnachie et al. 2008, Dollarhide 2019). In addition, several techniques are used in order to determine the physical condition of the waterlogged wood. For instance, physical resistance monitoring techniques such as pin test, Pilodyn, Sibbert drill, and electrical resistance monitoring, wood-water amount related analyses such as MWC, basic density (BD), loss of wood substance, and visual analyses techniques such as optical microscope and electron microscope are used in order to determine the physical condition of the waterlogged wood (Grattan 2000, Ogilvie 2000, Rodgers 2004, Jensen and Gregory 2006, Gregory et al. 2007, Capretti et al. 2008, Heritage 2010, Macchioni et al. 2012, Pizzo et al. 2010, Babinski et al. 2014, Oron et al. 2016, Kılıç and Kılıç 2018, Romagnoli et al. 2018, Han et al. 2020). Furthermore, a combination of these techniques can be applied.

37 shipwrecks, which are located in Istanbul, are considered as the world's largest medieval shipwreck collection. The shipwrecks were excavated by Directorate of Istanbul Archaeological Museums and conservation studies of the 31 of these shipwrecks have been carried out by the Istanbul University Yenikapı Shipwrecks Project (Kocabaş 2015). The members of the project undertook the conservation process of the shipwrecks. One of the important steps of these conservation processes was the determination of the physical condition of the wooden parts of the shipwrecks. The MWC and the BD values of the waterlogged woods were calculated in order to understand the physical condition of the waterlogged woods. The studies, which were conducted on Yenikapı shipwrecks, showed that there was an inverse proportion between MWC and BD values of the waterlogged wood and MWC values of the highly degraded woods were higher (Kılıç and Kılıç 2019). On the other hand, inorganic residues, which penetrated into the structure of the woods, could cause failure in these values (Kılıç 2017). For instance, corrosion products such as corroded nails could penetrate into woods. The basic principle of the MWC analysis is calculating the amount of the water inside the woods. Highly degraded woods have more gaps inside the wood. Normally, these gaps of the waterlogged wood are filled with water and the amount of the water inside the wood indicate the physical degradation level of the waterlogged wood. The water can be removed easily with heat and the MWC value can be calculated using differences between the weights of the wood. On the other hand, iron corrosion products are stable and cannot be removed with heat. Therefore, the weight of the wood, before and after having been put in an oven, was similar. Corrosion products which have penetrated the gaps in the woods cause failures in the MWC and the BD calculations. In general, the wooden parts which were penetrated with corrosion products can be identified easily by naked eye observation. Therefore, the results could be ignored easily (Kılıç and Kılıç 2019). On the other hand, corrosion product can only penetrate the core of the wood. In this situation the parts of the woods contaminated with iron corrosion products cannot be identified easily. In order to determine iron corroded areas, SEM can be used as a monitoring technique. SEM is a useful tool for the investigation of the surface appearance of waterlogged wood (Charola and Koestler 2006). SEM images with high resolution can provide a determination

of the accumulation of the iron corrosion products inside the gaps of the wood. In addition, XRF analyses were done in order to determine inorganic compounds in the woods. The Yenikapı Shipwrecks Project handled hundreds of waterlogged wood pieces from dozens of shipwrecks, so the simplicity and the cost of the analysis techniques are very fundamental. On the other hand, there are important points to be considered in order to make these simple calculations correctly. Samples taken near the corroded parts of the woods have low MWC values due to the iron compounds in the samples. Therefore, the aim of this study is the determination of deviations in the samples which have low MWC values via SEM images.

MATERIAL AND METHODS

The study was done on the samples of YK (Yenikapı) 29 which is one of the 37 Yenikapı shipwrecks. YK 29 is a merchantman, and it is dated to the 8–9th century based on stratigraphy (Fig. 1). The shipwreck's extant length is 7.90 m and width 4.5 m. The planks of the ship were nailed to the frames with iron nails (Kocabaş 2015).
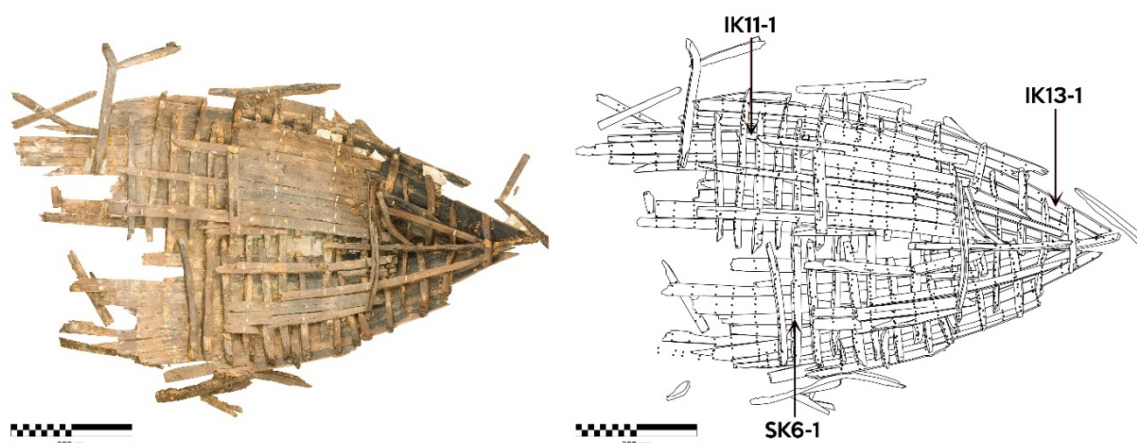

Fig. 1: Photo-mosaic image of YK 29 shipwreck (left), representation of the sample taken points on the drawing of YK 29 shipwreck (right) (IU Yenikapı shipwrecks project archive).

Samples were taken from 3 different planks (IK11-1, IK13-1, and SK6-1) which were in the desalination tanks at the IU Yenikapı Shipwrecks Research Laboratory. In order to calculate MWC and BD values, small pieces, not less than 1 g, were taken (Fig. 1). Before the measurement, the dirt on the surface of the samples was cleaned. These waterlogged samples were weighed in air and in water. Then, samples were oven-dried to a constant weight and finally weighed again. An analytical balance with an accuracy up to 0.0001 g was used for weighing (Kılıç and Kılıç 2019). The following equations were used in order to calculate MWC and BD values (Babinski et al. 2014).

$$MWC = 100 \times (m_w - m_d)/m_d \qquad (1)$$
$$BD = m_d / V_w \qquad (2)$$

where: MWC - maximum water content (%), BD - basic density ($g \cdot cm^{-3}$), m_w - mass of waterlogged sample (g), m_d - mass of oven-dry sample (g), and V_w - volume of waterlogged sample (cm^3).

In order to examine the physical condition of the samples in detail, SEM (Scanning Electron Microscope) images of the samples were taken with a FEI Quanta 450. Samples were prepared in transverse section direction (approximately 0.5 - 1 cm^3) with razor blade for SEM. After these analyses, XRF analyses were done in order to determine iron amounts of the samples. XRF analyses were carried out on a Spectro xSort handheld XRF Analyzer.

RESULTS AND DISCUSSION

The MWC and the BD values of the samples are presented in Tab. 1 (Akgün 2020). The samples, which were taken from IK13-1 and SK6-1, had low MWC values and high BD values. In addition, the MWC value of the sample, which was taken from IK11-1, was higher and the BD value of the sample was lower. The wood species of the samples is cypress (*Cupressus* L.) (Akkemik 2015).
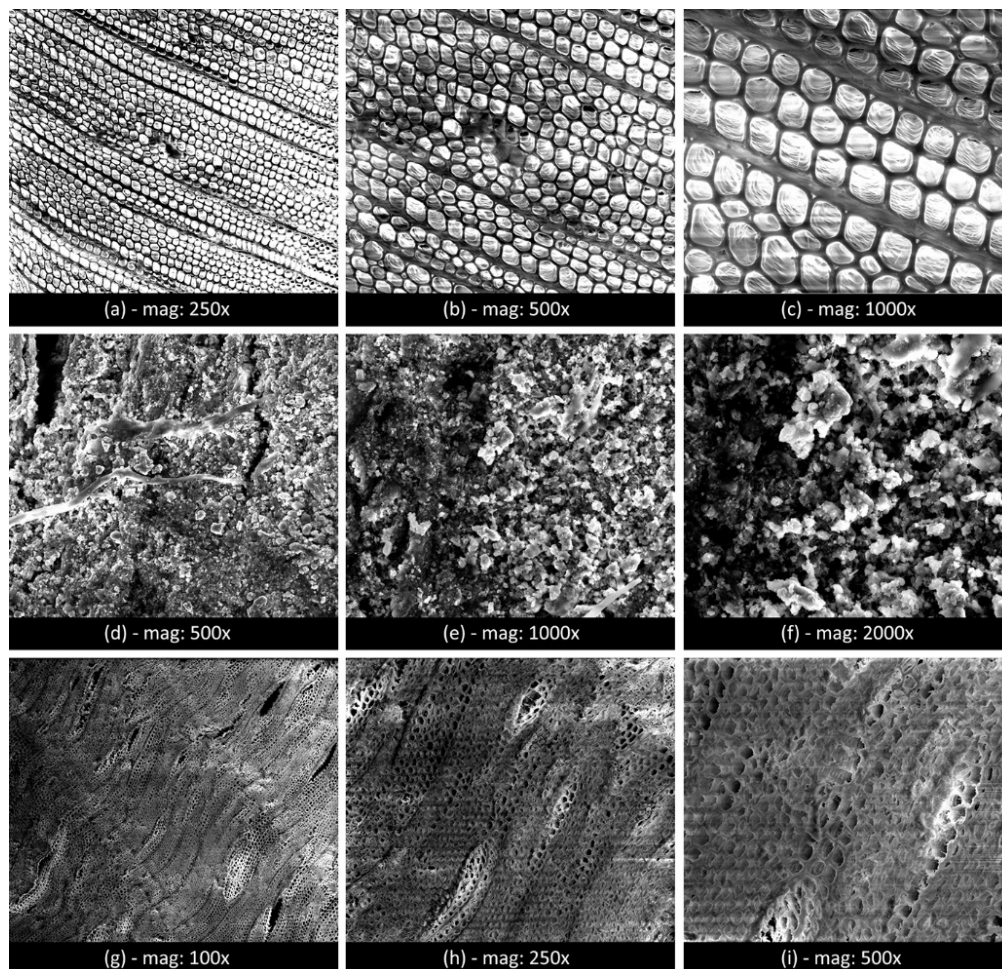
Fig. 2: SEM images of the samples. a-c: cross-section of the sample taken from IK13-1, d-f: cross-section of the sample taken from SK6-1, cross-section of the sample taken from IK13-1, g-i: cross-section of the sample taken from IK11-1.

According to MWC and BD values of the samples, the sample taken from IK13-1 should be recognized as highly preserved due to low MWC value. The sample taken from IK11-1 should be recognized as highly degraded due to high MWC value. The MWC value of

the sample taken from SK6-1, was remarkably low for a waterlogged wood sample and the BD value was higher than the density of fresh cypress wood (the density of the fresh cypress wood is 0,45 $g \cdot cm^{-3}$) (Akgün 2020). Due to the suspicion caused by this value, it was decided to perform SEM. In order to determine the physical conditions of the samples, SEM images were taken.

When the SEM images of the sample taken from IK13-1 were examined, it was observed that the wood was highly preserved, and tracheid, ray, and tracheid tangential wall of the wood were almost intact. The SEM images of the sample showed that there was almost no degradation on the structure of wood cells (Figs. 2a-c). When SEM images of the sample taken from SK6-1 were examined, it was observed that SK6-1 was covered with iron corrosion products so the woody tissue could not be observed (Figs. 2d-f). When SEM images of the sample taken form IK11-1 were examined, the degradation of the wood cells could be observed. Especially, collapse of the wood cells could be detected (Figs. 2g-i).

After these SEM observations, XRF analyses were done in order to measure the iron amounts of the samples (Tab. 1).

Tab. 1: MWC values of the samples.

Sample	MWC (%)	BD ($g \cdot cm^{-3}$)	Iron amounts of the samples (%)
IK11-1	441	0.20	3.7
IK13-1	164	0.45	0.4
SK6-1	87	0.71	32.3

IK and SK: Plank.

Moreover, an additional sample was taken from a part which was distant from the corroded area of the SK6-1 wood and SEM images of the sample were taken in order to have an idea about the physical condition of the SK6-1 wood (Fig. 3).
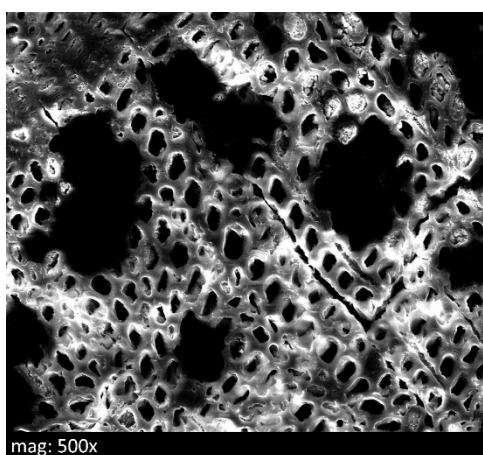
Fig. 3: SEM images of an additional sample taken from SK6-1.

When the SEM images were examined, the distortion occurring in the wood structure was observed. These images gave an idea about what might happen if the wood was not filled with corrosion products. For this reason, it is necessary to examine the woods with very low MWC values and very high BD values via microscopic methods especially via SEM.

CONCLUSIONS

The Yenikapı shipwrecks project handled hundreds of waterlogged wood pieces from dozens of shipwrecks, so the simplicity and the cost of the analysis techniques used for determination of the physical condition of the woods are very fundamental. With the help of determining the physical condition of the woods, conservation procedure of the wood can be maintained successfully. MWC and BD values can be calculated easily and economically but any contamination can cause incorrect results. In order to avoid any erroneous sampling due to the excessive number of the wooden parts, the size of the wooden parts of the shipwrecks, the sampling conditions (samples can be taken when the samples were in the desalination tank), and the sampling should be inspected well. Nevertheless, should be specifically examined with further analysis techniques such as SEM and XRF especially the wooden parts of the shipwrecks which were near the corroded iron nails. Iron corrosion products are stable against heat. In addition, the weight of the wood was similar before and after heating. Therefore, corrosion products which have penetrated the gaps in the woods cause failures in the MWC and the BD calculations. This study presented that usage of multiple analysis techniques is very beneficial for determining the physical condition of the waterlogged wood near the corroded parts.

ACKNOWLEDGEMENTS

REFERENCES

1. Akgün, C., 2020: The investigation of degradation degree of Yenikapı 29 shipwreck and conservation proposal. Istanbul University. Master's Thesis, 114 pp.
2. Akkemik, Ü., 2015: Woods of Yenikapi shipwrecks. Ege Publishing, 213 pp.
3. Babiński, L., Izdebska-Mucha, D., Waliszewska, B., 2014: Evaluation of the state of preservation of waterlogged archaeological wood based on its physical properties: basic density vs. wood substance density. Journal of archaeological science 46: 372-383.
4. Broda, M., Mazela, B., Krolikowska-Pataraja, K., Siuda, J., 2015a: The state of degradation of waterlogged wood from different environments. Annals of Warsaw University of Life Sciences-SGGW. Forestry and Wood Technology 91: 23-27.
5. Broda, M., Mazela, B., Królikowska-Pataraja, K., Hill, C.A., 2015b: The use of FT-IR and computed tomography non-destructive technique for waterlogged wood characterisation. Wood Research 60(5): 707-722.
6. Capretti, C., Macchioni, N., Pizzo, B., Galotta, G., Giachi, G., Giampaola, D., 2008: The characterization of waterlogged archaeological wood: the three Roman ships found in Naples (Italy). Archaeometry 50(5): 855-876.

7. Charola, A.E., Koestler, R.J., 2006: Methods in conservation. In: Conservation Science: Heritage Materials (Ed. May E., Jones M.). Pp. 13-31, RSC Publishing.

8. Christensen, B.B., 1970: Conservation of waterlogged wood in the National museum of Denmark. National Museum of Denmark. Copenhagen, 118 pp.

9. De Jong, J., 1977: Conservation techniques of old waterlogged wood from shipwrecks found in the Netherlands. In: Biodeterioration Investigation Techniques (Ed. Walters A.E.). Pp 295-338, Applied Science Publishers, London.

10. Dollarhide, K.D., 2019: A tale of two shipping crates from Brother Jonathan 1865. Texas A&M University. Doctoral dissertation, 129 pp.

11. Fix, P.D., 2015: Archaeological watercraft: A review and critical analysis of the practice. Texas A&M University. Doctoral dissertation, 387 pp.

12. Florian, M.E., 1990: Scope and history of archaelogical wood. In: Archeological wood – properties chemistry and preservation (Ed. Rowell R.M., Barbour R.J.). Pp 3-32, Advances in Chemistry Series 225, American Chemical Society.

13. Grattan, D.W., 2000: Wood (waterlogged) conservation. In: Archaeological method and theory: an encyclopedia (Ed. Ellis L.). Pp 665-667, Taylor & Francis.

14. Grattan, D.W., 1987: Waterlogged wood. In: Conservation of marine archaeological objects (ed. Pearson C.). Pp 55-67, Butterworth-Heinemann.

15. Gregory, D., Jensen, P., Matthiesen, H., Straetkvern, K., 2007: The correlation between bulk density and shock resistance of waterlogged archaeological wood using the Pilodyn. Studies in Conservation 52(4): 289-298.

16. Hamilton, D.L., 1996: Basic methods of conserving underwater archaeological material culture. US Department of Defense, Legacy Resource Management Program, 128 pp.

17. Han, L., Guo, J., Wang, K., Grönquist, P., Li, R., Tian, X., Yin, Y., 2020: Hygroscopicity of waterlogged archaeological wood from Xiaobaijiao No. 1 shipwreck related to its deterioration state. Polymers 12(4): 834: 1-15.

18. Hedges, J.I., 1990: The chemistry of archaeological wood. Archaelogical Wood – properties chemistry and preservation (Ed. Rowell R.M., Barbour R.J.). Pp 111-140, Advances in Chemistry Series 225, American Chemical Society.

19. Heritage, E., 2010: Waterlogged wood. Guidelines on the recording, sampling, conservation and curation, 35 pp.

20. Jensen, P., Gregory, D.J., 2006: Selected physical parameters to characterize the state of preservation of waterlogged archaeological wood: a practical guide for their determination. Journal of Archaeological Science 33(4): 551-559.

21. Kaye, B., Cole-Hamilton, D.J., 1998: Supercritical drying of waterlogged archaeological wood. In: Hidden Dimensions: the cultural significance of wetland archaeology (Ed. Bernick K). Pp 329-339, UBC Press.

22. Kılıç, A.G., 2017: Sulphur and iron analysis together with their distribution in woods and their removal from the woods of Yenikapı shipwrecks. Doctoral dissertation. Istanbul University, 193 pp.

23. Kılıç, N., Kılıç, A.G., 2018: Analysis of waterlogged woods: Example of Yenikapı Shipwreck. The Art-Sanat Journal 9: 1-11.

24. Kılıç, N., Kılıç, A.G., 2019: Physical properties for the characterization of waterlogged archaeological woods of eight Yenikapı shipwrecks from Byzantine period. Mediterranean Archaeology & Archaeometry 19(2): 133-148.

25. Kocabaş, U., 2015: The Yenikapı Byzantine-era shipwrecks, Istanbul, Turkey: A preliminary report and inventory of the 27 wrecks studied by Istanbul University. IJNA. 44-1: 5–38.

26. Koman, S., Feher, S., 2015: Basic density of hardwoods depending on age and site. Wood Research 60(6): 907-912.

27. Macchioni, N., Pizzo, B., Capretti, C., Giachi, G., 2012: How an integrated diagnostic approach can help in a correct evaluation of the state of preservation of waterlogged archaeological wooden artefacts. Journal of archaeological science 39(10): 3255-3263.

28. McConnachie, G., Eaton, R., Jones, M., 2008: A re-evaluation of the use of maximum moisture content data for assessing the condition of waterlogged archaeological wood. E-preservation Science. 5: 29-35.

29. Ogilvie, T., 2000: Water in archaeological wood: a critical appraisal of some diagnostic tools for degradation assessment. Doctoral dissertation. Durham University, 331 pp.

30. Oron, A., Liphschitz, N., Held, B.W., Galili, E., Klein, M., Linker, R., Blanchette, R.A., 2016: Characterization of archaeological waterlogged wooden objects exposed on the hyper-saline Dead Sea shore. Journal of Archaeological Science: Reports 9: 73-86.

31. Pizzo, B., Giachi, G., Fiorentino, L., 2010: Evaluation of the applicability of conventional methods for the chemical characterization of waterlogged archaeological wood. Archaeometry 52(4): 656-667.

32. Rodgers, B.A., 2004: Archaeological wood. The archaeologist's manual for conservation: A guide to non-toxic. Minimal Intervention Artifact Stablization, 214 pp.

33. Romagnoli, M., Galotta, G., Antonelli, F., Sidoti, G., Humar, M., Kržišnik, D., Cufar, K., Petriaggi, B.D., 2018: Micro-morphological, physical and thermogravimetric analyses of waterlogged archaeological wood from the prehistoric village of Gran Carro (Lake Bolsena-Italy). Journal of Cultural Heritage 33: 30-38.

ASLI GÖKÇE KILIÇ*
ISTANBUL UNIVERSITY
FACULTY OF LETTERS
MUSEOLOGY DEPARTMENT
ISTANBUL
TURKEY
*Corresponding author: gokcegokcay@istanbul.edu.tr

NAMIK KILIÇ
ISTANBUL UNIVERSITY
FACULTY OF LETTERS
DEPARTMENT OF CONSERVATION OF MARINE ARCHAEOLOGICAL OBJECTS
ISTANBUL
TURKEY

CEM AKGÜN
YILDIZ TECHNICAL UNIVERSITY
FACULTY OF ARCHITECTURE
DEPARTMENT OF CONSERVATION AND RESTORATION OF CULTURAL
PROPERTY
ISTANBUL
TURKEY

DEVELOPMENT OF A MACHINE FOR CHOPPING WOOD RESIDUES

GAMAL NASR, MOHAMED IBRAHIM, FETOUH HASHIM

CAIRO UNIVERSITY

EGYPT

ABSTRACT

CAD software and FEM analysis were used to modify the drum of threshing machine into machine for chopping wood residues. The operating parameters that affecting the performance of the chopping machine are drum speed (450, 1000 and 1200 rpm), three stages of serrated disk arrangement clearance between drum flail knives (0.7, 1.5 and 3 cm) and three levels of feeding capacity (W1 = 300, W2 = 360 and W3 = 420 kg·h^{-1}). The developed machine was operated by the addition of two types of knives (sharp free knives + serrated discs) to the original knife existing already in the machine. The machine was evaluated in terms of production capacity, cutting efficiency, power requirements and energy consumption. Using the modified (serrated) saw disk mill and flail knives reduced the energy requirement for chopping and raised fine degree of the chopped materials and solve the clogging problem. The cutting productivity and cutting efficiency raised with reducing the clearance between flail knives (0.7, 1.5 and 3 cm) while the power requirements and energy consumption reduced.

KEYWORDS: CAD, FEM analysis, chopping machine, serrated disc mills, knives sharps and wood residues.

INTRODUCTION

The first step towards solving residues problem, in order to be used as lignocelluloses raw materials in several industries, is to cut, crush and mill these residues using hammer mill machines to minimize the volume (Bejo et al. 2009). Ariavie et al. (2010) stated that, the fine particles of biomass improve density and the quality of briquettes. A briquetting plant used to produce the briquettes from residues essentially have hammer mill consists of a rotating shaft with free- swinging hammers, which reduce the size of particle to a predetermined size. Anup et al. (2012) used the hammer mill hammers like projection mounted on a shaft. The hammer revolves at high speed to chop the materials fed into pieces by beating. The one end of shaft coupled with blower to transport the chopped material from mill.

CAD (computer aided design) means that is a project assisted by a computer. CAD is the use of computer technology to aid in the design of a product. CAD system develop project functions, mainly based on the design of the item which one wants to create by using a series of tools provided by a data processing system to improve the efficiency and speed of the operations which are usually made by hand. CAD offers solutions reduce product time-to-market and improve communication efforts between design and production. Cellulose is one of the highly abundant natural polymers found in earth. It can be extracted from several sources including bagasse, wood, cotton, pineapple leaves and sisal fibers amongst others (Linganiso et al. 2019). Several authors state that the wood density varies not only by tree species but also with the vertical or radial location within the trunk or in the tree crown (Husch et al. 2003, Tomczak, and Jelonek 2013) followed by the annual rings width, the proportion of early and late wood, the tree age and the site on which the tree grows (Zeidler and Borůvka 2016, Schönfelder et al. 2017 and Jelonek et al. 2009).

The main objective of this research is to modify the performance of hammer mill equipment during cutting and crushing wood residues.

MATERIAL AND METHODS

A local hammer mill machine was developed for chopping wood residues. Development of cutting rotate drum was provided in three arrangement steps: *(1)* knives have been replaced by other knives with sharp edge, *(2)* knives have been replaced by knives with sharp edge beside (9 inches) saw disk which have been set on the rotating drum, and *(3)* knives have been replaced by knives with sharp edge beside (14, 12, 9 inches) saw disk mills. The machine was modified from old drum to the new one as shown in Fig. 1 to be more suitable for chopping many types of residues. Each knife is fastened by four bars and rotates with high speed corresponding to a lower speed of feeding drums. The swinging knives were fitted to the flange by four bars and bolts.

a)   *b)*

Fig. 1: a) The old drum under study before modification and b) after modification.

The action of these knifes interacted between themselves actions to help in cut the materials easily, reduce the impact force and prevent the straw around the drum. All disks with different diameters rotate with the main shaft at the same high speed. The maximum force

required to cut the wood sample in a direction perpendicular to the growth of the tree fibers Kováč et al. (2014), Kuvik et al. (2017) and Krilek et al. (2015).

Factors under study

The developed machine was evaluated at drum speed, clearance between drum knives, feeding capacity and stages of serrated disk arrangement. According to literature data (Srivastava et al. 2006, CIGR 1999), in reference to this information, machine productivity, power consumption, consumed energy and cutting efficiency were evaluated at each combination of variables.

Tab. 1: Experimental plan for evaluating the machine.

Variables	Levels
Drum speed, rpm	450, 1000, 1200
Clearance between drum knives, cm	0.7, 1.5, 3.00
Feeding capacity, kg h^{-1}	W1 = 300, W2 = 360, W3= 420
stages of serrated disk arrangement	Stage 1, Stage 2 , Stage 3

Finite element modeling using of CAD software

Computer aided design of machine was made by using "SolidWorks" software. Typical dimensions of the machine such as blade size, distance etc. and their 3D models can be easily made in short time. Input commands are provided for cutting tool features such as tool diameter, length of cut etc. Finite element modeling (FEM) was used to conduct a simulation study for stress analysis. A numerical model of chopping machine was created by using three-dimensional software. Deformation under static analysis was found, maximum strain values were obtained. The static results were analyzed and verified by simulation.

The properties of wood residues

The chopping machine was tested with different variety of wood with width in range 4-15 cm, length 18-50 cm and thickness 4-10 cm at 7.3% moisture content on wet base obtained from carpentry workshops. The samples were taken periodically from the machine outlet and placed in polyethylene bags. The samples were even dried at 70°C for 48 h (Nwaigwe et al. 2012) by using electrical oven. Moisture content (MC) was determined according to Eq. 1:

$$MC = m - m_0 / m \quad (\%) \tag{1}$$

where: MC - moisture content %, m - sample weight before drying, m_0 - weight after drying (g).

Performance evaluation of the developed machine

Evaluation of the hammer mill was performed taking the following measuring parameters:

Machine productivity

El Shal et al. (2010) mentioned that actual capacity of the machine is the actual rate of productivity by the amount of actual time consumed in operation (lost + productive time). Lost time is considered as the time spends in refilling the machine hopper, simple repairs and interruptions. Machine chopper productivity (*P*) was calculated by using Eq. 2 (Mady 1999):

$$P = W \times 3600 / T \qquad (kg \cdot h^{-1}) \qquad (2)$$

where: W - mass of the sample (kg), T - time (s).

Required power and consumed energy

El-Hanfy and Shalby (2009) stated that, the average of cutting length reduced and the distribution percentage of short pieces raised by rising the cutting speeds and overlapping between fixed and rotary knives.

Power consumption *(Pc)* was determined by measuring the volume of diesel fuel required and refueling the machine tank after finishing the operation time. The power was calculated by using Eq. 3. The consumed energy (CE) is power per unit productivity; it was calculated by the using Eq. 4. (El-Fatih et al. 2010):

$$Pc = \quad FC \times \rho f \times LCV \times 427 \times \Eta_m \times \Eta_{th} \quad / 3600 \times 75 \times 1.36 \qquad (kW) \qquad (3)$$

$$CE = Pc / P \qquad (kW.h.kg^{-1}) \qquad (4)$$

where: *FC* – fuel consumption ($l \cdot h^{-1}$), *ρf* – fuel density (Diesel 0,85 $kg \cdot l^{-1}$), *LCV* – lower calorific value of fuel (11000 $kcal \cdot kg^{-1}$), thermo- mechanical equivalent (427 $kg \cdot m \cdot kcal^{-1}$), *$\Eta_m$* – engine mechanical efficiency (85% Diesel engine), *$\Eta_{th}$* – engine thermal efficiency (25% diesel engine).

Cutting efficiency

Nwaigwe et al. (2012) noted that, the efficiency of the modified chopping materials mill is given by using Eq. 5:

$$Em = (Amount\ passing\ sieve\ /\ Total\ weight\ of\ sample) \times 100 \qquad (5)$$

RESULTS AND DISCUSSION

Finite element modeling

The applied mechanism here is impact loading where the time of application of force is less than the natural frequency of vibration of the body. Since the hammers are rotating at high speed, the time for which the particles come in contact with the hammers is very small, so here impact loading is applied. Swinging instead of hammers was used to avoid the hammers from getting stocked in case a hammer comes in contact with a material it cannot break at first impact.

A solid model is the complete type of geometric model used in CAD systems as sown at (Figs. 2 and 3). The shaft is considered to be subjected to torsion and bending. The model is considered for the horizontal shaft impact chopping to find out the relation between the feed, the crusher and the output parameters. Attrition method has the material scrubbed between the hammers and the screen bars. Attrition consumes more power and causes heavier wear on hammers and screen bars. Many studies have been investigated on elastic constants of wood through using different testing methods (Aira et al. 2014), non-destructive method (Tomazello et al. 2008, Xu et al. 2020), and resonant beam technique (Gerhard et al. 2020).
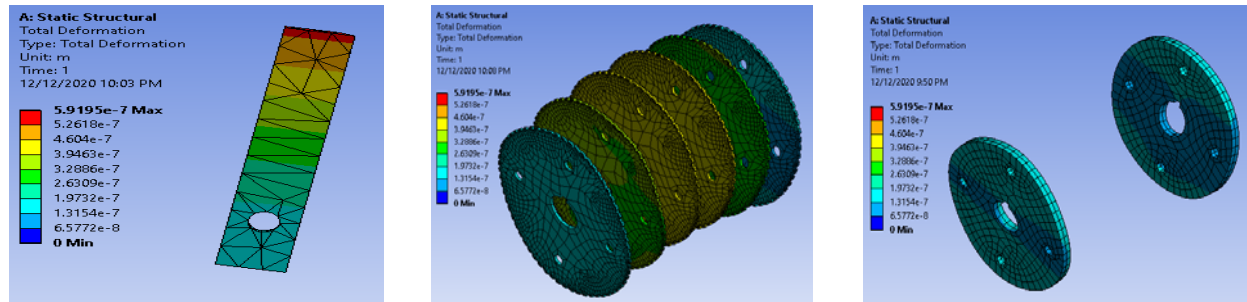

Fig. 2: Model analysis of the knife, disk and flange deformations in Ansys Pro.
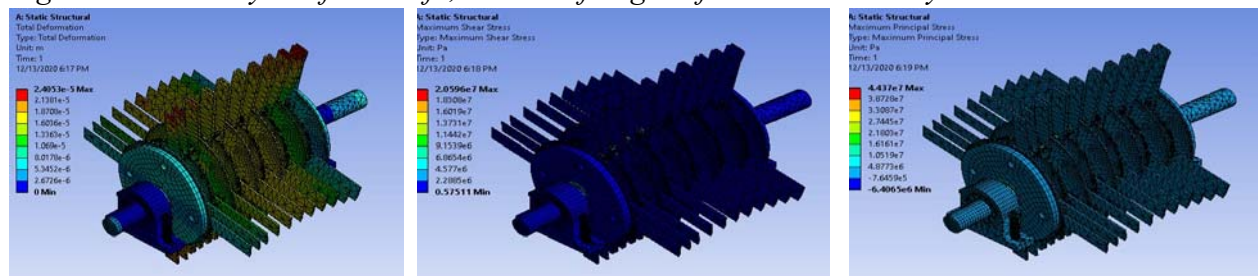
Fig. 3: Model analysis of the drum deformation, shear stress and principal stress in Ansys Pro.

Evaluation of the productivity with wood residues

The data in Fig. 4 shows that the cutting productivity raised with rising the cutting drum speed and reducing the clearance between flail knives (0.7, 1.5 and 3 cm).

Fig. 4: The relationship between cutting drum speed and productivity at three levels of feeding capacity (w1,w2 and w3) for wood residues at 7.2% moisture content.

Power requirement

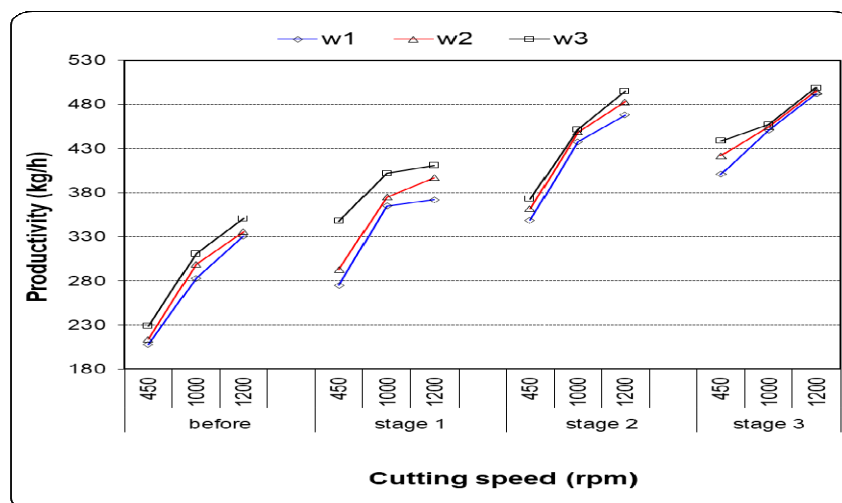The data in Fig. 5 shows that the power requirements reduced with rising cutting drum speed while the power requirements reduced with reducing the clearance between flail knives (0.7, 1.5 and 3 cm). The results show that the power consumption and energy requirement for cutting different residues was raised with rising drum speed, feed rate and moisture content but the power consumption and energy requirement were reduced by rising the concave clearance, the results agree with Arfa (2007).

Fig. 5: The relationship between cutting drum; speed and power requirements at three levels of feeding capacity (w1,w2 and w3) for wood residues at 7.2% moisture content.

Energy consumption

The data in Fig 6 show that the energy consumption reduced with rising cutting drum speed and with reducing the clearance between flail knives (0.7, 1.5 and 3 cm).

Fig. 6: The relationship between cutting drum speed and energy consumption at three levels of feeding capacity (w1,w2 and w3) for wood residues at 7.2% moisture content.

Cutting efficiency

The data in Fig. 7 show that the cutting efficiency raised with rising the cutting drum speed while the cutting efficiency raised with reducing the clearance between flail knives (0.7, 1.5 and 3 cm). It was possible to separately observe the amount of cutting force for cutting knifes thickness Kováč et al. (2014), Kuvik et al. (2017) and Krilek et al. (2015).
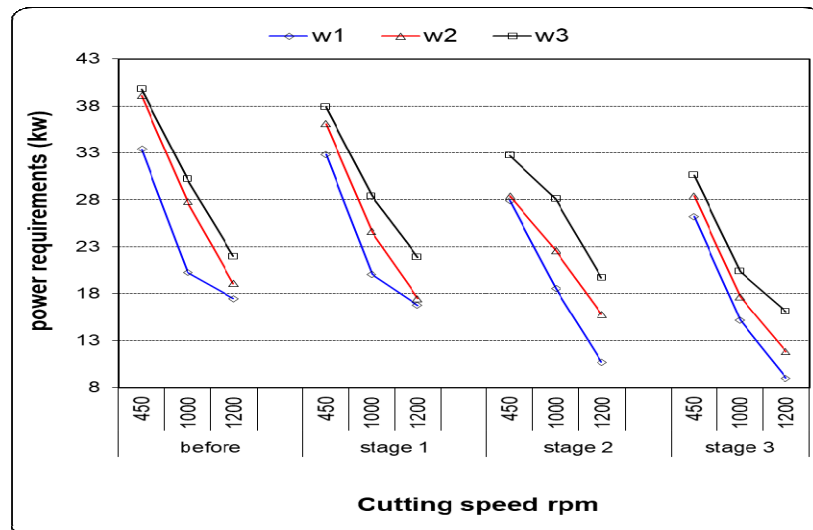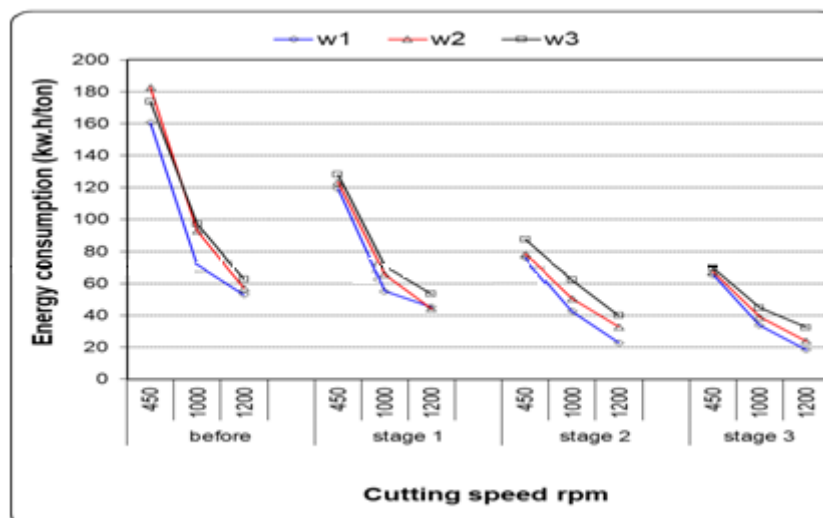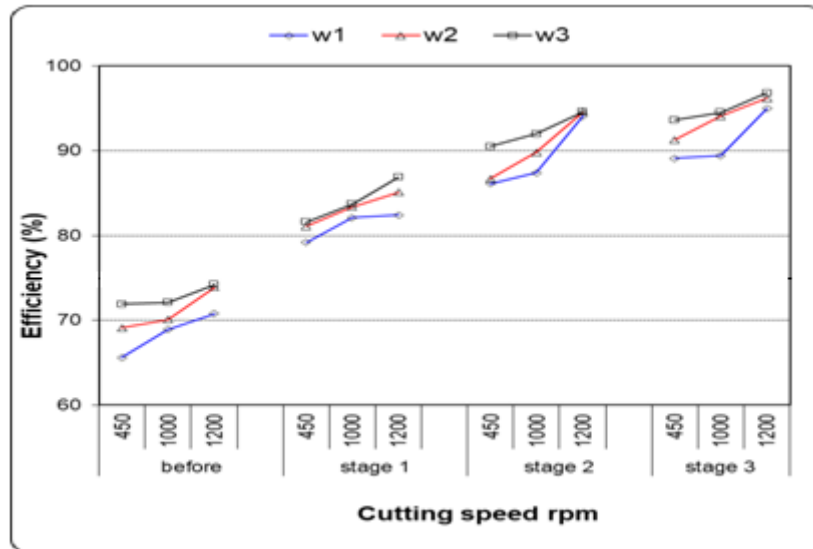

Fig. 7: The relationship between cutting drum speed and efficiency at three levels of feeding capacity (w1,w2 and w3) for wood residues at 7.2% moisture content.

CONCLUSIONS

From the above mentioned study, it can recommend that: *(1)* The addition of the serrated disc mills and the distance between reduce sharp flail knives themselves support the process of cutting force. *(2)* Using the modified (serrated) saw disk mill and flail knives reduced the energy requirement for chopping and raised fine degree of the chopped materials. *(3)* Reducing the serrated disk arrangement clearance between drum knives (0.7, 1.5 and 3 cm) solve the clogging problem and reduced the energy requirement for chopping and raised fine degree of the chopped materials.

REFERENCES

1. Abd El-Mottaleb, A.F., El-Dahhshhan, W.A., Bejo, L., 2009: Optimization of milling farm residues using a local hammer mill. Misr Journal of Agricultural Engineering 26(3): 1172-1189.
2. Aira, J.R., Arriaga, F., González, G.L., 2014: Determination of the elastic constants of Scots pine (*Pinus sylvestris* L.) wood by means of compression tests. Biosystem Engineering 126: 12–22.

3. Anup, A., Bijagare, P.G., Mehar, V.N., Mujbaile, 2012: Design optimization & analysis of drive shaft. VSRD International journal of mechanical, automobile and production engineering 2(6): 210- 215.

4. Arfa, G.K., 2007: Subdual of stationary thresher machine for chopping residues. Misr Journal of Agricultural Engineering 24(3): 504-521.

5. Ariavie, G.O, Ebunilo, P.O., Obanor, A.I., 2010: Design and preliminary testing of a hammer mill with end suction lift capability suitable for commercial processing of grains and solid minerals in Nigeria. International journal of Engineering Science and Technology 2(6): 1581-1593.

6. CIGR, 1999: Handbook of agricultural engineering. Vol. III. Plant production engineering. The International Commission of Agricultural Engineering. Published by the American Society of Agricultural Engineers.

7. El-Hanfy, E.H., Shalby, S.A., 2009: Performance evaluation and modification of the Japanese combine chopping unit. Misr Journal of Agricultural Engineering 26(2): 1021-1035.

8. El-Fatih, A., Arif, E.M. and Atef, A.E., 2010: Evaluate the modified chopper for rice straw composting. Journal of Applied Sciences Research 6(8): 1125-1131.

9. El-Shal, M.S., Tawfik, M.A., El-Shal, A.M. and Metwally, K.A., 2010: Study the effect of some operational factors on hammer mill. Misr Journal of Agricultural Engineering 27(1): 54-74.

10. Gerhard, S., Maierhofer, J., Loidli, D., Puchegger, S., Stanzl-Tschegg, S., 2020: Elastic constants of six wood species measured with the resonant beam technique. Wood Research 65(2): 347-352.

11. Husch, B., Beers, T.W., Kershaw, J.A., 2003: Forest mensuration. John Wiley & Sons. New Jersey, 443 pp.

12. Jelonek, T., Pazdrowski, W., Tomczak A., 2009: The effect of biological class and age on physical and mechanical properties of European larch (*Larix decidua* Mill.) in Poland. Wood Research 54(1): 1-14.

13. Kováč, J., Krilek, J., Kučera, M., Barcík, Š., 2014. The impact of design parameters of a horizontal wood splitter on splitting force. Drvna Industrija 65(4): 263-271.

14. Krilek, J., Kováč, J., Barcík, Š., Svoreň, J., Štefánek, M., Kuvik, T., 2015: The influence of chosen factors of a circular saw blade on the noise level in the process of cross cutting wood. Wood Research 61(3): 475-486.

15. Kuvik, T., Krilek, J., Kováč, J., Štefánek, M., Dvořák, J., 2017: Impact of the selected factors on the cutting force when using a chainsaw. Wood Research 62(5): 807-814.

16. Linganiso, L.Z., Buthelezi, T., Motaung, T.E., 2019: A comparative study of sugarcane bagasse and soft wood. Wood Research 64: 273-280.

17. Mady, M.A., 1999: Developing a manual cutting machine suitable for mechanical cutting stalks. Misr Journal of Agricultural Engineering 16 (3):449-459.

18. Nwaigwe, K.N., Nzediegwu, C., Ugwuoke, P.E., 2012: Design, construction and performance evaluation of a modified cassava milling machine. Research Journal of Applied Sciences, Engineering and Technology 4(18): 3354-3362.

19. Schönfelder, O., Zeidler, A., Borůvka, V., Bílek, L., 2017: Influence of site conditions and silvicultural practice on the wood density of the Scots pine (*Pinus sylvestris* L.) – a case study from the locality of Doksy, Czech Republic. Journal of Forest Science 63(10): 457–462.
20. Srivastava, A.K, Goering, C.E., Rohrbach, R.P., Buckmaster, D.R., 2006: Engineering principles of agricultural machine. 2nd ed. St. Joseph, Michigan: ASABE, 71 pp.
21. Tomazello, M., Brazolin, S., Chagas, M.P., Oliveira, J.T.S., Ballarin, A.W., Benjamin, C.A., 2008: Application of X-ray technique in nondestructive evaluation of eucalypt wood. Maderas-Ciencia y Tecnologia 10(2): 139-149.
22. Tomczak, A., Jelonek, T., 2013: Radial variation in the wood properties of Scots pine (*Pinus sylvestris* L.) grown on former agricultural soil. Forest Research Papers 74: 171-177.
23. Xu, W., Fang, X.Y., Han, J.T., Wu, Z.H., Zhang, J.L., 2020: Effect of coating thickness on sound absorption property of four wood species commonly used for piano soundboards. Wood and Fiber Science 52(1): 28-43.
24. Zeidler, A., Borůvka, V., 2016: Wood density of northern red oak and Pedunculate oak grown in former brown coal mine in the Czech Republic. BioResources 11(4): 9373-9385

GAMAL NASR, MOHAMED MAHMOUD IBRAHIM, FETOUH HASHEM*
CAIRO UNIVERSITY
FACULTY OF AGRICULTURE
AGRICULTURAL ENGINEERING DEPARTMENT
CAIRO, EGYPT
*Corresponding author: eng_fetouhhashem@yahoo.com

HARDWOOD TRADE IN SELECTED COUNTRIES OF EASTERN EUROPE

AGNESA MRAČKOVÁ, MILAN ŠIMEK
MENDEL UNIVERSITY IN BRNO
CZECH REPUBLIC

EVA HAVIAROVÁ
PURDUE UNIVERSITY
USA

ZOLTÁN PÁSZTORY
UNIVERSITY OF WEST HUNGARY
HUNGARY

ABSTRACT

This study focuses on trade of hardwood products in selected countries of Eastern Europe, specifically the Czech Republic, Slovakia, and Hungary. It was supported by a survey conducted with companies producing products made of hardwoods. It monitors trade trends in the wood products industry, specifically focusing on lumber, wooden veneers, furniture production, musical instruments, and wooden accessories. It also addresses the current and potential import and use of the US hardwood lumber in these countries. The study is also pointing out the shortcomings of the monitored markets. The online questionnaire and follow-up phone calls were used to obtain information from companies in countries of interest. Results showed that 83.3% of Czech respondents already use imported hardwoods in their production, followed by Hungary (69.2%) and Slovakia (54.6%). Despite the relatively high values of imported hardwood products, the overall results show that there is only a small potential for an increase in import of the US hardwoods in the wood products industry in chosen countries. The utilization of tropical hardwood species will continue because of their superior properties for specialized products such as musical instruments. Results also point out the grooving importance of certified hardwoods, their utilization, and trade.

KEYWORDS: Hardwood trade, hardwood products, US hardwoods, Eastern Europe.

INTRODUCTION

Over the last two decades, ongoing economic globalization has brought considerable changes in how wood products companies use and trade the material for their production. This study aimed to better understand the supply and trade of hardwood resources, such as lumber veneer, and finished products, such as furniture, in the selected countries of Eastern Europe, with the vision to facilitate potential opportunities for better international cooperation. Despite the pronounced downturn in many hardwood markets during this time, some evidence suggests that the smaller, customized manufacturing sector has fared better than the more traditional mass producers (Bumgardner et al. 2007, Buehlmann et al. 2008, Lihra et al. 2008). These smaller, customer-oriented manufacturers offer customized services and products and serve niche markets (Anderson 2006). However, their aggregate material consumption increases the importance of hardwood lumber producers (Luppold and Bumgardner 2008). This situation is very similar in Eastern European countries where the wood products industry plays a vital role and is represented mainly by smaller customized manufacturers. These producers need a steady supply of material to produce high-quality products, which they sell locally and globally. It is believed that adequate material supply should be available from local resources since Eastern European countries are highly forested. For numerous reasons, some producers are experiencing a shortage in the material supply of their choice and seeking imported resources. Hardwood lumber consumption and trade are difficult to measure. Estimates of consumption for individual industries exist based on survey data (Forbes et al. 1993), but these estimates are only snapshots and are not current. It is also essential to understand that the international hardwood lumber market seen can change quickly. The market that existed in the 1990s is not the same market the wood products industry faces today (Grzegorzewska and Sedliacikova 2021 Grzegorzewska et al. 2020). The systemic transformation that followed the collapse of communist regimes in the early 1990s in European countries of the so-called Eastern Bloc affected all areas of the economy, including forestry and forest products (Zälïtis 2015). Nevertheless, forest-based sectors in these regions continue to contribute significantly to the quality of life and sustainable natural resource utilization. For example, given the current state of the forestry and forest-based sectors in Slovakia, innovation trends in these sectors are oriented toward efficient wood processing, technological innovations, new software solutions, better services, and other approaches (Orazio et al. 2017, Hajduchova et al. 2016). The wood trade manners and market decisions on the Slovakian market were also researched and presented (Halaj et al., 2018). Due to the growing global demand for wood and wood products, it is crucial to be competitive in the international market to use the potential gains of this increased demand. The raw material path is relatively long, as wood is processed into the final products and delivered to a consumer. It passes several production stages and different markets until the final product fulfills the consumers' needs (Parobek et al. 2014). In environmentally sensitive markets, forest products' competitiveness can be influenced by factors related to the origin of wood material from sustainable and renewable sources (Paluš and Kaputa 2009).

Trade is usually associated with large economies, but also for small and vulnerable economies, exports and imports are essential in sustaining growth and external viability. Their long-term survival is dependent on their ability to compete with exports of similar products

from other countries on the international market. It is also known that a nation engaging in trade gains has a comparative advantage not because it can produce goods or services cheaper but because it is relatively more efficient than other nations in producing these goods or services (Carvalho et al., 2009). The importance of globalization in the development of world markets has been evident in recent decades, and its impact can be observed as well on the wood products market. Several studies reflect the global changes in industrial wood and wood products markets (Hurmekoski 2013, Buongiorno 2015, Zhang 2012, Dragicevic 2017, Knauf 2017, Latta et al. 2016, Wear et al., 2016). Economic growth represents one of the most important factors, which creates ideal conditions for timber market development. Following the theory of derived demand, the demand for wood depends on the demand for final wood products (Parobek et al. 2014).

The set of economic and political decisions have also impacted the whole wood market sector. The EU industrial wood and wood products trade is nearly 50% of the global trade. Therefore, the EU represents one of the world's most robust trading blocks. There was a significant shift in wood flows in Eastern Europe, namely in the Czech Republic. The exported volume of roundwood from the Czech Republic increased by almost 43% between 2015 and 2017, and it was the largest export of raw roundwood among all EU members. The share of the EU's import of roundwood worldwide has been stable over the past five years and reached about 40%. The share of exports was about 30% (Dzian et al. 2019).

The overall scope of this study is to find out more about how forest products companies in Eastern Europe source the material for their production and if there is an interest to expand their trade of hardwood resources (import or export) to other markers. The online survey was used as the primary tool to collect information from targeted companies to determine if they are producing their products from domestic or imported wood products, their raw material preferences, trends in management, and marketing practices.

MATERIALS AND METHODS

Steps of survey creation and data collection

The surveying process was preceded by secondary research, which aimed to target companies involved in producing hardwood products in selected countries of the Czech Republic, Slovakia, and Hungary. The database included companies producing and displaying on their website products made of hardwoods such as veneers, musical instruments, or hardwood accessories. The created database of companies included only publicly available information, company name, contact person and their job title, company headquarters, date of company establishment, number of employees, and turnover, if available. The industry experts and industry association representatives in all targeted countries reviewed the created hardwood products company database. This step was followed by developing an online questionnaire. The initial e-mail was sent to selected companies to acquaint them with the research scope and obtain permission to send them additional e-mails with the actual web-based questionnaire. Altogether, 80 companies were approached to participate in this survey, representatives from the secondary and the tertiary wood products sector, which are companies producing and trading targeted hardwood products. Surveying took place in the official

languages of each addressed country. Two e-mails with a link to the online questionnaire were mailed to companies, with a one-week separation between mailings. The response rate after the first e-mail was low at 13%. A week later, the second e-mail was sent immediately after a telephone call reminder, reaching out to the previously contacted company representatives. This approach was very successful and yielded a high response rate (on average, 45%). Some company representatives were friendly and agreed to participate in an extended phone interview, discussing the given topic further. This information was collated and reported in the result section.

Questionnaire structure

In a qualitative study, as in research methods in general, rigorous data collection procedures are the main factors that influence quality and trustworthiness (Kitto et al. 2008) and critically influence the study results (Gibbs et al. 2007). Eastern European wood product manufacturers producing or having the potential to produce their products from hardwoods imported from other markets (including popular tropical wood species) were examined by voluntary questionnaire. A systematic literature review was carried out (Campbell et al. 2014), exploring empirical and theoretical scientific papers or research reports that focused on developing semi-structured interview guidelines. In the end, the final version of the questionnaire containing 18 questions was developed.

All collected information was identified, grouped, labeled, and sorted into sub-categories based on their similarities and differences. After these steps, sub-categories were further grouped and allocated to the main studied categories, covering various methodology phases (Elo and Kyngäs 2008).

RESULTS AND DISCUSSION

Firm characteristics

In total, 25 Czech (CZ), 25 Slovak (SR), and 30 Hungarian (HU) companies participated in the survey. The response rate in the Czech Republic was 48%, in Slovakia 44%, and in Hungary 43.3%. The overall response rate of the questionnaires was 45%. There were 36 valid questionnaires and one incomplete and therefore excluded this questionnaire. Almost half of the responses came from the production sector of manufacturing furniture, interior products, and parquet flooring (47.2%). Other respondents were producers of veneers (11.1%), musical instruments (13.8%), and lumber producers (13.8%). A small range of addressed companies was also involved in the production of wooden accessories (8.3%) and shipbuilding (5.5%). Regarding the geographic location, the highest concentration of respondents from the Czech Republic (75%) was located in the eastern part of the country. In Slovakia, almost half of the responding companies came from the western half of the country and the other half from central Slovakia. In Hungary, the responding companies are located in the country's center, close to the country capital. Companies were divided by size into micro enterprises, small enterprises, medium enterprises, and large enterprises, following the EU regulations. The most suitable criteria for determining the enterprise's size were the number of employees (EU regulation) or the company's annual turnover. Company size was defined base on the number of employees.

The results showed that companies' ratio, with the variable number of employees in the Czech Republic and Hungary, is better represented than in Slovakia. While focusing on products from solid wood or veneer, small and medium-sized businesses are dominant in all three targeted countries. Thirty respondents were classified as micro-enterprises, with up to 9 employees. With the increasing number of employees, the number of businesses was decreasing. However, large enterprises of 100 to 500 employees were also found in the Czech Republic and Hungary. It could be concluded from collected responses that the addressed companies engaged in the production of secondary wood products, such as furniture, wood accessories, parquet, or musical instruments, were of a small or medium size. On the other hand, primary wood products companies, those processing logs, veneers, or other semi-products, usually have a higher number of employees (one Hungarian company had over 500). Employees' annual turnover can be a very delicate subject, even though this is one of the criteria that every enterprise must disclose through its financial statements. In addition to specific turnover intervals, there was an option not to answer this question, but it was answered by 16.7% of respondents. However, 50% of respondents reported an annual turnover below 2 million €. Another 33.3% reported the annual turnover in the range from 5 to 10 million €. The rest of the companies selected a turnover above 10 million €.

Import of foreign hardwood species

A significant number of respondents (69%) reported that they import foreign wood species. The lowest balance was reported in Slovakia (54.4%), while the highest in the Czech Republic (83.3%) and Hungary (69.2%). The question about foreign hardwood species' utilization included temperate hardwoods and other tropical hardwood species, mainly those coming from Africa and Asia. The most popular wood species were American black walnut (60%) and mahogany (44%). Regarding the US hardwoods, 70% of Czech and 83.3% of Slovak respondents reported working their experience mostly with American black walnut.

In comparison, 44.4% of Hungarian respondents used Hard maple, as is shown in Fig. 1. It is also important to note that some Czech and Hungarian companies also import a low quantity of local hardwood species. Specifically, species such as European beech or Pin oak.

One of the objectives was to learn about US hardwood species and their proportional representation in production by selected countries. Thus, from a total of 36 respondents, 69.4% reported experience of working with US hardwood species. Fifteen firms (60%) reported using the American black walnut (*Juglans nigra*), followed by Hard maple (*Acer saccharum*), which was identified by eight respondents (32%). In contrast, seven respondents (28%) reported using the Northern white/red oak (*Quercus Alba/ Quercus nigra*). However, American black cherry (*Prunus serotina Ehrhart*) and hickory (*Carya ovata*) were reported as the least used wood species. American black cherry was selected by four companies (16%) and hickory only by two companies (8%). Importing foreign wood species was attributed to their exceptional appearance and superior properties, reported by 48% of companies. Responses showed that 40% of the surveyed companies import foreign wood species for strategic (marketing) reasons, mainly the interest of their customers. However, specific results differ in each country and almost in every company. The most frequent reason was the customer demand, selected by 36% of respondents. Three Czech companies producing wood accessories, musical

instruments, and veneers chose foreign species for their superior structure/texture compared to the domestic hardwood species. One company mentioned that they import wood species from abroad precisely because of better acoustic/resonance properties.
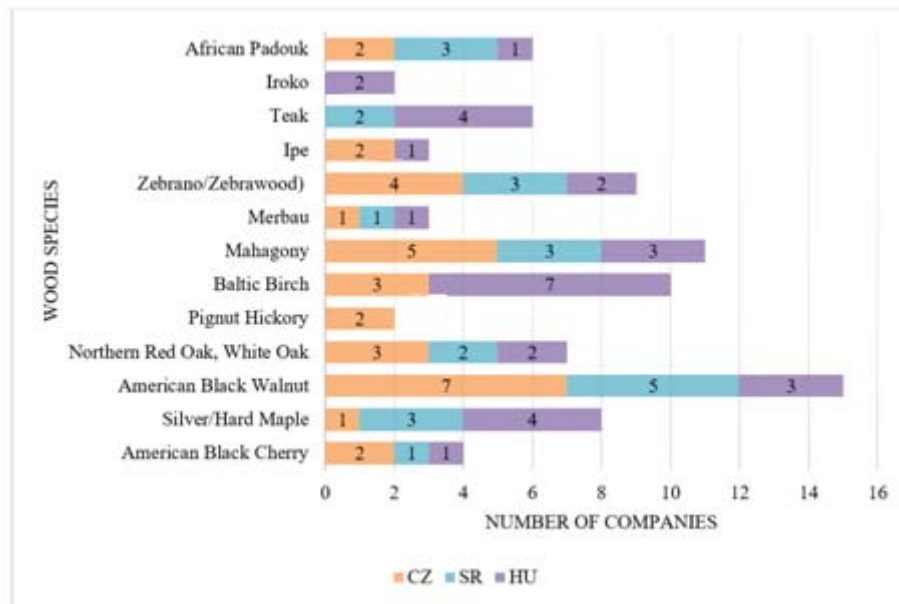

Fig. 1: Imported wood species from abroad by EU countries (CZ, SR, HU).

Production characteristics

Respondents were also asked to comment on their production and the type of imported hardwoods. 65.2% of respondents import wood in the form of lumber, and 56.5% of surveyed companies import and used hardwood veneers. In respect of hardwood logs import, the semi-finished products category was selected only by 17.4% of respondents. It should also be noted that out of 25 companies, just about 8%, only trade and do not process the imported commodities. To evaluate the import of the US hardwoods, it was necessary to exclude companies that import tropical wood species from other continents. The remaining results are not 100% decisive, as most companies import in addition to the US hardwood species also other tropical wood species. For example, if a company reported working with American black walnut and mahogany, they reported a product type importing solid wood and veneer. We wouldn't know which wood species were imported for what type of products. The results showed that the most imported product type of the US hardwood species is lumber, reported by 61.1% of companies from a total of 18 companies. Furthermore, a significant imported product type was the US hardwood veneers (55.6%). The last negligible type of products is semi-finished products (16.6%) and furniture (5.5%).

The following question was related to the perception of better physical and mechanical properties of foreign wood species, mainly concerning musical instrument manufacturers. Thus, the responses received were quite surprising; even though none of the Hungarian companies works in the production of musical instruments, many responded that foreign wood species have better physical and mechanical properties than those of domestic wood species. These respondents work mainly with tropical wood species, such as mahogany, teak, wenge, or iroko, so this statement belongs to those species. The only company from the furniture

manufacturing sector that works with Hard maple reported better physical and mechanical properties than domestic wood species. Altogether, 40% of the surveyed companies said the physical and mechanical properties of foreign wood species are better; the remaining 60% do not consider that the US hardwoods have better physical and mechanical properties than the domestic wood species.

Business environment and customers

Regarding the results, up to 64% of 25 respondents were buying foreign wood species through trade party representatives. Direct trade with the manufacturer/producer was reported by 32% of companies, and 4% of respondents chose not to answer this question. More than half of the companies buy foreign wood species through third-party representatives, which bear witness to an underdeveloped international trade. In the case of the US hardwood products supply, a minimum quantity of goods to the buyer may be determined, which must be loaded on the means of transport to ensure meaningful logistics. For this reason, transportation costs are increasing, and thus direct trade for the addressed countries is almost unrealistic. For long-term contracts, the deliveries' sequence can be managed through shipping consents (consensus letters), regulating the balance and continuity of supply concerning the buyer's storage and processing capacities (Paluš 2013). Trade party representatives are located primarily in Western European countries, specifically Germany, England, and France, where the US hardwoods business is already part of the developed wood sector.

Respondents were also asked if they are selling products made of imported wood species internationally. The survey showed that 76% of respondents' trade abroad their products of mentioned wood species. This situation could be because there is a lack of demand for these products on the domestic market, or a higher price of the final product, targeting more affluent customers. This could mean that such a clientele could stagnate in the country where these products are produced. If the company imports foreign timber, then processing it into a product and exports that product to the external market, under ceteris paribus, the company becomes more competitive on domestic and foreign markets. The remaining 24% of the addressed companies do not export their products made of imported wood species, which would mean the exact opposite of the reasons mentioned above. Regarding US hardwoods, the results have the same tendency; 78% of respondents and US hardwood species users stated that their products are also exported abroad. All Hungarian companies export products made of imported material abroad, which can be seen as a lack of demand from Hungarian customers.

The following results are related to sales trends in the woodworking industry, concerning the activities with the imported wood species and commenting on a global perspective. Given the question about performing sales, the results could predict regarding specific industry's area. The results showed that the Czech and Hungarian companies prefer to operate via the B2C (business to customer) model, while Slovak companies also sell via B2B (business to business). 75% of the surveyed companies realized their sales through B2C and 55.6% through B2B. Hungarian companies do not sell online. Online sales were mentioned by five Czech and two Slovak companies. It is also important to note that some companies perform their sales in variable ways. Hungarian companies also stated that they were using another way of selling their products but did not specify the method. In the case of trading and processing the US

hardwood species, the results are changing only slightly, shown in Fig. 2. In the Czech Republic, sales through the B2B model are dominant, but on the other hand, we see the highest number of online sales. Of course, online sales are not performed by companies that process veneers or lumber, as they are bulky semi-finished products and subject to further processing. Thus, companies automatically introduce online sales by producing products such as accessories, furniture, or musical instruments. The B2C model is still dominant in Slovakia and Hungary, so consumers are the target group.
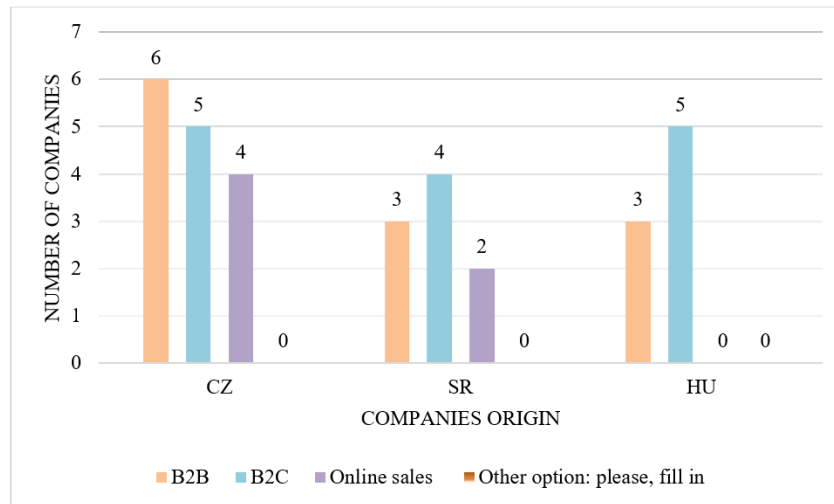

Fig. 2: Sales performance overview based on responses from US hardwood species processing companies.

Sustainable forest management

Forest management and certification play a supportive role in realizing wood production by evaluating social, economic, and ecological objectives. The number of certified forests is increasing rapidly worldwide. The results show that more and more companies prefer wood material of known origin and thus certified wood. Only 27.8% of responding companies from three countries said they did not care about the wood origin. This may result from several limitations on certified raw materials in Eastern EU countries. Final consumers create public opinion, but demand is created at the level of buyers of certified wood. Two certification systems, FSC and PEFC, were used prevalently by the respondents. These two certifications are strongly enforced in the countries of Europe. Some companies claim that they require both PEFC and FSC. Up to 57.7% (Fig. 3) of companies said they required an FSC certification, 15.4% required a PEFC certification, and 23.1% said they needed a different certification. Only one of the companies named CITES certification as an alternative. Focusing on the results obtained from woodworking firms utilizing US resources, the results are as follows. The largest percentage of respondents use the FSC certification, 66.7%. Four companies require PEFC certification, which is 26.7%. The remaining 26.7% use unknown certifications.
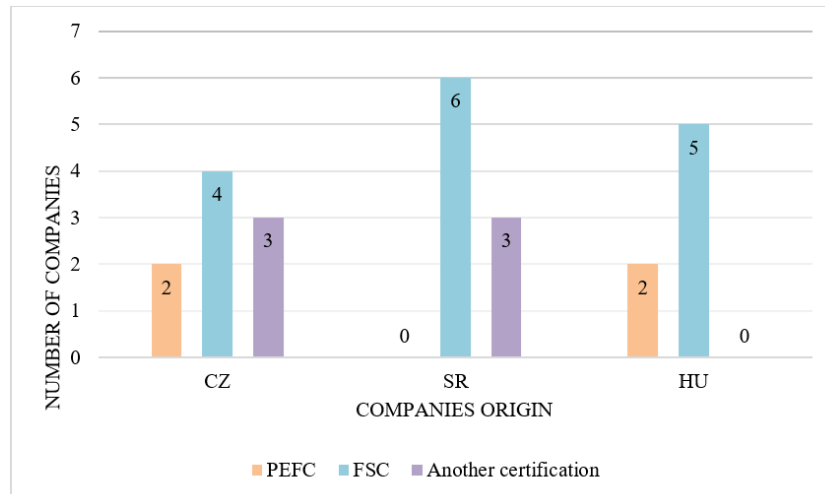
Fig. 3: Wood certification overview responded by addressed companies.

CONCLUSIONS

The main goal of this research was to evaluate the current and potential use of foreign hardwood species in chosen EU countries. Mainly small and medium-size wood processing companies were involved. The survey results showed that there is already ongoing business with well-functioning trade and use of foreign wood species. It showed that 83.33% of Czech respondents already use imported hardwoods in their production, followed by Hungary (69.24%) then Slovakia (54.55%). Compared to the Czech Republic and Hungary, the lower percentage of imported hardwoods users in Slovakia could be attributed to sufficient domestic resources. American walnut is the most popular foreign wood species on the Czech and Slovak markets, and up to 60% of respondents expressed interest in this type of wood species. Hard maple is recognized and valued by Hungarian companies, followed by Black cherry and hickory. The results also showed that 48% of the US hardwoods are imported due to their unique structure and properties that the other wood species cannot replace. 40% of their import is attributed to strategic reasons, such as particular demand from customers. The work aimed to determine if there is a direct business connection between the producer of US hardwood species and the users in Eastern European countries, but this question did not yield very positive results. Up to 77.78% of respondents said that they are importing US hardwoods through sales representatives, which means that import runs through the intermediate links in Western Europe. Because of this, shipping costs are increased. Transport costs will also be increased in direct trade between producer and user if the capacity of transfer is not met. 78% of the surveyed companies said they exported products made of US hardwoods to the external markets. The Hungarian market is focusing mainly on external markets, thus ensuring greater competitiveness. The Czech Republic and Slovakia focus their production mainly on the domestic market. The second outlet of the questionnaire was focused on a potential trade with the foreign wood species. In this survey, 11 respondents were involved, of which only 19% expressed interest in a possible trade with foreign wood species. This interest came from the Hungarian companies, which expressed interest in the US hardwood species such as American walnut, Hard maple, and other African wood species. The vast majority of addressed

companies that do not yet work with foreign wood species and are not very interested came from Slovakia. A similar response was also recorded in the Czech Republic, where companies expressed low interest in foreign wood species.

The application of tropical wood species is still essential in producing musical instruments, such as decorative veneers on the back and side of the guitar. Tropical woods with the highest density (mahogany or wengé) are used for guitar components and so-called bridges. However, the distinctive texture of tropical wood species from afar is not as popular as before, and the current production represents around 2%. The risk of imports is associated with logistics, whether the economic crisis is also one reason for low use.

In terms of sales, it was expected that the bulk of sales would happen through the B2C mechanism, in which the highest emphasis is placed on the targeted customer. This hypothesis was confirmed since the B2C mechanism prevailed in every studied country, where the predominance of small and medium-sized enterprises is most common, and this mechanism most profitable. The growing importance of online sales was observed mainly in the Czech Republic but also in Slovakia when respondents launched online sales. Of course, online sales are challenging for some companies dealing with bulky products. However, with smaller products such as furniture, musical instruments, or wooden accessories, the online sale could be an excellent move and an advantage to combat growing competition.

In recent years, the awareness of sustainable forest management is on a growing trajectory, which is also very strongly reflected in the responses about the importance of the origin of raw material (wood). In the Czech Republic and Slovakia, it is possible to speak unambiguously about the interest in certified wood products, while it is not so clear in Hungary. Their forest areas are so far not prevalently certified. Only in 2016, Hungarian Forest Certification Non-Profit Ltd. became a member of PEFC certification. Currently, no forests in Hungary are certified by PEFC. Nevertheless, the PEFC and FSC chain of custody management is used in Hungary, mainly due to the large export of their products abroad. However, it should be noted that the demand for certified wood and wood products is increasing every year. This statement is based on statistics of ever-growing areas of certified forests and a new chain of custody certificates, especially FSC certification.

REFERENCES

1. Anderson, C., 2006: The long tail. Hyperion, New York, 238 pp.
2. Buehlmann, U., Bumgardner, M., Schuler, A., Crissey. J., 2008: Managing the downturn. Modern Woodworking. April 2008, Pp 40–49.
3. Bumgardner, M., Romig, R., Luppold, W., 2007: Wood use by Ohio's Amish furniture cluster. Forest Product Journal 57(12): 6–12.
4. Buongiorno, J., 2015: Income and time dependence of forest product demand elasticities and implications for forecasting. Silva Fennica 49(5): 17.
5. Campbell M., Egan M., Lorenc, T., Bond, L., Popham, F., Fenton, C., 2014: Considering methodological options for reviews of theory: illustrated by a review of theories linking income and health. Systematic Reviews 3: 114.

6. Carvalho, K.H.A., Silva, M.L., Soares, N.S., 2009: Competitiveness of Brazilian wood pulp in The International Market. Cerne 15(4): 383–390.

7. Dragicevic, A.Z., Barkaoui, A., 2017: Forest-based industrial network: Case of the French timber market. Forest Policy and Economics 75: 23–33.

8. Dzian, M., Paluš, H., Parobek, J., 2019: Global trends affecting the EU timber trade. In: Digitalisation and circular economy: forestry and forestry based industry implications (ed. Chobanova R). Pp 297-301, USB & WoodEMA. Varna.

9. Elo, S., Kyngäs, H., 2008: The qualitative content analysis process. Journal of Advanced Nursing 62(1): 107–115.

10. Forbes, C.L., Sinclair, S.A., Luppold, W., 1993: Wood material use in the furniture industry: 1990-1992. Forest Products Journal 43(7/8): 59–65.

11. Gibbs, L., Kealy, M., Willis, K., Green, J., Welch, N., Daly, J., 2007: What have sampling, and data collection got to do with good qualitative research? Australian and New Zealand Journal of Public Health 31(6): 540–544.

12. Grzegorzewska, E., Sedliacikova, M., 2021: Labour Productivity in the Sustainable Development of Wood-based Industry: A Case for the European Union Countries, Bioresources, 16(2): 3643-3661.

13. Grzegorzewska, E., Sedliacikova, M., Drabek, J., 2020: Evaluating the international competitiveness of Polish furniture manufacturing industry in comparison to the selected EU countries, Acta Facultatis Xylologiae Zvolen 62(2): 149-164.

14. Hajduchova, I., Sedliacikova, M., Halaj, D., 2016: The Slovakian Forest-Based Sector in the Context of Globalization, Bioresources 11(2): 4808-4820

15. Halaj, D., Sedliacikova, M., Mala, D., 2018: Customer Behavior on the Slovakian Roundwood Market: A Case Study. Bioresources 13(3): 6003-6020.

16. Hurmekoski, E., Hetemäki, L., 2013: Studying the future of the forest sector: Review and implications for long-term outlook studies. Forest Policy and Economics 34: 17–29.

17. Kitto, S.C., Chesters, J., Grbich, C., 2008: Quality in qualitative research. Medical Journal of Australia 188(4): 243–246.

18. Knauf, M., 2017: Market potentials for timber-concrete composites in Germany's building construction sector. European Journal of Wood and Wood Products 75(4): 639–649.

19. Latta, G.S., Plantinga, A.J., Sloggy, M.R., 2016: The effects of internet use on global demand for paper products. Journal of Forestry 114(4): 433–440.

20. Lihra, T., Buehlmann, U., Beauregard, R., 2008: Mass customization of wood furniture as a competitive strategy. International Journal of Mass Customisation 2(3/4): 200–215.

21. Luppold, W., Bumgardner, M., 2008: Forty years of hardwood lumber consumption: 1963 to 2002. Forest Products Journal 58(5): 6–12.

22. Orazio, C., Cordero Montoya, R., Régolini, M., Borges, J., Garcia-Gonzalo, J., Barreiro, S., Botequim, B., Marques, S., Sedmák, R., Smreček, R., Brodrechtová, Y., Brukas, V., Chirici, G., Marchetti, M., Moshammer, R., Biber, P., Corrigan, E., Eriksson, L.O., Favero, M., Galev, E., Hengeveld, G.M., Kavaliauskas, M., Mozgeris, G., Navrátil, R., Nieuwenhuis, M., Paligorov, I., Pettenella, D., Stanislovaitis,A., Tomé, M., Trubins, R., Tuček, J., Vizzarri, M., Wallin, I., Pretzsch, H., Sallnäs, O., 2017: Decision support tools

and strategies to simulate forest landscape evolutions integrating forest owner behaviour: A review from the case studies of the European Project, INTEGRAL. Sustainability 9(4): 599.

23. Paluš, H., 2013: Market and trade in wood and wood products (in Slovak). Zvolen, 225 pp.

24. Paluš, H., Kaputa, V., 2009: Survey of attitudes towards forest and chain of custody certification in The Slovak Republic. Drewno 52(182): 65−81.

25. Parobek, J., Paluš, H., Šupín, M., Kaputa, V., 2014: Analysis of wood flows in Slovakia. Bioresources 9(4): 6453−6462.

26. Štěrbová, M., Loučanová, E., Paluš, H., Ivan, Ľ., Šálka, J., 2016: Innovation strategy in Slovak forest contractor firms. A SWOT analysis. Forests 7(6): 12.

27. Wear, D.N., Prestemon, J.P., Foster, M.O., 2016: US forest products in the global economy. Journal of Forestry 114(4): 483-493.

28. Zhang, H., Buongiorno, J., 2012: Markets, government policy, and China's timber supply. Silva Fennica 46(4): 595−608.

AGNESA MRAČKOVÁ, MILAN ŠIMEK*
MENDEL UNIVERSITY IN BRNO
FACULTY OF FORESTRY AND WOOD TECHNOLOGY
DEPARTMENT OF FURNITURE, DESIGN AND HABITATION
ZĚMĚDĚLSKÁ 1
613 00 BRNO, CZECH REPUBLIC
*Corresponding author: simek@mendelu.cz

EVA HAVIAROVÁ
PURDUE UNIVERSITY
DEPARTMENT OF FORESTRY AND NATURAL RESOURCES
175 MARSTELLER STREET
WEST LAFAYETTE, IN 47907, USA

ZOLTÁN PÁSZTORY
UNIVERSITY OF WEST HUNGARY
FACULTY OF WOOD SCIENCES
4 BAJCSY-ZSILINSZKY E STR.
SOPRON 9400, HUNGARY